Methacrylate based nanogels as drug delivery system and Pickering-Ramsden emulsion stabiliser

A thesis submitted in partial fulfilment of the requirements of the Degree of Doctor of Philosophy

Giorgio Chianello

School of Biological and Chemical Sciences, Queen Mary University of London

Supervisor: Prof. Marina Resmini

2016

Statement of originality

I, Giorgio Chianello confirm that the research included within this thesis is my own work or that where it has been carried out in collaboration with, or supported by others, that this is properly acknowledged below and my contribution indicated. Previously published material is also acknowledged below.

I attest that I have exercised reasonable care to ensure that the work is original, and does not to the best of my knowledge break any UK law, infringe any third party's copyright or other Intellectual Property Right, or contain any confidential material.

I accept that the College has the right to use plagiarism detection software to check the electronic version of the thesis.

I confirm that this thesis has not been previously submitted for the award of a degree by this or any other university.

The copyright of this thesis rests with the author and no quotation from it or information derived from it may be published without the prior written consent of the author.

Signature:

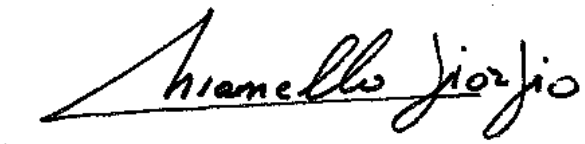

Date: 31/08/2016

Details of collaboration:

Biological studies were performed in collaboration with Dr. Lino Ferreira, Ms. Josephine Blersch and Ms. Michela Comune from Biocant Technological Park in Cantanhede, Portugal. TEM images were recorded by Dr. Giulia Mastroianni (Queen Mary Univerisity of London).

Part of the work described in this thesis has been declared of potential interest for the filing of a patent, which is currently being written. This has delayed publication of the work.

This thesis is dedicated to my beloved Pupi (Valentina Cartaino)

For her unconditioned support and love during these years

and to my grandfathers

Angelo Chianello (il Capitano) who I am sure would have been so proud to have his first grandson doing a PhD. I sincerely wished he could have been here today (1922 -2008).

Nicola Carlisi (il Professore) a man who has left a mark on every person he has met, for his honesty, fondness, self-denial and kindness. Hope one day I will be able to leave such a legacy. (1935-).

Abstract

A novel methacrylate based nanogel system has been designed and developed for drug delivery applications. Methacrylates are optimal tuneable materials in terms of polarity, with combination of hydrophobic and hydrophilic moieties. Synthesis of these nanogels (NGs) was achieved via high dilution radical polymerisation using 2-(*tert*-butylamino)ethyl methacrylate (tBAEMA) as functional monomer, methacrylic acid (MAA) or ethylene glycol methyl ether methacrylate (EGMMA) as co-monomer and *N*,*N*′-methylenebis(acrylamide) (MBA) as cross-linker. Fabricated nanoparticles (NPs) were shown to possess water solubility higher than 2 mg/mL and diameter ranging from 5 to 20 nm (depending on nanogels' composition) as confirmed by either dynamic light scattering (DLS) and transmission electron microscopy (TEM). Moreover, nanogels produced have shown the ability to be employed as Pickering-Ramsden emulsion stabiliser. Their reduced size together with their emulsion capabilities make these nanoparticles a promising system for drug delivery, in particular taking into account skin as administration route. The size is in fact small enough to favour their penetration through the *stratum corneum*. Furthermore, in the view of their ability to form emulsions, nanogels could be used both as drug carrier and emulsifier in a final pharmaceutical formulation. NGs proved to be able to incorporate both small molecule such as fenoprofen (an anti-inflammatory non-steroidal drug) and big macromolecule such as siRNA. Cytotoxicity and cell metabolism were also evaluated by transfecting normal human dermal fibroblasts (NHDF), keratinocytes (HaCaT) and HeLa cells with nanogels. Data showed that nanoparticles did not affect viability, cells' morphology and adenosine triphosphate (ATP) levels up to high concentration of 100 μg/mL. In addition, preliminary studies indicated the ability of the nanogels to internalise and release their payload inside cells. In conclusion, the results confirmed that this novel system possesses all the desired characteristics to be used as a promising platform for drug delivery.

Acknowledgement

First of all, I would like to express my profound gratitude to Prof. Marina Resmini for the continuous support and guidance throughout all my PhD. She has always been able to use the right words at the right moment. She has been a true life coach and group leader. I am also thankful to her for the opportunity she gave me to acquire industrial experience by working, for a period of 4 months, at Polyintell, a polymer producing company based in France. This has been possible due to a previous collaboration with the company established during the European project IRMED coordinated by Prof. Resmini.

I owe a great debt of gratitude towards Dr. Lino Ferreira and my "sisters" Josephine Blersch and Michela Comune (Biocant technological park, Portugal) for the fantastic opportunity, they gave me, to undertake a fruitful and rewarding collaborative work. They introduced me to the world of experimental cell biology and have provided me precious guidance and useful tools for my future carrier.

My gratitude goes to Dr. Giulia Mastroianni for her scientific help and her kindness.

I must thank Mark Freely for proof-reading part of this thesis, for being a good friend and for making me discover wall climbing.

I also need to thank Joey McMorrow for proof-reading part of this thesis and for his great sense of humour which always put a smile upon my face.

A very special thanks goes to my "bro" Gabriele, Fosca, Yolanda, Judith, Katarzyna and Dolça for being a constant source of positive energy, unforgettable moments and also precious research advices and support.

Dr. Paolo Bonomi, Dr. Diana Velluto and Dr. Sofia Papadimitriou must be mentioned for their valuable advices and help during the early days of my PhD.

A huge thank you to all the NANODRUG "family", PIs, ESRs and ERs who have been a great inspiration for me and who I shared great moments with.

Thanks to all the members of Resmini's group and the friends from the School of Biological and Chemical Sciences, at Queen Mary University of London, for all the beautiful memories that I will always bring with me.

A big thank you goes to all the academic, administrative and technical staff of Joseph Priestley (JP) building for making the working place such a friendly, stimulating and entertaining environment in particular Jay Cumber, Agha Shah, Sylvie Fritche, Jalal Hamdan, Prof. Mike Watkinson, Dr. Matteo Palma, Dr. Elisa Piccaro, Dr. Tippu

Scheriff, Dr. Nathalie Labrasseur, Dr. Gregory Chass, Dr. Chris Bray, Dr. David Palomas, Dr. Harold Thoms, Sunita Devi-Paul, Indigo Dean, John Hayes and Janet MacPherson. They all contributed to make the chemistry department “shine” both professionally and socially.

Thanks to my very good “London” friends Philipp, Vanessa, Nelson, Taimur, Anna, Ben, Trini, Gabi, Javi, Sergio, Carolina, Nick, Rheza, Marco, Paola R., Paola C., Cinzia and Carlo for making my life and experiences in the city wonderful.

My Queen Mary basketball team (Los malakas and the boss) also deserve a special mention, in particular Lazaros, Ismael, Antonio, Christian and Marc for the very good times I had with them both inside and outside the court.

Special thanks to my best friend, a brother to me, Andrea who has always been there for me throughout all my life.

I want also to thank Florent for his invaluable help during my time in France, he is definitely one of the kindest person I ever had the fortune to meet.

Finally, a huge thank you goes to my parents and the rest of my big family for their endless love and encouragement.

Financial support from the European Commission initial training network (ITN) NANODRUG (grant agreement number 289454) is gratefully acknowledged.

Table of Contents

List of abbreviations

°C	Degree Celsius
ε	Extinction coefficient
δ	Chemical shift in spectra of nuclear magnetic resonance
Δ	Bending in IR spectra
δ/MPa	Solubility parameter or Hildebrand parameter
λ	Wavelength
λ_{ab}	Absorption wavelength
λ_{em}	Emission wavelength
µg	Microgram/s
µL	Microlitre/s
µm	Micrometre/s
µM	Micro molar
Ac	Acetone
AFM	Atomic force microscopy
AIBN	Azobisisobutyronitrile
APS	Ammonium persulfate
ATP	Adenosine triphosphate
AU	Arbitrary units
br	Broad (NMR signal)
BSA	Bovine serum albumine
$CDCl_3$	Deuterated chloroform
$(CD_3)_2SO$	Deuterated dimethyl sulfoxide
$CHCl_3$	Chloroform
CO_2	Carbon dioxide
Conc.	Concentration
C_M	Monomer concentration
CY5	Cyanine 5
d	Doublet (NMR signal)
D_2O	Deuterium oxide
Da	Dalton

DDS	Drug Delivery System
DEAEMA	Diethylamminoethyl methacrylate
DLS	Dynamic Light Scattering
DMARDs	disease-modifying anti-rheumatic drugs
DMEM	Dulbecco's modified Eagle's medium
DMSO	Dimethyl sulfoxide
EE	Encapsulation efficiency
EGMMA	Ethylene glycol methyl methacrylate
Et_2O	Diethyl ether
Fen.	Fenoprofen
g	Gram/s
g	Gravity centrifugal force
GFP	Green fluorescent protein
J	Coupling constant
HaCaT	Immortalised human keratinocytes
HCl	Hydrochloric acid
HDRP	High dilution radical polymerisation
HeLa	Henrietta Lang cells
He-Ne	Helium-Neon
HEMA	2-Hydroxyethyl methacrylate
^{1}H-NMR	Proton nuclear magnetic resonance
HPLC	High pressure liquid chromatography
Hz	Hertz
IMC	Initial monomer concentration
K_2CO_3	Potassium carbonate
K_a	Acid dissociation constant
K_b	Base dissociation constant
LMA	Lauryl methacrylate
m	Multiplet (NMR signal)
MAA	Methacrylic acid
MAF	2-(2-(3,4-bis(butylthio)-2,5-dioxo-2,5-dihydro-1H-pyrrol-1-yl)acetoxy)ethyl methacrylate
MBA	N,N'-methylenebis(acrylamide)

MeOH	Methanol
mg	Milligram/s
mL	Millilitre/s
mmol	Millimole/s
MSmons	Mass of monomers
MScl	Mass cross-linker
mV	MilliVolt/s
MN	Methyl myristate
MRGC	Experimental code standing for Marina Resmini Giorgio Chianello
MWCO	Molecular weight cut off
NaOH	Sodium hydroxide
NG	Nanogel
NGs	Nanogels
NHDF	Normal human dermal fibroblast
nm	Nanometre/s
Nmons	Number of moles of monomers
NMR	Nuclear nagnetic resonance
NPs	Nanoparticle
NSAID	Non-steroidal anti-inflammatory drug
OA	Oleic acid
OC	Octanol
p	-log operator
P	precipitate
PBS	Phosphate buffer solution
Pdi	Polydispersity index
PES	Polyethersulfone
PI	Propidium iodide
ppm	Part per million
quin	Quintet (NMR signal)
RA	Rheumatoid arthritis
RBF	Round bottom flask
R_f	Retardation factor
RNA	Ribonucleic acid

rpm	Round per minute
r.t.	Room temperature
s	Singlet (NMR signal)
SC	Stratum corneum
SD	Standard deviation
sex	Sextet (NMR signal)
siRNA	Short interfering RNA or silencing RNA
Solv.	Solvent
st	Streaching in IR spectra
t	Triplet (NMR signal)
T%	Transmittance percentage
tBAEMA	tert-buthylamminoethyl methacrylate
TEA	Triethylamine
TEM	Transmission Electron Microscope
TLC	Thin layer chromatography
UV	Ultra violet
UV-VIS	Ultra violet-visible
v/v	Volume/volume ratio
W	Water
XL	Cross-linker
XLs	Cross-linkers

Chapter I: Introduction

1.1 Drug Delivery System

1.1.1 Overview and desirable properties

Drug discovery intended as the use of natural extracts, goes back to the early stages of human civilization. [1] Foundations of modern chemistry and physics were laid between the end 1800s and the beginning of 1900s. This was the time when synthetic bioactive compounds were introduced and pharmaceutical companies were founded. [1, 2] At the beginning of the previous century it was paramount to discover and develop new drugs capable to suppress most of the human diseases that were, until then, incurable. Sulfanilamides (prepared by P. Gelmo and investigated by J. Domagk J. Tréfouël, T. Tréfouël, F. Nitti and D. Bovet) and penicillin, discovered by A. Fleming and further studied by H. Florey and E. B. Chain, are among the most famous example of drug identified and then produced at industrial scale [1]. Although drug discovery is still progressing, from 1960-70, thanks to pioneering work carried out by J. Folkman, T. Higuchi, A. Zaffroni and A. Michaels the pharmaceutical industry moved the attention towards the development of new ways of drug administration that would be able to optimise the pharmacological properties of already known bioactive compounds. [3, 4] Pharmacological activity of a molecule, alone, is often not enough to induce safe and reliable therapeutic effects. Peptide therapeutics, for instance, cannot be administered orally due to their poor stability and weak resistance against enzymatic degradation. [5, 6] There are several desirable characteristics that a drug should possess in order to be employed in the treatment of a disease: the ability to maintain a concentration in the body as stable as possible and within the therapeutic window (Figure 1.1); the capacity to selectively target a specific district of the human body; the resistance against environmental condition (such as the acidity inside the stomach) that could lead to the premature degradation of the drug before the induction of the final effect; possess an adequate speed of action according to the disease that is intended to address and the power to respond to particular stimuli just to name few.

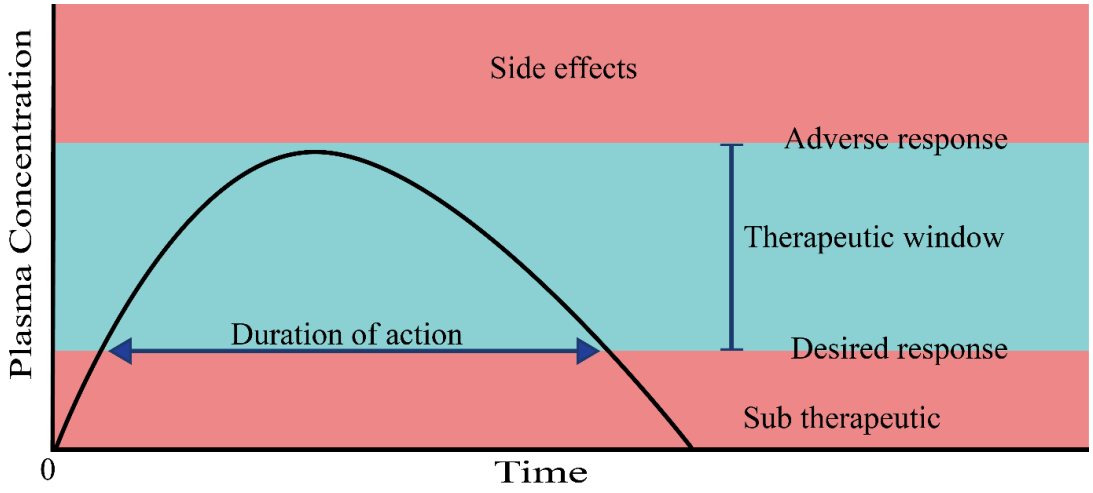

Fig. 1.1 Schematic explanation of drug concentration fluctuation in the body over time and possible effects.

In order to enhance erratic properties of investigational drugs, pharmaceutical industries employ what is called a drug delivery system (DDS).

DDS is a way of administering a pharmaceutical compound to achieve a therapeutic effect in humans or animals. [7] The purpose of a DDS is to alter drug pharmacokinetics and to act indirectly on its pharmacodynamics. DDS can potentially provide several advantages. Among them:

- Promote drug solubility and stability.
- Protect the drug from the external environment.
- Increase patient compliance through the introduction of a new route of administration (for instance from injection to oral administration), lowering numbers of administrations, reduction of side effects, covering unpleasant smells, colours and taste of a free drug.
- Site targeting and side effect avoidance. Some drugs express a therapeutic effect on specific organs while, at the same time, they show toxic or adverse effects on others.
- Stabilising the drug release rate and avoid any side effects related to drug level fluctuation. [8,9]

The major carriers for drug delivery available today can be divided into two groups: prodrug and drug encapsulating systems.

A prodrug is a pharmacologically inactive medication that is designed to be activated after enzymatic or chemical reaction inside the body. The drug is therefore chemically modified in order to optimise its ADME (administration, distribution, metabolism and excretion) profile. The results are: the increase in drug solubility, as more than 30% of drugs show poor hydrophilicity; facilitate permeability across physiological membranes and introduce site targeting, by the addition of a targeting moiety linked to the drug through a spacer, as visually explained in the example below (Fig. 1.2). [10]

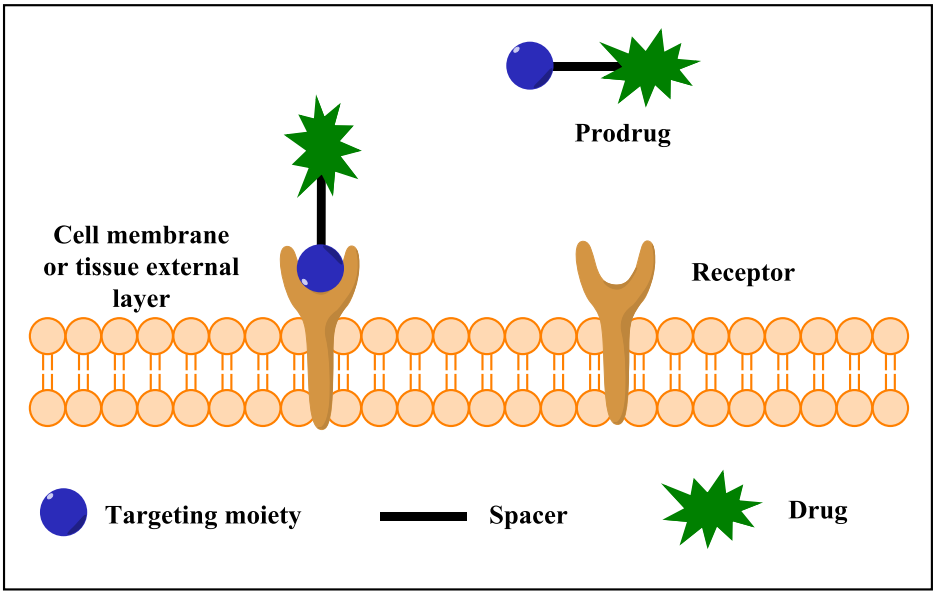

Fig. 1.2 Schematic showing targeted prodrug.

Although prodrugs offer several advantages there are few downsides that limit their application. First of all not all the drug can be chemically modified in the desired way; some of them for instance are not able to endure the reaction's conditions needed for the chemical modification, while some others do not possess the required functional groups that are essential for further modification. Furthermore, sometimes the chemical modification or linkage of the therapeutic compound to a carrier is not sufficient to protect the drug from the harshness of the external environment. Lastly, genetic polymorphisms or age-related physiological changes may vary the pharmacokinetics of the prodrug. [10]

In order to overcome all the above mentioned limitations, drugs can be embedded inside particles or the cavity of a three-dimensional structure. This approach in fact allows the fabrication and subsequent chemical modification of a final system without direct interaction with the drug, at least during initial studies. Once the system is fully

synthesised, characterised and tested, the drug can then be uploaded inside. Another important feature is the possibility to tune the drug release rate by modifying the chemistry of the drug encapsulating systems, a property that cannot be achieved by a prodrug. Moreover, drug encapsulating systems can be designed in order to respond to multiple biomedical relevant changes such as pH or temperature as well as enzymatic cleavage at the same time, without the need of drug chemical modification.

When the development of a new DDS is being considered, it is important to remember that, in addition to the therapeutic improvement, DDS should also possess as many of the following characteristics as possible:

- Biocompatibility, probably one of the most important requirement for a DDS.
- Biodegradability.
- Absence or reduced toxicity.
- Low cost.
- Ease of synthesis, in terms of equipment, labour and manufacturing time needed.
- High raw materials availability, possibly from multiple sources/providers.
- Absence of flavour, a desirable property when taking into account oral administration for example.
- Absence of unpleasant colours.

However, it is also necessary to specify that the desired properties of a DDS also depend on the route of drug administration and targeted disease.

1.1.2 Route of drug administrations: overview and comparison

Drug administration can be classified into two groups according to either the localisation of the final pharmaceutical effect or the route of drug administration. In the first case it is possible to identify two subcategories: 1) local, when the drug exerts its therapeutic effect in the area of application or in a specific compartment of the human body; 2) systemic, when the bioactive compound produces a generalised effect in multiple or all body apparatuses. The second group can be further subdivided into five

major routes of drug administration: parenteral, oral, pulmonary, trans-mucosal, and transdermal. Each of which have pros and cons.

Parenteral, otherwise known as injection, is the fastest and more reliable way of administration as the drug quickly reaches the bloodstream or tissue which is penetrated. Injection is further categorised according to the site of needle penetration in: intravascular, intramuscular, intraosseous, epidural, intravitreal and subcutaneous, just to mention a few. The advantages of this route are: speed of action; precision and accuracy; first pass effect avoidance, which is the chemical processing operated by the liver when a molecule is adsorbed by the gastrointestinal tract and the opportunity to use this route when a patient is unconscious or has his/her gastrointestinal tract compromised (for instance vomiting or blockage). [11]

At the same time parenteral administration shows several disadvantages: It is invasive and could lead to inflammation of the tissue perforated; must be performed by trained personnel to avoid risk of embolism or critical tissue damage; can be painful and has low patient compliance due to the pain related to needle perforation or irritating properties of formulation administered. [11]

Oral, or enteral, administration is generally the preferred patient administration route. It is non-invasive, provides ease of administration and is normally well accepted by patients unless showing unpleasant organoleptic properties. The latter case however can be easily masked using formulation excipients able to cover distasteful characteristics. On the other hand, this way is not suitable for formulations that are not able to resist the gastrointestinal environment, for patients who are either unconscious or have a malfunctioning gastrointestinal tract and for drugs that get immediately metabolised by the liver or that need to act fast, in case of emergency. [11]

Pulmonary administration comprises all the pharmaceutical formulations administered through the airways. It is a relatively fast administering route, it has intermediate patient compliance, it can profit from an extensive exchange surface and offers first pass effect bypass. Although this route is being currently explored and the number of formulations are increasing, there are several issues that restrict its use. The number of drugs that can be administered through this route are still very limited, the process of formulation production is complicated and expensive, it requires the use of a complex and

sometimes expensive external device and it requires either training or experienced personnel to be performed. [12, 13]

Trans-mucosal administration is the delivery of therapeutic agents across the mucous membrane. It includes: rectal, vaginal, and urethral delivery. Most of the DDS administered through this route exert local therapeutic effects with only few of them that can go systemic. In regards to the advantages, this route can benefit from: avoidance of first pass effect, avoiding harsh condition of the stomach, the possibility to be used on unconscious subjects and prolong residence time at the site of administration. However trans-mucosal administration often shows low patient compliance and it presents significant difference in drug adsorption profiles depending on mucosa condition. Furthermore, some medication can produce irritation and several drugs can be degraded by the environmental conditions of the body apparatuses of this route of administration. [14]

Transdermal delivery involves the administration of biologically active compound through the skin. This route demonstrated high potential, not yet fully exploited, in providing an alternative to hypodermic injection and oral administration. With the latter it shares few properties such as high patient compliance and ease of administration. The skin can provide several advantages over the aforementioned routes: first pass effect avoidance; the capacity to exert local or systemic effect depending on DDS degree of penetration in the superficial or deep strati of the skin respectively; the possibility to be used on unconscious patients; an extensive surface of application available; the invasive character and the constant and controllable drug release. [15]

However, some physical obstacles limit its use, like penetration capacity of DDS that have to cross the tight junction of the skin and, as the oral route, the impossibility to administer therapeutic agents that are required to act immediately. [15] Despite all the mentioned limitations, DDS research is rapidly progressing in order to address and overcome these restrictions.

1.1.3 Modern DDS technology

Nature and the physiological body functions already perform at a level that is close to perfection. All movements, sensing and body's basal activities are the results of reactions that take place at the molecular level. Thanks to the tremendous advancement in technology, today it is possible to detect, image, manufacture and modify materials at the nanoscale. Therefore, it is clear that the development of a DDS that could act at the same scale as biological processes would be extremely beneficial and could potentially open new applications. For these reasons, in the last twenty years there has been a growing interest and investments in nanotechnology research and in nanomedicine, with a particular interest in drug delivery. [16-18]

''There's Plenty of Room at the Bottom," Richard P. Feynman 1959. This sentence is considered the birth point for nanotechnology, a field of research and material development that has casted new light on understanding and fine modelling matter.

1.2 Nanomedicine

1.2.1 Introduction, applications and advantages

Nanotechnology is defined as the science that studies, produces and manipulates materials which have at least one dimension in the size range 1-100nm. In order to provide a visual explanation of this extremely reduced magnitude, scientist use to make a comparison with the human hair which has a diameter of 80,000nm (Figure 1.3). [19]

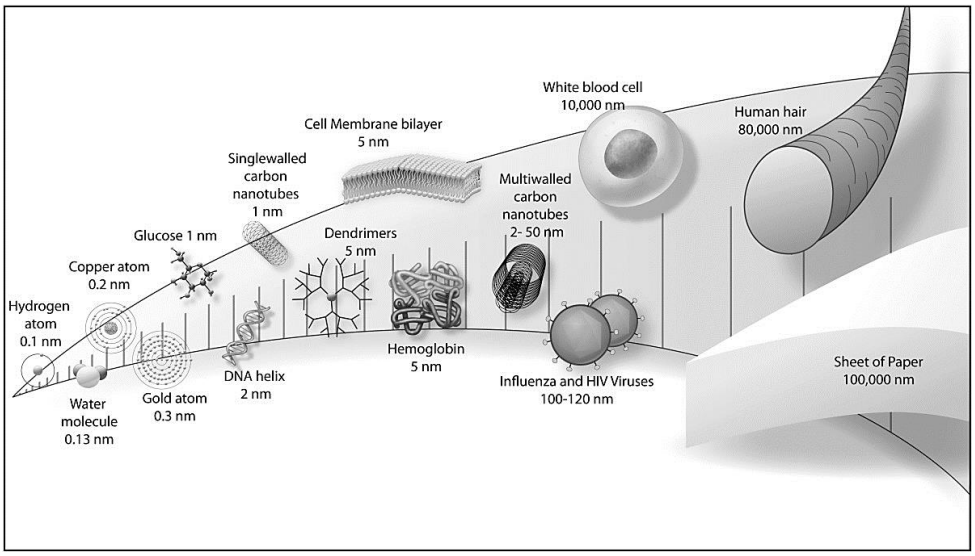

Fig. 1.3 Representation of nanoscale objects. From R. A. Yokel et al. *J. Occup. Med. Toxicol.*, **2011**, 6, 1-27 [a]

Although this is the most accepted definition, some researchers believe that 100 nm cut-off would exclude physiochemical behaviours that occur at a slightly larger scale. For instance, the plasmon-resonance, reported in literature, for 150 nm diameter gold nanoshells or the enhanced permeability and retention (EPR) effect that arise in the size range between 100-200 nm. [20]

Nanotechnology is an extremely broad field of research that includes applications in food industry, electronics, energetic sector etc. [21-23] Nanomedicine is the application of nanotechnology in medical science. It comprises two main employments areas: diagnostics, the detection or monitoring of chemicals, diseases, biomarkers etc. and therapeutics the use of nanomaterials to improve and sustain therapeutic effects of bioactive compounds.

Drug delivery is a segment of the nanomedicine sector which attract consistent funding [24]. As mentioned previously, there is currently an exceptional and rapid growth of research involving nanoparticles (NPs) as drug delivery systems due to their promising characteristics.

For instance, one of the great assets of nanomaterials is their high surface to volume ratio when compared to bulk materials [25] (Figure 1.4). This provides the particles with a very extensive surface area of interaction between the material and the external environment. A fundamental consequence of the increased surface to volume ratio is the high loading capacity of nanoparticles resulting in a lower quantity of nanomaterial required to encapsulate a certain amount of drug, compared to bulk materials. This leads

to two main advantages: reducing the amount of materials required for the synthesis and most importantly decrease the chances of side effects or toxicity associated with the material. Below is a visual explanation of the increment of surface to volume ratio related to scaling size down.

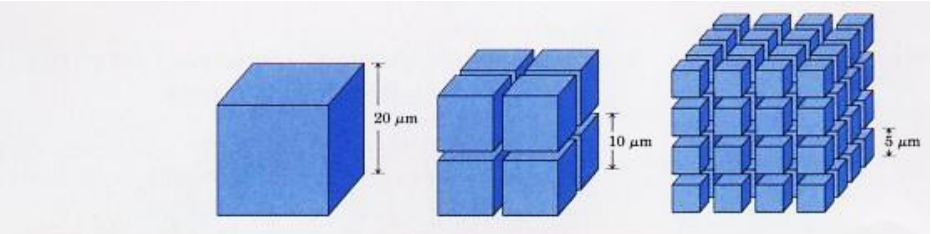

Number of cubes, n	1	8	64
Length of a side, l (μm)	20	10	5
Total surface area, $l^2 \times 6n$ (μm^2)	2,400	4,800	9,600
Total volume, $l^3 \times n$ (μm^3)	8,000	8,000	8,000
Surface area: volume ratio, $\frac{6}{l}$	0.3	0.6	1.2

Fig. 1.4 Surface to volume ratio explained. From Lehninger, D. Nelson; M. Cox. Principles of biochemistry, 2nd edition [b]

As an example, a cube with a side of 1cm has a volume of 1 cm^3 and a surface of 6 cm^2. If this cube was cut into 10nm cubes, while keeping the same total volume of 1 cm^3, the new surface area would then become 600 m^2, significantly increasing the surface to volume ratio from 6:1 up to 6,000,000:1.

Moreover, together with the modern advancement in biotechnology, nanomedicine could provide solid foundations for the development of personalised medicine systems. "The right patient with the right drug at the right dose at the right time" [26]. The development of a drug can require up to 20 years and very high costs, therefore the selection or modification of a suitable delivery system could provide tailoring of pharmacodynamics in a relatively short time and with a tremendous impact on costs.

Furthermore, another advantage of nanomaterials is the promise of active site targeting by tuning the chemistry of nanoparticle or nano-devices in order to provide them with stimuli response capabilities or specific receptor recognition [27, 28].

Although nanomedicine has proven to be an extremely promising research field, pharmaceutical industries and several research groups express concerns regarding the

long term effects of nanomaterials both on living beings and the environment [28-30]. It is in fact still unclear the fate of many NP systems in terms of biodegradability and accumulation in the body or the environment. Nevertheless, the advances both in terms of novel materials and technological instrumentations are continuously improving the knowledge in this area, further enhancing the potential for medical applications.

One of the disadvantages of drug delivery is the extended timeframe needed for preclinical and clinical studies in order to assess safety of the materials, this of course applies also to nanomaterials to an even larger extent due to the additional characterisation tests required. This is probably the biggest limitation for the pharmaceutical industry since it implies higher costs and reduced revenues due to shorter intellectual property coverage. However, the market has already found its own solution to this issue by employing small and medium sized enterprises (SMEs), a growing business which develops the technology and then license it out to big pharma companies. As proven by the European Medicine Agency (EMA) annual reports, SMEs are playing and are expected to play a more important role in the pharmaceutical sector. [31]

Nevertheless, the potential advantages provided by nanomaterials for medicine are attractive, therefore justifying the continuous effort and resources invested. This is also proven not only by the growing number of scientific publications but also by a series of formulations in the process approval or already approved and present in the market by the American Food and Drug Administration (FDA). [32, 33] Renagel® -cross-linked poly allylamine hydrochloride for the control of hyperphosphatemia in adult patients receiving hemodialysis or peritoneal dialysis, Marqibo® -Vincristine sulfate encapsulated in sphingomyelin/cholesterol (60/40, molar) 100 nm liposomes for the treatment of adult patients with Philadelphia chromosome–negative (Ph–) acute lymphoblastic leukemia and Eligard® - Leuprolide acetate incorporated in nanoparticles composed of biodegradable poly-DL-lactide-co-glycolide for managing advanced prostate cancer, just to name few [32].

Several of the DDS systems currently under development or already available in the market are described in more details in the next section.

1.2.2 Overview of existing nano drug delivery systems

In the last six decades numerous DDSs have been developed in order to enhance the therapeutic profile of drugs [34]. As scientific literature can prove there are several different systems currently under development and used today. They can be classified in diverse ways: inorganic or organic according to their chemical composition; self-assembled or synthesised in regards to the production process required; polymeric or oligomeric taking into account their basic structure lengths; natural or synthetic when considering the material source etc. However, three main categories can be identified to describe most of the DDS known: inorganic, non-polymeric and polymeric materials.

1.2.2.1 Inorganic nanomaterials

Inorganic nanomaterials are all those systems not based on carbon chemistry. Mesoporous silica and gold nanoparticles (NPs) are among the most studied and used inorganic systems. Herein a brief description, of the two NPs is provided.

Mesoporous silica nanoparticles (MPSNPs) are solid materials with honeycomb-like structure able to adsorb large amount of molecules due to their extremely high surface area [35]. They are used in several applications as sensors, catalyst and drug delivery systems [35, 36]. Nonetheless, studies have demonstrated toxicity related to MPSNPs. [37]

Gold nanoparticles are colloidal gold shell coated nanoparticles (Figure 1.5). They are currently object of a large number of studies and applications such as diagnostics, drug delivery, photochemistry etc. [38] However, there is a concern regarding the fate of these particles that still needs to be addressed. It has been proven in fact that gold nanoparticles deposit in the liver and spleen and although there is no evidence of short term side effects, their long term reactivity still needs to be studied [39]. Furthermore, their cost may need to be considered.

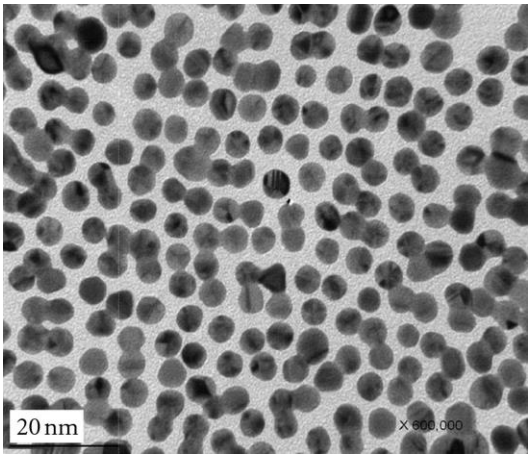

Fig. **1.5** Transmission electron microscope (TEM) image of gold NPs. From S.-H. Kim et al. *J. Nanomater.*, **2012**, Article ID 504026. (OPEN ACCESS).[c]

Inorganic NPs are considered stable under different temperatures and pH conditions however they do not generally biodegrade which may give rise to concerns for the long term administration. [40]

1.2.2.2 Non polymeric organic nanomaterials

The best known example of non-polymeric organic nanomaterials is represented by liposomes. These are vesicles constituted by one or more lipid bilayer with the polar heads of the lipid oriented toward the extravescicular solution (water in the human body) and the inner cavity, and the hydrophobic chains forming the bilayer (Figures 1.6 and 1.7) [41-43]. Hydrophilic molecules can be retained in the centre of the liposomes while hydrophobic ones can fit within the bilayer. Their size range, between 20 nm and 5µm, lies between micro and nano systems. They are a versatile DDS because of their wide size range and similarity to cells, perhaps at the same time they show limitations in achieving active site targeting and controllable drug release rate. [42-44]

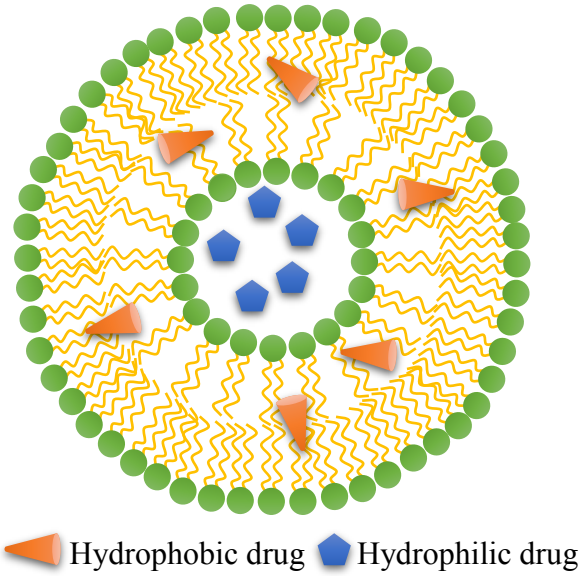

, **1.6** Liposomes schematic views. Where green circle represent the hydrophylic moyety of the lipid surfactant and the yellow chains the hydrofobic region of the surfactant.

1.2.2.3 Polymeric nanomaterials

The majority of modern drug delivery systems can be included in the category of polymeric materials. They are the most versatile systems as their broad chemical composition and architecture can give rise to numerous particles with diverse tuneable properties which can be tailored according to the final application. Moreover, polymers can also be used as coating agents for inorganic nanoparticles [40, 45; 46]. Some examples of polymeric materials are reported below.

Micelles (Figure 1.7) are described as self-assembled colloidal particles, with a size ranging generally between 5 and 100 nm and constituted by amphiphilic polymeric molecules or surfactants that associate in aqueous medium to form core-shell structures. [47-50]

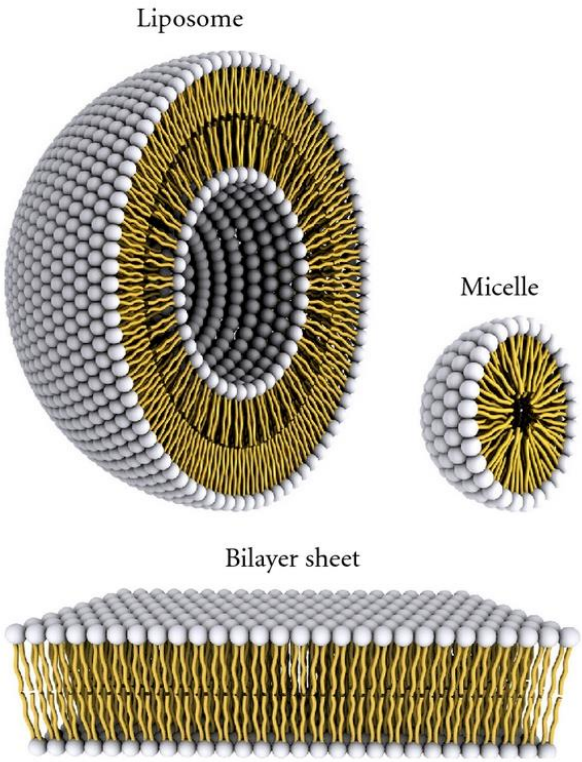

Fig. 1.7 Schematic representation of micelles, liposomes and bilayer sheet. From D. Bitounis et al. *ISRN Pharmaceutics*, **2012**, Article ID 738432. doi:10.5402/2012/738432 (OPEN ACCESS). [d]

A surfactant is a molecule that possesses two regions, one hydrophobic and the other hydrophilic. Depending on the nature of the solvent the surfactant will expose the segment that shows affinity to the solvent on the outside and the lyophobic part on the inside (away from solvent) forming an inner core in order to minimise the free energy (Figure 1.8) [47, 48].

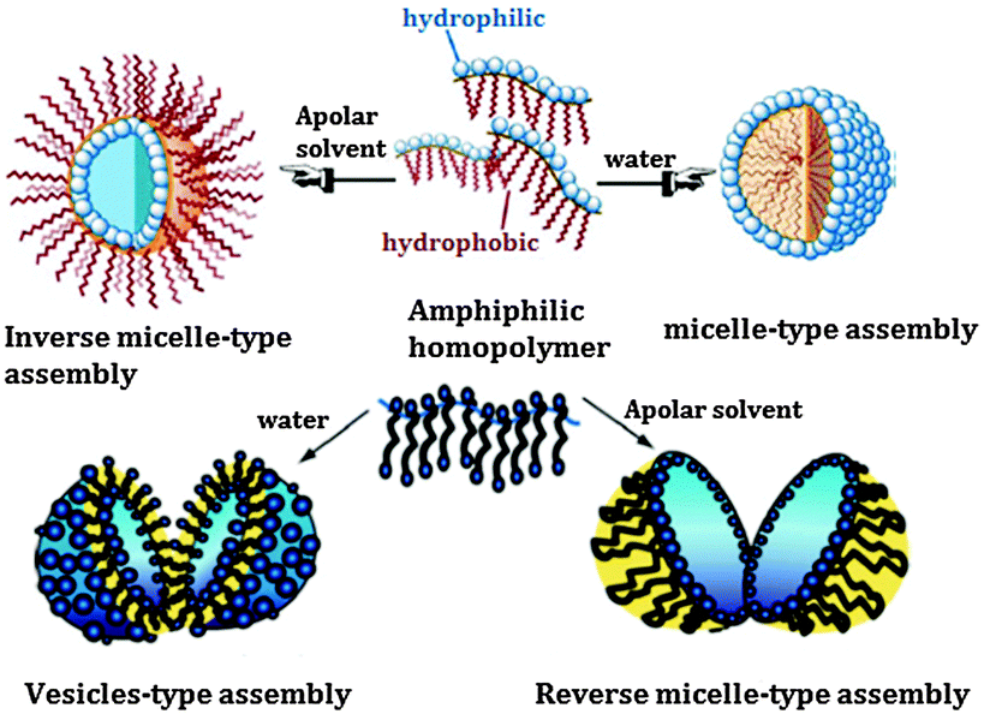

Fig. 1.8 Difference between direct and inverse micelles. From J. Zhang et al. *Chem. Commun*., **2015**, 51, 11541-11555. **License Number:** 3991880626562. [e]

It is possible to describe two different kinds of particles: direct micelles (polar solvent) and inverse micelles (apolar solvents). Micelles are being extensively studied for their promising characteristics such as small particle size, high loading capacity, general biocompatibility and ability to modulate drug release kinetics which makes them suitable for drug delivery and image diagnostics applications. [49, 51-53] The formation of the micelles generally relies on non-covalent bonds and micelles are in fact generally considered as not static systems. In fact, the building blocks (surfactants) micelles are made of, can reshuffle and are in dynamic equilibrium with free surfactants. However, this property is not always an advantage, such as in drug delivery applications, where this can lead to premature drug bleeding from the particles. For this reason, a particular subset of micelles, characterised by stable chemical cross-linking has been developed and studied. [54] Micelles are the main competitor of the drug delivery system described in this work and could be considered a valuable alternative. However, nanogels possess some characteristics not achievable by micelles such as imprinting capabilities (further described in the following section) which provide high specificity and molecule recognition abilities.

Dendrimers are defined as nanosized, radially symmetric branched macromolecules (Figure 1.8) that are extremely homogenous with organised structures and high potential for drug delivery and diagnostics. [55] On the other hand, they are difficult to synthesise, generally expensive and do not provide enough space for drug loading. [56]

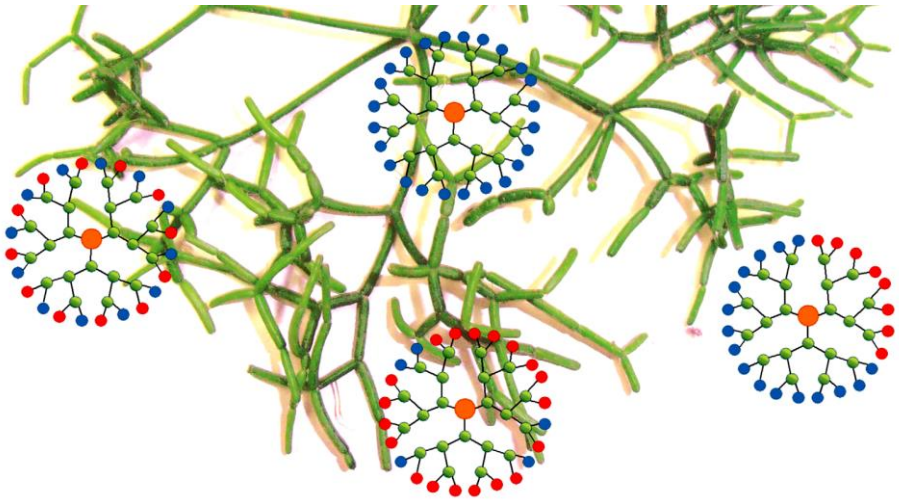

Fig. 1.9 Schematic representation of dendrimers. From M. Sowinska et al. *New J.Chem.*, **2014**, 38, 2168-2203. **License Number:** 3934721385025 [f]

Finally, there are nanogels, which are nanosized networks of physically or chemically crosslinked polymers that swell in particular solvents. Nanogel is the system object of this study and is further described in the following section.

These are some of the main systems employed today for drug delivery. However, several more are currently being used or under development.

1.2.3 Nanogels: properties, uses and advantages

The term "nanogel" was introduced by S. V. Vinogradov and A. V. Kabanov while describing swollen chemically cross-linked networks of cationic and neutral branched polyethylene glycol-crosslinked-polyethylenimine (PEG-cl-PEI) polymers, which were developed for the delivery of antisense oligonucleotides [57]. Nanogels (NGs) are swollen nanosized networks composed of hydrophilic or amphiphilic polymer chains.

They are defined as nanoscale stable colloidal systems formed by physically or chemically cross-linked polymer networks [58, 59] (Figure 1.10).

NGs are soft particles that show features of hydrogels and NPs at the same time. They are flexible, stretchable and able to swell as hydrogels and offer all the potential pharmacokinetics improvements of NPs. Due to their ability to swell and adsorb large amounts of water, NGs are generally inert and show characteristics between solids and fluids while their porous structure provides them with high loading capabilities. [58]

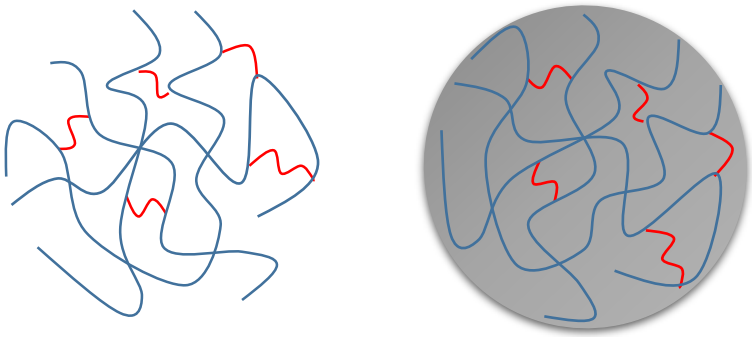

Fig. 1.10 Schematic representation of crosslinked structure of nanogels. Polymer chains are drawn in blue and inter-chain crosslinking in red. Image on the right showing the possibility to approximate nanogels to spheres

In the last few decades, a large number of nanogels have been developed for application in nanomedicine due to their promising characteristics. NGs possess high loading capacity, stability and responsiveness to physical changes, such as ionic strength, pH and temperature [61, 62]. As reported in the literature, several applications have been or are currently under investigation, such as NGs with catalytic activity [63] or thermo-responsive profile [62]. Furthermore, they satisfy most of the requirements for an ideal drug delivery system. [64]

NGs provide drug protection, they can avoid premature interaction between the drug and the human body or the external environment. In this way they can decrease side effects and protect the drug from premature degradation. They can be designed to respond to particular stimuli such as pH or temperature variation. The responsive characteristics of NGs can act as a passive site targeting or as a controller for the release rate. The latter feature is fundamental when the therapeutic window of a drug is particularly narrow, which means that fluctuations in drug concentration would probably cause side effects. NGs can show high penetration efficiency due to their reduced size and deformability, therefore they show high potential for penetration in all

districts of the human body. Moreover, they can be chemically functionalised in order to gain site targeting properties. This is an excellent way to reduce side effects and lower the amount of drug needed in order to produce the desired therapeutic effect. [60] Lastly, NGs show ease of synthesis which is a fundamental characteristic for industrial scale production of a DDS.

There are different synthetic methodologies for the preparation of nanogels: 1) physical self-assembly of interactive polymers; 2) cross-linking of preformed polymers; 3) polymerisation of monomers in homogeneous or heterogeneous phase and 4) template-assisted nanofabrication. The first three methods are, in most cases, relatively inexpensive and simple processes while the fourth is more complex but leads to formation of very homogenous NPs. [65]

Physical self-assembly of interactive polymers leads to the formation of micelle-like particles, therefore their stability may not be as high as chemically crosslinked particles. Cross-linking of preformed polymers and polymerisation of monomers (in the homogeneous or heterogeneous phase) are perhaps the most used synthetic techniques. The first approach generally produces NGs with larger pore size however does not allow the same property control as the latter.

Template-assisted nanofabrication or photolithographic technique utilises a preformed and inert stamp that forces polymerisation into the stamp cavities, molding gels into defined 3D structures that can then be washed out from the support (Figure 1.11). [66]

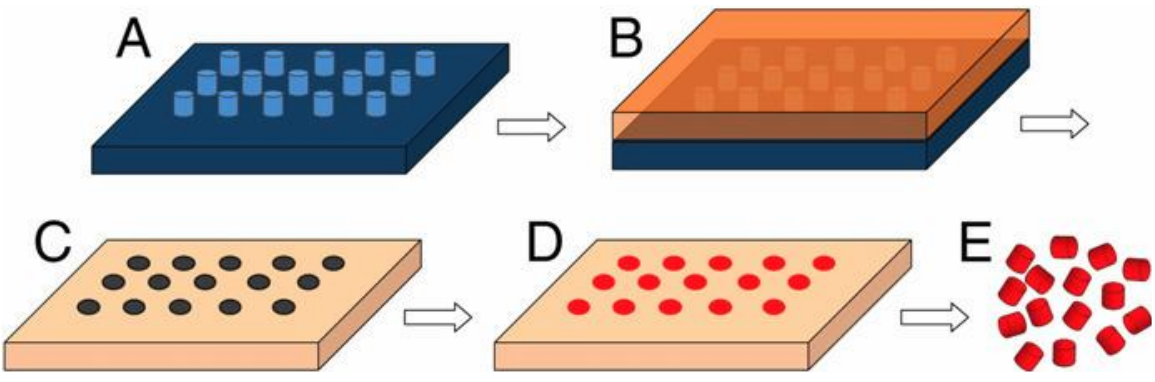

Fig. 1.11 The process of template assisted nanofabrication. A: pattern formation of vertical posts onto a silicon template. B: aqueous gelatine solution is poured to for a gel imprint. C: once solidified, the gel mold is peeled off. D: the mold cavities are filled with polymerisation mixture. E: polymerisation solvent is evaporated and the

mold dissolved to yield 3D constructs with shape complementary to the mold cavities. From G. Acharya et all *J. Control. Release*, **2010**, 141, 314-319. **License Number:** 3937560904561. [g]

This approach leads to the formation of a very homogenous batch and shape of defined particles. However, instruments performing electron beam lithography (EBL), the technique used for the synthesis of the stamps, are extremely expensive (over $1million) and require highly skilled personnel to ensure correct operation.
Polymerisation of monomers in the homogeneous or heterogeneous phase is therefore the preferred way of synthesis and it can be further divided into different techniques.

Precipitation is one of the methods employed. It involves the dissolution of the monomers into a solvent where the nanogels, as soon as they are formed, are insoluble. Therefore, nanogels precipitate and are recovered from the solution by centrifugations/washes and filtration. However, this process generally requires the use of either toxic surfactant such as sodium dodecyl sulphate (SDS) [67, 68] or toxic solvents like dimethylformamide (DMF). [69]

Heterogeneous emulsion is one of the most used techniques and can be subdivided into: membrane emulsification, inverse emulsion and reverse micellar methods. [70] The first approach involves the extrusion of one of the two phases (oil or water) through a porous membrane. The small, homogeneous pores allow one phase to be injected into the other to form small liquid droplets. The second method employs a homogenizer or a high-speed mechanical stirrer to mix the oil and water phases to form droplets. [70] The reverse micellar process utilises a high concentration of surfactants able to form reverse micelles inside the oil phase and adsorb water in their inner core where the nanogel formation will take place. All these synthetic procedures include the employment of organic solvent or oil phases and surfactant to stabilise the emulsion droplets. These not only add complexity and higher cost to the synthetic environment but also introduce elements that may not be completely removed from the final product and therefore cause unpredictable effects both in terms of biocompatibility and physico-chemical properties of the nanogels.

Lastly, high dilution radical polymerisation, a homogenous phase approach, is probably the simplest method for the synthesis of nanogels. This is the technique that was chosen for this work and it is explained in more details in chapter 2.

Further feature of NGs include their suitability to be used in imprinting procedures. This technique utilises a template approach that can be divided into three key steps. Firstly, the functional monomer(s), through physical interactions, arrange themselves around a template molecule. Later this complex is cross-linked during a polymerisation process. Finally, the removal of the template from the polymeric matrix leaves a 3-D cavity complementary in terms of shape and functionality to a target analyte (substrate) [71, 72] (Figure 1.12).

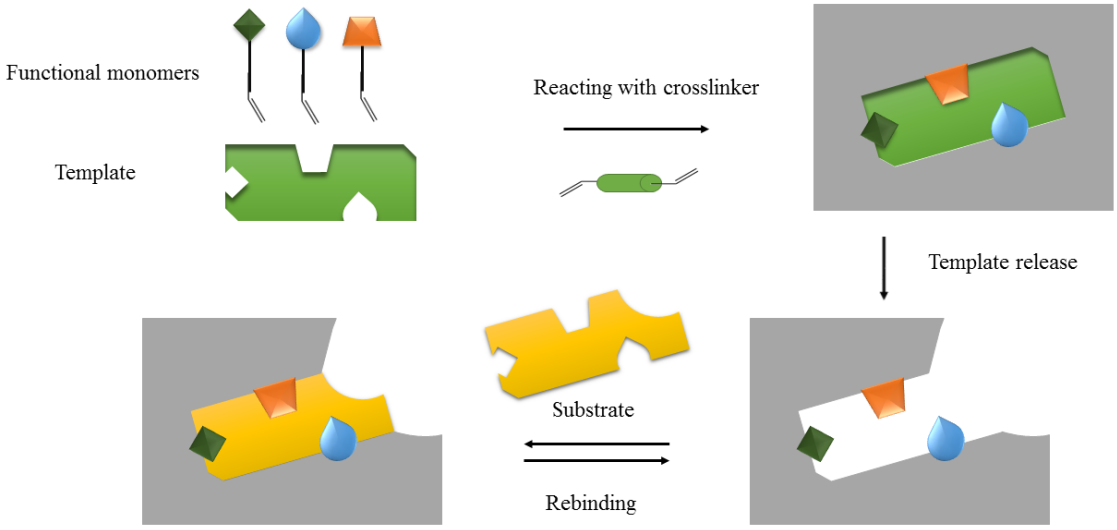

Fig. 1.12 Schematic representation of imprinting process.

Imprinting technology is currently studied and used for a wide range of applications such as sensors, catalyst, potential drug delivery system, for purification or isolation procedures etc. [73-75] The approach can be extremely beneficial for the development of DDS as imprinted nanogels can accommodate bioactive molecules in their drug complementary cavity with higher specificity than non-imprinted particles. Moreover, when considering the design of a multidrug formulations, the production of two or more highly specific and selective nanoparticles could allow avoidance of drug cross interaction, simultaneous drug administrations, improvement of patient compliance (due to reduced number of doses) and lowering the amount of excipients required.

NGs are extremely versatile materials [76] that can be used not only on their own but also as hybrid or composite. Plasmonic, magnetic and core shell nanogels are some of the main examples of hybrid and composites that combine properties of different

systems. Extensive works from Molina et al. and Maya et al. show the large number of current preparations employing nanogel technology [77, 78]. Below are reported some of the recent formulations deduced from the before mentioned reviews.

Drug loaded NGs	Characteristics	Cancer cells
Virus mimetic (VM) nanogel Doxorubicin-(poly(Lhistidine-co-phenylalanine) (poly(His32-co-Phe6))-PEG-BSA	pH-induced reversible swelling/deswelling of the core, enhanced Doxorubicin (Dox) release at the endosomal pH (6.4) and release reduced at cytosolic pH (6.8-7.4)	Human ovarian carcinoma (A2780)
Curcumin-chitin	Transdermal delivery of anticancer agents, excellent skin penetration and retention, cationic charged nanogels (CCNGs) interact with negatively charged skin lipids and interaction with hydrophobic moiety	Human melanoma (A375)
Doxorubicin-dextran-chitosan	Long circulating nanoparticles (NPs), enhanced regression in tumour volumes in vivo, 50% survival rate for 9 days and reduced toxicity compared to free drug	Macrophage tumour cells (J77A1)

Table 1.1 A selection of the nanogels under examination for the treatment of cancer. [78]

NGs	Cell imaging	Characteristics
Poly-N-isopropyl acrylamide (Nipam)-Gold NPs	Human cervical cancer cells (Hela)	Simultaneous optical temperature sensing, cell imaging and combined chemo-photothermal treatment. Superior Hela cells death when irradiated with 515nm laser
CdSe quantum dots (QD) hydroxypropylcellulose-poly acrylic acid (HPC-PPA)	Mouse melanoma (B16F10)	Dual temperature and pH responsive, emit at two different fluorescence wavelengths, combining a pHsensitive NIR emission (741 nm) and a less sensitive visible emission (592 nm)

Table 1.2 A selection of the nanogels for imaging purposes. [78]

Table 1.1 and 1.2 provide few examples of NGs currently under investigation while Table 1.3 (below) shows formulations already undergoing preclinical and clinical studies.

Phase	Hybrid NGs	Application
Preclinical	Plasmonic@NG	Cancer therapy
	Core-shell NGs	Neurodegenerative disorders
	Core-shell NGs	Treatment of acute pulmonary inflammation
	Cholesterol-bearing pullulan (CHP)-W9- peptide	Bone loss disorder
Clinical	CHP	Vaccines

Table 1.3 Hybrid nanogels in preclinical and clinical phase [77]

The main reasons for the versatility of nanogels are: 1) the wide spectrum of materials that can be used for their preparation, ranging from synthetic biopolymers such as hyaluronic acid or chitosan to vinyl polymers like poly-acrylamides or poly-methacrylates [78-82] 2) the possibility of tuning their properties (such as size or rigidity) by modifying the percentages of building blocks and synthetic conditions.

Natural monomers and polymers are usually employed for their faster biodegradability while synthetic monomers and polymers, in particular vinyl compounds, should be preferred when higher stability is required.

The work herein presented focused on the development of a novel methacrylate based nanogels for drug delivery purposes. For this reason, a brief introduction on methacrylates and their characteristics is reported in the following section.

1.3 Methacrylates

1.3.1 Current uses and applications

Methacrylates are ester derivatives of metacrylic acid (Figure 1.13) and are commonly used in the production of polymer plastics.

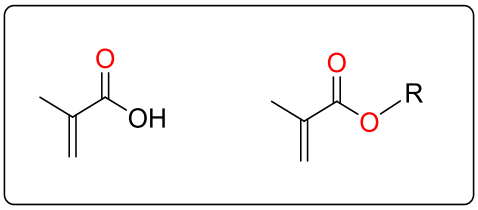

Fig. 1.13 Methacrylic acid left and methacrylate right

Methacrylic acid was first obtained in 1865 by E. Frankland [83] while its first polymeric form was discovered in 1880 by F. Engelhorn. [84]

Polymethylmethacrylate (known as acrylic glass) is probably the most diffused and used methacrylate polymer. Plexiglas, Perspex and Lucite are some of its commercial names. Its development is dated 1901 and credited to the German chemist O. Röhm who in 1933, together with Walter Bauer, branded the polymer as Plexiglas which was first sold by the Rohm and Hass. [85, 86] Since then it has been used in numerous applications such as protection glass, for orthopaedics, material for contact lenses, electrochemical chip supports etc. [87-89]

A number of methacrylate based polymers are currently employed or under development, offering a wide range of materials with diverse characteristics and applications. Methacrylate based polymers are in fact used for the production of platform for antibodies immobilisation, molecular imprinted matrixes for filtration cartridges, antibacterial coating materials, molecularly imprinted sensor for food chemistry, hydrophobic fabrics, nanoparticles for drug delivery and nanogels just to name few. [90-96] Moreover methacryaltes are often used in combination with preformed materials as coating or functionalising agents. [97-99]

1.3.2 Methacrylates structure, properties and biological uses

Methacrylates are optimal tuneable materials in terms of polarity, due to the modifiable ester group which can lead to formation of systems ranging from highly hydrophobic to highly hydrophilic. Also their size and steric interactions can vary according to the length, arrangement and chemical composition of the ester chain (Figure 1.14).

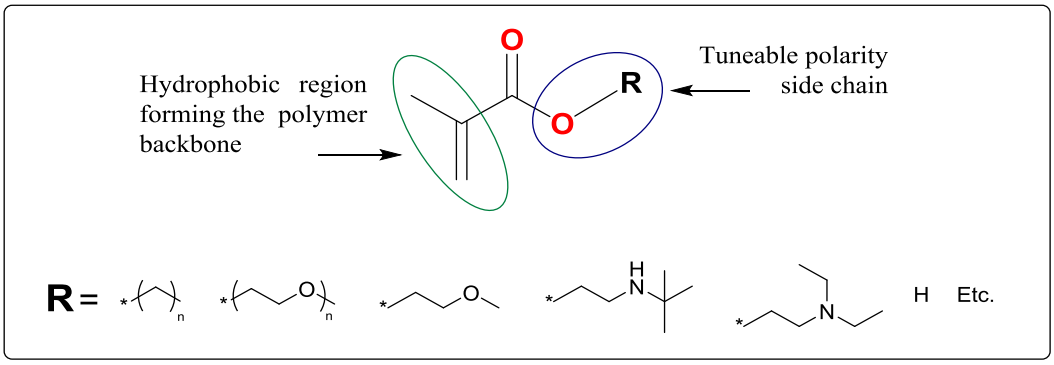

Fig. 1.14 Basic chemical structure of methacrylates and few examples of ester chains.

Furthermore, by modifying the ester group, the resulting material can gain numerous physical-chemical characteristics including the ability to respond to stimuli such as pH or temperature, solubility improvements or decrement, surface tension reduction or emulsion formation capabilities. [100-103] The latest characteristic deserves a particular mention as the nanogels object of this study have been found to be able to form Pickering-Ramsden emulsions. Those are emulsions stabilised by nanoparticles rather than surfactants and they are introduced and further discussed in chapter 3. Due to the tuneable characteristics and the vast library of chemical structures, methacrylates are widely employed materials for the development of drug delivery systems and for other biological applications. Works in the literature report on numerous methacrylate particles and polymers developed for the treatment of cancer, as antimicrobial systems, as drug release modulator coating polymers such as EUDRAGIT ® and as dental or bone materials, just to name few of the various biological applications involving methacrylates. [100, 104-112]

EUDRAGIT® in particular, deserves a more in depth mention due to its large use in the pharmaceutical industry and for its chemical structure similarity to the nanogels object

of this study. [113-116] A number of ester copolymers of methacrylic and acrylic acid are commercialised under the name of EUDRAGIT® (Figure 1.15). [113, 116]

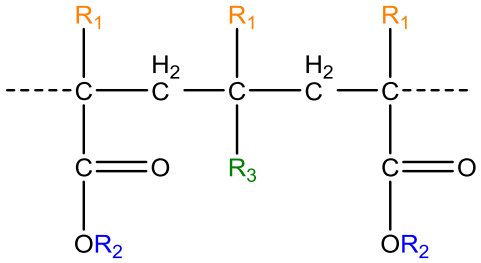

R_1= -CH_3, -H; R_2= -CH_3, -CH_2CH_3; R_3= -COOH Eudragit L and S

R_1= -CH_3, -H; R_2= -CH_3, -CH_2CH_3; R_3= -$COOCH_2CH_2N(CH_3)_3Cl$ Eudragit RL and RS

R_1= -CH_3, -H; R_2= -CH_3, -CH_2CH_3; R_3= -$COOCH_3$ Eudragit NE

Fig. 1.15 Structures of main Eudragit polymers

Eudragits are non toxic, non adsorbable and non biodegradable polymer which can dissolve or increase their porosity at various pH ranges according to their chemical structures. Because of their pH responsiveness they are often used as coating agent in pharmaceutical formulations in order to gain sustained release. [113]

However, Eudragit cannot be directly compared to methacrylate based nanogels as its structure is linear and not cross-linked. Therefore, Eudragit does not have the capacity to incorporate molecules, such as conventional nanoparticles, but simply coat them. Eudragit is in fact used as an eccipient, coating agent or co-polymer. [114, 115, 117; 118]

In conclusion the great potential offered by nanomaterials, in particular nanogels, combined with the adjustable properties of methacrylates were the leading forces that triggered the development of the novel methacrylate based nanogels object of this study.

Before starting the description of the chemical and biological characteristics of the nanogels, a brief introduction of the aims and objectives of this work are given in the following section.

1.4 Aims and Objectives

The aim of this project was the synthesis of a novel methacrylate based nanogel characterised by reduced size, high biocompatibility and stimuli response capabilities for drug delivery application, in particular targeting the skin.

The work reported in this thesis was focused on three main objectives:

1. Synthesis and characterisation of the nanogels.
2. *In vitro* toxicity and cell metabolism studies.
3. Preliminary testing of drug upload and release.

Each of the objectives is covered in a dedicated chapter. Here below a short outline of the content of each chapter is given.

Chapter II covers the production and characterisation of novel polymeric NPs via high dilution radical polymerisation, the initial screening of different monomers, reaction conditions and monomers/cross-linker ratios. The numerous polymerisations were performed in order to identify best formulation in terms of solubility, size, shape and stimuli response. The incorporation of elsewhere synthesised fluorescent probe was also carried out in the view of potential *in vitro and ex vivo* monitoring of nanoparticles. Particle size was assessed both via dynamic light scattering (DLS) and transmission electron microscopy (TEM). This part of the project has been carried out at the School of Biological and Chemical Sciences, Queen Mary University of London, under the direct supervision of Prof. Marina Resmini. Dr. Giulia Mastroianni has to be acknowledged for TEM imaging.

In chapter III the nanogel ability to form Pickering-Ramsden emulsions and their stimuli responsiveness were investigated. This part of the project has been carried out at the School of Biological and Chemical Sciences, Queen Mary University of London, under the direct supervision of Prof. Marina Resmini. Chapter IV focuses on the biological experiments in order to assess biocompatibility of the nanomaterial produced. Different cell lines were employed to test cytotoxicity, cellular morphological modification and adenosine triphosphate (ATP) cellular levels. This work was carried out in collaboration with Dr. Lino Ferreira, Ms Michela Comune and Ms Josephine Blersch at Biocant Technological Park, Cantanhede, Portugal.

In chapter V, preliminary data of drug encapsulation and release are discussed. This chapter is divided in two parts the first regards the incorporation and release of macromolecules of biological relevance such as siRNA, the second instead treats the incorporation of small conventional anti-inflammatory drugs such as fenoprofen. The first part of this study was carried out in collaboration with Dr. Lino Ferreira, Miss Michela Comune and Ms. Josephine Blersch at Biocant Technological Park, Cantanhede, Portugal. The second part was carried out at the School of Biological and Chemical Sciences, Queen Mary University of London, under the direct supervision of Prof. Marina Resmini.

A brief introduction is given for each chapter in order to place the work into context and facilitate the reading.

Two additional chapters are also part of this thesis: chapter VI that includes all the experimental procedure details and chapter VII where conclusion and future works are reported.

Images references

a) **1.3** R. A. Yokel; R. C. MacPhail. Engineered nanomaterials: exposures, hazards, and risk prevention. *J. Occup. Med. Toxicol.*, **2011**, 6, 1-27. (OPEN ACCESS).

b) **1.4** Lehninger, D. Nelson; M. Cox. Principles of biochemistry, 2nd edition. *Worth Publishers,* Inc., New York, John Wiley and Sons, **1992**, 1012 pages. **License Number:** 3937580045115.

c) **1.5** S.-H. Kim, E.-M. Kim, C.-M. Lee, D. W. Kim, S. T. Lim, M.-H. Sohn; H.-J. Jeong. Synthesis of PEG-Iodine-Capped Gold Nanoparticles and Their Contrast Enhancement in Vitro and in Vivo for X-Ray/CT. *J. Nanomater.,* **2012**, Article ID 504026, 9 pages. (OPEN ACCESS).

d) **1.7** D. Bitounis, R. Fanciullino, A. Iliadis; J. Ciccolini, Optimizing Druggability through Liposomal Formulations: New Approaches to an Old Concept. *ISRN Pharmaceutics,* **2012**, Article ID 738432, 11 pages, 2012. doi:10.5402/2012/738432 (OPEN ACCESS).

e) **1.8** J. Zhang, K. Liu, K. Müllen; M. Yin. Self-assemblies of amphiphilic homopolymers: synthesis, morphology studies and biomedical applications. *Chem. Commun*., **2015**, 51, 11541-11555. **License Number:** 3991880626562.

f) **1.9** M. Sowinska; Z. Urbanczyk-Lipkowska. Advances in the chemistry of dendrimers. *New J.Chem.,* **2014**, 38, 2168-2203. **License Number:** 3934721385025.

g) **1.11** G. Acharya, C. S. Shin, M. McDermott, H. Mishra, H. Park, I. C. Kwon; K. Park. The hydrogel template method for fabrication of homogeneous nano/microparticles. *J. Control. Release,* **2010**, 141, 314-319. **License Number:** 3937560904561.

References

1. R. Ng. Appendix I: history of drug discovery and development. From "Drugs: From Discovery to Approval, Second Edition". *Wiley-Blackwell,* **2008**.
2. J. Drews. Drug Discovery: A Historical Perspective. *Science*, **2000**, 287, 1960-1964.
3. N. A. Peppas. Historical perspective on advanced drug delivery: How engineering design and mathematical modeling helped the field mature. *Adv. Drug Deliver. Rev.*, **2013**, 65, 5-9.
4. A. S. Hoffman. The origins and evolution of "controlled" drug delivery systems. *J. Control. Release*, **2008**, 132, 153-163.
5. K. Fosgerau; T. Hoffmann. Peptide therapeutics: current status and future directions. *Drug Discov. Today,* **2015**, 20, 122-128.
6. J. Shaji; V. Patole. Protein and Peptide Drug Delivery: Oral Approaches. *Indian J Pharm Sci.,* **2008**, 70, 269–277.
7. G. Tiwari, R. Tiwari, B. Sriwastawa1, L Bhati2, S Pandey, P Pandey, S. K Bannerjee. Drug delivery systems: An updated review. *Int. J. Pharm. Investig.,* **2012**, 2, 2-11.
8. T. M. Allen; P. R. Cullis. Drug Delivery Systems: Entering the Mainstream. *Science,* **2004**, 303, 1818-1822
9. K.P. S. Kumar, D. Bhowmik, S. Srivastava, S. Paswan; A.S. Dutta. Sustained Release Drug Delivery System Potential. *The Pharma Innovation*, **2012,** 1(2), 48-60.
10. K. M. Huttunen, H. Raunio, J. Rautio. Prodrugs-from Serendipity to Rational Design. *Pharmacol. Rev.,* **2011**, 63, 750-771.
11. P. Verma, A.S. Thakur, K. Deshmukh, Dr. A.K. Jha; S. Verma. ROUTES OF DRUG ADMINISTRATION. *I.J.P.R.S.*, **2010**, 1, 54-59
12. N. R. Labiris; M. B. Dolovich. Pulmonary drug delivery. Part I: Physiological factors affecting therapeutic effectiveness of aerosolized medications. *Br. J. Clin. Pharmacol.* **2003**, 56, 588-599.
13. J. S. Patil, S. Sarasija. Pulmonary drug delivery strategies: A concise, systematic review. *Lung India*, **2012**, 29, 44-49.
14. Pooja Abhang, Munira Momin, Mayur Inamdar; Swapan Kar. Transmucosal Drug Delivery- An Overview. *Drug Deliv. Letters*, **2014**, 4, 26-37.
15. Mark R. Prausnitz; Robert Langer. Transdermal drug delivery. *Nat. Biotechnol*., **2008**, 26, 1261-1268.
16. www.researchandmarkets.com Global Nanotechnology Market Outlook 2022. RNCOS E-Services Private Limited, Report ID: 3512791, **2015.**
17. S. S. Dewan et al. www.bccresearch.com Global Markets and Technologies for Advanced Drug Delivery Systems. Report Code: PHM006J, **2014**.
18. www.researchandmarkets.com Global Nanomedicine Market & Pipeline Insight 2015. Report ID 3160605, **2015.**

19. T. Theis, D. Parr, P. Binks, J. Ying, K. E. Drexler, E. Schepers, K. Mullis, C. Bai, J. J. Boland, R. Langer, P. Dobson, C. N. R. Rao; M. Ferrari. Nan´o·tech·nol´o·gy n. *Nature Nanotechnology*, **2006**, 1, 8-10
20. M. L. Etheridge, S. A. Campbell, A. G. Erdman, C. L. Haynes, S. M. Wolf, J. McCullough. The big picture on nanomedicine: the state of investigational and approved nanomedicine products. *Nanomed-Nanotechnol,* **2013**, 9, 1-14.
21. Q. Chaudhry; L. Castle. Food applications of nanotechnologies: An overview of opportunities and challenges for developing countries. *Trends Food Sci. Tech.,* **2011**, 22, 595-603.
22. D. K. Kim, Y. Lai, B. T. Diroll, C. B. Murray; C. R. Kagan. Flexible and low-voltage integrated circuits constructed from high-performance nanocrystal transistors. *Nat. Commun.,* **2012**, 3:1216 doi: 10.1038/ncomms2218.
23. O. Neumann, A. S. Urban, J. Day, S. Lal, P. Nordlander; N. J. Halas. Solar Vapor Generation Enabled by Nanoparticles. *ACS Nano*, **2013**, *7* (1), 42–49.
24. V. Morigi, A. Tocchio, C. B. Pellegrini, J. H. Sakamoto, M. Arnone; E. Tasciotti. Nanotechnology in Medicine: From Inception to Market Domination. *J. Drug Deliv.*, **2012**, 1-7.
25. E. Roduner. Size matters: why nanomaterials are different. *Chem. Soc. Rev.*, **2006**, 35, 583-592.
26. M. A. Hamburg. Paving the Way for Personalized Medicine. *FDA report,* **2013**, 1-61.
27. S. M. Moghimi, A. C. Hunter; J. Clifford Murray. Nanomedicine: current status and future prospects. *FASEB J.,* **2005**, 19, 311-330.
28. R. L. Juliano. The future of nanomedicine: Promises and limitations. *Science and Public Policy*, **2012**, 39, 99-104.
29. A. Baun; S. F. Hansen. Environmental Challenges for Nanomedicine. *Nanomedicine,* **2008**, 5, 605-608.
30. P. J. A. Borm, D. Robbins, S. Haubold, T. Kuhlbusch, H. Fissan, K. Donaldson, R. Schins, V. Stone, W. Kreyling, J. Lademann, J. Krutmann, D. Warheit; E. Oberdorster. The potential risks of nanomaterials: a review carried out for ECETOC. *Particle and Fibre Toxicology*, **2006**, 3(11).
31. Annual report from the SME Office – 2014. EMA/699351/2014, **2015.**
32. V. Weissig, T. K. Pettinger; N. Murdock. Nanopharmaceuticals (part 1): products on the market. *Int. J. Nanomed.*, **2014**, 9, 4357-4373.
33. V. Weissig; D. Guzman-Villanueva. Nanopharmaceuticals (part 2): products in the pipeline. *Int. J. Nanomed.,* **2015**, 10, 1245-1257.
34. K. Park. Controlled drug delivery systems: Past forward and future back. *J. Control. Release*, **2014**, 190, 3-8.
35. I. I. Slowing; J. L. Vivero-Escoto, C.-W. Wu; V. S.-Y. Lin. Mesoporous silica nanoparticles as controlled release drug delivery and gene transfection carriers. *Adv. Drug Deliver. Rev.,* **2008**, 60, 1278-1288
36. S. Kwon, R. K. Singh, R. A. Perez, E. A. Abou Neel, H.-W. Kim; W. Chrzanowski. Silica-based mesoporous nanoparticles for controlled drug delivery. *J. Tissue Eng.,* **2013**, 4, 1-18.

37. I. Passagne, M. Morille, M. Rousset, I. Pujalté; B. L'Azou. Implication of oxidative stress in size-dependent toxicity of silica nanoparticles in kidney cells. *Toxicology*, **2012**, 299, 112-124.
38. E. C. Dreaden, A. M. Alkilany, X. Huang, C. J. Murphy; M. A. El-Sayed. The golden age: gold nanoparticles for biomedicine. *Chem. Soc. Rev.*, **2012**, 41, 2740-2779.
39. N. Lewinski, V. Colvin; R. Drezek. Cytotoxicity of Nanoparticles. *Small*, **2008**, 4, 1, 26-49.
40. A.H. Faraji; P. Wipf. Nanoparticles in cellular drug delivery. *Bioorgan. Med. Chem.*, **2009**, 17, 2950-2962.
41. K. A. Edwards; A. J. Baeumner. Analysis of liposomes. *Talanta* **2006**, 68, 1432–1441
42. S. S. Chrai, R.Murari; I. Ahmad. Liposomes: A review--part 1: Manufacturing issues. *BioPharm*, **2001** 14(11), 10-14
43. S. S. Chrai, R.Murari; I. Ahmad. Liposomes: A review--part 2: Drug Delivery Systems. *BioPharm*, **2002,** 15, 40-43, 49.
44. A. A. Gabizon, H. Shmeeda; A. Zalipsky. Pros and Cons of the Liposome Platform in Cancer Drug Targeting. *J. Liposome Res.*, **2006,** 16, 175-183.
45. O. S. Muddineti, B. Ghosh; S. Biswas. Current trends in using polymer coated gold nanoparticles for cancer therapy. *Int. J. Pharm.*, **2015**, 484, 252-267.
46. S. Bhattacharyya, H. Wang; P. Ducheyne. Polymer-coated mesoporous silica nanoparticles for the controlled release of macromolecules. *Acta Biomater.*, **2012**, 8, 3429-3435.
47. Kf C. Oerlemans, W. Bult, M. Bos, G. Storm, J. F. W. Nijsen; W. E. Hennink. Polymeric Micelles in Anticancer Therapy: Targeting, Imaging and Triggered Release. *Pharm, Res.*, **2010**, 27, 2569–2589.
48. K. Letchford; H. Burt. A review of the formation and classification of amphiphilic block copolymer nanoparticulate structures: micelles, nanospheres, nanocapsules and polymersomes. *Eur. J. Pharm. Biopharm.*, **2007**, 65, 259-269.
49. V. P. Torchilin. Micellar Nanocarriers: Pharmaceutical Perspectives. *Pharm. Res.*, **2007**, 24, 1-16.
50. G. Dikmen, L. Genç; G. Güney. Advantage and Disadvantage in Drug Delivery Systems. *J. Mat.s Sci. Eng.*, **2011**, 5, 468-472.
51. M. Yokoyama. Clinical Applications of Polymeric Micelle Carrier Systems in Chemotherapy and Image Diagnosis of Solid Tumors. *J. Exp. Clin. Med.*, **2011**, 3, 4, 151-158.
52. N. Nishiyama; K. Kataoka. Current state, achievements, and future prospects of polymeric micelles as nanocarriers for drug and gene delivery. *Pharmacol. Ther.*, **2006**, 112 630-648.
53. J. Hu, S. Miura, K. Na; Y. H. Bae. pH-responsive and charge shielded cationic micelle of poly(L-histidine)-block-short branched PEI for acidic cancer treatment. *J. Control. Release*, **2013**, 172, 69-76.
54. W. Chen, Y. Cheng; B. Wang. Dual-Responsive Boronate Crosslinked Micelles for Targeted Drug Delivery. *Angew. Chem. Int. Ed.*, **2012**, 51, 5293- 5295.

55. E. Abbasi, S. F. Aval, A. Akbarzadeh, M. Milani, H. T. Nasrabadi, S. W. Joo, Y. Hanifehpour, K. Nejati-Koshki; R. Pashaei-Asl. Dendrimers: synthesis, applications, and properties. *Nanoscale Res. Lett.*, **2014**, 9:247.
56. M. Sowinska; Z. Urbanczyk-Lipkowska. Advances in the chemistry of dendrimers. *New J.Chem.*, **2014**, 38, 2168-2203.
57. S. Vinogradov, E. Batrakova; A. Kabanov. Poly(ethylene glycol)–polyethyleneimine NanoGel™ particles: novel drug delivery systems for antisense oligonucleotides. *Colloids and Surfaces B: Biointerfaces*, **1999**, 16, 291-304
58. A. V. Kabanov; S. V. Vinogradov. Nanogels as Pharmaceutical Carriers: Finite Networks of Infinite Capabilities. *Angew. Chem. Int. Ed*., **2009**, 48, 5418-5429.
59. S. V. Vinogradov, T. K. Bronich; A. V. Kabanov. Nanosized cationic hydrogels for drug delivery: preparation, properties and interactions with cells. *Adv. Drug Deliver. Rev.*, **2002**, 54, 135–147.
60. H. Zhang, Y. Zhai, J. Wang; G. Zhai. New progress and prospects: The application of nanogel in drug delivery. *Mater. Sci. Eng.*, **2016**, 60, 560-567.
61. T. Hoarea, S. Young, M. W. Lawlor; D. S. Kohanec. Thermoresponsive nanogels for prolonged duration local anesthesia. *Acta Biomaterialia* **2012**, 8, 3596-3605.
62. R. T. Chacko, J. Ventura, J. Zhuang; S. Thayumanavan. Polymer nanogels: A versatile nanoscopic drug delivery platform. *Adv. Drug Deliver. Rev.*, **2012**, 64, 836–851.
63. P. Bonomi, A. Servant, M. Resmini. Modulation of imprinting efficiency in nanogels with catalytic activity in the Kemp elimination. *J. Mol. Recognit*., **2012**, 25, 352-360.
64. G. Soni; K. S. Yadav. Nanogels as potential nanomedicine carrier for treatment of cancer: A mini review of the state of the art. *Saudi Med. J.*, **2014**, doi:10.1016/j.jsps.2014.04.001
65. F. Sultana, Manirujjaman, Md. Imran-Ul-Haque, M. Arafat; S. Sharmin. An Overview of Nanogel Drug Delivery System. *J. Appl. Pharm. Sci.*, **2013**, 3, 95-105.
66. J. K. Oha, R. Drumright, D. J. Siegwartb; K. Matyjaszewski. The development of microgels/nanogels for drug delivery applications. *Prog. Polym. Sci.*, **2008**, 33, 448–477.
67. Sodium dodecyl sulfate. Safety Data Sheet (MSDS). Sigma Aldrich **2015**.
68. N. Singh; L. A. Lyon. Synthesis of multifunctional nanogels using a protected macromonomer approach. *Colloid. Polym. Sci.* **2008**, 286, 1061-1069.
69. M. Giulbudagian, M. Asadian-Birjand, D. Steinhilber, K. Achazi, M. Molina; M. Calderón. Fabrication of thermoresponsive nanogels by thermo-nanoprecipitation and in situ encapsulation of bioactives. *Polym. Chem.*, **2014**, 5, 6909–6913.
70. S. B. Sengel; N. Sahiner. Poly(vinyl phosphonic acid) nanogels with tailored properties and their use for biomedical and environmental applications. *Eur. Polym. J.*, **2016**, 75, 264-275

71. F. Mirata; M. Resmini. Molecularly Imprinted Polymers for Catalysis and Synthesis. *Advances in Biochemical Engineering/Biotechnology*, **2015**, 107-129.
72. M. Resmini. Molecularly imprinted polymers as biomimetic catalysts. *Anal. Bioanal. Chem.*, **2012**, 402, 3021-3026.
73. P. Ski. Molecularly imprinted polymers as the future drug delivery devices. *Acta Poloniae Pharmaceutica -Drug Research*, 70, **2013**, 4, 601-609.
74. A. Gültekin, G. Karanfil, S. Sönmezoğlu; R. Say. Development of a highly sensitive MIP based-QCM nanosensor for selective determination of cholic acid level in body fluids. *Mater. Sci. Eng. C*, **2014**, 42, 436-442.
75. R. Schirhagl. Bioapplications for Molecularly Imprinted Polymers. *Anal. Chem*., **2014**, 86, 250-261.
76. R. Yoshida; T. Okano. Stimuli-Responsive Hydrogels and their application to functional materilas. *Biomedical Applications of Hydrogels Handbook*, **2010**, 19-43.
77. M. Molina, M. Asadian-Birjand, J. Balach, J. Bergueiro, E. Miceliac; M. Caldero´. Stimuli-responsive nanogel composites and their application in nanomedicine. *Chem. Soc. Rev.*, **2015**, 44, 6161-6186.
78. S. Maya, B. Sarmento, A. Nair, N. S. Rejinold, S. V. Nair; R. Jayakumara. Smart Stimuli Sensitive Nanogels in Cancer Drug Delivery and Imaging: A Review. *Curr. Pharm. Design*, **2013**, *19*, 7203-7218.
79. F. Brunel, L. Véron, C. Ladaviere, L. David, A. Domard; T. Delair. Synthesis and Structural Characterization of Chitosan Nanogels. *Langmuir*, **2009**, 25(16), 8935-8943.
80. C. Yang, X. Wang, X. Yao, Y. Zhang, W. Wu; X. Jiang. Hyaluronic acid nanogels with enzyme-sensitive cross-linking group for drug delivery. *J. Control. Release*, **2015**, 205, 206-217.
81. L. Wu, H. Zhou, H.-J. Sun, Y. Zhao, X. Yang, S. Z. D. Cheng; G. Yang. Thermoresponsive Bacterial Cellulose Whisker/Poly(NIPAM-co-BMA) Nanogel Complexes: Synthesis, Characterization, and Biological Evaluation. *Biomacromolecules*, **2013**, 14, 1078-1084.
82. Y. Tian, S. Bian; Wuli Yang. A redox-labile poly(oligo(ethylene glycol) methacrylate)-based nanogel with tunable thermosensitivity for drug delivery. *Polym. Chem*., **2016**, 7, 1913-1921.
83. E. Frankland. *Ann.*, **1865**, 136, 12.
84. F. Engelhorn et al. *Ann.*, **1880**, 200, 70.
85. J. Schwartz. The Right Chemistry: 108 Enlightening, Nutritious, Health-Conscious and Occasionally Bizarre Inquiries into the Science of Daily Life. **2012.**
86. Evonik industries. www.evonik.com. Plexiglas, Polymers for a clear, transparent view. 02/05/2016.
87. P. F. Holmes, M. Bohrer; J. Kohn. Exploration of polymethacrylate structure-property correlations: Advances towards combinatorial and high-throughput methods for biomaterials discovery. *Prog Polym Sci*., **2008**, 33(8), 787-796.

88. M. Arora, E. K. S. Chan, S. Gupta; A. D. Diwan. Polymethylmethacrylate bone cements and additives: A review of the literature. *World J. Orthop.,* **2013**, 4(2), 67-74.
89. J. Liu, L. Wang, W. Ouyang, W. Wang, J. Qin, Z. Xu, S. Xu, D. Ge, L. Wang, C. Liu; L. Wang. Fabrication of PMMA nanofluidic electrochemical chips with integrated microelectrodes. *Biosens. Bioelectron.,* **2015**, 72, 288-293.
90. Samira Hosseini, F. Ibrahim, H. A. Rothan, R. Yusof, C. van der Marel, I. Djordjevic; L. H. Koole. Aging effect and antibody immobilization on COOH exposed surfaces designed for dengue virus detection. *Biochem. Eng. J.,* **2015**, 99, 183-192.
91. M. E. Çorman, C. Armutcu, S. Özkara, L. Uzun; A. Denizli Molecularly imprinted cryogel cartridges for the specific filtration and rapid separation of interferon alpha. *RSC Adv.,* **2015**, 5, 45015-45026.
92. B. L. Wang, T. W. Jin, Y. M. Han, C. H. Shen, Q. Li, Q. K. Linab; H. Chen. Bio-inspired terpolymers containing dopamine, cations and MPC: a versatile platform to construct a recycle antibacterial and antifouling surface. *J. Mater. Chem. B,* **2015**, 3, 5501-5510.
93. T. Eren, N. Atar, M. L. Yola; H. Karimi-Maleh. A sensitive molecularly imprinted polymer based quartz crystal microbalance nanosensor for selective determination of lovastatin in red yeast rice. *Food Chem.,* **2015**, 185, 430-436.
94. M. Rabnawaz, Z. Wang, Y. Wang, I. Wyman, H. Hu; G. Liu. Synthesis of poly(dimethylsiloxane)-block-poly[3-(triisopropyloxysilyl) propyl methacrylate] and its use in the facile coating of hydrophilically patterned superhydrophobic fabrics. *RSC Adv.,* **2015**, 5, 39505-39511.
95. A. Jäger, E. Jäger, F. Surman, A. Höcherl, B. Angelov, K. Ulbrich, M. Drechsler, V. M. Garamus, C. Rodriguez-Emmenegger, F. Nalletd; P. Štěpáneka. Nanoparticles of the poly([N-(2hydroxypropyl)]-methacrylamide)-b-poly[2-(diisopropylamino)ethyl methacrylate] diblock copolymer for pH-triggered release of paclitaxel. *Polym. Chem.,* **2015**, 6, 4946-4954.
96. X. T. Cao, A. M. Showkat; K. T. Lim. Synthesis of nanogels of poly(e-caprolactone)-b-poly (glycidyl methacrylate) by click chemistry in direct preparation. *Eur. Polym. J.,* **2015**, 68, 267-277
97. F. Zhang, S. Yu, G. Hou, N. Xu, Z. Wu; L. Yue. Miniemulsion-based assembly of iron oxide nanoparticles and synthesis of magnetic polymer nanospheres. *Colloid. Polym. Sci.,* **2015**, 293:1893-1902.
98. F. Jiang, Y. Zhang, Z. Wang, W. Wang, Z. Xu; Z. Wang. Combination of Magnetic and Enhanced Mechanical Properties for Copolymer-Grafted Magnetite Composite Thermoplastic Elastomers. *ACS Appl. Mater. Interfaces,* **2015**, 7, 10563-10575.
99. H. Hemmatpour, V. Haddadi-Asl; H. Roghani-Mamaqani. Synthesis of pH-sensitive poly (N,N-dimethylaminoethyl methacrylate)-grafted halloysite nanotubes for adsorption and controlled release of DPH and DS drugs. *Polymer,* **2015**, 65, 143-153.

100. A. J. Morse, S. P. Armes, K. L. Thompson, D. Dupin, L. A. Fielding, P. Mills; R. Swart. Novel Pickering Emulsifiers based on pH-Responsive Poly(2-(diethylamino)ethyl methacrylate) Latexes. *Langmuir*, **2013**, 29, 5466-5475.
101. A. J. Morse, J. Madsen, D. J. Growney, S. P. Armes, P. Mills; R. Swart. Microgel Colloidosomes Based on pH-Responsive Poly(tert-butylaminoethyl methacrylate) Latexes. *Langmuir*, **2014**, 30, 12509-12519.
102. A. J. Morse, S. P. Armes, P. Mills; R. Swart. Stopped-Flow Kinetics of pH-Responsive Polyamine Latexes: How Fast Is the Latex-to-Microgel Transition? *Langmuir*, **2013**, 29, 15209-15216.
103. S. Yusa, M. Sugahara, T. Endo; Y. Morishima. Preparation and Characterization of a pH-Responsive Nanogel Based on a Photo-Cross-Linked Micelle Formed from Block Copolymers with Controlled Structure. *Langmuir*, **2009**, 25(9), 5258-5265.
104. Y. Li, B. Xu, T. Bai; W. Liu. Co-delivery of doxorubicin and tumor-suppressing p53 gene using a POSS-based star-shaped polymer for cancer therapy. *Biomaterials*, **2015**, 55, 12-23.
105. A. Kumar, S. V. Lale, S. Mahajan, V. Choudhary; V. Koul. ROP and ATRP Fabricated Dual Targeted Redox Sensitive Polymersomes Based on pPEGMA-PCL-ss-PCL-pPEGMA Triblock Copolymers for Breast Cancer Therapeutics. *ACS Appl. Mater., Interfaces*, **2015**, 7, 9211-9227.
106. L. Deng, J. Ren, J. Li, J. Leng, Y. Qu, C. Linc; D. Shic. Magnetothermally responsive star-block copolymeric micelles for controlled drug delivery and enhanced thermo-chemotherapy. *Nanoscale*, **2015**, 7, 9655-9663.
107. J. An, Q. Luo, M. Li, D. Wang, X. Li; R. Yin. A facile synthesis of high antibacterial polymer nanocomposite containing uniformly dispersed silver nanoparticles. *Colloid, Polym. Sci.*, **2015**, 293, 1997-2008.
108. H. Zuo, D. Wu; R. Fu. Preparation of Antibacterial Poly(methyl methacrylate) by Solution Blending with Water-Insoluble Antibacterial Agent Poly[(tert-buty1amino) ethyl methacrylate]. *J. Appl. Polym. Sci.*, **2012**, 125, 3537-3544.
109. K. P. Seremeta, D. A. Chiappetta; A. Sosnik. Poly(-caprolactone), Eudragit® RS 100 and poly(-caprolactone)/Eudragit® RS 100 blend submicron particles for the sustained release of the antiretroviral efavirenz. *Colloid. Surface. B*, **2013**, 102, 441-449
110. R. I. Moustafine, I. M. Zaharov; V. A. Kemenova. Physicochemical characterization and drug release properties of Eudragitw E PO/Eudragitw L 100-55 interpolyelectrolyte complexes. *Eur. J. Pharm. Biopharm.*, **2006**, 63, 26-36.
111. L. Cheng, M. D. Weir, H. H. K. Xu, J. M. Antonuccie, A. M. Kraigsleye, N. J. Line, S. Lin-Gibson; X. Zhou. Antibacterial amorphous calcium phosphate nanocomposites with a quaternary ammonium dimethacrylate and silver nanoparticles. *Dent. Mater.*, **2012**, 28, 561-572.

112. Z. Liu, Y. Tang, T. Kang, M. Rao, K. Li, Q. Wang, C. Quan, C. Zhang, Q. Jiang; H. Shen. Synergistic effect of HA and BMP-2 mimicking peptide on the bioactivity of HA/PMMA bone cement *Colloid. Surface. B,* **2015**, 131, 39-46.
113. S. Thakral, N. K. Thakral; D. K. Majumdar. Eudragit®: a technology evaluation. *Expert. Opin. Drug Deliv.,* **2013**, 10, 131-149.
114. M. Z. I. Khan, Z. Prebeg; N. Kurjakovic. A pH-dependent colon targeted oral drug delivery system using methacrylic acid copolymers I. Manipulation of drug release using Eudragit® L100-55 and Eudragit® S100 combinations. *J. Control. Release,* **1999**, 58, 215-222.
115. S. Haznedar; B. Dortunç. Preparation and in vitro evaluation of Eudragit microspheres containing acetazolamide. *Int. J. Pharm.,* **2004**, 269, 13-140.
116. EUDRAGIT ® Brouchure. Evonik industries. http://healthcare.evonik.com/product/health-care/en/products/pharmaceutical-excipients/EUDRAGIT/Pages/default.aspx
117. R. Pignatello, C. Bucolo, P. Ferrara, A. Maltese, A. Puleo; G. Puglisi. E udragit RS100® nanosuspensions for the ophthalmic controlled delivery of ibuprofen. *Eur. J. Pharm. Sci.,* **2002**, 16, 53-61.
118. B. Mukherjee, S. Mahapatra, R. Gupta, B. Patra, A. Tiwari; P. Arora. A comparison between povidone-ethylcellulose and povidone-eudragit transdermal dexamethasone matrix patches based on in vitro skin permeation. *Eur. J. Pharm. Biopharm.,* **2005**, 59, 475-483.

Chapter II: Results and discussion (materials)

2.1 Nanogel preparation

Nanogels (NGs), were selected as the matrix for the development of a novel drug delivery system. They offer several advantages as described in section 1.2.3 and can be employed for the tailored release of bioactive compounds throughout several routes of administration [1-3], however the focus of this work was transdermal delivery. Certain properties have to be considered when using skin as a route of administration. Several are the features (deformability, charge, toxicity etc.) that play a role in skin penetration however size and partition coefficient are perhaps the most important [4-5]. Due to the tight junction of the stratum corneum (the outermost layer of skin) and its high content of lipids, it is fundamental to employ NPs with appropriate polarity and reduced diameter [4]. While it is generally accepted that NPs should possess a diameter smaller than 40nm [6, 7] in order to penetrate through the SC, it is difficult to determine an optimal partition coefficient. An extremely hydrophobic entity would remain trapped in the lipid layers of the skin while a highly hydrophilic one (optimal for systemic applications) would not be able to enter due to the inability to interact with lipids. Therefore, it is necessary to utilise materials with intermediate properties.

NGs are promising platform for skin delivery due to their size, flexibility and tuneable properties but, in order to achieve all the mentioned desired characteristic, it is essential to select a suitable synthetic procedure and identify the right monomers, cross-linkers (XLs), initiators and solvents.

2.1.1 High Dilution Radical Polymerisation

In section 1.2.3 several synthetic techniques used for the production of nanogels were described. High dilution radical polymerisation (HDRP) was selected as synthetic procedure taking into account simplicity of the method, homogeneous and reduced size NPs obtained. In addition, the extensive works carried out by several members of Resmini's group [8, 9] was also considered. HDRP or solution polymerisation was first explored by N. Graham and A. Cameron [10]. As the name suggest it involves generation of radicals which can be achieved via photolysis or thermal decomposition of an

initiator molecule. Polymers are then formed by consecutive addition of free radicals building blocks. In high dilution conditions the particle-particle interactions are strongly disfavoured, therefore limiting formation of larger size constructs. The solvent plays a fundamental role in the polymerisation due to its interactions with monomers and cross-linkers (XLs). A porogen with high polymer chain solvation power is required to prevent chain-chain interactions that could result in polymer contraction and collapse of aggregates. Given a set of cross-linkers, monomers and initiators, a solvent able to fully dissolve all the components, to ensure homogeneous condition, should be chosen. Furthermore, it is essential to mention that only certain monomers' concentrations (C_M) and building blocks ratios can be chosen to form nanogels and avoid macrogelation or suspension formation. For every system it is possible to correlate composition to nanogel/macrogel formation by plotting the media solubility parameter (a value that expresses the solvation power of solvents) against initial monomer concentrations (IMC) (Figure 2.1).

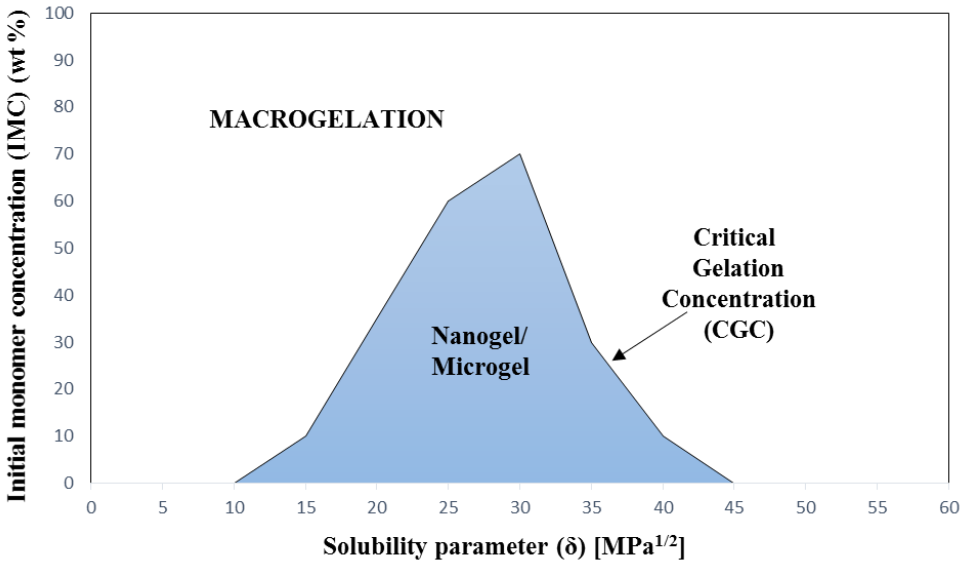

Fig. 2.1: Example of plot of critical gelation concentration as function of IMC against solubility parameter of the solvent or solvent mixture used for polymerization.

Nanogels or microgels are formed when IMC is within the critical gelation concentration (CGC), while C_M higher than CGC would culminate in macrogelation.

Overall HDRP offers several advantages: a) bypassing the use of surfactants with the consequent simplification of purification processes and reduction of compounds

required for the synthesis b) one pot reaction c) lower costs d) possibility to tune particle size and properties by altering NG composition and polymerisation conditions e) production of homogenous particles which require relatively short time for fabrication.

The characteristics and advantages of using nanogels for drug delivery purposes were previously described in chapter 1. It is important to point out that those properties are dependent both on synthetic protocol and selected building blocks. In the next section the process and rationale behind these selections are described.

2.1.2 Choice of monomers, cross-linker, initiator and solvents

Monomers and cross-linkers are responsible for the final physico-chemical properties of nanogels. Therefore, their choice is fundamental for the development of the delivery system. Literature data clearly identify small size and balanced polarity as key features for successful skin penetration [4-7]. In view of these facts two formulations, one based on lauryl methacrylate (LMA) and one on ethylene glycol methyl methacrylate (EGMMA), were initially selected for further studies (Figure 2.2).

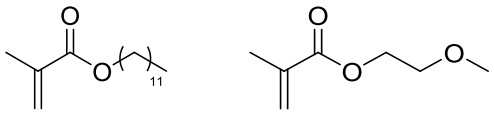

Fig. 2.2 left: lauryl methacrylate and right: ethylene glycol methyl methacrylate

The choice was driven by the different polarity of the two monomers. LMA has low hydrophilicity due to the long carbon chain while EGMMA has higher water solubility due to the ethylene glycol moiety. The initial idea was to obtain two nanogels' preparations, evaluate their possible different interaction with the skin and eventually test combinations of the two monomers to fine tune polarity. Moreover, the two systems present the advantage that following ester hydrolysis a negative charge would be formed (Figure 2.3), providing the particles with a negative surface charge, a feature that is often reported to improve cell internalisation [11] and body clearance rate [12].

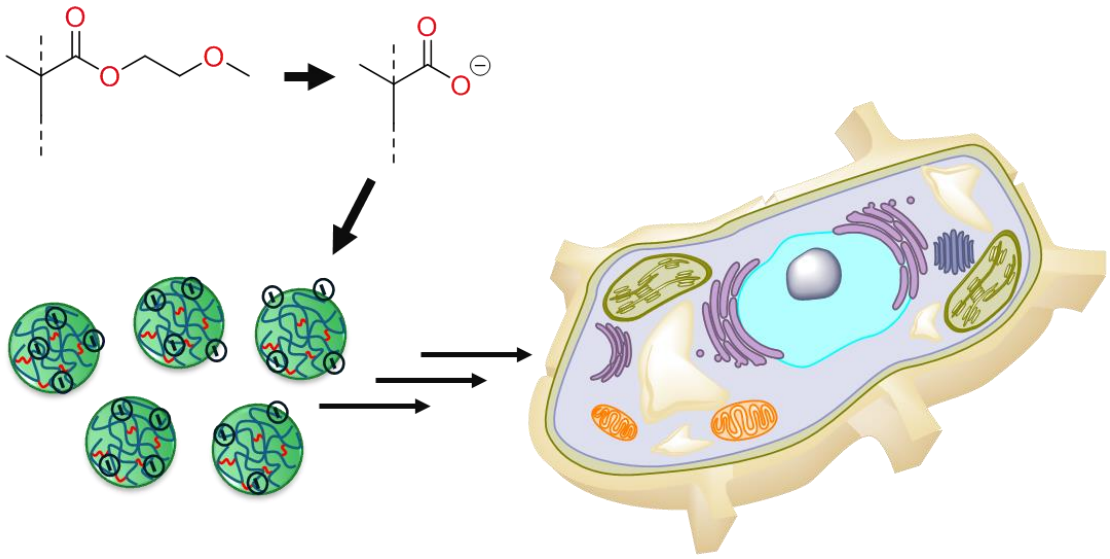

Fig. 2.3 Formation of negative charge subsequent to hydrolysis of ester bond leading to increased cellular uptake.

In order to form the network structure, the use of a polymer chains interconnecting agent (cross-linker) is required, therefore both LMA and EGMMA were copolymerised with the widely used N,N′-methylenebis(acrylamide) (MBA) [13-15] as cross-linker. It was agreed to fix MBA maximum molar concentration at 20% of the total polymerisation mixture so that the overall methacrylate nature of the nanoparticles was retained. Previously reported methacrylate based nanogels or microgels employ either toxic aromatic XLs such as divinyl benzene (DVB) [16] or degradable ones as ethylene glycol diacrylate (EGDA) and derivatives [17, 18]. Herein it was proposed to utilise MBA as a less toxic and chemically resistant cross-linker to lower risk of toxicity and premature degradation of the nanogel's network. Moreover, it is interesting to note that MBA is one of the smallest cross-linkers available, and this feature was expected to influence the size of the nanogel, leading to a compact structure and reduced particle size.

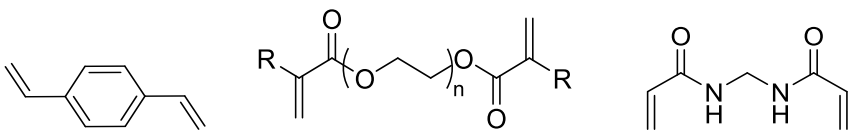

Fig. 2.4 From left to right chemical structures of: DVB; EGDA with n=1 and R=H while n=2,3… and R=H or CH_3 for derivatives; MBA.

A number of minimum requirements were identified to assess suitability of NGs for transdermal application: water solubility greater or equal to 1 mg/mL, due to the expected interaction with biological fluids (water based) and to allow further biological testing such as cytotoxicity analysis; reduced particle size (< 40 nm) screened via dynamic light scattering and polymerisation yields over 50%.

Dimethyl sulfoxide (DMSO) and deionised water were the main solvents employed as polymerisation media. The first for its ability to solvate both polar and non-polar compounds, the latter for its capacity to form hydrogen bonding and to verify whether an organic solvent free (greener) approach was achievable. Two widely used initiators were also selected: azobisisobutyronitrile (AIBN) (Figure 2.5) to be used in DMSO polymerisations [18] and ammonium persulfate (APS) (Figure 2.6) for water preparations [19].

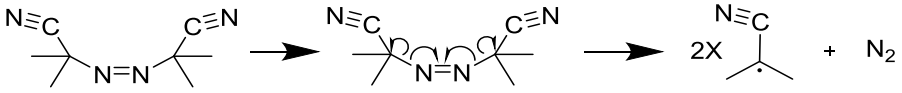

Fig. 2.5 AIBN structure and radical generation mechanism

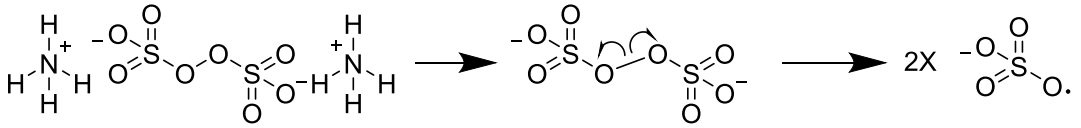

Fig. 2.6 APS structure and radical generation mechanism

Choice of AIBN and APS were based on proven efficacy shown on numerus researches reported in literature [16, 19, 20; 21]. Unfortunately, preparations based on lauryl methacrylate had to be discarded at an early stage of the project due to their total insolubility in aqueous media.

Initially, polymerisations using EGMMA, as the functional monomer, were carried out in DMSO for its high solvation power and ideal Hildebrand solubility parameter that was previously shown within the Resmini group to lead to nanogels with low

polydispersity. However, the solvent was soon found to be not suitable for the production of methacrylate nanogels as it was leading to formation of particles poorly soluble in water and with large diameter (over 200 nm). Several solvent mixtures with different Hildebrand (solubility) parameter were then evaluated, in order to find an optimal environment for the synthesis of NGs. DMSO (solubility parameter δ/MPa= 26.4) was therefore not completely abandoned and was used in conjunction with water at different ratios (Table 2.1). Nonetheless, even in this cases, polymerisations did not produce nanogels with the desired solubility and particle size.

NGs	EGMMA	MBA	AIBN	C_M%	Solvent	Yield
MRGC 120	80%	20%	1%	0.1%	W : D 9:1	82%
MRGC 121	80%	20%	1%	0.1%	W : D 8:2	52%
MRGC 123	80%	20%	1%	0.1%	W : D 4:6	45%
MRGC 124	80%	20%	1%	0.1%	W : D 2:8	40%

Table 2.1: Summary of nanogels' preparations in water : DMSO (W:D). Initiator percentage is referred to total number of double bonds in the polymerisation mixture.

Results showed that polymerisation yield was decreasing as function of DMSO increase. Using the solubility theory, which states that materials with similar intermolecular attractive forces are expected to be miscible, and considering the more similar solubility parameter values of DMSO to methacrylate monomers (example 2-hydroxyethyl methacrylate δ/MPa= 25) than water (δ/MPa= 48) [22-24], It was hypothesised that strong DMSO-methacrylates interactions could have prevented polymers elongation and particle formation, leading to yield decrease.

After discarding DMSO due to the poor water solubility and large particle size of nanogels produced, isopropyl alcohol (IPA) was employed as replacement of DMSO, due to its similar Hildebrand parameter (δ/MPa= 24.9), to understand whether the previously mentioned hypothesis was confirmed or not. Also these attempts resulted unsuccessful. The use of IPA led in fact to macrogelation and yields lower than 40% (Table 2.2).

NGs	EGMMA	MBA	APS	C_M%	Solvent	Yield
MRGC 125	80%	20%	2%	0.5%	W:IPA 5:5	20%
MRGC 126	80%	20%	2%	0.1%	W:IPA 5:5	4%
MRGC 127	80%	20%	2%	0.5%	W:IPA 4:6	18%
MRGC 128	80%	20%	2%	0.1%	W:IPA 4:6	1%

Table 2.2: Summary of nanogels preparations in water : isopropyl alcohol (W:IPA) mixtures.

Despite the unsuccessful polymerisations, a correlation between water percentage and yield obtained was identified. This was indeed the trigger that directed towards the selection of water as the only solvent of reaction. Water with its higher Hildebrand parameter (δ/MPa= 48) seemed to favour nanogel formation, probably due to a lower interaction with monomers which made them more available for polymer conversion. Therefore, if a modification of the environmental synthetic condition will be required in the future, for instance for the imprinting of molecules not soluble in water, solvent with high δ/MPa, such as short carbon chain glycols (δ/MPa= 30-35) or glycerol (δ/MPa= 36.2) should perhaps be considered.

Water polymerisation of EGMMA gave rise to formation of nanogels in high yield (over 90%), however their solubility (< 1 mg/mL) and size (90-250 nm) were still not suitable for skin delivery purposes. Moreover, in agreement with the solubility theory, water proved to possess lower dissolution power compared to DMSO since preparations using C_M 1% lead to macrogelation/precipitation. It should be also noted that the particle size was found to increase when increasing C_M (Table 2.3).

NGs	APS	AIBN	C_M%	Solvent	Y	Size I	Size V	Size N	Pdi
MRGC 110	0%	1%	1%	DMSO	60%	241±79 nm	244±91 nm	155±60 nm	0.250
MRGC 129	2%	0%	0.5%	WATER	92%	239±50 nm	241±57 nm	212±49 nm	0.015
MRGC 131	2%	0%	0.1%	WATER	95%	135±32 nm	135±35 nm	108±26 nm	0.028
MRGC 135	2%	0%	0.05%	WATER	60%	118±26 nm	118±28 nm	95±22 nm	0.015

Table 2.3 Main EGMMA (80%) : MBA (20%) preparations.Y is the yield of polymerisation. I for intensity V for volume and N for number size distributions. All data are mean values of triplicate with standard deviation.

A number of different alternative approaches were then investigated and although not successful in terms of yielding the desired nanogels, these studies provided some interesting information regarding the polymerisation conditions and are briefly summarised below.

In order to test alternative radical initiation procedures and to assess possible properties modification of nanogels, both thermal and ultraviolet (UV) methods were tested. UV is a generally faster technique useful in the presence of thermosensitive species, but at the same time it requires more sophisticated apparatus and cannot be employed when photosensitive monomers, such as fluorophores, are present in the polymerisation mixture. Although particle size resulted slightly smaller (≈ 70 nm by number distribution) the yield obtained was significantly lower (Table 2.4).

NG	Y	Size I	Size V	Size N	Pdi
MRGC 140 (UV)	58%	130±49 nm	100±45 nm	70±22 nm	0.128
MRGC 131 Thermal	95%	135±32 nm	135±35 nm	108±26 nm	0.028

Table 2.4 comparison between UV and thermal radical initiation. UV performed at room temperature in water and thermal at 70 ºC in water. Both polymersiatios performed in water with EGMMA (80%), MBA (20%). 2% of APS and C_M 0.1%. Y is yield of polymerisation. I for intensity V for volume and N for number distributions. Standard deviation reported as ± (mean value of triplicates) and as seen on DLS measurments.

It was then decided to increase the percentage of cross linker as an additional attempt to reduce particle size, due to the formation of denser core and closer polymer chains, before testing new nanogels' compositions (Table 2.5).

NG	EGMMA	MBA	Y	Size I	Size V	Size N	Pdi
MRGC 136	70%	30%	99%	141±31 nm	135±35 nm	115±27 nm	0.010
MRGC 131	80%	20%	95%	135±32 nm	135±35 nm	108±26 nm	0.028

Table 2.5 No effect of cross-linker percentage on particle size. Both polymersiatios performed in water with 2% of APS and with C_M 0.1%. I for intensity V for volume and N for number distributions.

However, as shown in Table 2.5, also the increment of MBA percentage did not produce any size contraction. It was hence chosen to employ new monomers in order to improve nanogels' characteristics.

After considering different methacrylate alternatives to overcome the poor aqueous solubility issue and to attempt to reduce particle size, 2-(diethylamino)ethyl methacrylate (DEAEMA) (Figure 2.7) was introduced as co-monomer.

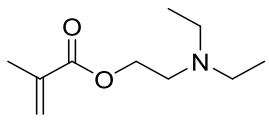

Fig. **2.7** DEAEMA chemical structure

DEAEMA had been extensively used in the production of nanoparticles for different applications such as for the synthesis of drug delivery systems or bile acids adsorbents [17, 25-27] consequently it was considered a good candidate for NGs synthesis.

The main reasons behind this choice were the presence of an amino group characterised by higher hydrophilicity and possible pH responsiveness capabilities [28]. Moreover, previous works by Morse et al. [20] showed that the monomer could have potentially provided emulsion stabilising properties.

Combination of EGMMA, DEAEMA and MBA were therefore screened by keeping EGMMA : DEAEMA ratio 1:1. Results suggested that C_M had to be kept under 0.5% in order to avoid formation of precipitate during polymerisation; DMSO was also found not suitable to be used as porogen for the production of nanoparticles, as in the case of EGMMA polymerised with MBA.

While testing different reaction conditions, a corrrelation was identified between cross-linker percentage and yield achieved (Table 2.6), in the range between 5 and 20% of cross-linker. Higher methylenebis(acrylamide) percentage was in fact leading to higher yield. Furthermore, nanogels produced, showed large particles size (> 300 nm by intensity, volume and number distribution) and poor water solubility (< 1 mg/mL) hence still not usable for transdermal delivery.

NG	EGMMA	MBA	APS	AIBN	DEAEMA	C_M%	Solvent	Yield
141	40%	20%	5%	0%	40%	0.5%	Water	P
142	40%	20%	5%	0%	40%	0.1%	Water	87%
148	40%	20%	0%	5%	40%	0.1%	DMSO	0%
146	40%	20%	0%	5%	40%	1%	DMSO	10%
159	42.5%	15%	5%	0%	42.5%	0.5%	Water	84%P
160	42.5%	15%	5%	0%	42.5%	0.1%	Water	57%
155	45%	10%	5%	0%	45%	0.5%	Water	77%P
147	45%	10%	5%	0%	45%	0.1%	Water	48%
144	47.5%	5%	5%	0%	47.5%	0.5%	Water	40%P
145	47.5%	5%	5%	0%	47.5%	0.1%	Water	24%

Table 2.6 DEAEMA : EGMMA 1:1 preparations. Formation of precipitate is indicated with P.

2-(diethylamino) ethyl methacrylate was therefore tested on its own and cross-linked with MBA (90:10) to understand the monomer contribution to nanogel's water solubility. The yields obtained appeared to be low (lower than 40% with C_M 1%), probably due to prevalent formation of short dead polymer chains and low amount of MBA used. The solubility (up to 1 mg/mL) instead, proved to be more suitable for the planned application. It was hypothesised that hydrogen bonding interaction between the two monomer may play a role in the formation of nanogels. When EGMMA and DEAEMA are placed together in the polymerisation mixture their interactions bring them closer, so when the polymerisation is initiated there are more chances to build larger polymer network which will then be retained during the purification via dialysis.

It was then decided to increase the percentage of DEAEMA in the polymerisation mixture to evaluate whether solubility and particle size could have been improved. Therefore DEAEMA : EGMMA : MBA water polymerisation, 60:20:20, 60:25:15, 60:30:10 and 65:30:5 were performed at various C_M confirming the previously observed trend of cross-linker/yield correlation . Furthermore, as previously observed, C_M had to be kept at 0.1% to avoid precipitation also in these preparations (Table 2.7).

NG	EGMMA	MBA	APS	DAEEMA	C_M%	Solvent	Yield
181	20%	20%	5%	60%	0.50%	Water	81%P
184	25%	15%	5%	60%	0.50%	Water	75%P
183	30%	10%	5%	60%	0.50%	Water	72%P
151	30%	10%	5%	60%	0.1%	Water	46%
152	30%	5%	5%	65%	0.1%	Water	27%

Table 2.7 Preparations containing DEAEMA as functional monomer. Formation of precipitate is indicated with P.

It is worth mentioning that 2-(diethylamino) ethyl methacrylate is reported to provide thermo-responsive capabilities to particles [29]. It was therefore decided to test this property. In order to evaluate thermoresponse of nanogels, UV thermal analysis was selected as analytical method and was performed on 4 different 1 mg/mL nanogel dispersions (Table 2.8).

NG	EGMMA	MBA	APS	DEAEMA	C_M%	Solvent	Yield
143	45%	10%	5%	45%	0.5%	Water	28%
144	47.5%	5%	5%	47.5%	0.5%	Water	40%
151	30%	10%	5%	60%	0.1%	Water	46%
152	30%	5%	5%	65%	0.1%	Water	27%

Table 2.8 Summary of nanogels' preparations tested for thermoresponsiveness.

The concept is that by increasing the temperature, amine groups from DEAEMA rearrange within the nanogels' structure moving towards the inner part of the polymeric network, pushing water molecules away. This leads to a decrease in nanoparticles' hydrophilicity which can be visually seen as an increased turbidity of the solution. The turbidity increment then prevents, partially or totally, the transmittance of UV light from the sample to the detector.

The point of the curve (obtained via UV scan) where the slope is at its highest, generally corresponding to 50% transmittance, is considered the transition temperature of the material.

UV profile of nanogels, reported below, showed that MRGC 143 and MRGC 151 were indeed capable to respond to temperature variation. Moreover, their response temperature appeared to be close to body temperature (37 ºC) as seen in thermal UV Figures 2.8 and 2.9.

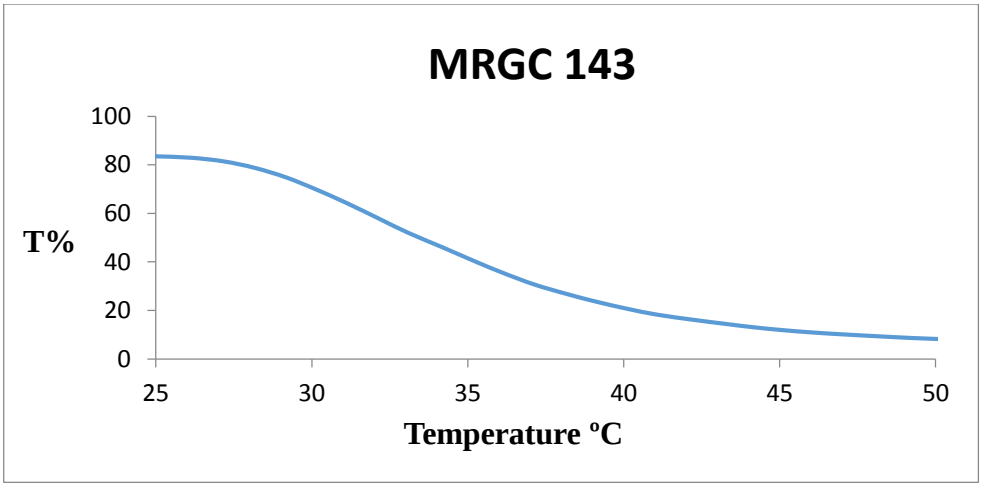

Fig 2.8 MRGC 143 UV thermal profile.

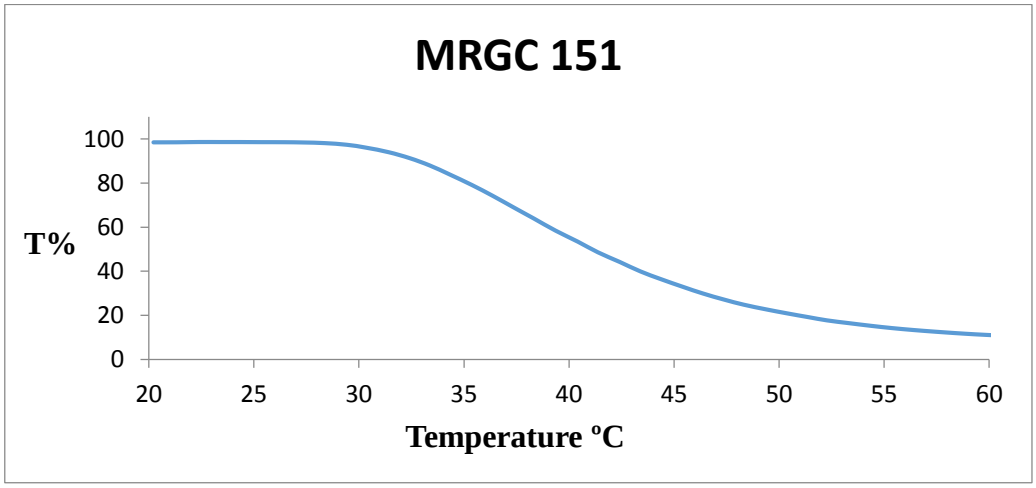

Fig. 2.9 MRGC 151 UV thermal profile.

In addition, results appeared to suggest that reduction of cross linker percentage led to shifting of thermal response towards higher temperature, not fully recorded because over the optimal thermal conditions for measurements in water as at a temperature higher than 60 ºC the solvent would start evaporating fast, potentially compromising UV readings. The shift can be visualised in Figures 2.10 and 2.11 reported below.

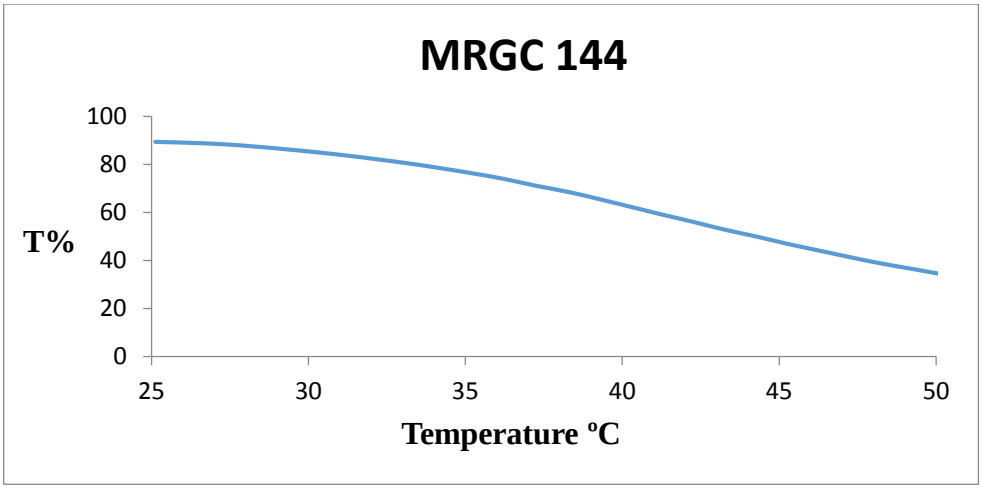

Fig. 2.10 MRGC 144 UV thermal profile

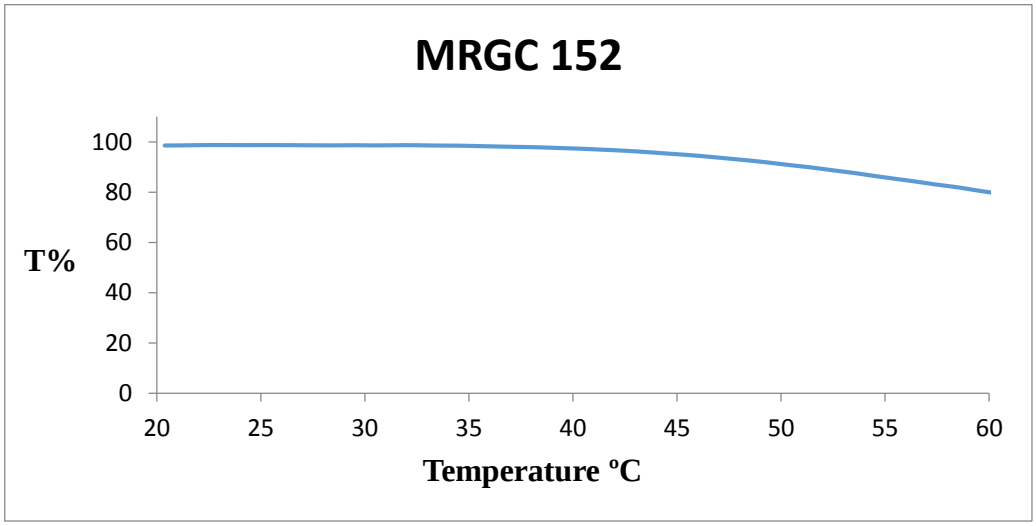

Fig. 2.11 MRGC 152 UV thermal profile

Although the data provided some evidence of thermo-responsive behaviour, the desired increase in solubility (equal or over 1 mg/mL) expected as a result of the increase in percentage of DEAEMA in the mixture, was not observed. Moreover, it was noted that C_M of 0.1% would have drastically limited the scalability of the process for potential industrial applications. For these reasons, DEAEMA was replaced with 2-(tert-butylamino) ethyl methacrylate (tBAEMA) for its chemical similarity but higher solubility provided by the secondary amine which could form an additional hydrogen bond compared to the tertiary amine of DEAEMA (Figure 2.8).

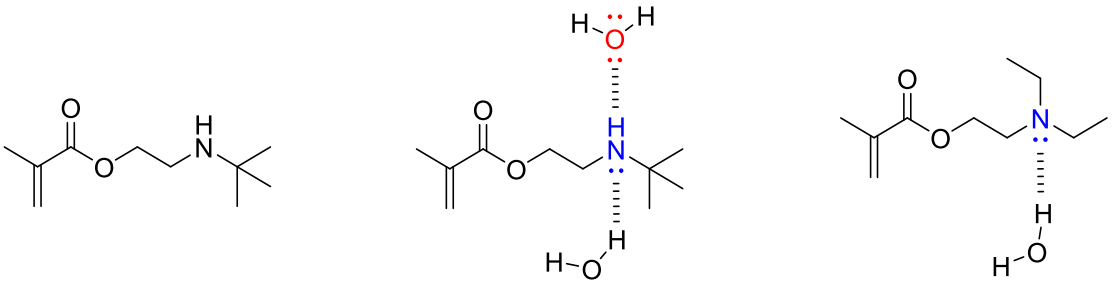

Fig. **2.8** tBAEMA chemical structure (left); comparison of water hydrogen bonding formation with tBAEMA (centre) and DEAEMA (right).

Moreover, due to different pK_b values, secondary amines are stronger bases than tertiary leading to increased formation of positive ions more soluble in water media (Figures 2.12 and 2.3).

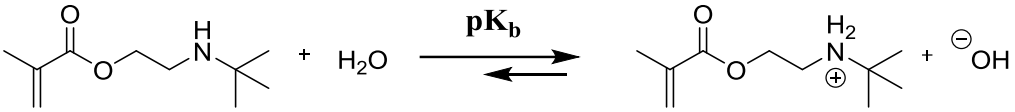

Fig. **2.12** tBAEMA protonation (pK_a = 7.3; pK_b = 6.7) [31]

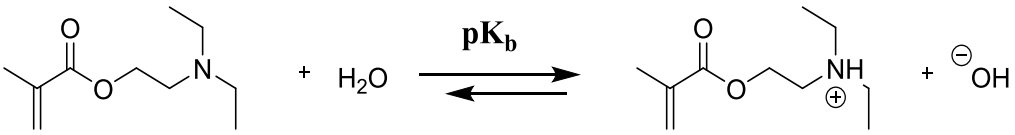

Fig. **2.13** DEAEMA protonation (pK_a = 6.9; pK_b = 7.1) [15]

tBAEMA has been previously employed for various applications such as antimicrobial agents [30,31] or Pickering emulsifier [32] and was shown by previous work to be able to provide all the potential advantages that were expected from DEAEMA [16, 28]. Therefore, it was considered a good candidate for the improvement of nanoparticles' properties.

In order to evaluate the impact of the new monomer on the solubility of the nanoparticles, tBAEMA was first tested together with MBA but without EGMMA as co-monomer. A series of different polymers were prepared using a combination of different percentages of cross-linker and C_M (Table 2.9).

NG	MBA	APS	tBAEMA	C_M%	Solvent	Yield
167	10%	5%	90%	1%	Water	47%
165	10%	5%	90%	0.5%	Water	30%
166	10%	5%	90%	0.1%	Water	29%
173	15%	5%	85%	0.5%	Water	57%
174	15%	5%	85%	0.1%	Water	43%
168	20%	5%	80%	0.5%	Water	53%
172	20%	5%	80%	0.1%	Water	58%

Table 2.9 tBAEMA:MBA preparations. Red high lined value seemed not to follow the trend of yield increase due probably to material loss during nanogels' purification and collection processes. However due to time constrains the preparation was not repeated.

Comparison of the preparations reported on Table 2.9 with those obtained employing only DEAEMA suggested that tBAEMA use was leading to production of better nanogels as they showed no sign of macrogelation even at C_M 1% and higher solubility in water (>2 mg/mL). Similarly, to what was noted previously, the results suggested a direct correlation of C_M and cross-linker percentages used with the overall yields that were obtained. On the other end all the polymer preparations, analysed by dynamic light scattering in order to evaluate particle size, were found to be over 200 nm in diameter. This size was deemed too large for skin penetration and therefore these preprations were not considered suitable.

EGMMA was then introduced to complete the comparative study. Taking in to account previously tested DEAEMA based polymerisations, different tBAEMA : EGMMA : MBA ratios were selected and consequently tested in order to identify a potential good candidate for the proposed application. After screening various compositions, an optimal mixture constituted by 60% of tBAEMA as functional monomer, 20% of EGMMA as co-monomer and 20% of cross-linker (MBA) (Table 2.10) were identified.

NG	tBAEMA	EGMMA	MBA	Yield	Size I	Size V	Size N	Pdi
186	75%	20%	5%	50%	204±76 nm	8±3 nm	7±2 nm	1.000
185	65%	20%	15%	64%	725±128 nm	17±3 nm	16±3 nm	0.730
176	60%	30%	10%	55%	166±52 nm	4±1 nm	4±1 nm	0.380
180	60%	20%	20%	76%	34 ± 30 nm	9 ± 5 nm	6 ± 2 nm	0.400
178	50%	30%	20%	75%	42±25 nm	7±5 nm	5±2 nm	0.405

Table 2.10 Preparations containing tBAEMA as functional monomer. Optimal formulation highlighted in green. All polymersiatios performed in water with 5% of APS and with C_M 0.5%. I for intensity V for volume and N for number distributions.

Careful analysis of the new polymers suggested that their characteristics were better suited for the desired application as drug delivery system for the skin. Among the different preparations polymer MRGC 180 showed: yield over 75%, water solubility greater than 2 mg/mL and particle size in the range 5-15 nm (by number and volume distribution) confirmed by both dynamic light scattering (DLS) measurements and transmission electron microscopy (TEM) imaging (Figure 2.14) which are discussed in more details in the following sections.

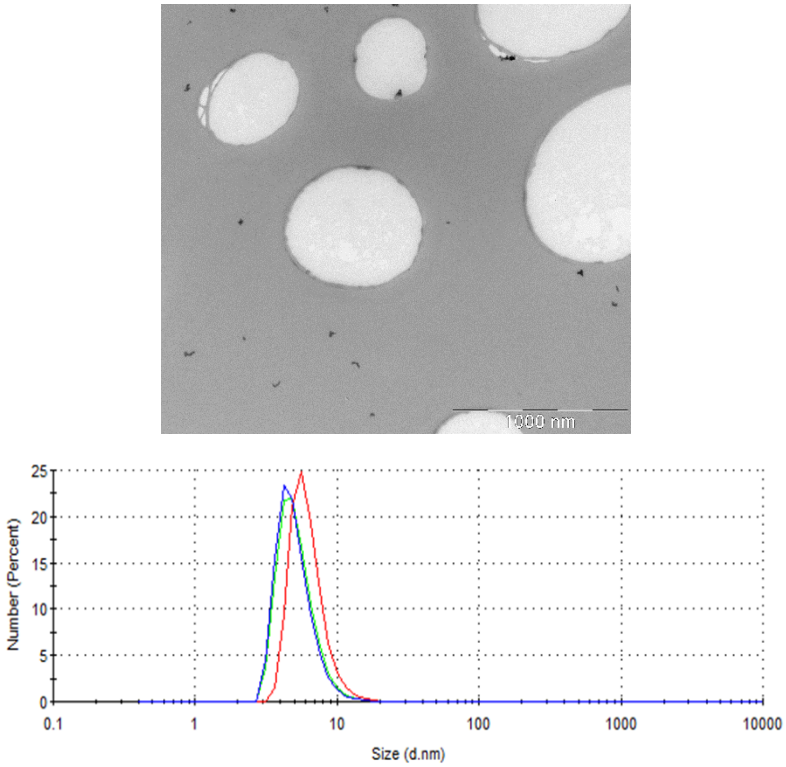

Fig. **2.14** TEM image (top) and triplicate overlap of DLS distribution signals by number (bottom) for MRGC 180

In the view to investigate systems with different polarity, it was decided to prepare additional nanogels by replacing EGMMA with methacrylic acid (MAA) (Figure 2.15) to further improve hydrophilicity of the nanoparticles.

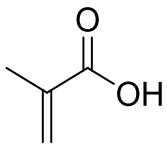

Fig. **2.15** MAA chemical structure.

Nanogels were then obtained using the previously identified composition of 60:20:20 (tBAEMA : MAA : MBA) (Table 2.11). Their synthesis in water at C_M 0.5% achieved a substantial yield of over 90%, water solubility higher than 5 mg/mL and particle size in the range 5-20nm (by number and volume distribution).

NG	tBAEMA	EGMMA	MAA	Y	Size I	Size V	Size N	Pdi
180	60%	20%	0%	76%	34 ± 30 nm	9 ± 5 nm	6 ± 2 nm	0.400
196	60%	0%	20%	94%	45 ± 30 nm	14 ± 9 nm	9 ± 3 nm	0.285

Table 2.11 Nanogels containing tert-buthylaminoethyl methacrylate as functional monomer and ethylene glycol methyl ether methacrylate (EGMMA) or methacrylic acid (MAA) as co-monomer. Polymerisations performed in water MBA at 20% and C_M 0.5%

Along with the desired size and solubility, these nanogels were shown to possess additional capabilities such as pH responsiveness and emulsion stabilising properties which are further discussed in the following chapter.

This work represents the first attempt to synthesize nanogels using tBAEMA as functional monomer in combination with EGMMA or MAA as co-monomers and MBA as cross-linker hence this is the first reported study for these novel nanomaterials.

Beside the synthesis of nanoparticles with optimal characteristics for drug delivery, the ability to monitor them *in vitro*, *ex vivo* and *in vivo* provides a great benefit to further demonstrate the suitability of the DDS for the intended application. For this reason, it was proposed to incorporate a fluorescent probe into the nanogels.

2.1.3 Fluorescent tag selection

One of the big challenges in the development of a new drug delivery system is to demonstrate whether the carrier is able to be internalised inside cells or to be distributed within a tissue. Fluorescent labelling is a widely used technique to address these objectives [33, 34]. Two are the approaches used for the introduction of a fluorophore moiety into a delivery system: covalent and non-covalent [35-37]. The first implies the chemical link between the fluorescent tag and the particle, the latter instead envisages the adsorption of the probe into the particle via physical interactions. Although the second approach does not significantly modify the structure of the cargo it does not grant accurate quantification due to possible fluorescent leakage. Covalent approach is

for this reason the best approach when certain localisation and quantification is requested.

The selection of a chemically attached fluorophore, to be used as tag for nanogels, has to consider few key parameters: chemical similarity in order to react at a rate comparable to monomers used and to avoid significant alteration of the structure; photo-stability and minimal impact on nanoparticles properties (size, polarity, responsiveness etc.). Furthermore, it must be pointed out that tag incorporation planned in this study was aimed only for the demonstration of cell internalisation and potential skin penetration. Therefore, the final pharmaceutical formulation would not contain the probe that served exclusively as proof of concept.

A number of different candidates were first evaluated, based on to experience accumulated in the group:

a) 1,3-dioxo-1H-benzo[de]isoquinolin-2(3H)-yl-ethyl) acrylamide (naphtalic based fluorophore NBF) (Figure 2.16) previously developed and employed by Dr. P. Bonomi [38], former postdoctoral fellow in the Resmini team.

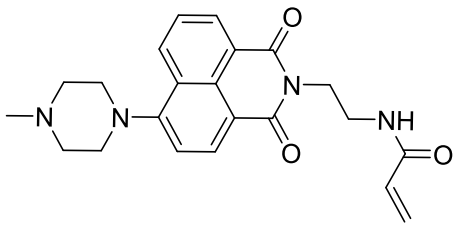

Fig. **2.16** 1,3-dioxo-1H-benzo[de]isoquinolin-2(3H)-yl-ethyl) acrylamide chemical structure.

b) 7-[4-(Trifluoromethyl)coumarin]acrylamide (TFMCA) (Figure 2.17) reported in literature [39] and already tested by Dr. J. Ray, former PhD student of Resmini's group.

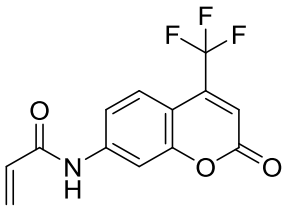

Fig. **2.17** 7-[4-(trifluoromethyl)coumarin] acrylamide chemical structure.

Both NBF and TFMCA were selected for their acrylamide polymerisable moiety which should possess similar reactivity to MBA. However due to their bulkiness and almost total insolubility in water they were soon discarded.

Further evaluation of literature reports led to the identification of a new fluorophore, developed by O'Reilly et al., named 2-(2-(3,4-bis(butylthio)-2,5-dioxo-2,5-dihydro-1H-pyrrol-1-yl)acetoxy)ethyl methacrylate {methacrylate fluorophore} (MAF) (Figure 2.18), [33, 40-42;].

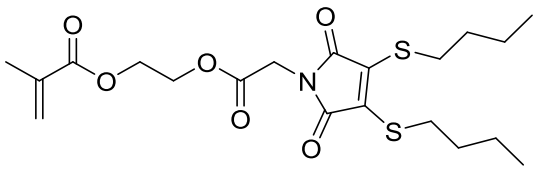

Fig. **2.18** MAF chemical structure.

Due to the reported high quantum yield (54%) [33] and MAF's chemical similarity to monomers used, the fluorophore appeared to possess good characteristics to be employed as nanogels' tag. Moreover, the maximum emission ($\lambda_{em} \approx 540$ nm) [33] of MAF was considered an optimal value for the avoidance of fluorescence signal overlapping with cell nuclei' staining agent Hoechst H33342 ($\lambda_{em} \approx 460$) and dead cells' staining dye propidium iodide ($\lambda_{em} \approx 620$) used to evaluate cell viability profile of nanogels, reported in chapter 4.

Synthesis of MAF was achieved, following the published literature procedure [40-42], in 3 steps as shown in the Figure 2.19 below.

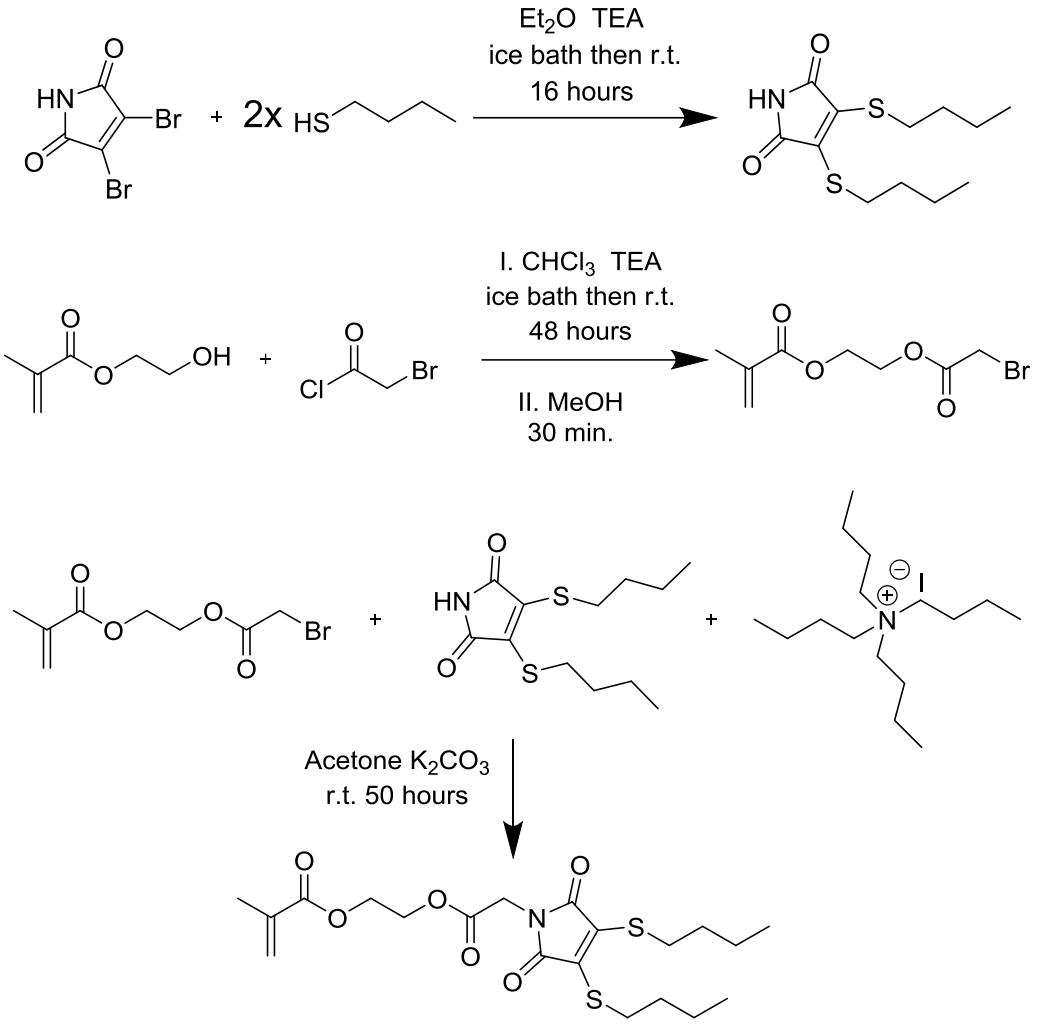

Fig. **2.19** MAF synthetic pathway.

MAF synthesis was confirmed both by ^{1}H-NMR and fluorimetry studies (Figure 2.20 and 2.21).

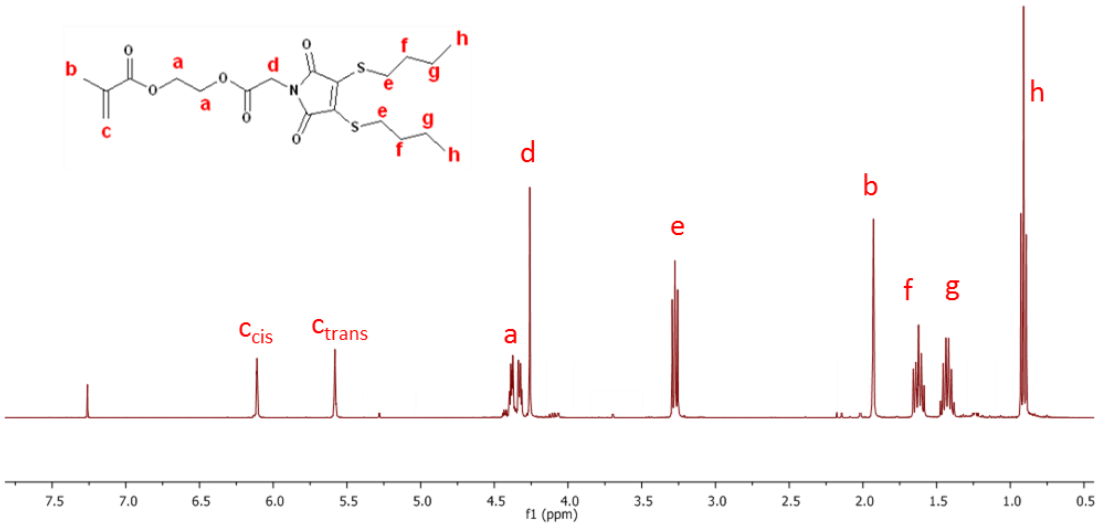

Fig. 2.20 ^{1}H-NMR of MAF

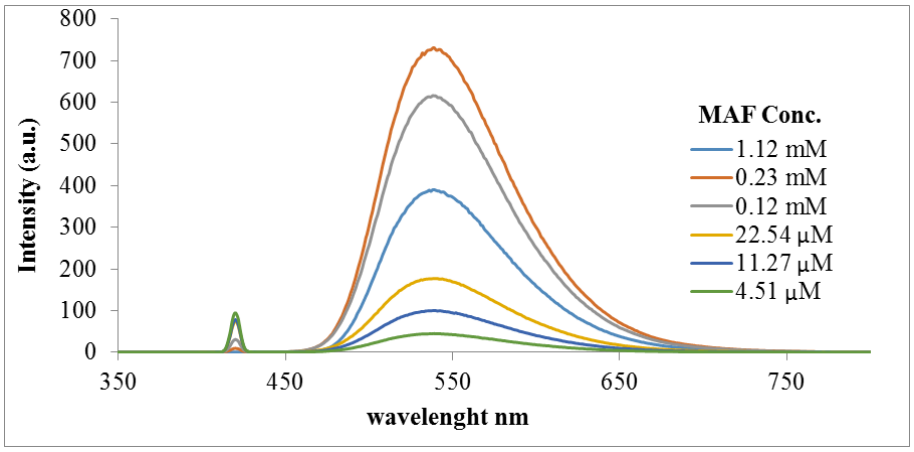

Fig. 2.21 fluorescence profile of MAF in chloroform. Excitation set at λ= 417 nm. The analysis showed that concentrations equal or higher than 0.23mM give rise to fluorescent self-quenching.

Following its synthesis, it was required to identify the appropriate conditions for its incorporation into the nanoparticles via covalent bond. Polymerisations in water were first carried out setting MAF percentage at 5% and using tBAEMA : EGMMA : MBA or tBAEMA : MAA : MBA ratios of 55:20:20. The low fluorophore percentage was selected to minimise the potential effect of the fluorescent tag on the nanoparticles properties. Despite a number of attempts, the fluorescent nanogels could not be obtained with the desired solubility. Some changes in the solvent solution were then evaluated and after testing different approaches, a mixture of water and acetone (1:1)

was found to be a good system for the preparation of the fluorescent polymers (Table 2.12).

NG	tBAEMA	EGMMA	MAA	MAF	Solvent	Yield	Size I	Size V	Size N
MRGC 211	55%	20%	0%	5%	W:Ac 1:1	51%	116 ± 36 nm	97 ± 35 nm	75 ± 22 nm
MRGC 209	55%	0%	20%	5%	W:Ac 1:1	69%	78 ± 28 nm	58 ± 22 nm	45 ± 13 nm

Table 2.12 Chemical composition, yield and diameter of fluorescent nanoparticles. Cross-linker percentage was set at 20% and C_M at 0.5%. Polymerisation was carried out for 72 hours at 40 ºC. W is water and Ac is acetone. I stands for intensity, V for volume and N for number Dynamic light scattering (DLS) measurements. Standard deviation reported as ± (mean value of triplicates) and as seen on DLS measurments.

In order to evaluate the incorporation efficiency of the fluorescent tag into the nanogels, UV spectroscopy was selected as analytical method over fluorescence spectroscopy due to its higher accuracy. Given the insolubility of nanogels in chloroform, MAF calibration and NGs spectra were recorded by using samples dissolved in a mixture of acetone : water = 7:3 which was found to be the optimal ratio in order to dissolve both fluorophore on its own and fluorescent labelled nanoparticles (Figures 2.22 and 2.23).

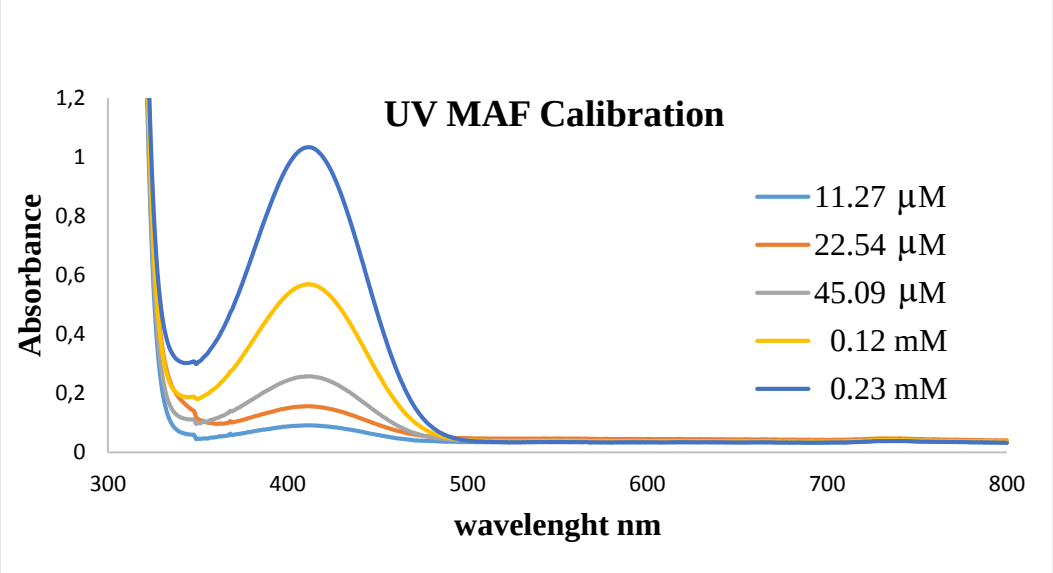

Fig. 2.22 UV calibration of MAF dissolved in a mixture water : acetone 3:7

The maximum fluorophore absorbance was observed at λ_{ab} = 411 nm (close to the value of fluorescent excitation). Therefore, absorbance values, obtained at this wavelength, at five different fluorophore concentrations were used to produce a calibration curve in order to extrapolate the molar extinction coefficient ε, using Lambert-Beer law, then used for the evaluation of fluorophore's incorporation into nanogels.

For comparative purposes, previously achieved nanogels (MRGC 180 and 196) were synthesised in the same solvent mixture, used for fluorescent nanoparticles production, showing no significant difference in terms of size and water solubility (Table 2.13).

NGs	tBAEMA	EGMMA	MAA	MAF	Solvent	Yield	Size I	Size V	Size N
MRGC 180	60%	20%	0%	0%	Water	76%	34 ± 30 nm	9 ± 5 nm	6 ± 2 nm
MRGC 214	60%	20%	0%	0%	W:Ac 1:1	86%	150 (87%) ± 64 nm	12 ± 3 nm	10 ± 2 nm
MRGC 211	55%	20%	0%	5%	W:Ac 1:1	51%	116 ± 36 nm	97 ± 35 nm	75 ± 22 nm
MRGC 196	60%	0%	20%	0%	Water	94%	45 ± 30 nm	14 ± 9 nm	9 ± 3 nm
MRGC 213	60%	0%	20%	0%	W:Ac 1:1	91%	100 (84%) ± 11 nm	11 ± 2 nm	10 ± 2 nm
MRGC 209	55%	0%	20%	5%	W:Ac 1:1	69%	78 ± 28 nm	58 ± 22 nm	45 ± 13 nm

Table 2.13 Summary of fluorescent and non-fluorescent preparations. All polymerisation at C_M 0.5% with MBA at 20%. Reaction time of 72 hours at 40 ° C for water : acetone volume ratio 1:1 and at 70 ° C for water preparations. I stands for intensity, V for volume and N for number Dynamic light scattering (DLS) measurements. Standard deviation reported as ± (mean value of triplicates) and as seen on DLS measurments.

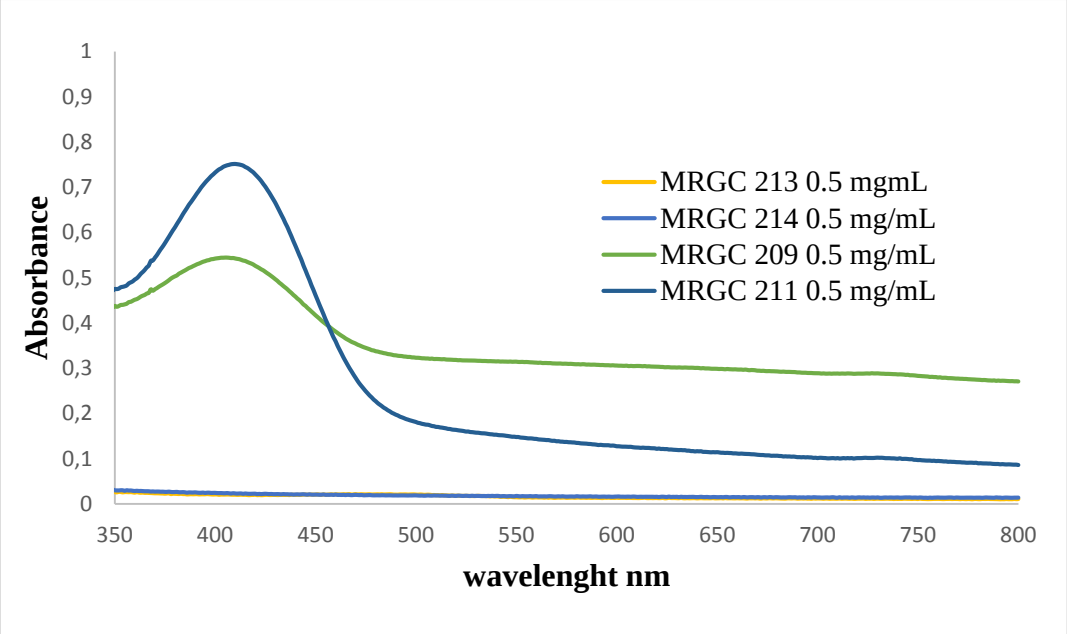

Fig. 2.23 UV profile of fluorescent (MRGC 209 and 211) and non-fluorescent (MRGC 213 and 214) nanogels dissolved in a mixture water : acetone 3:7

Figure 2.23 shows the UV spectra for nanogels MRGC 209 and MRGC 211 both used at the same concentration of 0.5 mg/mL. Comparison of the UV spectra of the two fluorescently labelled nanogels with their non-fluorescent analogues (MRGC 213 and MRGC 214) clearly provides evidence of incorporation of the fluorescent tag into the polymer matrix. The difference in absorbance between the two polymers could be taken as evidence of variation in tag incorporation, however potential fluorophore-monomers interactions as a result of the different monomers present in the two polymer structures could also justify such differences.

A very simple estimate of fluorescent tag incorporation was done by using the extinction coefficient to determine the concentration of fluorophore in the polymer, while the theoretical content of MAF was estimated in each case and was based on the assumption that all nanogel's components (included MAF) contributed to the final yield proportionally to their molar percentages initially fed into the polymerisation mixture. MRGC 209 showed a tag incorporation of 78% while MRGC 211 higher than 100%, indicating that degree of probe inclusion into nanogels' structure resulted to be proportionally over the initial 5% fed into polymerisation mixture.

It is interesting to note that the yields obtained and particles size for the nanogels containing the fluorescent probe were found to be different from the NGs synthesised without the tag (Table 2.14).

NG	tBAEMA	EGMMA	MAA	MAF	Y	Size II	Size V V	Size N N
MRGC 209	55%	0%	20%	5%	69%	78 ± 28 nm	58 ± 22 nm	45 ± 13 nm
MRGC 213	60%	0%	20%	0%	91%	100 (84%) ± 11 nm	11 ± 2 nm	10 ± 2 nm
MRGC 211	55%	20%	0%	5%	51%	116 ± 36 nm	97 ± 35 nm	75 ± 22 nm
MRGC 214	60%	20%	0%	0%	86%	150 (87%) ± 64 nm	12 ± 3 nm	10 ± 2 nm

Table 2.14 Chemical composition, yield and particles' size fluorescent (MRGC 209 and 211) and non-fluorescent (MRGC 213 and 214) nanogels. All polymerisation at C_M 0.5% with MBA at 20%. Reaction time of 72 hours at 40 ° C in water : acetone volume ratio 1:1. I stands for intensity, V for volume and N for number Dynamic light scattering (DLS) measurements. Standard deviation reported as ± (mean value of triplicates) and as seen on DLS measurments.

Lower yields observed could have been due to radical quenching operated by MAF while increased particle size was probably caused by the larger dimensions of the fluorophore compared to monomers.

The larger diameter of the tagged nanogels could have significant implications in terms of final properties of the drug delivery system such as penetration throw the skin, cell internalisation and toxicity, compromising the assumption that nanoparticles labelled and non-labelled would behave in similar manner. Moreover, also water solubility of fluorescent NGs proved to be lower compared to non-fluorescent equivalents (≤ 1 mg/mL). An obvious next step would be reducing the percentage of MAF, however due to time constrains these formulations were not prepared. Nevertheless, an alternative way to evaluate cell internalisation was identified and it is described in chapter 5.

2.1.4 Nanogels isolation

After performing the polymerisation and before the characterisation, the nanogels need to be purified in order to get rid of any unreacted monomers, cross-linker and initiator as well as dead short polymer chains. Dialysis, over deionised water, through a cellulose membrane was selected as the most suitable technique. Due to the reduced size of nanoparticles produced the smallest commercially available membrane with molecular cut off of 3500 Da was employed, to avoid the loss of nanogels via diffusion. This method was well established within the Resmini group and was previously shown to work very effectively [43]

Following the dialysis step the purified nanogels solutions were freeze dried in order to yield soft powders. The reasons of this treatment were: a) to calculate yield of polymerisation; b) to obtain a material with extended shelf life compared with a solution; c) work with known amount of material and d) reduce space required for storage.

Nanogels were then reconstituted in the appropriate solvent in order to perform characterisation and analysis, which are described later in this and in following chapters.

2.2 Characterisation

A number of experiments were carried out in order to gain structural information of the nanogels and confirm their formation over simple polymer chains. These tests include infra red spectroscopy, nuclear magnetic resonance, dynamic light scattering, zetapotential and transmission electron microscopy. All these studies are reported in the individual sections below.

2.2.1 Fourier transform infra red (FT-IR) spectroscopy

Fourier transform infra red (FT-IR) spectroscopy was employed in order to confirm the presence of main functional groups of the monomers within the different polymeric structures.

First, each individual monomer was analysed alone to identify the characteristic peaks that would allow to confirm their presence in the final polylmer structure. These are shown, with their main signals assignmentin in the captions, in Figures 2.24-2.27 below.

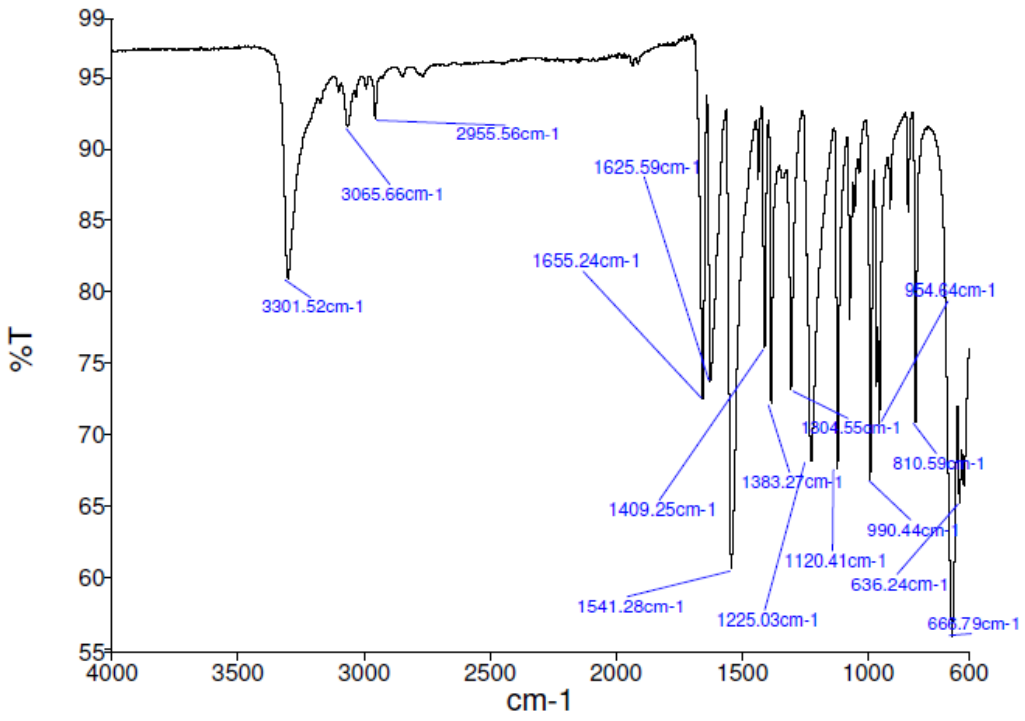

Fig. 2.24 FT-IR of MBA. Main significant signals: 3301 cm^{-1} (N-H st); 1655 cm^{-1} (C=O st); 1625 cm^{-1} (N-C=O st); 1541 cm^{-1} (NH **Δ**). St is streaching and Δ is bending.

Figure 2.24 shows signals for the stretching and bending of the secondary amide (both nitrogen and carbonyl) at 3301, 1655, 1625 and 1541 cm^{-1} which characterise N,N′-methylenebis(acrylamide) (MBA).

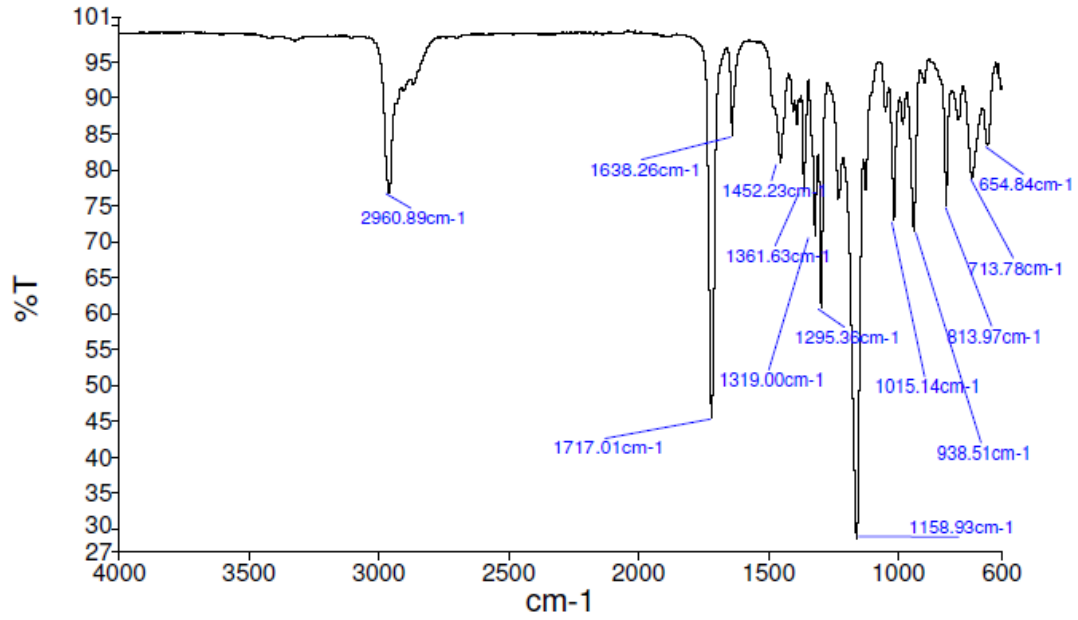

Fig. 2.25 FT-IR of tBAEMA. Main significant signals: 2960 cm^{-1} (NH st); 1717 cm^{-1} (C=O st); 1159 cm^{-1} (C-O st).

In Figure 2.25 the characterist peaks of ester and secondary amine for 2-(tert-butylamino) ethyl methacrylate (tBAEMA) are present (2960, 1717 and 1159 cm^{-1}).

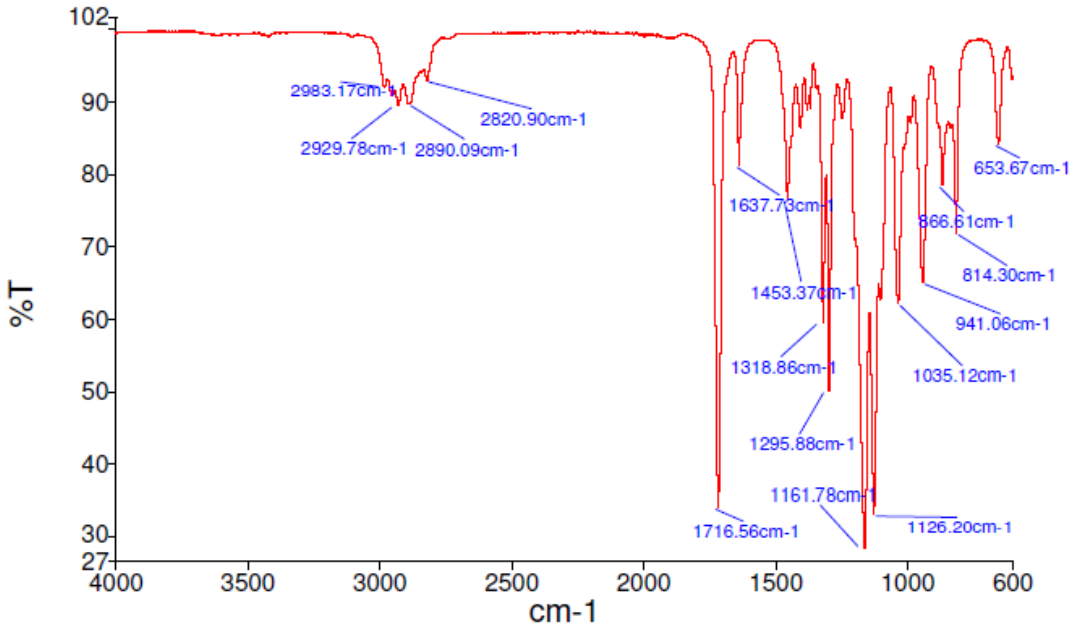

Fig. 2.26 FT-IR of EGMMA. Main significant signals: 1716 cm^{-1} (C=O st); 1161, 1126 cm^{-1} (C-O st).

FT-IR spectrum of ethylene glycol methyl methacrylate (EGMMA) shows (Figure 2.26) signals for the ester group (1716 and 1161 cm^{-1}) as for tBAEMA but without the presence of the amine signal.

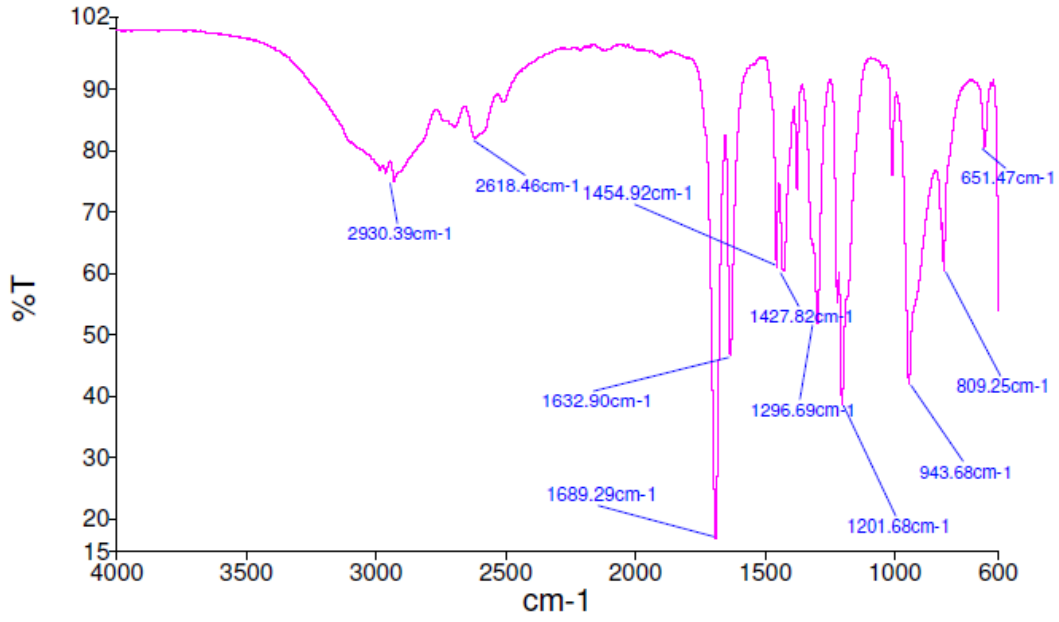

Fig. **2.26** FT-IR of MAA. Main significant signals: 2931 cm^{-1} (O-H st); 1689 cm^{-1} (C=O st).

Finally, Figure 2.26 shows the characteristic broad peak for the hydroxyl/alkoxyde group (2931 cm^{-1}) toghether with the carbonyl signal (1689 cm^{-1}) of the methacrylic acid (MAA)

Having identified the main functional group signals, also the six selected final preparations were analysed and are shown in Figures 2.27-2.32 below.

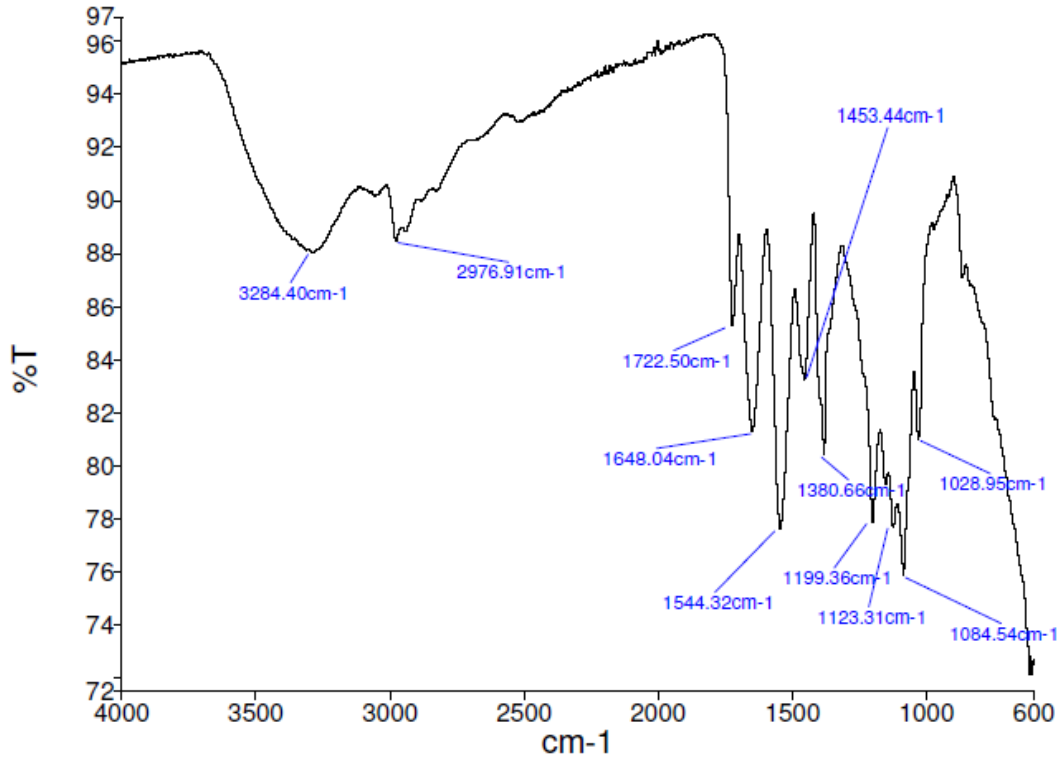

Fig. 2.27 FT-IR of MRGC 180. Main significant signals: 3294 cm^{-1} ($R_2HH_2^+$ st); 2976 cm^{-1} (NH free st); 1722, 1648 cm^{-1} (C=O st); 1544 cm^{-1} (NH **Δ**).

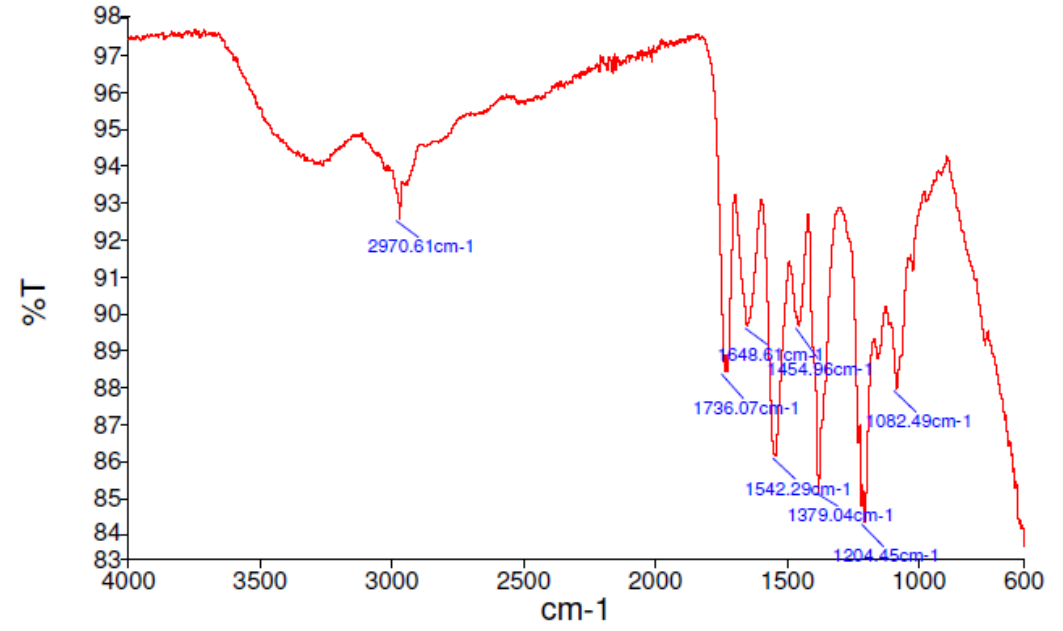

Fig. 2.28 FT-IR of MRGC 196. Main significant signals: 3284 cm^{-1} ($R_2HH_2^+$ st); 2970 cm^{-1} (NH free st); 1736, 1649 cm^{-1} (C=O st); 1542 cm^{-1} (NH **Δ**).

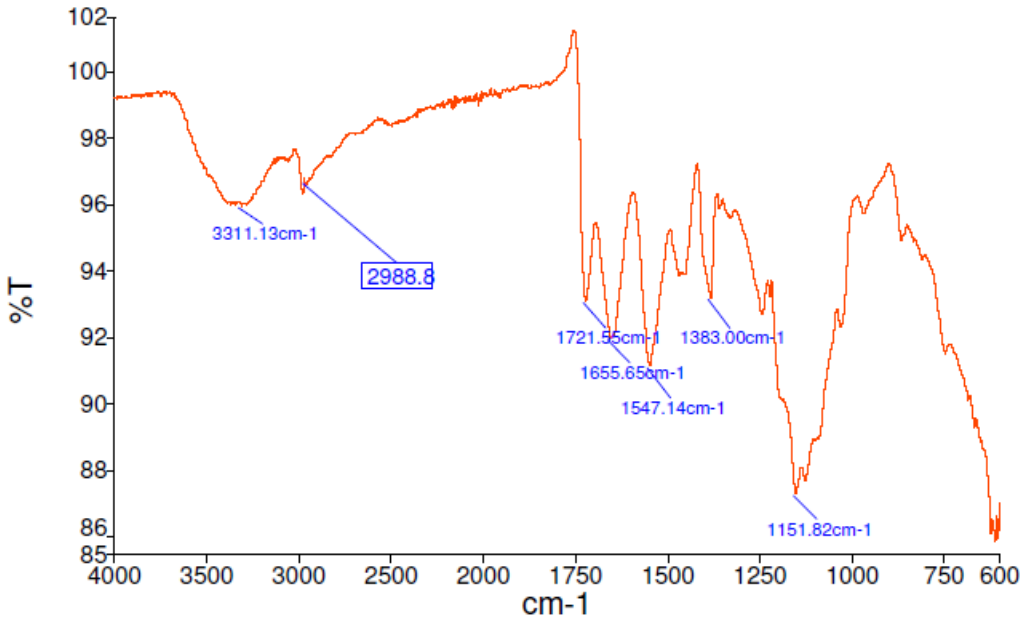

Fig. 2.29 FT-IR of MRGC 214. Main significant signals: 3311 cm^{-1} ($R_2HH_2^+$ st); 2988 cm^{-1} (NH free st); 1721, 1655 cm^{-1} (C=O st); 1547 cm^{-1} (NH **Δ**).

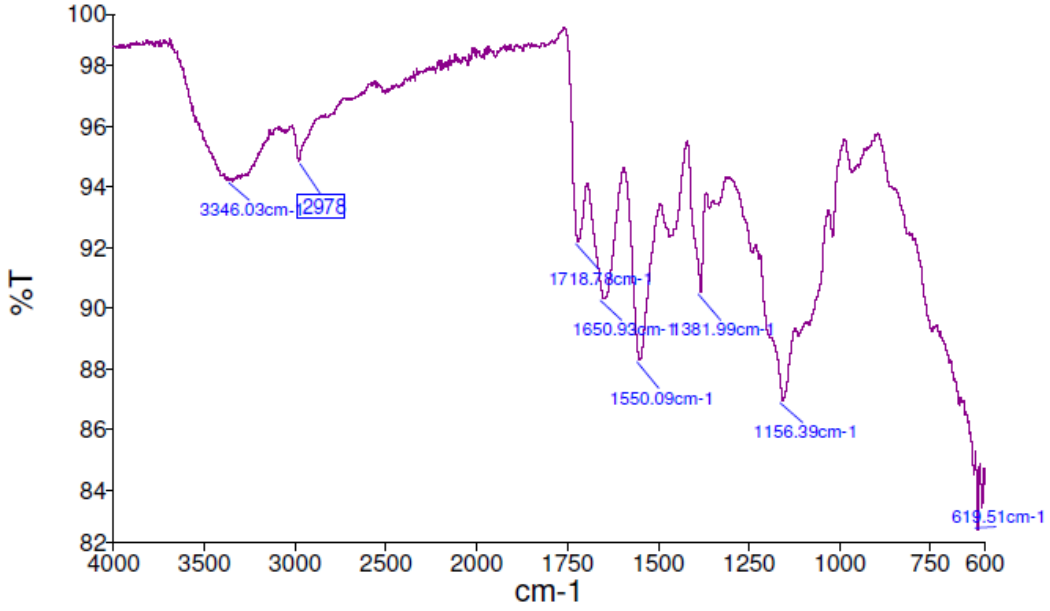

Fig. 2.30 FT-IR of MRGC 213. Main significant signals: 3346 cm^{-1} ($R_2HH_2^+$ st); 2978 cm^{-1} (NH free st); 1718, 1650 cm^{-1} (C=O st); 1550 cm^{-1} (NH **Δ**).

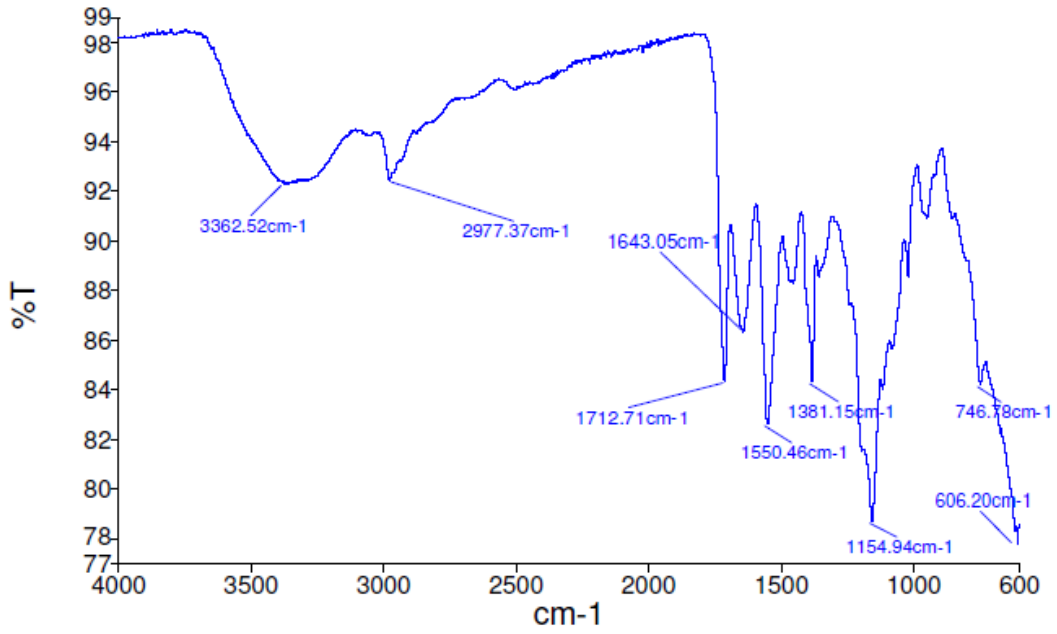

Fig. 2.31 FT-IR of MRGC 209. Main significant signals: 3362 cm^{-1} ($R_2HH_2^+$ st); 2977 cm^{-1} (NH free st); 1712, 1643 cm^{-1} (C=O st); 1550 cm^{-1} (NH **Δ**).

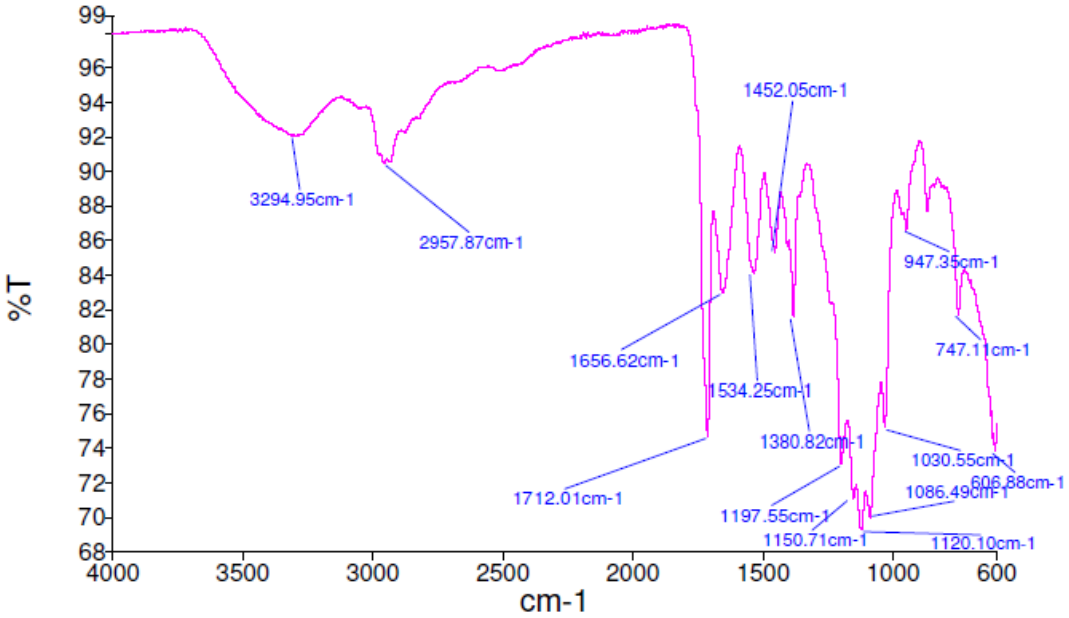

Fig. 2.32 FT-IR of MRGC 211. Main significant signals: 3294 cm^{-1} ($R_2HH_2^+$ st); 2957 cm^{-1} (NH free st); 1712, 1656 cm^{-1} (C=O st); 1534 cm^{-1} (NH **Δ**).

In all the polymers it is possible to identify the broad signal for the protonated amine (around 3300 cm^{-1}) and the streaching of the secondary amine (around 2970 cm^{-1}) from tBAEMA toghether with the ester (around 1710 cm^{-1}) and the MBA amide (around 1650 cm^{-1}) signals.

Therefore, FT-IR analysis confirmed the presence of the main functional groups within the polymer structure of nanogels. It is relevant to note that although it was not possible to resolve the peaks between 1200-1000 cm^{-1}, the nanogels MRGC 180, 211 and 214 showed a partial splitting of signals in this region (as seen in EGMMA) due to the presence of the ether group of EGMMA while MRGC 196, 209 and 213 did not show such splitting.

In order to further confirm formation of polymeric structure of nanogels it was decided to carry out proton magnetic nuclear resonance analyses.

2.2.2 Proton nuclear magnetic resonance (^{1}H-NMR)

Previosly it was mentioned that proton NMR was employed in order to to confirm completion of polymeristaion

As for the FT-IR experiments, each monomer and cross-linker were dissolved in deuterated water and characterised (Figure 2.33)

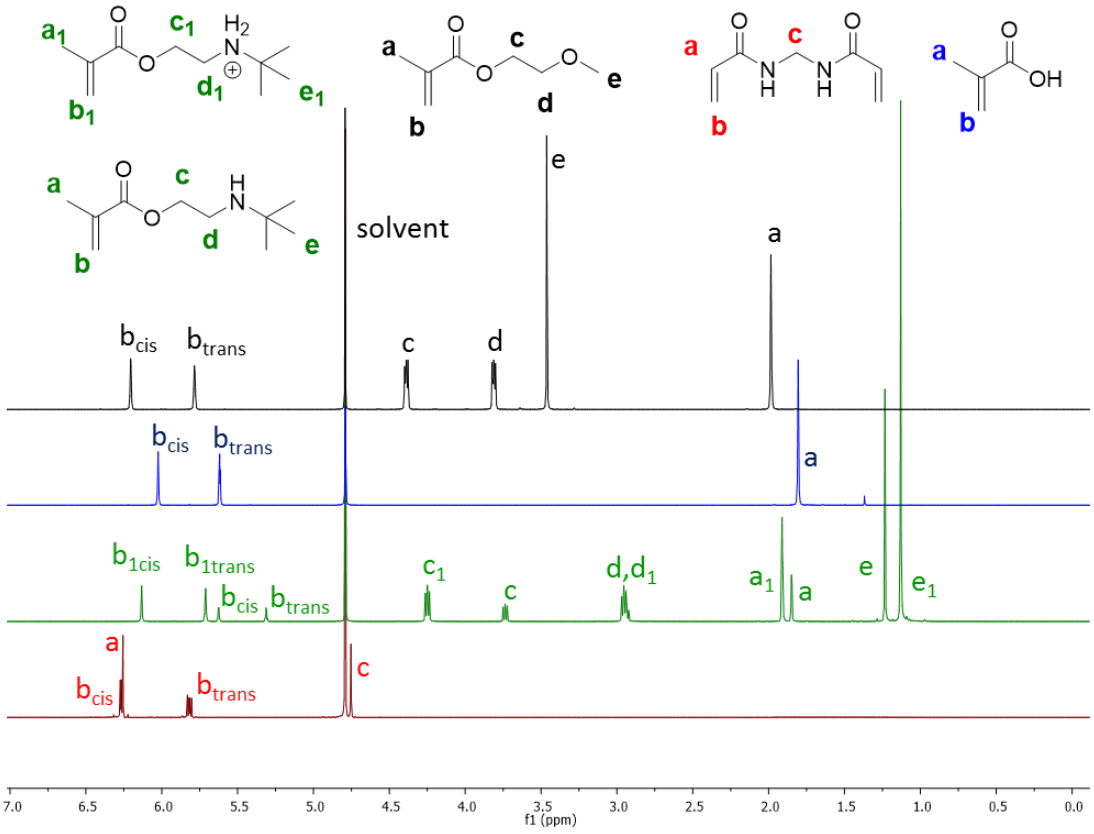

Fig. 2.33 ^{1}H-NMR assignment of monomers and cross-linker. Black EGMMA, Blue MAA, green tBAEMA and red MBA.

In a fist stage the two main preparations (MRGC 213 and MRGC 214) were characterised via ^{1}H-NMR (Figures 2.34 and 2.35).

Figure 2.34 below shows the ^{1}H-NMR characterisation for MRGC 213.

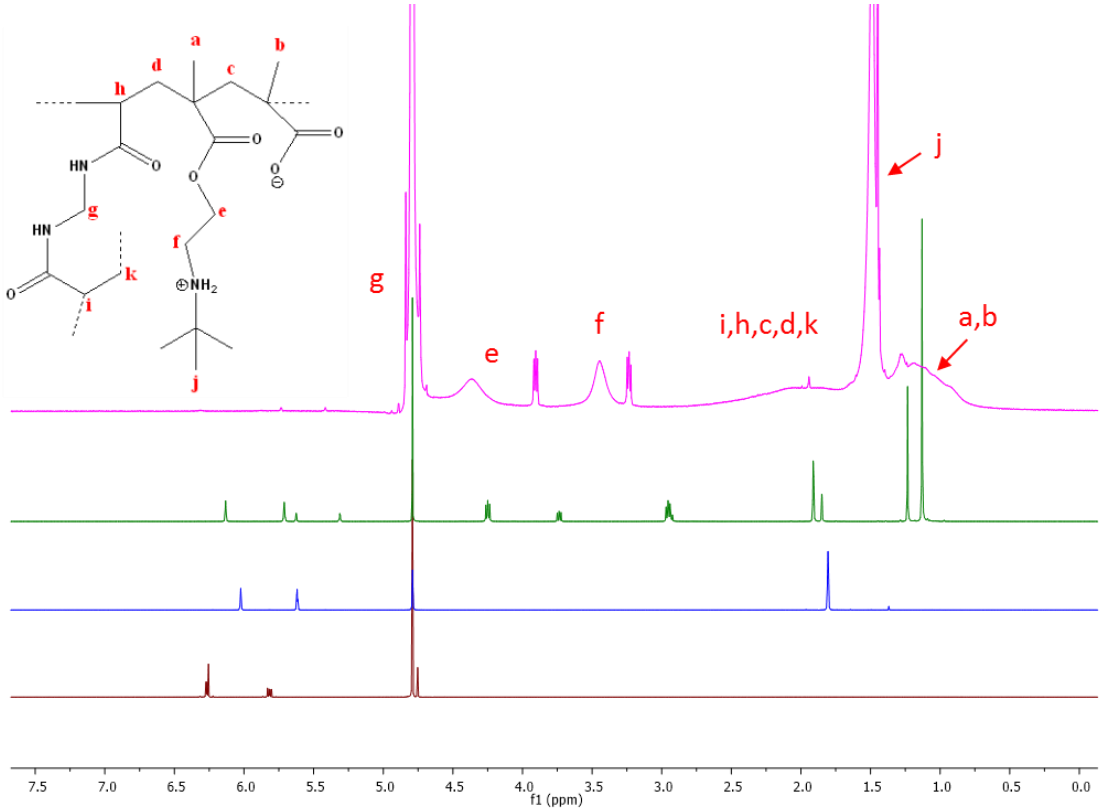

Fig. 2.34 ^{1}H-NMR assignment of MRGC 213. Magenta MRGC 213, green tBAEMA, blue MAA and red MBA.

Signals for protons attached to carbon e (4.36 and 3.90 ppm), f (3.45 and 3.23 ppm) and j (1.49 and 1.45 ppm) are present in two forms, this was due to presence of protonated and unprotonated secondary amine of tBAEMA. Moreover, there is only 0.5% trace of remaining double bond meaning that practically all the monomers had reacted to form the final cross-linked structure. Integration of peaks also reveal that monomers and cross-linker ratios were maintained durng polymerisation.

Similar results were obtained for MRGC 214 and are shown in Figure 2.35 below.

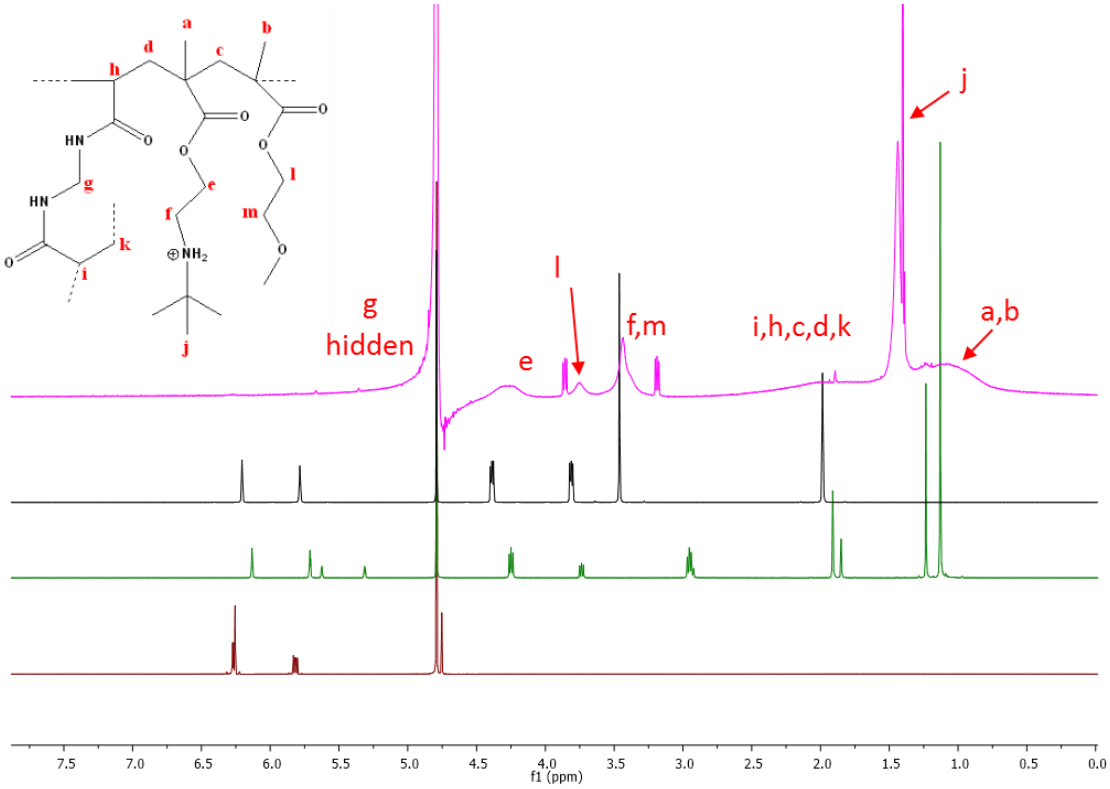

Fig. 2.35 ^{1}H-NMR assignment of MRGC 213. Magenta MRGC 214, black EGMMA, green tBAEMA and red MBA.

The chemical differences between MRGC 213 and 214 can be easily visualised in Figure 2.35 (signals l and m). In the first case MAA was employed as co-monomer while in the latter EGMMA was used. The extra signals of the 4 protons of the ethyl groups of EGMMA for MRGC 214 (protons attached to carbons l and m) are found at 3.75 pmm (2 protons from carbon l) and hidden within the signal of the 2 protons connected to carbon f which belong to the tBAEMA monomer.

Further studies involved the analyses of the fluorescent nanogels (MRGC 209 and MRGC 211). These analyses showed very similar chemical shift and spectra compared to non fluorescent nanoparticles and can be visually correlated from Figure 2.36.

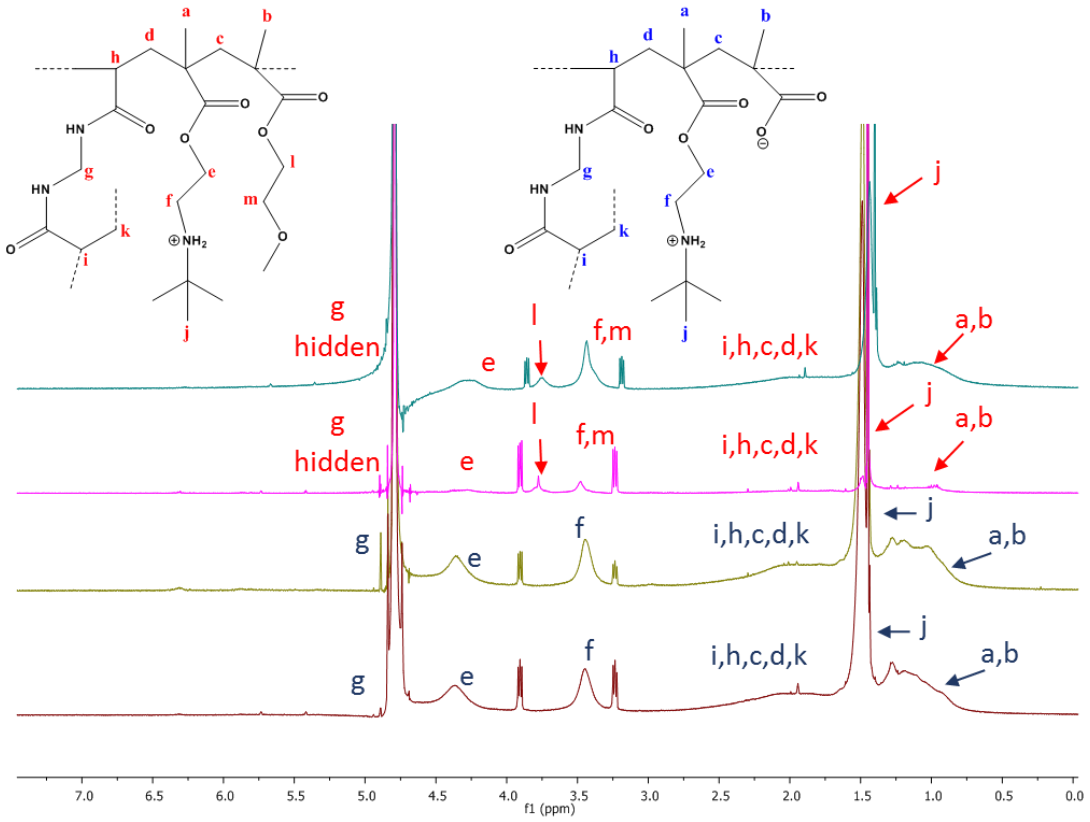

Fig. 2.36 ^{1}H-NMR assignment of fluorescent and non fluorescent nanogels. Blue MRGC 214, Magenta MRGC 211, yellow MRGC 209 and red MRGC 213.

It is important to note that due to the reduced percentage of fluorophore (5 %) and the reduced solubility of fluorescent nanogels (≤ 1 mg/mL) the signals of the fluorophore could not be detected.

The data obtained by NMR, all related to the polymers isolated following dialysis, confirmed that no monomers could be identified in the isolated nanoparticles. In the case of the non-fluorescent polymers this was further supported by a very high chemical yield of polymerisation, over 80%, while for the fluorescent polymers this was lower, as previously reported. Having confirmed the completion of reaction and formation of nanogels the next step was to analyse their particle size, solution stability and morphology via dynamic light scattering, transmission electron microscopy and emulsion formation analyses. These studies are reported in the following sections (2.2.3 - 2.2.5).

2.2.3 Dynamic Light Scattering and Zeta Potential

Previous sections of this chapter highlighted the importance of size for skin penetration. Therefore, a careful evaluation of the particle size was an important part of this work. Dynamic light scattering (DLS), also known as Photon Correlation Spectroscopy (PCS), is a widely used technique for the measurement of nanoparticles' average diameter in solution [20, 21; 32]. DLS instruments estimate hydrodynamic diameter by correlating random Brownian motion with time-dependent variation in the light scattering intensity arising from particles in solution [44, 45].

The instrument records average size using 3 different methods:

- Intensity: the contribution of each particle in the distribution relates to the intensity of light scattered by the particle. Bigger particles produce higher intensity peaks
- Volume: the contribution of each particle in the distribution relates to its volume, therefore a larger volume will give higher contribution to the analysis. This is useful from a commercial perspective as the distribution represents the sample composition in terms of its volume/mass.
- Number: each particle is given equal weighting irrespective of its size. This is the most accurate measurement, especially when considering very small nanoparticles. [45]

Figure 2.37 below provide a visual explanation of the differences between the three measurement techniques.

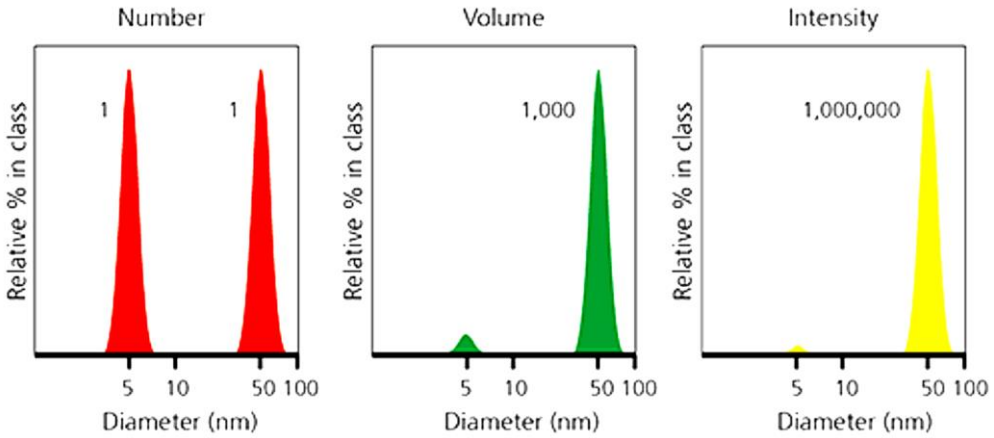

Fig. 2.37 Sample consisting of equal numbers of particles with diameters of 5 nm and 50 nm measured by number, volume and intensity. Zetasizer user manual 2013. Malvern.com

In a purely monodispersed solution, and in the absence of any large impurities such as dust, the *intensity*-size distribution, in a given DLS measurement, is most reliable. The important point to note is that in the intensity versus size plot in the DLS technique, the types of materials giving rise to the intensity are not important. The material properties are accounted for only when the intensity size distribution is converted into a *volume* or *number distribution* plots using the Mie theory. Hence the contribution to the measured intensity by each particle is only taken into account in a *volume-size* distribution plot. [Malvern Instrument, UK]

The intensity is proportional to the square of the molecular weight and in a real system, having a multimodal particle size distribution, the interpretation of the data in terms of *intensity* could be misleading. This is because a very small number of aggregates or impurities such as dust particles can dominate the intensity distribution. The data in *intensity*, *volume* or *number weight* as a function of particle size, for example, have different sensitivities, 10^6, 10^3 and 1.

For example, one million particles of 10 nm size and only **one** 100 nm will have peaks of roughly the same intensity (Figure 2.38).

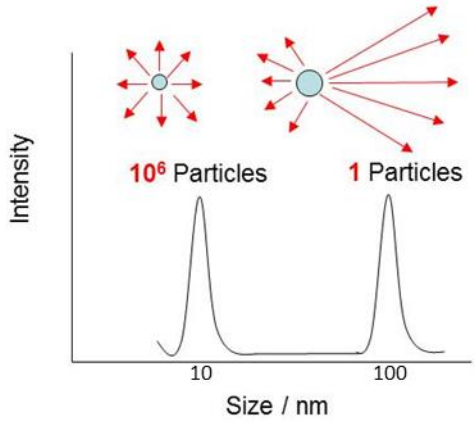

Fig. 2.38 Contribution to size distribution by intensity of particles of different hydrodynamic diameter.

Gustav Mie developed an exact solution (without any need for approximation) to Maxwell's electromagnetic equations for scattering from spheres. The solution is sensitive to smaller sizes (wide angle scatter), a different range of absorption characteristic, and only requires the refractive indexes of particle and bulk medium. [46]

Mie scattering theory (Lorenz-Mie theory) is normally applied to all the intensity data. Now the particles cannot be considered as point sources of scattered light. Destructive inferences are taken into account from light originating at different parts of our solution. Mie theory is a complete solution of Maxwell's equation for electromagnetic radiation being scattered by all the particles in a given solution. Mie scattering analysis is normally used and the data are then represented as a volume-size distribution.

In the view of this and due to reduced hydrodynamic diameter of nanogels, size distribution by number and volume were considered to be a more accurate representasion of the nanoparticle characterists. Moreover, in order to avoid operator inaccuracy or erroneous data collection and to produce significant results, all the measurements were recorded as triplicate and samples were tested randomly twice or thrice on the same day and on different days.

Results for the fluorescent and non-fluorescentformulations, summarised in Table 2.15, are shown in Figures 2.39 to 2.44.

NGs	tBAEMA	EGMMA	MAA	MAF	Solvent	Yield	Size I	Size V	Size N
MRGC 180	60%	20%	0%	0%	Water	76%	34 ± 30 nm	9 ± 5 nm	6 ± 2 nm
MRGC 214	60%	20%	0%	0%	W:Ac 1:1	86%	150 (87%) ± 64 nm	12 ± 3 nm	10 ± 2 nm
MRGC 211	55%	20%	0%	5%	W:Ac 1:1	51%	116 ± 36 nm	97 ± 35 nm	75 ± 22 nm
MRGC 196	60%	0%	20%	0%	Water	94%	45 ± 30 nm	14 ± 9 nm	9 ± 3 nm
MRGC 213	60%	0%	20%	0%	W:Ac 1:1	91%	100 (84%) ± 11 nm	11 ± 2 nm	10 ± 2 nm
MRGC 209	55%	0%	20%	5%	W:Ac 1:1	69%	78 ± 28 nm	58 ± 22 nm	45 ± 13 nm

Table 2.15 Summary of 6 preparations selected. All polymerisation at C_M 0.5% with MBA at 20%. Reaction time of 72 hours at 40 ° C for water : acetone volume ratio 1:1 and at 70 ° C for water preparations. I stands for intensity, V for volume and N for number DLS measurements. Standard deviation reported as ±.

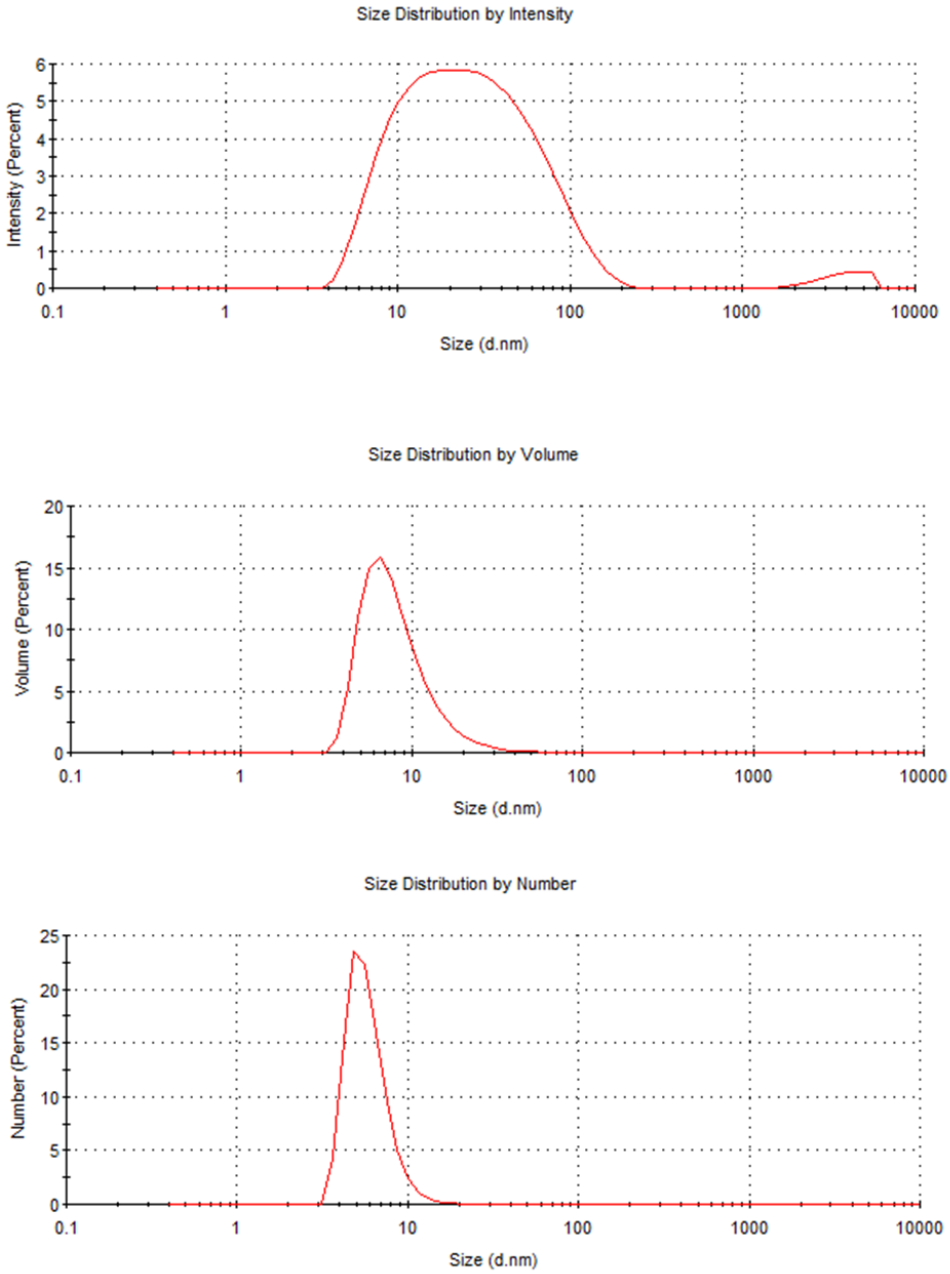

Fig. 2.39 DLS measurements of MRGC 180 by intensity volume and number (top to bottom). Polydisprsity index (Pdi): 0.40

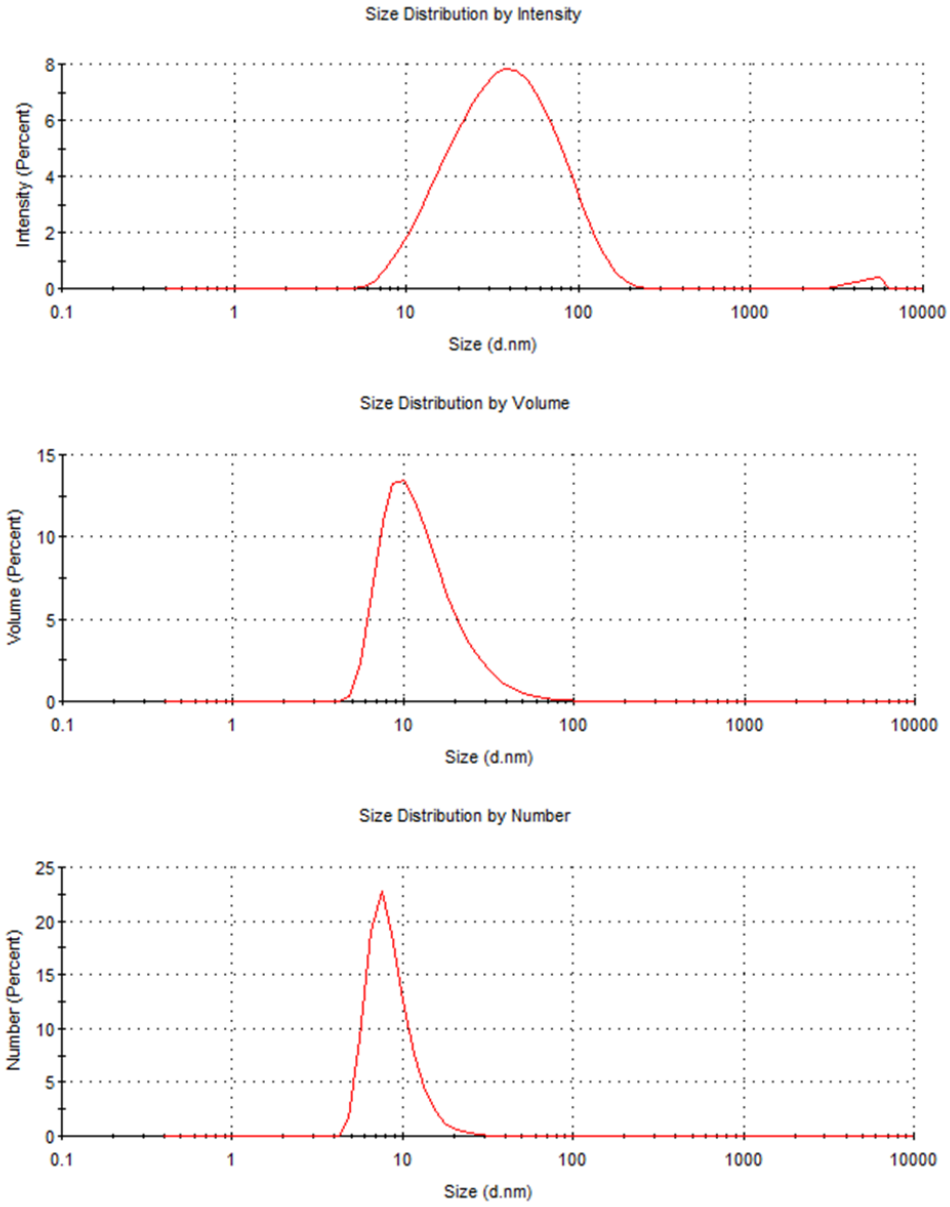

Fig. 2.40 DLS measurements of MRGC 196 by intensity volume and number (top to bottom). Pdi: 0.28

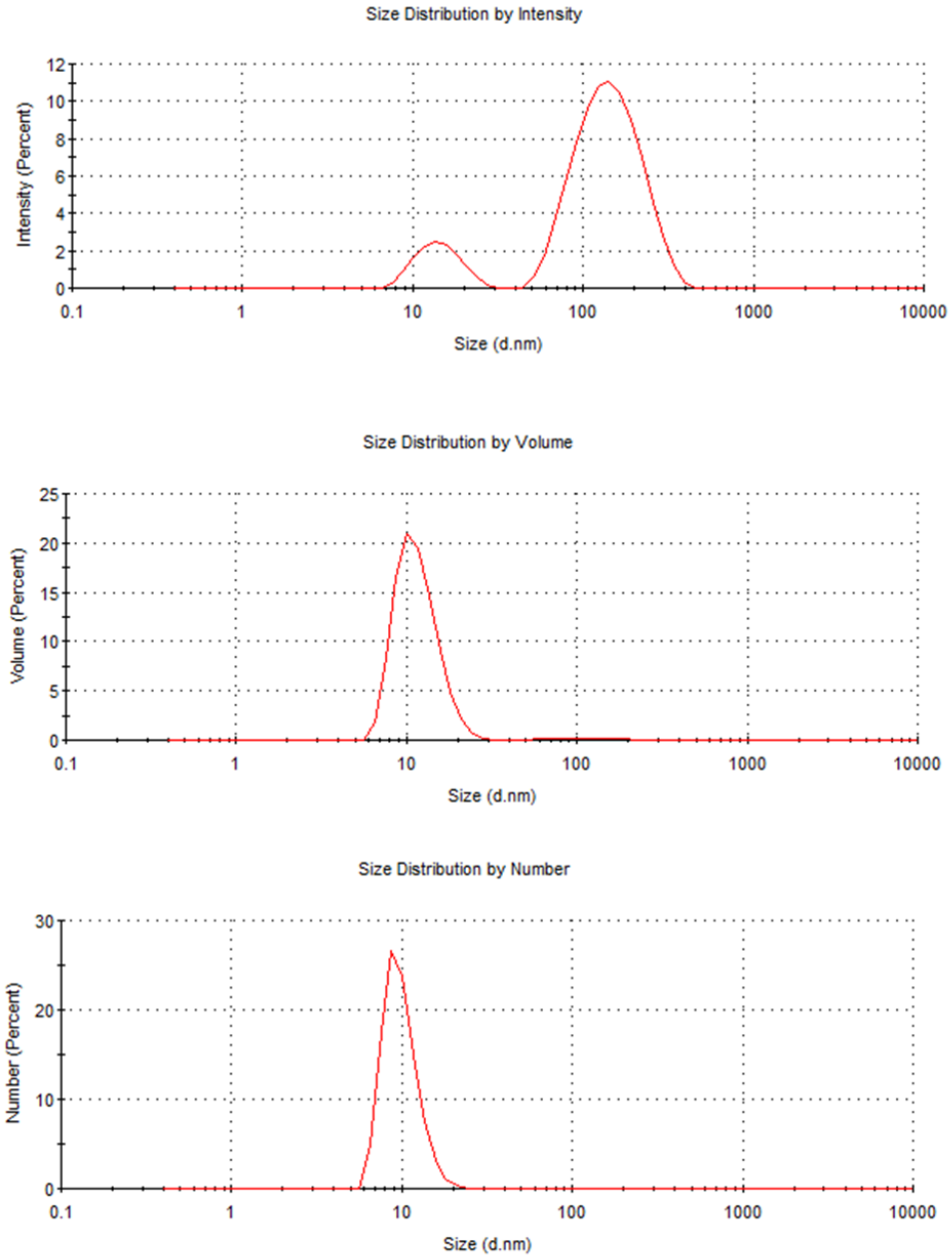

Fig. 2.41 DLS measurements of MRGC 214 by intensity number and volume (top to bottom). Pdi: 0.52

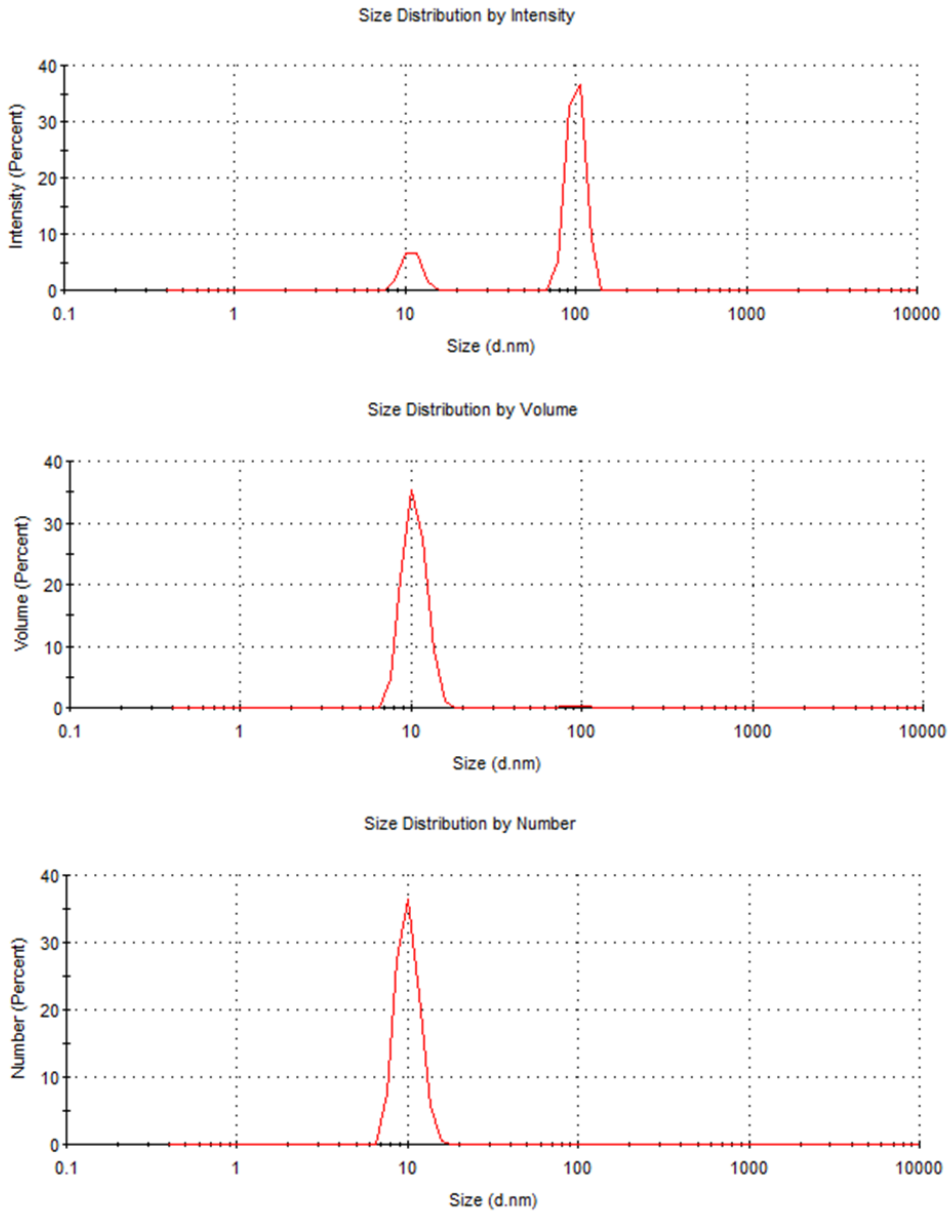

Fig. 2.42 DLS measurements of MRGC 213 by intensity volume and number (top to bottom). Pdi: 0.59

As briefly mentioned in section 2.1.3, no significant difference was found in particle size for NGs synthesised in pure water or in the 1:1 mixture of water and acetone. This could be easily visualised by comparing Figure 2.38, 2.39, 2.40 and 2.41.

The high polydispersity index (Pdi) values of these formulations can be explained considering what was previously said in this section regarding DLS measurments.

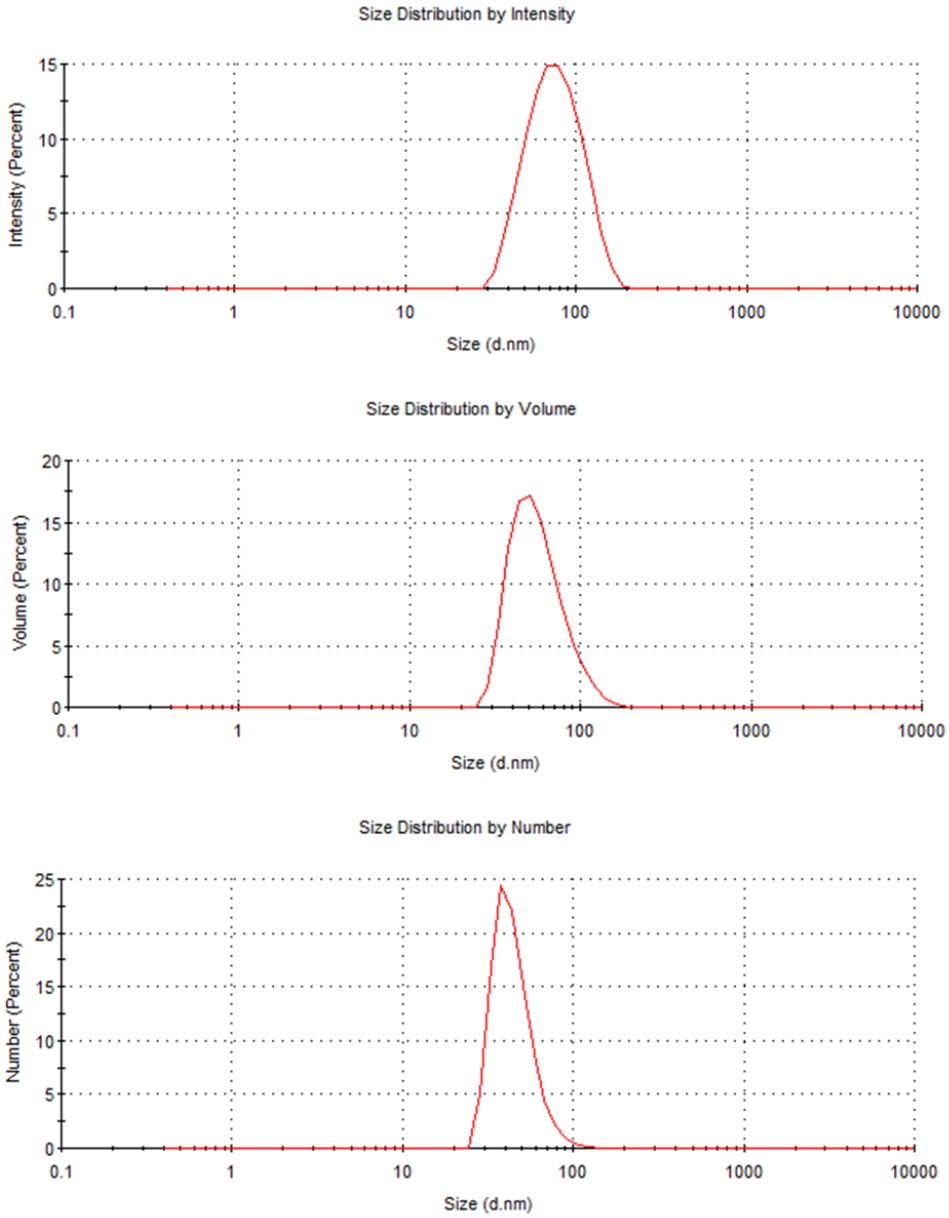

Fig. 2.43 DLS measurements of MRGC 209 by intensity volume and number (top to bottom). Pdi: 0.20

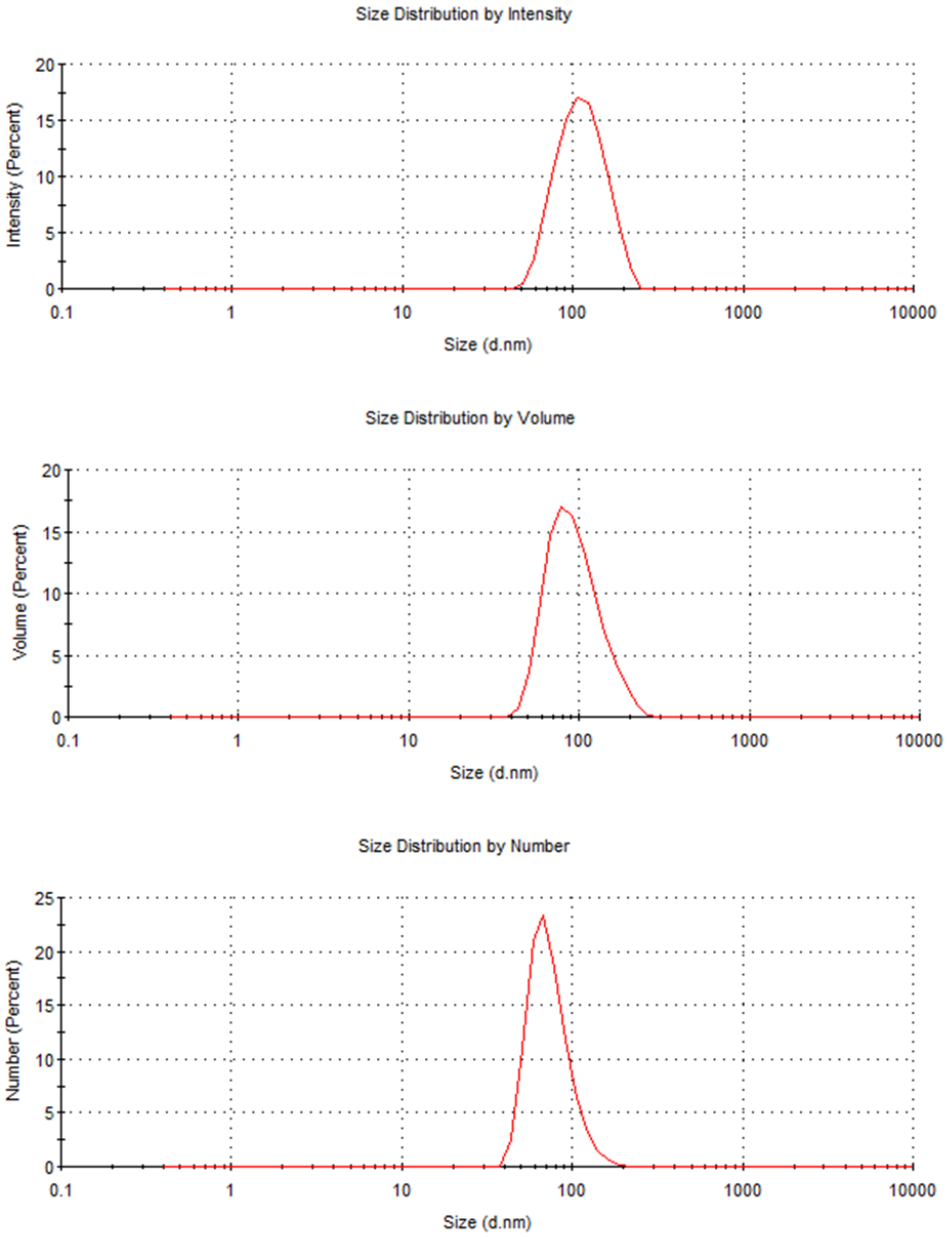

Fig. 2.44 DLS measurements of MRGC 211 by intensity volume and number (top to bottom). Pdi: 0.10.

Figures 2.42 and 2.43 showed larger hydrodynamic diameter of fluorescently labelled nanoparticles. In section 2.1.3 was in fact acknowledged that monomers polymerised in the presence of MAF resulted in formation of nanogels with lower yield and larger particle size.

After measuring particle size via DLS it was also decided to assess solution stability via Zetapotential measuremnts. These studies are reported in the following section.

2.2.4 Zetapotential

DLS instruments are generally equipped with an electrical circuit that can apply current through a solution. This is done by using a specific cuvette equipped with metallic plates on each sides which are in contact with the solution of particles. When electrical current is applied to the sample the movement of the particles is recorded by measuring the fluctuation in intensity of laser light scattered by the particles and zeta potential values are extrapolated.

Particles in solution are surrounded by charges which form two main liquid layers around them. The inner one, where ions are strongly bound with the particle, called the Stern layer and the outer diffuse region called the slipping plane where the ions are free to move. When a particle moves the charges within the slipping plane move together with it and vice versa, when an electrical potential is applied the particle is pushed by the ions surrounding its surface (Figure 2.45). Zeta potential (ζ potential) is the electrical potential difference between the Stern layer and the medium. Its value gives an indication of colloidal dispersion stability. Particles with zeta potential over +30 mV or lower than -30 mV are generally considered very stable while those with values comprised between -10 to +10 mV are considered unstable as they may tend to aggregate, flocculate or precipitate. [45]

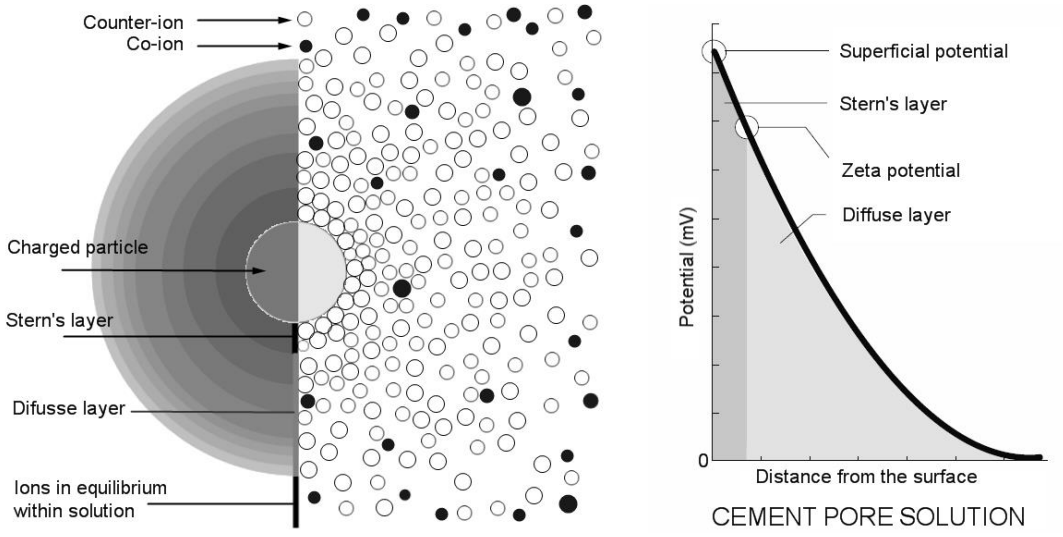

Fig. **2.45** Visual explanation of zeta potential R. Talero, C. Pedrajas and V. Rahhal (2013). Performance of Fresh Portland Cement Pastes – Determination of Some Specific Rheological

Parameters, Rheology - New Concepts, Applications and Methods, Associate Prof. Rajkumar Durairaj (Ed.), InTech, DOI: 10.5772/53761. (Open Access)

ζ-potential data, reported on Table 2.16, were the results of triplicate analyses as for particle size measurements.

NG	tBAEMA	EGMMA	MAA	MAF	Solvent	Size Volume	Size Number	Zeta
MRGC 180	60%	20%	0%	0%	Water	9 ± 5 nm	6 ± 2 nm	-33 ± 4 mV
MRGC 214	60%	20%	0%	0%	W:Ac 1:1	12 ± 3 nm	10 ± 2 nm	17 ± 3 mV
MRGC 211	55%	20%	0%	5%	W:Ac 1:1	97 ± 35 nm	75 ± 22 nm	-20 ± 5 mV
MRGC 196	60%	0%	20%	0%	Water	14 ± 9 nm	9 ± 3 nm	-21 ± 6 mV
MRGC 213	60%	0%	20%	0%	W:Ac 1:1	11 ± 2 nm	10 ± 2 nm	18 ± 7 mV
MRGC 209	55%	0%	20%	5%	W:Ac 1:1	58 ± 22 nm	45 ± 13 nm	18 ± 3 mV

Table 2.16 Summary of 6 preparations selected. All polymerisation at C_M 0.5% with MBA at 20%. Reaction time of 48 hours at 40 ° C for water:acetone volume ratio 1:1 and at 70 ° C for water preparations. Standard deviation reported as ±.

Focusing the attention on non-fluorescent particles, data suggested that the reaction environment played an important role in assembly of the polymer chains. Polymersitaion performed in water led to production of systems with negative ζ-potential while water : acetone (1:1) environment produced particles characterised by positive ζ-potential (Table 2.17). These results were further confirmed by polymerisation replicates wich returned comparable values.

NG	tBAEMA	EGMMA	MAA	MBA	C_M	Solvent	Zeta
MRGC 180	60%	20%	0%	20%	0.5%	Water	-33 ± 4 mV
MRGC 214	60%	20%	0%	20%	0.5%	W:Ac 1:1	17 ± 3 mV
MRGC 196	60%	0%	20%	20%	0.5%	Water	-21 ± 6 mV
MRGC 213	60%	0%	20%	20%	0.5%	W:Ac 1:1	18 ± 7 mV

Table 2.17 ζ-potential comparison of nanogels produced in water and in mixture water : acetone 1:1.

Different solvent environments may induce different intermolecular interaction between monomers and crosslinker which resulted in diverse disposition within the nanogel network leading to different charge disposition around he particles.

Although dynamic light scattering (DLS) is an extensively used procedure that provides reliable results, it is always good practise to confirm the data obtained with additional analytical techniques. Moreover, DLS alone does not provide any information regarding nanoparticles morphology. It was therefore decided to pair DLS measurements with high resolution microscopy techniques, in particular with transmission electron microscopy. These analyses are reported in the following section.

2.2.5 Transmission Electron Microscopy

Transmission electron microscopy (TEM) is an extensively used and powerful technique to obtain highly magnified images of materials at a scale close to atomic level [47-49]. A focalised electron bean is transmitted to a support where the material is cast and by adsorbing part of the energy the material produces a contrasted area that is recorded as an image by a photographic device such as a CCD camera [50, 51]. TEM was therefore employed to gain information of nanogels morphology and to confirm DLS measurements. Moreover, by comparing TEM and DLS data it is also possible to gain information on NPs behaviour in solution and at the solid state.

Below are reported images from the 6 selected nanogels' preparations. All the images were taken using carbon oxide coated copper grids as support and without staining samples with contrast agents. The use of contrast agents was avoided due to the porous nature of nanogels that could lead to staining leakage which could then results in false positive assessments.

Nanogel MRGC 180 was one of the first preparation analysed (Figure 2.46). Pictures recorded showed that at the dry state particles had a tendency to aggregate into small cluster of 3 to 5 particles on average. However, their individual diameter appeared to be in line with DLS measurements.

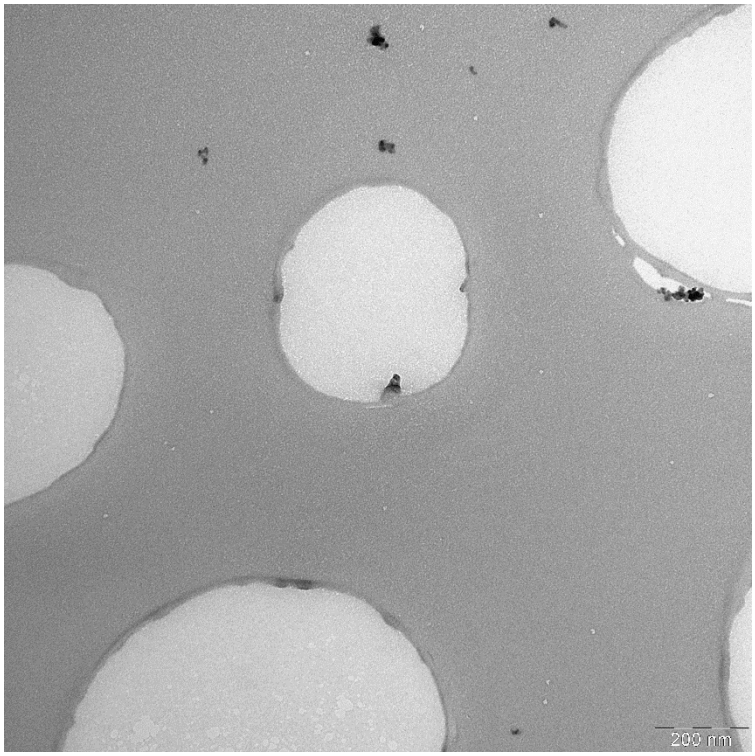

Fig. **2.46** TEM image of MRGC 180 at 1 mg/mL, scale bar 200 nm. Provided by Dr. Giulia Mastroianni.

Also NG MRGC 214 showed a similar cluster behaviour even though the number of particles was found to be higher and the individual particles could be more easily resolved (Figure 2.47).

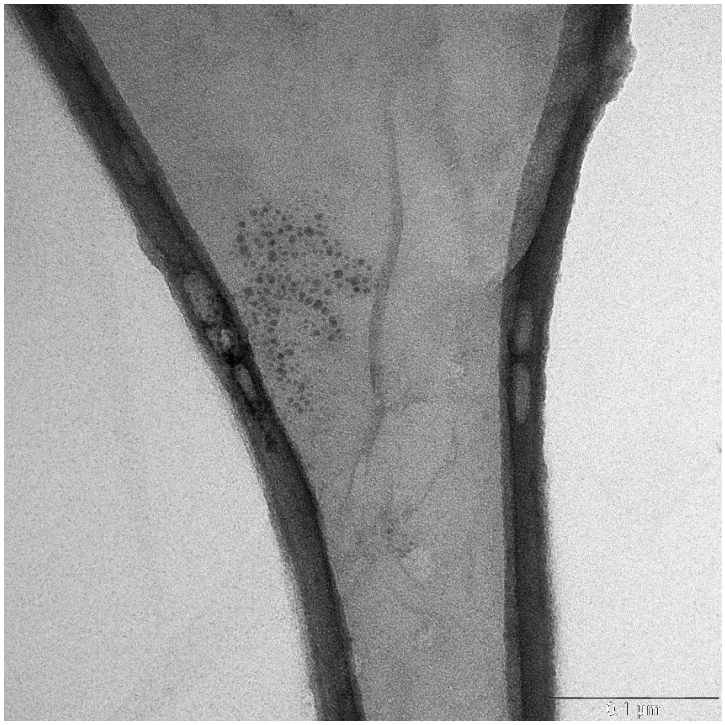

Fig. **2.47** TEM image of MRGC 214 at 1 mg/mL, scale bar 100 nm. Provided by Dr. Giulia Mastroianni.

As noted in previously performed DLS analyses, particle size of fluorescent nanogels appeared to be larger compared to non-labelled ones (MRGC 180 and MRGC 214), this can be seen by comparing Figure 2.45 and 2.46 with the image below (Figure 2.48).

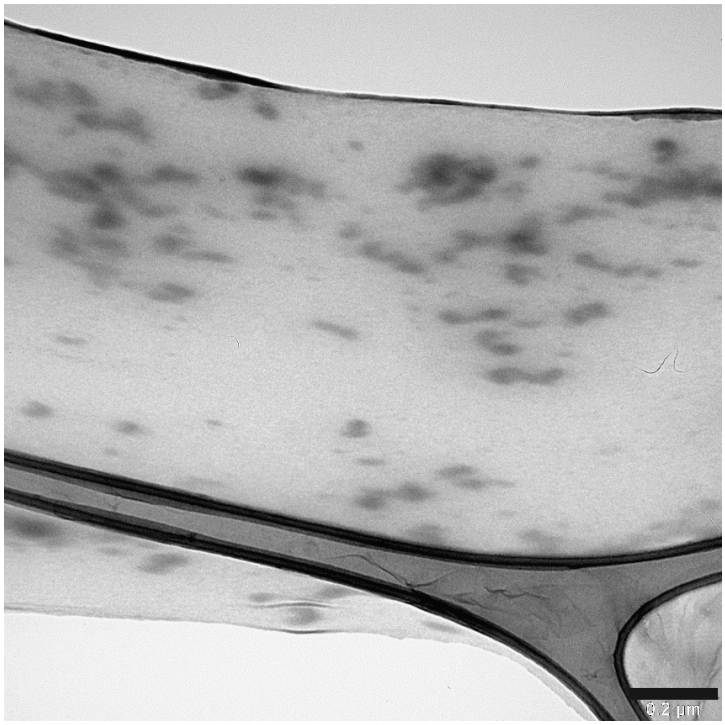

Fig. **2.48** TEM image of MRGC 211 at 1 mg/mL, scale bar 200 nm. Provided by Dr. Giulia Mastroianni.

Similar to MRGC180 and MRGC214 formation of cluster, in the dry state, were also observed for MRGC 196 (Figure 2.49). However, in this case clusters formed appeared to be constituted by a larger number of particles and characterised by high density.

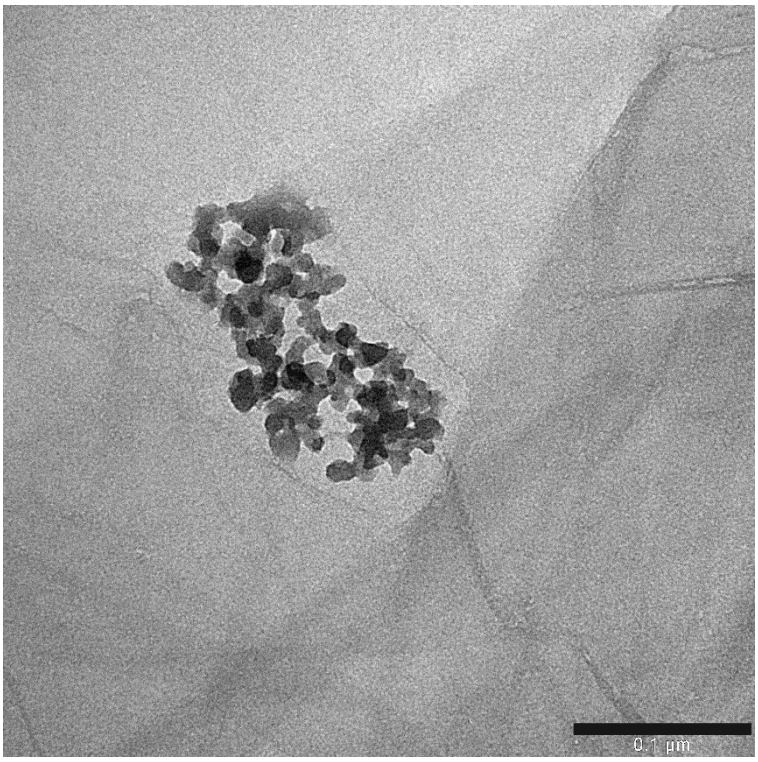

Fig. **2.49** TEM image of MRGC 196 at 1 mg/mL, scale bar 100 nm. Provided by Dr. Giulia Mastroianni

Nevertheless, this aggregation behaviour could potentially be limited using different techniques or a combination of them. Sonicating the water solution containing the nanogels for longer than 2 minutes (time used for the analysis herein reported) before casting onto TEM grids as well as reducing nanoparticles concentration could be good approaches to resolve clustering. Another way would be the employment of different drying methods. Solutions cast onto grids were in fact dried by first removing water excess by placing filter paper perpendicularly on the side of the grids. Then they were allowed to dry for few minutes at normal temperature and pressure conditions, although drying could have also been achieved with the aid of air or nitrogen flow or under vacuum. The casting procedure, described before, was previously developed and used by the group for acrylamide based nanogels. However, the nanoparicles in this study may have needed a different casting technique to optimise particles separation that due to time and resources constrains could not be performed on all nanogels.

A solution of MRGC 214 was therefore prepared by applying a combination of the previously mentioned propositions, in order to prove that clusters imaged were indeed particles' aggregates and to demonstrate the possibility to disaggregate these nanogels clumps. Sonication time was increased from 2 to 10 minutes and nanoparticles concentration decreased from 1 to 0.25 mg per mL. This new protocol resulted successful, in fact, although in the image below it can still be seen a small percentage of clusters (top left), the majority of particles appear separated (Figure 2.50).

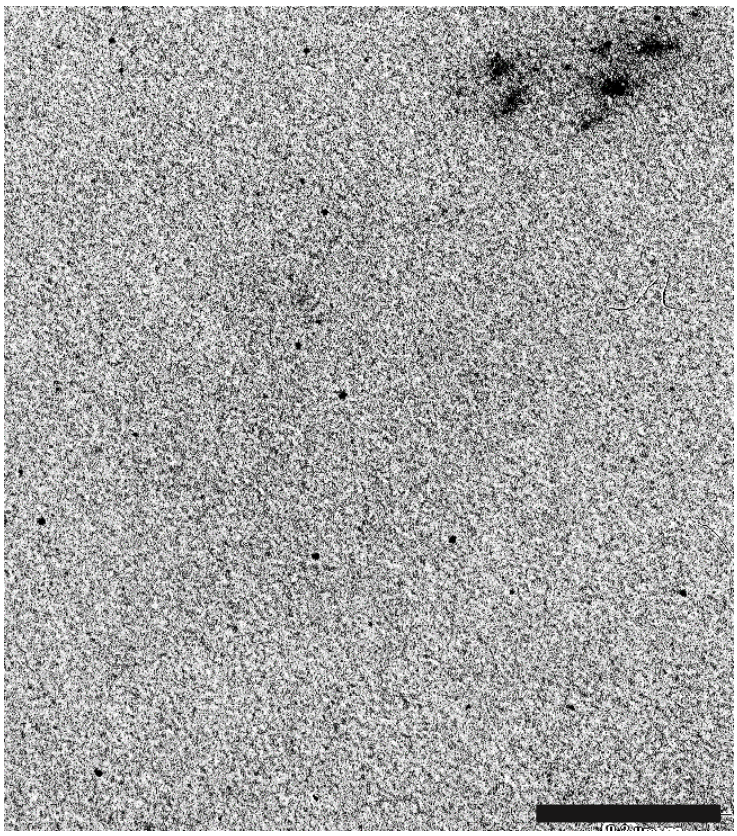

Fig. **2.50** TEM image of MRGC 214 at 0.25 mg/mL, scale bar 200 nm. Sonicated for 10 minutes. Provided by Dr. Giulia Mastroianni

Another method, based on a reported technique [52], for the avoidance of drying artefacts was tested simultaneously by using a MRGC 214 solution prepared following the same procedure as for the solution used for image 2.50. This technique involves the use of bovine serum albumin (BSA), a macromolecule invisible to the TEM that is able to form a corona layer around particles limiting their aggregation during drying. Figure 2.51 reported below shows the effect of BSA on a solution of MRGC 214 at a final

concentration of 0.5 mg per mL with BSA at a final concentration of 0.25 mg per mL of water.

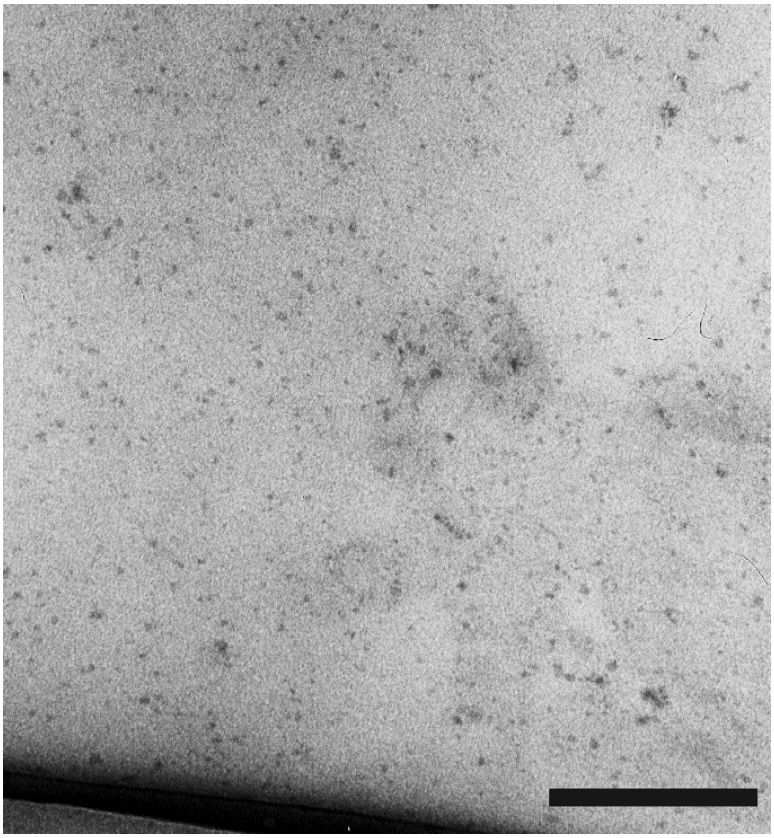

Fig. **2.51** TEM image of MRGC 214 at 0.5mg/mL plus BSA at 0.25 mg/mL, scale bar 200 nm. Sonicated for 10 minutes. Provided by Dr. Giulia Mastroianni

MRGC 213 together with MRGC 209 showed the best results in terms of particles separations (Figure 2.52 and 2.53) without the need to use any of the techniques previously described to resolve MRGC 214 clustering.

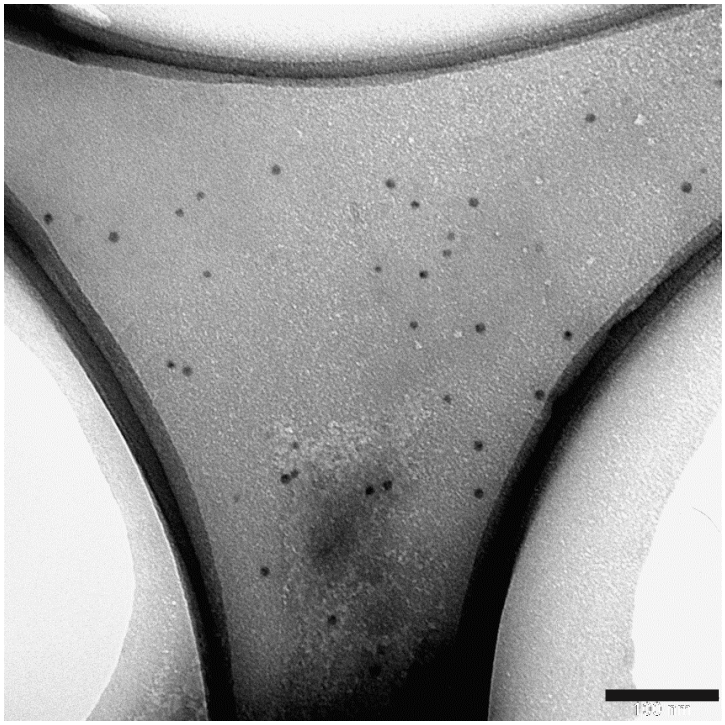

Fig. **2.52** TEM image of MRGC 213 at 1 mg/mL, scale bar 100 nm. Provided by Dr. Giulia Mastroianni

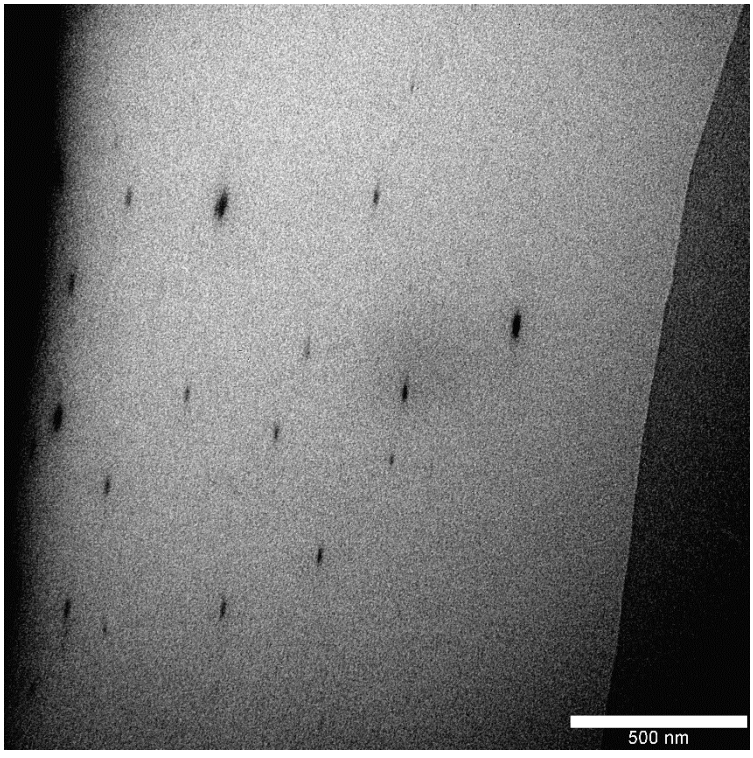

Fig. **2.53** TEM image of MRGC 209 at 1 mg/mL, scale bar 500 nm. Provided by Dr. Giulia Mastroianni

As seen from DLS measurements and as well as previously noted for MRGC 211, particle size of labelled nanogel MRGC 209 was confirmed to be in the range 70-100nm, which was significantly larger than non-fluorescent nanoparticles.

In conclusion TEM images confirmed results obtained with dynamic light scattering technique. Moreover, it was shown that nanogels produced in acetone: water (1:1) mixture were characterised by more homogenous and shape defined structures. In particular nanoparticles containing methacrylic acid as co-monomer (MRGC 209 and MRGC 213) did not show signs of particles' clustering, probably due to their higher solubility in water.

Given the requirements for skin delivery MRGC 213 and MRGC 214 were selected as the best candidates for transdermal application and further tested to assess their cytotoxity profile which is reported in chapter 4.

2.3 **Conclusions**

In this chapter the work towards the development of new nanogels with the ideal characteristics to be suitable for dermal drug delivery was described. In particular, the features that were being targeted were: small particle size, lower than 40nm, and good water solubility (equal or greater than 2 mg/mL).

A very significant part of the work was the identification of suitable monomers to be included in the polymer formulation. Nanogel production attempts included the use of tert-buthylamminoethyl methacrylate (tBAEMA), ethylene glycol methyl ether methacrylate (EGMMA), diethylamminoethyl methacrylate (DEAEMA) and methacrylic acid (MAA) as monomers and N,N'-methylenebis(acrylamide) (MBA) as crosslinker.

After considerable work on screening polymerisations, nanoparticles containing tert-buthylamminoethyl methacrylate as functional monomer and either ethylene glycol methyl ether methacrylate or methacrylic acid as co-monomers were identified as the most suitable formulations

In particular, nanogels. MRGC 213 and MRGC 214, best fitted the before mentioned requirements They were constituted by a molar ratio 60% of tBAEMA, 20% of MBA and 20% of either MAA or EGMMA respectively. These nanoparticles were synthesised in a mixture water acetone (1:1 v/v), under nitrogen atmosphere, via high dilution radical polymerisation (C_M 0.5%) and in the presence of APS, as initiator, set at a molar concentration of 5% of the overall monomers and cross-linker double bounds. The nanogels were characterised via FT-IR, H-NMR, DLS, Zetapotential measurement and TEM microscopy showing size lower than 20 nm and solubility greater than 3 mg/mL.

In section 2.1.2 was mentioned the use of *tert*-buthylamino ethyl methacrylate (tBAEMA) to confer emulsion capabilities to nanoparticles. In the view of this, nanogels were tested in order to evaluate their emulsion stabilising characteristics. Preliminary data on emulsion formation and disruption are described in the following sections.

References

1. D. A. Heller, Y. Levi, J. M. Pelet, J. C. Doloff, J. Wallas, G. W. Pratt, S. Jiang, G. Sahay, A. Schroeder, J. E. Schroeder, Y. Chyan, C. Zurenko, W. Querbes, M. Manzano, D. S. Kohane, R. Langer; D. G. Anderson. Modular 'Click-in-Emulsion' Bone-Targeted Nanogels. *Adv. Mater.* **2013**, 25, 1449-1454.
2. J. PK Tan, M. BH Tan; M. KC Tam. Application of nanogel systems in the administration of local anesthetics. *Local. Reg. Anesth.*, **2010**, 3, 93-100.
3. N. Sanoj Rejinold, T. Baby, K.P. Chennazhi, R. Jayakumar. Dual drug encapsulated thermo-sensitive fibrinogen-graft-poly(N-isopropyl acrylamide) nanogels for breast cancer therapy. *Colloid. Surface B*, **2014**, 114, 209-217.
4. B. Baroli. Penetration of Nanoparticles and Nanomaterial in the skin: Fiction or Reality? *J. Pharm. Sci*., **2010,** 99, 21-50.
5. C. Pegoraro, S. MacNeil; G. Battaglia. Transdermal drug delivery: from micro to nano. *Nanoscale*, **2012**, 4, 1881–1894.
6. A. Vogt, B. Combadiere, S. Hadam, K. M. Stieler, J. Lademann, H. Schaefer, B. Autran, W. Sterry; U. Blume-Peytavi. 40 nm, but not 750 or 1,500 nm, Nanoparticles Enter Epidermal CD1aþ Cells after Transcutaneous Application on Human Skin. *J. Invest. Dermatol.*, **2006**, 126, 1316-1322.
7. H. I. Labouta, L. K. El-Khordagui, T. Krausc; M. Schneider. Mechanism and determinants of nanoparticle penetration through human skin. *Nanoscale*, **2011**, 3, 4989-4999.
8. A. Servant, K. Haupt; M. Resmini. Tuning Molecular Recognition in Water-Soluble Nanogels with Enzyme-Like Activity for the Kemp Elimination. *Chem. Eur. J.*, **2011**, 17, 11052-11059.
9. A. R. Jorge, M. Chernobryva, S. E. J. Rigby, M. Watkinson; M. Resmini. Incorporation of Cobalt-Cyclen Complexes into Templated Nanogels Results in Enhanced Activity. *Chem. Eur. J.*, **2016**, 22, 3764-3774.
10. N. B. Graham; A. Cameron. Nanogels and microgels: The new polymeric materials playground. *Pure & Appl. Chem.***, 1998,** 70, 1271-1275.
11. E. Fröhlich. The role of surface charge in cellular uptake and cytotoxicity of medical nanoparticles. *Int. J. Nanomed.*, **2012**, 7, 5577-5591.
12. F. Alexis, E. Pridgen, L. K. Molnar; O. C. Farokhzad. Factors Affecting the Clearance and Biodistribution of Polymeric Nanoparticles. *Mol. Pharmaceutics*, **2008**, *5*(4), 505-515.
13. R. A. Stile, W. R. Burghardt; K. E. Healy. Synthesis and Characterization of Injectable Poly(N-isopropylacrylamide)-Based Hydrogels That Support Tissue Formation in Vitro. *Macromolecules*, **1999**, 32, 7370-7379.
14. O. Okay; W. Oppermann. Polyacrylamide-Clay Nanocomposite Hydrogels: Rheological and Light Scattering Characterization. *Macromolecules*, **2007**, 40, 3378-3387.

15. A. Kumar, G. Sharma, M. Naushad, P. Singh; S. Kalia. Polyacrylamide/Ni0.02Zn0.98O Nanocomposite with High Solar Light Photocatalytic Activity and Efficient Adsorption Capacity for Toxic Dye Removal. *Ind. Eng. Chem. Res.,* **2014**, 53, 15549-15560.
16. A. J. Morse, D. Dupin, K. L. Thompson, S. P. Armes, K. Ouzineb, P. Mills; R. Swart. Novel Pickering Emulsifiers based on pH-Responsive Poly(tert-butylaminoethyl methacrylate) Latexes. *Langmuir* **2012**, 28, 11733-11744.
17. A. Pikabea, J. Ramos; J. Forcada. Production of Cationic Nanogels with Potential Use in Controlled Drug Delivery. *Part. Part. Syst. Charact.* **2014**, *31*, 101–109.
18. L. Hou, K. Ma, Z. An; P. Wu. Exploring the Volume Phase Transition Behavior of POEGA- and PNIPAM-Based Core−Shell Nanogels from Infrared-Spectral Insights. *Macromolecules* **2014**, 47, 1144-1154.
19. P. Pasetto, S. C. Maddock; M. Resmini. Synthesis and characterization of molecularly imprinted catalytic microgels for carbonate hydrolysis. *Anal. Chim. Acta*, **2005**, 542, 66-75.
20. A. J. Morse, S. P. Armes, K. L. Thompson, D. Dupin, L. A. Fielding, P. Mills; R. Swart. Novel Pickering Emulsifiers based on pH-Responsive Poly(2-(diethylamino)ethyl methacrylate) Latexes. *Langmuir*, **2013**, 29, 5466-5475.
21. J. Tang, M. F. X. Lee, W. Zhang, B. Zhao, R. M. Berry; K. C. Tam. Dual Responsive Pickering Emulsion Stabilized by Poly[2-(dimethylamino)ethyl methacrylate] Grafted Cellulose Nanocrystals. *Biomacromolecules*, **2014**, 15, 3052−3060.
22. J. Burke. Solubility Parameters: Theory and Application. *The Book and Paper Group Annual*, **1984.** Independent publication.
23. H. J. Vandenburg, A. A. Clifford, K. D. Bartle, R. E. Carlson, J. Carroll; I. D. Newton. A simple solvent selection method for accelerated solvent extraction of additives from polymers. *Analyst*, **1999**, 124, 1707-1710.
24. Alan Y. Kwok, Greg G. Qiao, David H. Solomon. Synthetic hydrogels 3. Solvent effects on poly(2-hydroxyethyl methacrylate) networks. *Polymer,* **2004**, 45, 4017-4027.
25. Y. Nagasaki, T. Yamazaki, A. Kikuchi; M. Harada-Shiba. Elevated atherogenic index following oral administration of quaternized polyamine nanogels. *Colloid. Surface. B* **2014**, 113, 237-242.
26. S.Yusa, M. Sugahara, T. Endo; Y. Morishima. Preparation and Characterization of a pH-Responsive Nanogel Based on a Photo-Cross-Linked Micelle Formed From Block Copolymers with Controlled Structure. *Langmuir,* **2009,** 25(9), 5258-5265.
27. Q. Jin, G. Liu; J. Ji. Preparation of reversibly photo-cross-linked nanogels from pH-responsive block copolymers and use as nanoreactors for the synthesis of gold nanoparticles. *Eur. Polym. J.*, **2010**, 46, 2120-2128.
28. W. B. Liechty, R. L. Scheuerle; N. A. Peppas. Tunable, responsive nanogels containing t-butyl methacrylate and 2-(t-butylamino)ethyl methacrylate. *Polymer,* **2013**, 54, 3784-3795.

29. T. N. Nekrasova, L.N. Andreeva, O. V. Nazarova, M. A. Bezrukova, Y. I. Zolotova, R. T. Imanbaev, O. V. Skorbunova, V. D. Pautov; E. F. Panarin. Structural and dynamic characteristics of thermo- and pH-sensitive copolymers of 2-(diethylamino)ethyl methacrylate and 2-deoxy-2- methacrylamido-D-glucose. *Polymer*, **2015**, 77, 246-253.
30. T. Wang, J. Jiang, Y. Xiao, Y. Zou, J. Gaoa; J. Du. Preparation of polymersomes in pure water for facile antibacterial applications. *RSC Adv.,* **2015**, 5, 55602-55607.
31. J. Marra, A. G. Paleari, L. S. Rodriguez, A. R. P. Leite, A. C. Pero; M. A. Compagnoni. Effect of an acrylic resin combined with an antimicrobial polymer on biofilm formation. *J Appl Oral Sci.,* **2012**, 20(6), 643-648.
32. A. J. Morse, J. Madsen, D. J. Growney, S. P. Armes, P. Mills; Ron Swart. Microgel Colloidosomes Based on pH-Responsive Poly(tert-butylaminoethyl methacrylate) Latexes. *Langmuir,* **2014**, 30, 12509-12519.
33. M. P. Robin, J. E. Raymond; R. K. O'Reilly. One-pot synthesis of super-bright fluorescent nanogel contrast agents containing a dithiomaleimide fluorophore. *Mater. Horiz.,* **2015**, 2, 54-59.
34. A. B. Chinen, C. M. Guan, J. R. Ferrer, S. N. Barnaby, T. J. Merkel; C.A. Mirkin. Nanoparticle Probes for the Detection of Cancer Biomarkers, Cells, and Tissues by Fluorescence. *Chem. Rev.,* **2015**, 115, 10530-10574.
35. M. P Robin; R. K O'Reilly. Strategies for preparing fluorescently labelled polymer nanoparticles. *Polym. Int.,* **2015**, 64, 174-182.
36. O. S. Wolfbeis. An overview of nanoparticles commonly used in fluorescent bioimaging. *Chem. Soc. Rev.,* **2015**, 44, 4743-4768.
37. S. Lombardi Borgia, M. Regehly, R. Sivaramakrishnan, W. Mehnert, H. C. Korting, K. Danker, B. Röder, K. D. Kramer; M. Schäfer-Korting. Lipid nanoparticles for skin penetration enhancement—correlation to drug localization within the particle matrix as determined by fluorescence and parelectric spectroscopy. *J. Control. Release,* **2005**, 110, 151–163.
38. X.Ton, B. Tse Sum Bui, M. Resmini, P. Bonomi, I. Dika, O. Soppera; Karsten Haupt. A Versatile Fiber-Optic Fluorescence Sensor Based on Molecularly Imprinted Microstructures Polymerized in Situ. *Angew. Chem. Int. Ed.*, **2013**, 52, 8317-8321.
39. M. Sierant, S. Kazmierski, A. Rozanski, P. Paluch, U. Bienias; B. J. Miksa. Nanocapsules for 5-fluorouracil delivery decorated with a poly(2-ethylhexyl methacrylateco-7-(4-trifluoromethyl)coumarin acrylamide) cross-linked wall. *New J. Chem.,* **2015**, 39, 1506-1516.
40. Y. Kang, A. Lu, A. Ellington, M. C. Jewett; R. K. O'Reilly. Effect of Complementary Nucleobase Interactions on the Copolymer Composition of RAFT Copolymerizations. *ACS Macro Lett.* **2013**, 2, 581−586.
41. M. P. Robin, P. Wilson, A. B. Mabire, J. K. Kiviaho, J. E. Raymond, D. M. Haddleton; R. K. O'Reilly. Conjugation-Induced Fluorescent Labeling of Proteins and Polymers Using Dithiomaleimides. *J. Am. Chem. Soc.*, **2013**, 135, 2875−2878.

42. M. P. Robin; Rachel K. O'Reilly. Fluorescent and chemico-fluorescent responsive polymers from dithiomaleimide and dibromomaleimide functional monomers. *Chem. Sci.,* **2014**, 5, 2717-2723.
43. S. C. Maddock. Synthesis and characterization of novel imprinted microgels with hydrolytic catalytic activity. PhD thesis, **2002**.
44. D. Arzenšek, R. Podgornik, D. Kuzman. Dynamic light scattering and application to proteins in solutions. Seminar from the University of Ljubljana, **2010**.
45. Zetasizer Nano user manual. Malvern **2013**.
46. D. Arzensek, Dynamic Light Scattering and Application to Proteins in Solutions, Seminar for University of Ljubljana, **2010**, 1–18.
47. J. P. Patterson, A. M. Sanchez, N. Petzetakis, T. P. Smart, T. H. Epps, I. Portman, N. R. Wilson; R. K. O'Reilly. A simple approach to characterizing block copolymer assemblies: graphene oxide supports for high contrast multi-technique imaging. *Soft Matter,* **2012**, 8, 3322-3328.
48. T. M. Mayhewa, C. Mühlfeldb, D. Vanheckeb; M. Ochs A review of recent methods for efficiently quantifying immunogold and other nanoparticles using TEM sections through cells, tissues and organs. *Ann. Anat.,* **2009**, 191, 153-170.
49. Mühlfeld, B. Rothen-Rutishauser, D. Vanhecke, F. Blank, P. Gehr; M. Ochs. Visualization and quantitative analysis of nanoparticles in the respiratory tract by transmission electron microscopy. *Part. Fibre Toxicol.,* **2007**, 4:11 DOI: 10.1186/1743-8977-4-11
50. Z. L. Wang**.** Transmission Electron Microscopy of Shape-Controlled Nanocrystals and Their Assemblies. *J. Phys. Chem. B,* **2000**, *104*, 1153-1175.
51. W.D. Pyrz; Douglas J. Buttrey. Particle Size Determination Using TEM: A Discussion of Image Acquisition and Analysis for the Novice Microscopist.
52. B. Michen, C. Geers, D. Vanhecke, C. Endes, B. Rothen-Rutishauser, S. Balog; A. Petri-Fink. Avoiding drying-artifacts in transmission electron microscopy: Characterizing the size and colloidal state of nanoparticles. *Nature Sci. Rep*., **2015**, 5, Article number: 9793.

Chapter III: Pickering-Ramsden emulsions

3.1 Overview, advantages and applications

Pickering emulsion are emulsions stabilised by particles rather than surfactants. [1] They were named after S. U. Pickering who first described the phenomenon in 1907 [2] although W. Ramsden firstly observed it in 1903. [3] Emulsion are largely employed and still express great potential in various sectors such as pharmaceutical, cosmetic, food, agricultural and petroleum industries. [4-6] Apart from industrial applications, there are also many examples of natural Pickering emulsions in foods like milk, mayonnaise and dairy cream. [7] Emulsion stabilisation via particles shows some differences and offers several advantages over conventional surfactants: surface active molecules are well known to generate tissue irritation and cell damages reducing their usability for bio-medical applications [8]; particle-particle interactions and lateral capillary forces provide higher mechanical strength and rigidity to the interface compared to normal surfactants [9]; due to higher energy barrier required to desorb from the interface particles do not undergo fast absorption-desorption as tensioactive molecules [8]; particles can be designed to respond to stimuli and reversibly or irreversibly destabilise the emulsion after environmental changes [10]; lastly surfactants are genarally more difficult to recover from any given system than particles.

Given such advantages, the nanogels obtained in this work were also evaluated for emulsion forming capabilities that would provide an additional advantage for the application as dermal drug delivery systems. Many formulations for transdermal application are administered in form of ointment which are basically emulsions. Therefore, nanoparticles described in this work could be potentially employed both as a drug carrier and as emulsion adjuvant in a final pharmaceutical application.

Before presenting the results obtained regarding emulsion stabilisation, it is important to mention the differences that lay between emulsion formation led by hard and soft particles.

3.2 Soft particles against hard particles

When considering emulsions stabilised by particles it is important to acknowledge the distinct properties between hard and so called soft particles. For instance, titanium oxide particles are one type of rigid particles employed in the stabilisation of emulsions [11] while micro and nanogels are examples of soft particles due to their capacity to deform [12].

The deformability and ability to respond to stimuli are key parameters that are responsible for the diversity between soft and hard particles. The first has a significant impact in enhancing droplets accommodation and increasing inter-particles interactions given by possible particle-particle interpenetration [12]. The latter instead provides additional properties to the system as the emulsion can be destabilised on demand by tuning environmental conditions (for instance pH or temperature) [13].

The improved characteristics of nanogels over hard particles make them an excellent platform for the development of responsive materials for drug delivery.

In the next paragraph preliminary emulsion stabilisation properties of the nanogels, herein discussed, will be presented.

3.3 Emulsion preliminary studies

Emulsions are complex systems with many variables that play a role in their formation and stability. Oil phase selected, chemical nature and concentration of the emulsifier as well as environmental conditions (pH, ionic strength, temperature etc.) can affect the emulsion. In order to fully understand the effect of each individual parameter extensive studies are required. However, this was not the object of this work. Nevertheless, some initial studies were performed in order to identify compatible oil phases and carry out preliminary studies on stimuli responsiveness of emulsions and nanogel concentration effect on emulsion formation.

The selection of the oil phase is probably the most critical point of emulsion studies. The formation and properties of the emulsion depends on the chemical interaction

between the emulsifier and the oil phase [14]. Without interaction between the oil phase and the nanoparticles the emulsion would not form. Initially the idea was to evaluate oil phases with different polarity to identify the phase with better affinity to nanogels produced. Therefore, heptane, ndodecane, paraffin oil, methyl myristate (MM), octanol (OC) and oleic acid (OA) were selected as suitable candidates for testing (Figure 3.1). The incompatibility with totally apolar oils was proven at an early stage. In view of this fact heptane, n-dodecane and paraffin oil were discarded due to the nanogels's inability to form emulsion in their presence.

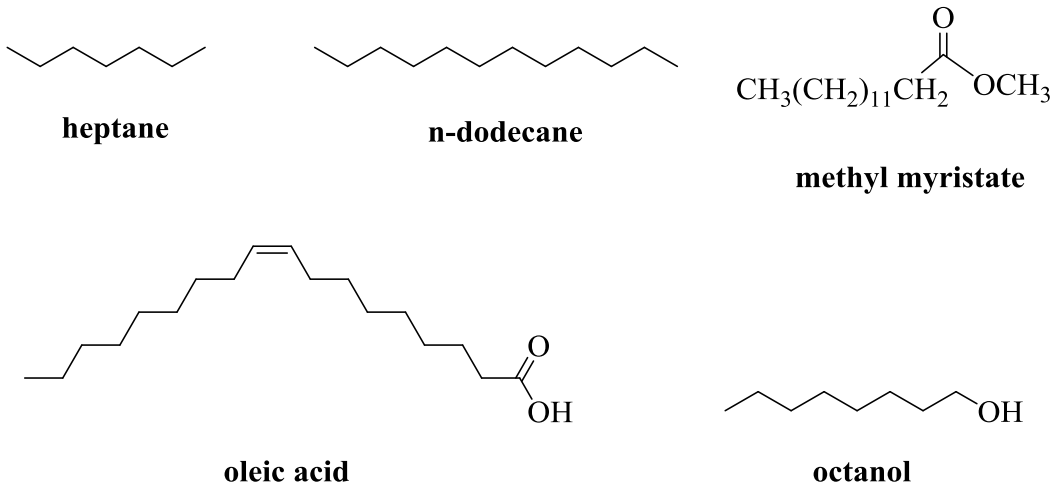

Fig. **3.1** chemical structure of oil phases used. Liquid paraffin is not herein displayed due to its multicomponent nature.

While the previously mentioned apolar phases did not form emulsions, methyl myristate appeared to possess intermediate characteristics. Figure 3.2 shows that emulsions were formed but after few seconds (< 15) they started separating from the centre.

Fig. 3.2comparison between water / oleic acid (left) and water / methyl myristate (right) systems. Vial on the right shows phase separation taking place from the centre of the emulsion.

Both the polar octanol and oleic acid led to formation of emulsions. Oleic acid in particular was selected as the optimal oil in terms of compatibility with nanogels but also considering its properties. Oleic acid is a natural occurring unsaturated fatty acid found in olive oil, several vegetables and adipose tissue of various animals. It is widely used as excipient in pharmaceutical formulations [15] containing bioactive compounds for the treatment of cardiac malfunctioning (Diltiazem), epilepsy or mental disorders (Carbmazepine) and as gastro protectant (Omeoprazole) to name a few [16].

One of the first studies conducted on emulsion was mixing volumes ranging from 0.5 to 1 mL of 1mg/mL aqueous solutions of nanogels with increasing amounts of oil phases ranging from 0.1mL up to double the initial volume of water phase used. The reason for this experiment was to assess optimal ratios between the phases. In the case of octanol the optimum ratio of water to oil was found to be 10:4. Oleic acid instead would form stable emulsions at various ratios (from 10:2 up to 10:15), however it was decided to fix phase's ratio at 1:1 or 1:0.5 (water:oil) as those systems seemed to produce the best emulsion performance.

As a proof of concept fluorescent labelled nanogels (MRGC 209 MRGC 211) were also tested and showed to be able to form emulsions (Figure 3.3). However, they were not analysed any further as this was beyond the scope of this work.

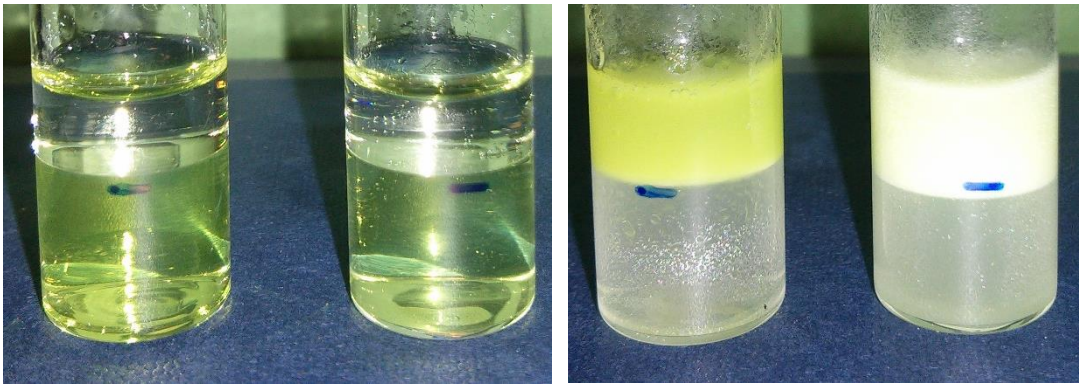

Fig. 3.3 Water/oleic acid systems of MRGC 211 and MRGC 209 before agitation (left) and after agitation (right) at 2500 rpm for 1 minute.

tBAEMA responsiveness to pH variation was previously referenced (section 2.1.2). For this reason, it was decided to confirm this property by testing emulsion stability in acidic, neutral and basic conditions. It is relevant to note that the pH was set both by using buffer solutions or dissolving the nanoparticles in either hydrochloric acid (HCl)

0.01M or sodium hydroxide (NaOH) 0.01M water solutions. The latter method offers the advantage of avoiding the interference of buffer salts, which could sit at the interface and therefore modify emulsion properties. On the other hand, the use of buffer solutions produces a system that better mimics the biological environment.

It was found that in acidic and neutral condition the nanogels were able to form stable emulsion while in basic condition the emulsions were disrupted or partially inverted.

Figure 3.4 below shows the effect, on the emulsion stability, after adding a few drops of NaOH 0.1M to an emulsion consisting of a nanogels' solution of 1 mg in 1mL of 0.01M HCl in water plus 1 mL of oleic acid (for a final nanogel's concentration 0.5mg/mL).

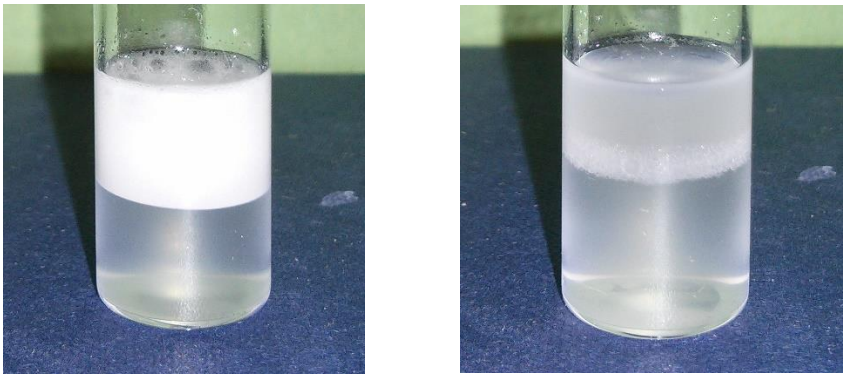

Fig. 3.4 Left: MRGC 180 1 mg in 1 mL of HCl 0.01M water solution (pH 4) plus 1 mL of oleic acid 1 hour after emulsion formation. Right: nanogels emulsion 10 minutes following addition of few drops of NaOH 0.1M (pH 12).

This behaviour can be easily explained as follow. Protonated secondary amines have a pKa in the range between 10 and 12, therefore their conjugated bases possess a pKb ranging from 2 to 4. This implies that tBAEMA can be considered a medium-weak base and therefore, in neutral and in basic conditions the extent of its protonation is moderate to low. On the contrary, in acidic conditions, due to the higher hydronium ion concentration the equilibrium is shifted towards the protonated species (Figure 3.5). The increase or reduction of positive charges, as a result of protonation-deprotonations of the amino groups from tBAEMA, leads to modification of the hydrophilic lipophilic balance (HLB) of nanogels resulting in either disruption (as previously seen in the case of MRGC 180) or inversion of the emulsion (Figures 3.6 and 3.7).

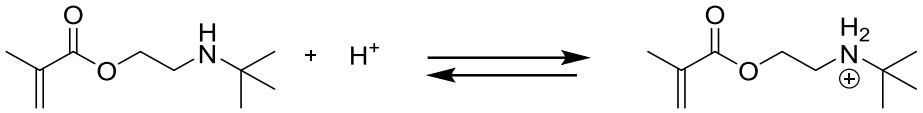

Fig. 3.5 Protonation of tBAEMA

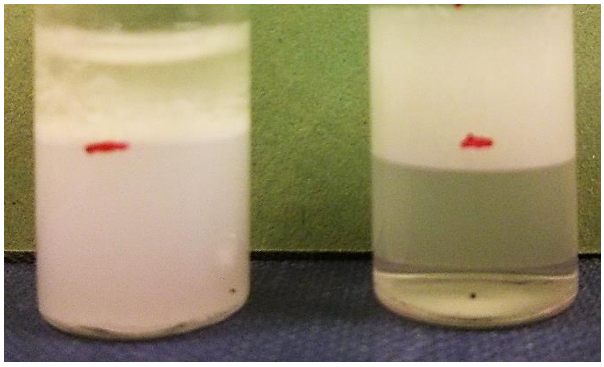

Fig. 3.6 0.5 mL of oleic acid plus 1 mL of MRGC 213 at 1 mg/mL 0.01M NaOH (left) or 0.01M HCl (right) water solution, 1 hour after agitation.

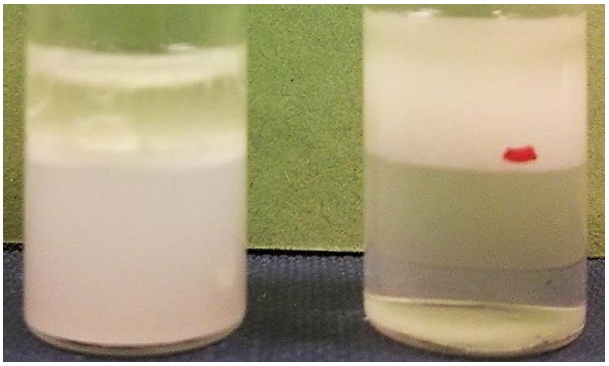

Fig. 3.7 0.5 mL of oleic acid plus 1 mL of MRGC 214 at 1 mg/mL 0.01M NaOH (left) or 0.01M HCl (right) water solution, 1 hour after agitation.

Overall MRGC 213 was shown to be the best preparation for the stabilisation of emulsions due to the presence of carboxylic acid groups (methacrylic acid) which conferred higher hydrophilicity and therefore greater interaction with the water phase.

Although transdermal delivery was selected as possible route of administrations for NGs, their pH responsive profile would be suitable also for oral administration. In the acid conditions of mouth and stomach the emulsion could potentially remain stable while breaking up in the intestine due to its basic environment.

The beahaviour of emulsion in buffer solutions proved to be different compared to HCl and NaOH pH adjusted solutions. While in a neutral enviroment the nanoparticles formed stable emulsions both in phosphate buffer solution (PBS) and in deionised water (Figures 3.8 and 3.9), basic conditions of pH 9.2, obtained through the use of carbonate/bicarbonate buffer, did not lead to emulsion inversion (Figure 3.6, 3.7 and 3.8) or breakage but to formation of an emulsion similar to those formed in neutral and acidic conditions (Figure 3.10). However, the reason for this behaviour, was not investigated any further due to time constrains and no hypothesis was formulated for this phenomenon.

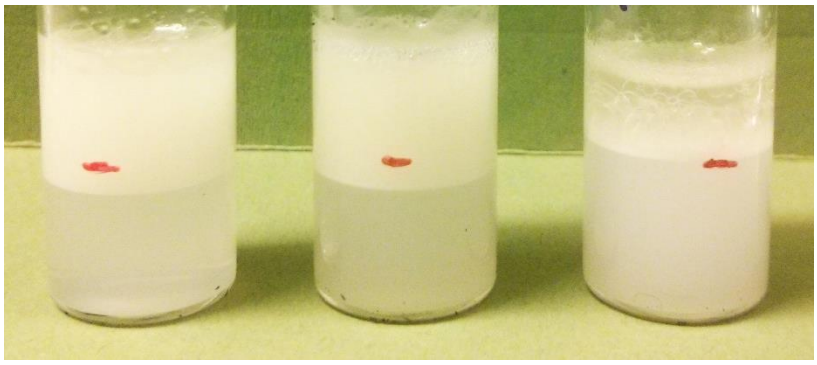

Fig. 3.8 0.5 mL of oleic acid plus 1 mL of MRGC 213 at at 1 mg/mL of aqueous citric acid buffer at pH 4 (left); phospate buffer solution at ph 7.4 (center) and 0.01M NaOH (right) 15 minutes after emulsion formation.

Fig. 3.9 0.5 mL of oleic acid plus 1 mL of a 1 mg/mL solution of MRGC 213 in deionised water.

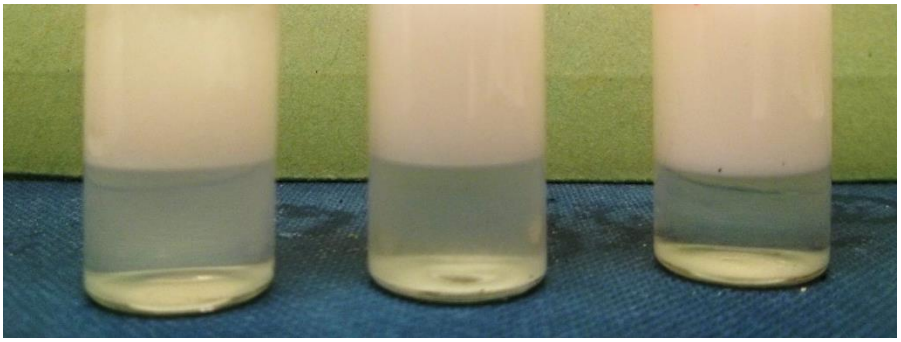

Fig. 3.10 0.5 mL of oleic acid plus 1mL of MRGC 213 at 1 mg/mL of aqueous citric acid/citrate buffer at pH 4 (left); phospate buffer at ph 7.4 (center) and carbonate/bicarbonate buffer at pH 9.2 (right) 15 minutes after emulsion formation.

With regards to the emulsions produced in acidic conditions at pH 4, achieved via the use of citric acid/citrate buffer, it should be noted that while their formation and short term (4 hours) stability was found to be similar to the emulsion adjusted with hydrochloric acid (Figures 3.7, 3.9 and 3.11), on the long term (< 24 hours) they proved not to be stable (Figure 3.11).

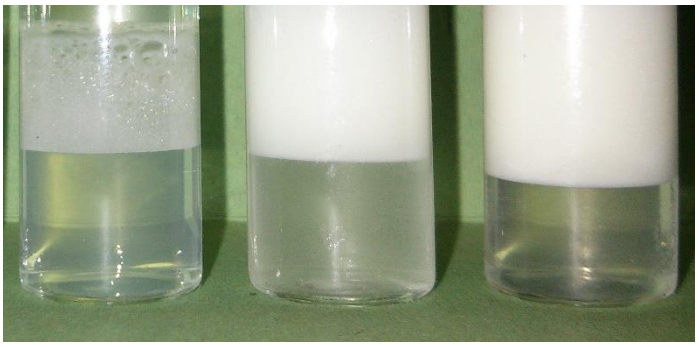

Fig. 3.11 0.5mL of oleic acid plus MRGC 213 1 mL at1 mg/mL of aqueous citric acid/citrate buffer at pH 4 (left); phospate buffer at ph 7.4 (center) and carbonate/bicrbonate buffer at pH 9.2 (right) one month after emulsion formation.

The bulky structure of citrate (Figure 3.12) compared to phosphates or carbonates could have caused the instability of the emulsion. In fact, phosphate and carbonate anions can bind with tBAEMA, through ionic interactions, while leaving the surface of the nanogels available for interactions with the oil and water phases. On the other hand, citrate, due to its tridentate and larger structure, could completely cover the

nanoparticles' surface offering highly hydrophilic moieties which would prevent interactions with the oil phase.

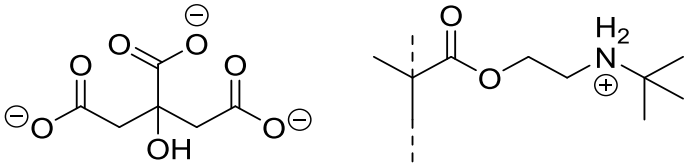

Fig. 3.12 Chemical structure of citrare (left) and tert-butylamino ethyl methacrylate within the nanogel's structure

These results seemed to indicate that selection of buffer solution played an important role on emulsion stability. Therefore, more in depth analyses will be required to fully comprehend mechanisms and elements driving the emulsion formation and stability, that due to time constrains could not be carried out.

In order to obtain more data on the ability of the nanogels to favour the formation of emulsions it was decided to investigate the impact of nanogel concentration. The images in Figure 3.13 show different samples of nanogels with concentrations ranging from 1mg/mL to 5 mg/mL before emulsion formation (A) and after the homogenisation (B). It was demonstrated that an increment in nanoparticle concentration led to larger emulsion volumes (Figure 3.13 B). From image B it can be easily observed that the emulsion phase is significantly increasing and the height of the emulsion is becoming more significant with increase in concentration.

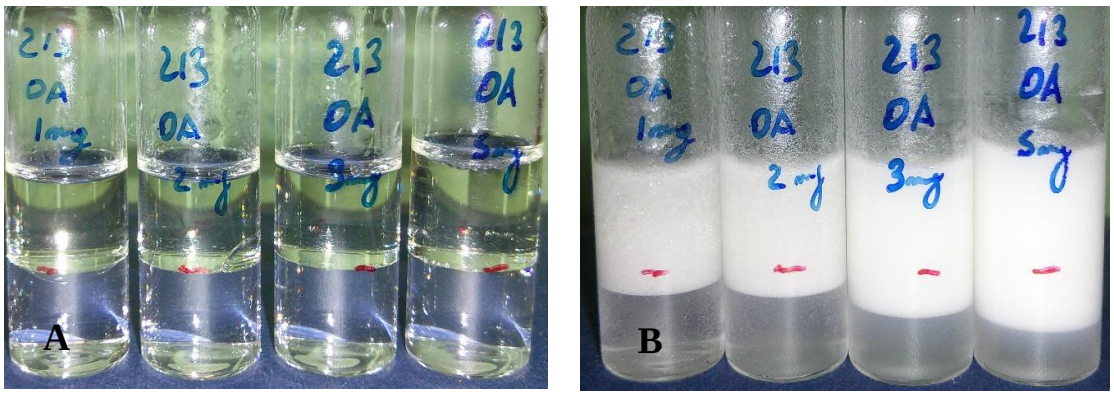

Fig. **3.13** Nanogels at increasing concentration, ranging from 1 to 5 mg/mL, before agitation (left). Emulsion formation after agitation at 2500 rpm for 1 minute. Red marks indicate level of phase's separation plane before agitation (right).

While macroscopic emulsion stability (over one month) could be assessed with naked eye. It was proposed to employ optical microscopy to confirm microscopic stability and to visualise behaviour of the emulsions (Figure 3.14).

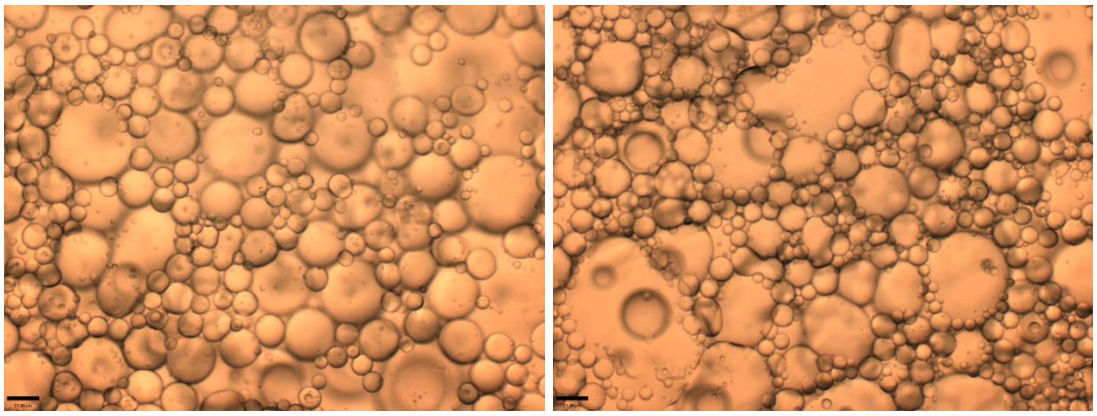

Fig. 3.14 Stability of oleic acid : water emulsions: MRGC 213. Left, emulsion prepared few minutes before analysis. Right, same emulsion after one week. Scale bar 53 µm. Images recorded with the support of Dr. Katarzyna Zielinska.

Figure 3.14 and 3.15 (below) show no significant difference in droplet size and morphology between emulsions freshly prepared and emulsions 1 week after formation confirming emulsion stability under both macroscopic and microscopic perspective.

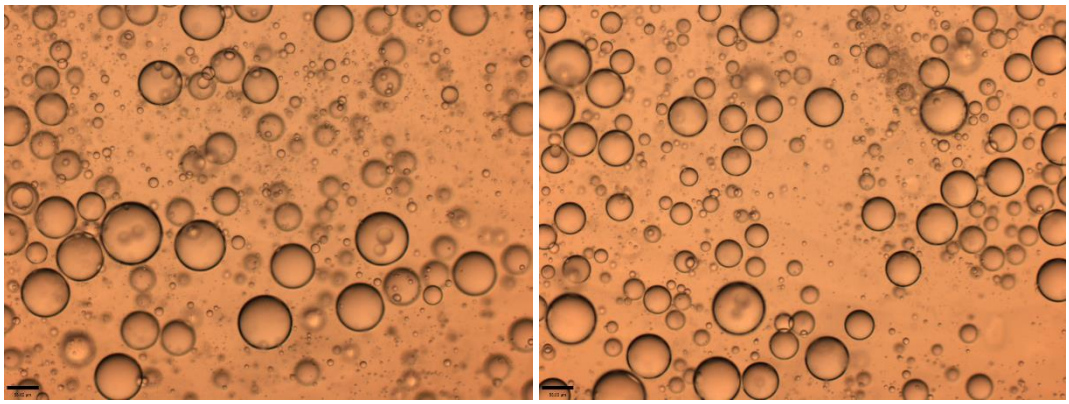

Fig. 3.15 Stability of oleic acid : water emulsions: MRGC 214. Left, emulsion prepared few minutes before analysis. Right, same emulsion after one week. Scale bar 53 µm. Images recorded with the support of Dr. Katarzyna Zielinska.

It is important to note that as soon as the emulsions are casted and spread on top of the glass for microscopy analysis, the emulsions quickly start to break therefore, the test has to be run promptly. The smallest droplets seen in the pictures represent the real emulsion droplets while the larger ones are the result of emulsion breakage due to collapsation of small droplets to form

large clusters. Comparing Figure 3.14 with 3.15 it can be noted that the smallest droplets (1-5 μm) possess similar size however, the pictures appear very different. This is due to the fact that emulsions formed by MRGC 214 break faster than those formed with MRGC 213. As the emulsions are water in oil this can be easily explained by the presence of extra charges (MAA) and higher acqueous solubility of MRGC 213 which can produce stronger interaction with the water phase and therefore keep it in the oil phase for a longer time.

3.4 **Conclusions**

In conclusion MRGC 213 and MRGC 214nanoparticles were shown to be able to form stable Pickering emulsions which could be broken, following pH modifications.

These properties further expand the capabilities of these novel methacrylate based NGs. However additional test will have to be performed in order to fully understand the behaviour of the nanoparticles in more complex systems such as biological fluids or cell media.

After nanogels synthesis and the evaluation of their Pickering-Ramsden emulsion formation capabilities, the focus was moved on the evaluation of the biological properties of the nanoparticles in order to assess their suitability for drug delivery applications. These characteristics are discussed in the following chapter.

References

1. Y. Chevalier; M. A. Bolzinger. Emulsions stabilized with solid nanoparticles: Pickering emulsions. *Colloids and Surfaces A: Physicochem. Eng. Aspects*, **2013**, 439, 23-34.
2. S.U. Pickering**. Emulsions.** *J. Chem. Soc., Trans.***, 1907**, 91, 2001-2021.
3. W. Ramsden. *Proc. Roy.* Soc., **1903**, 72, 156-164.
4. R. J. G. Lopetinsky, J. H. Masliyah; Z. Xu. Solids-Stabilized Emulsions: A Review. In: B. P. Binks, T. S. Horozov editors. Colloidal particles at liquid interfaces. Cambridge: *Cambridge University Press*, **2006**, 186-224.
5. J. Tang, P. J. Quinlan; K. C. Tam. Stimuli-responsive Pickering emulsions: recent advances and potential applications. *Soft Matter*, **2015**, 11, 3512-3529.
6. E. Dickinson. Food emulsions and foams: Stabilization by particles. *Curr. Opin. Colloid. In.*, **2010**, 15, 40-49.
7. B. P. Binks; T. S. Horozov. Colloidal particles at liquid interfaces: an introduction. In: B. P. Binks, T. S. Horozov editors. Colloidal particles at liquid interfaces. Cambridge: *Cambridge University Press*, **2006**, 1-73.
8. A. Schrade, K. Landfestera; U. Ziener. Pickering-type stabilized nanoparticles by heterophase polymerization. *Chem. Soc. Rev.*, **2013**, 42, 6823-6839.
9. K. D. Danov; P. A. Kralchevsky. Capillary forces between particles at a liquid interface: General theoretical approach and interactions between capillary multipoles. *Adv. Colloid. Interfac.*, **2010**, 154, 91-103.
10. S. Fujii, E. S. Read, B. P. Binks; S. P. Armes. Stimulus-Responsive Emulsifiers Based on Nanocomposite Microgel Particles. *Adv. Mater.*, **2005**, 17, 1014-1018.
11. T. Chen, P. J. Colver; S. A. F. Bon. Organic–Inorganic Hybrid Hollow Spheres Prepared from TiO_2-Stabilized Pickering Emulsion Polymerization. *Adv. Mater.* **2007**, 19, 2286-2289.
12. M. Destribats, V. Lapeyre, M. Wolfs, E. Sellier, F. Leal-Calderon, V. Ravaine; V. Schmitt. Soft microgels as Pickering emulsion stabilisers: role of particle deformability. *Soft Matter*, **2011**, 7, 7689-7698.
13. S. Wiese, Y. Tsvetkova, N. J. E. Daleiden, A. C. Spieß; W. Richtering. Microgel stabilized emulsions: Breaking on demand. *Colloid. Surface A*, **2016**, 495, 193-199.
14. E. S. Read, S. Fujii, J. I. Amalvy, D. P. Randall; S. P. Armes. Effect of Varying the Oil Phase on the Behavior of pH-Responsive Latex-Based

Emulsifiers: Demulsification versus Transitional Phase Inversion. *Langmuir*, **2004**, 20, 7422-7429.

15. R. G. Strickley. Solubilizing Excipients in Oral and Injectable Formulations. *Pharmaceut. Res.*, **2004**, 21, 201-230.
16. Drugs.com. www.drugs.com/inactive/oleic-acid-44.html (20/04/2016).

Chapter IV: Results and discussion (biological)

4.1 Introduction

The biological works carried out and presented in this chapter and in chapter 4 are the result of a secondment, lasted for a total period of 2 months, at the Technological Park of Cantanhede in Portugal, under the co-supervision of Dr. L. Ferreira and with the collaboration of his research team, in particular Miss J. Blersch and Dr M. Comune. This was part of the European funded PhD program, initial training network (ITN) NANODRUG, undertaken by the candidate presenting this thesis.

Chapter two described the nanogels (NGs) under a material stand point. It is important to place the drug delivery system (DDS) in to the context of its intended application. Therefore, after a brief introduction on the skin (selected as route of administration), this chapter presents the biological properties of NGs in terms of cell cytotoxicity and trafficking.

The dermal delivery route was chosen, for this project, for its great potential which have not been yet fully exploited [1]. This was further strengthened by a number of collaborations available within the Resmini's research group via NANODRUG, the European Marie Curie ITN that supported financially this study.

4.1.1 Skin as route of administration

The skin is the most extensive and accessible organ of the body (Figure 4.1). Its main functions are: defending the body from the external environment, regulating the temperature, controlling the output of water and the sensation [2, 3].

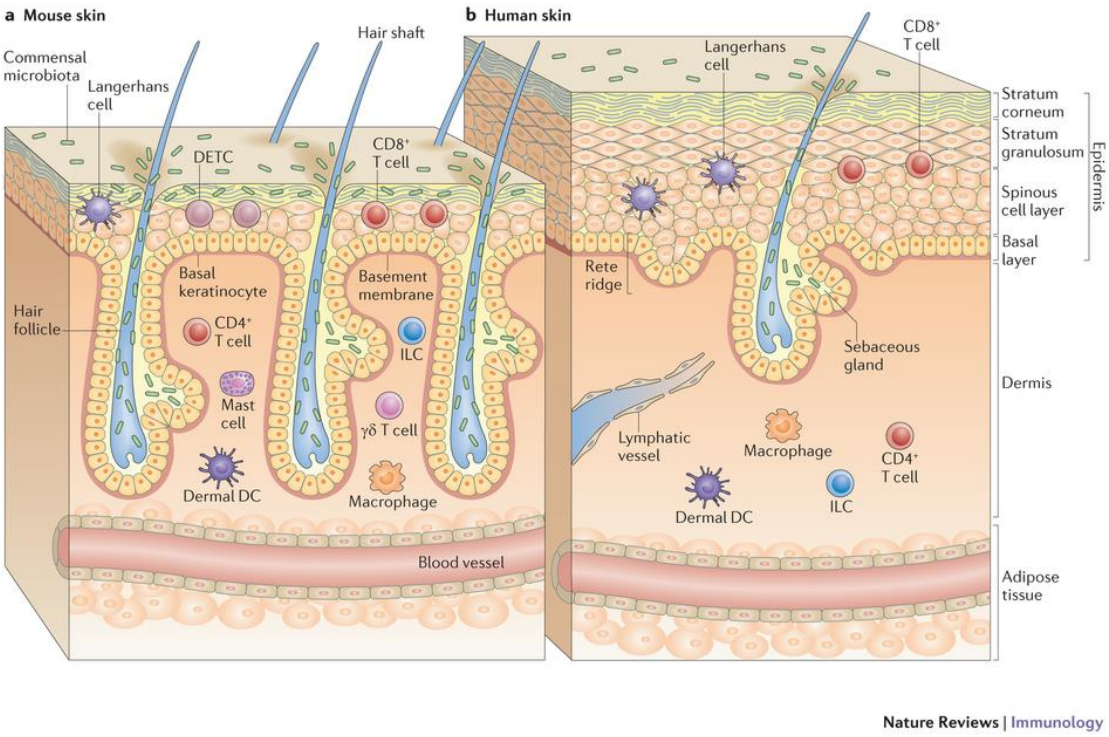

Fig. 4.1 Structure and cellular components of the skin in mice and humans. From M. Pasparakis et al. *Nat Rev. Immunol.*, **2014**, 14, 289-301. **License Number:** 3962990247987.[a].

It is constituted by three layers: epidermis, dermis and hypodermis. Epidermis, the external layer, consists of five individual layers: the stratum germinativum (basal layer), stratum spinosum, stratum granulosum, stratum lucidum (found in thick skin) and stratum corneum (SC) the outermost layer (Figure 3.2). Cells of this layer are: keratinocytes, dendritic melanocytes, Langerhans cells and tactile Merkel cells. Moving towards the surface keratinocytes differentiate and slowly undergo apoptosis, lose the nucleus, grow in size, get flatter, start to adhere each other and become less and less hydrated. Epidermis has the function to protect the body from external environment in particular the SC has the major defensive function. In this layer keratinocytes are called corneocytes, they are highly keratinized, with a hexagonal shape and organised in cluster. The macrostructure of the SC is generally described with the brick and mortar model, where the corneocytes are the bricks and the lipidic matrix (secreted at the stratum granulosum–stratum corneum interface) around them is the mortar. [3-5]

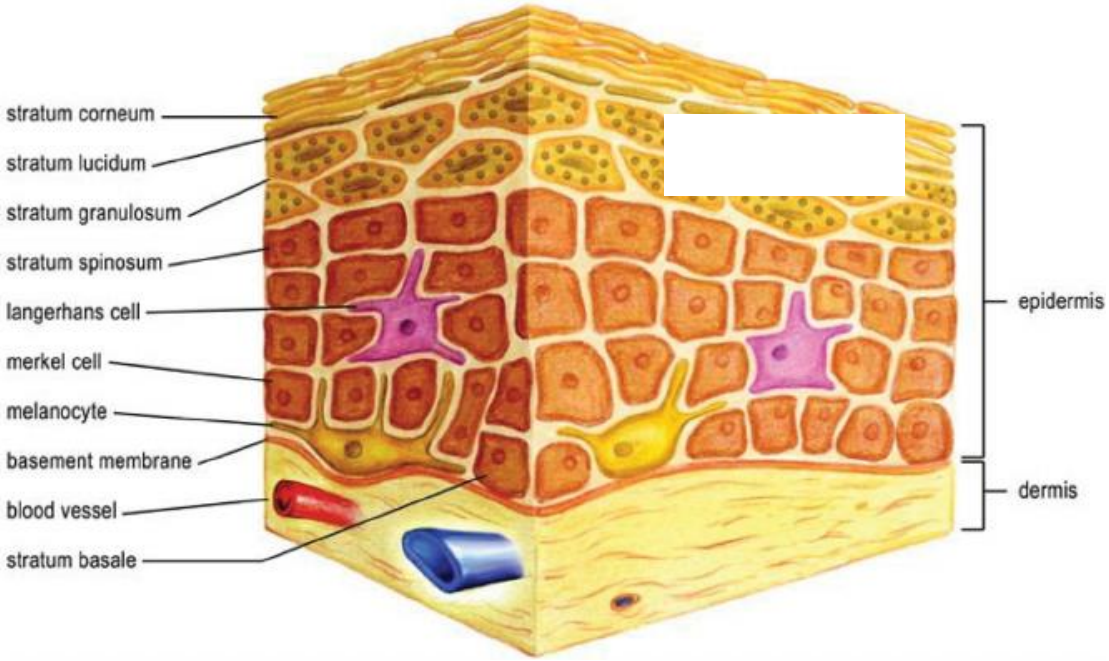

Fig. 4.2 Detailed structure of epidermis. From M. A. Farage et al. *Cutan. Ocul. Toxicol.*,**2007**, 26, 343-357. Permission granted free of charge from Taylor & Francis for thesis use. [b]

Dermis, the intermediate layer, is a highly vascularised tissue that is responsible for bringing nutrients to the epidermis and clearing the skin from metabolic products and permeated compounds. This is the target layer for drugs that are required to be administered systemically. [3-5]

Hypodermis, the deepest layer, is a tissue rich in collagen and fat, which has the function to insulate the body, protect from external shock and offers support to the outer layers and it does not play any role in dermal drug delivery. [3, 4]

There are three routes to skin permeation: two trans-epidermal (intracellular and intercellular) and one transapendageal (transport of drugs through hair follicles and sweat glands) which are shown in Figure 4.3. Although transapendageal route can be used in order to administer large and polar compounds it has a minor impact due to the relatively small area (around 0.1% of the total skin surface). On the other end administration via both intracellular and intercellular routes is limited by the size of the drug delivery system.

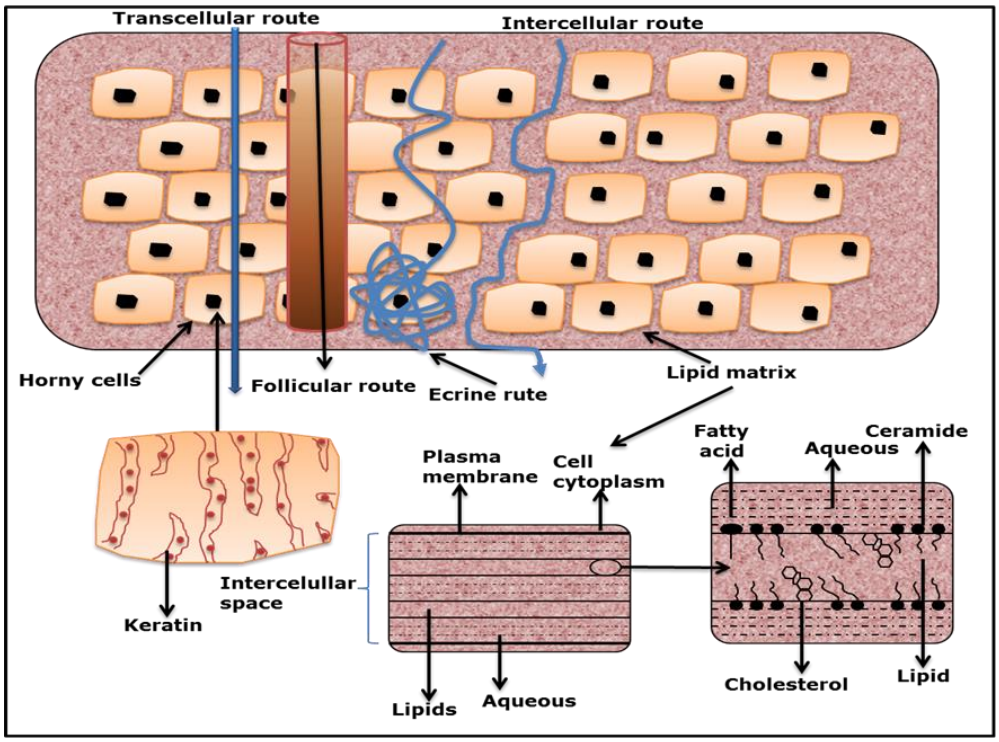

Fig. 4.3 Schematic for the routes of skin penetration. From J. J. Escobar-Chávez et al. *Ali Demir Sezer (Ed.), InTech*, **2012** DOI: 10.5772/50314. (OPEN ACCESS) [c]

It has been hypothesised that only particles with a size lower than 40 nm may permeate through the epidermis [6, 7]. Moreover, other factors have to be taken into account for the development of transdermal drug delivery system (TDDS) such as: pH, partition coefficient, level of skin hydration, thickness and condition of the specific area of skin treated. [2-4]

Dermal drug delivery offers several advantages compared to oral and parental administration:

- Both topical and systemic drug delivery can be achieved.
- pH influence and harsh condition of gastro-intestinal tract is avoided.
- The first pass effect (hepatic metabolism) is bypassed.
- An easy way of access is provided.
- It is a non-invasive approach.
- Patient compliance gets improved. [2-4]
- Several are the drugs, for topical treatment, that can be administered through the skin some example may be: anaesthetics such as Lidocaine or Benzocaine,

antifungal such as Miconazole or Ketoconazole, anti-inflammatory such as Ketoprofen or Diclofenac etc.

Despite the potential advantages that drug delivery can offer there are still a number of issues that need to be addressed in order to fully understand all the possible applications and limitations.

Before presenting the results obtained, an overview of cell lines and biological assays used in this study are described in order to justify the experimental work that was undertaken to demonstrate NGs suitability for transdermal application.

4.1.2 Skin cell lines

In order to evaluate the potential of these novel methacrylate based nanogels, described in chapter two, as a drug delivery system (DDS) for dermal administration, the first step involved the study of how the nanoparticles would interact with cells.

Cytotoxicity, cellular metabolism alteration and cell internalisation (described in the following chapter) are the most important parameters that need to be investigated in order to demonstrate the suitability of the nanogels for further pharmacological employment.

The selection of cells should always consider the final application of the DDS tested. In this case the anatomy of the skin, which is constituted by 4 main cell lines, was taken into account. Cells of the tissue are: keratinocytes (major component), fibroblast (connective tissue), Langerhans (immune system) and melanocytes (pigment producing cells) [8, 9]. In the view of this fact, immortalised human keratinocytes (HaCaT) and normal dermal human fibroblast (NDHF) were selected as model cells.

Before starting to describe the cell lines chosen and the data collected, it is important to briefly describe the techniques selected for the biological analysis of the nanogels.

4.1.3 Cytotoxicity and metabolism tests

Variations of cell viability and metabolic molecules concentration are important guidelines to understand the effects of a given entity to the normal biological functioning of cell cultures and allow to make preliminary consideration on the entity's safety and usability. In this study, in particular, the interest lied on the biocompatibility of the nanogels, essential requirement for pharmacological applications.

There are numerous tests available that could be used to evaluate cytotoxicity together with a variety of markers for the assessment of metabolic homeostasis of cells.

Cell toxicity can be determined by: 1) analysis of morphological changes in the cell structure; 2) assessment of cell membrane integrity measured by using dyes that enter cells only when they are dead or that are actively up taken by living cells; 3) alteration of cell growth and 4) metabolic alteration which can be as well correlated to cell toxicity. [10]

Profiting of the collaboration and expertise of Dr. Lino Ferreira and its team from Biocant Technological Park in Cantanhede, Portugal, it was decided to employ two widely used techniques in order to evaluate nanoprticles' biocompatibility: the propidium iodide and the adenosine triphosphate (ATP) levels assays, which are described in the following sections.

4.1.3.1 Propidium iodide assay

Propidium iodide (PI) (Figure 4.4) is a red fluorescent dye that intercalates into the DNA and does not permeate through membranes in viable cells [11].

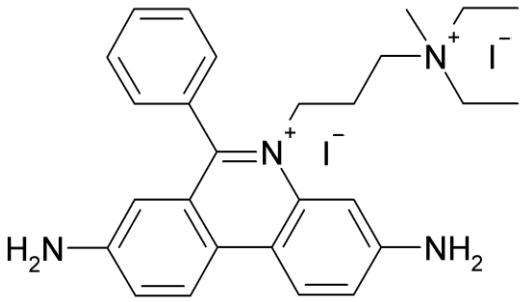

Fig. 4.4 Chemical structure of propidium iodide

Due to its characteristics it is used to identify dead cells by fluorometric analysis of cells' nuclei. When a cell dies, its nucleus membrane integrity gets compromised and becomes permeable to PI that is then free to bind nucleic material [12]. PI assay is more reliable than tests which are based on dyes actively taken up by viable cells such as Almar Blue (resazurin). This is due to several factors: 1) different cell lines may have different dye absorption rate making a comparison between them rather difficult; 2) interaction between entity tested and resazurin or use of same cell internalisation pathway could lead to false positive or negative and 3) cell metabolism modification could have an impact on dye internalisation not necessarily related to cell viability [13]. Although its advantages, PI has few limitations. Since it binds both DNA and RNA it could produce false positive when binding free nucleic acid material [14]. Moreover, conventional PI tests employs flow cytometry or microscopy [14-16] which can present disadvantages like the need to sacrifice part of the cell culture, risk of cell integrity loss and lower throughput [17]. To overcome this issues the PI assays, presented later in this chapter, were performed coupling PI and Hoechst 33342 (H33342) cell nuclei staining [18] (Figure 4.5) with high content analysis (HSA). HSA is an accurate and reliable technique widely used for drug delivery applications, which combines molecular tools of cell biology with automated high-resolution microscopy and automated analysis [19]. It is important to point out that while PI does not penetrate inside viable cells, Hoechst 33342 is always able to permeate cell membranes.

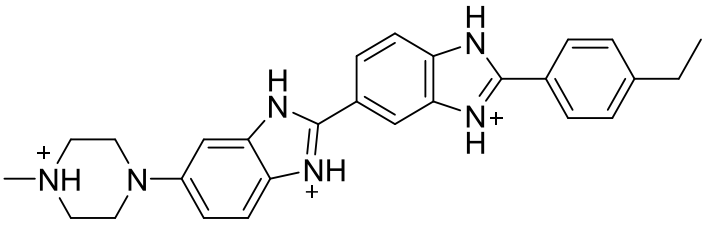

Fig. 4.5 Chemical structure of Hoechst 33342

In order to evaluate cytotoxicity, cell line cultures were incubated, at 37 ºC under 5% CO_2 atmosphere, together with increasing concentration of nanogels (ranging from 10 to 400 µg/mL) and monitored at different time points (4 and 24 hours mainly) by PI incorporation. Cells were cultured in Dulbecco's modified Eagle's medium (DMEM) supplemented with 10% (v/v) of fetal bovine serum and 1% (v/v) penicillin/streptomycin and incubated with Hoechst 33342 and PI, for 15 minutes, prior imaging.

The analyses were performed using an InCell analyser, a high content screening microscope which can imaged entire cell plates in relatively short amount of time.

The microscope can simultaneously image different fluorescent channels together with the brightfield (optical microscopy). Moreover, the instrument provides a large amount of data easy to process and allows the combination of channels for a more accurate analysis and the possibility to extrapolate more information regarding the cell culture.

Via software it is then possible to implement a segmentation around the nuclei using the Hoechst 33342 channel (stain binding the cell nuclei). This means that the software will then be able to count cells and identify dead ones by overlapping H33342 with PI channels (Figure 4.6). This is further explained in section 4.2.1.

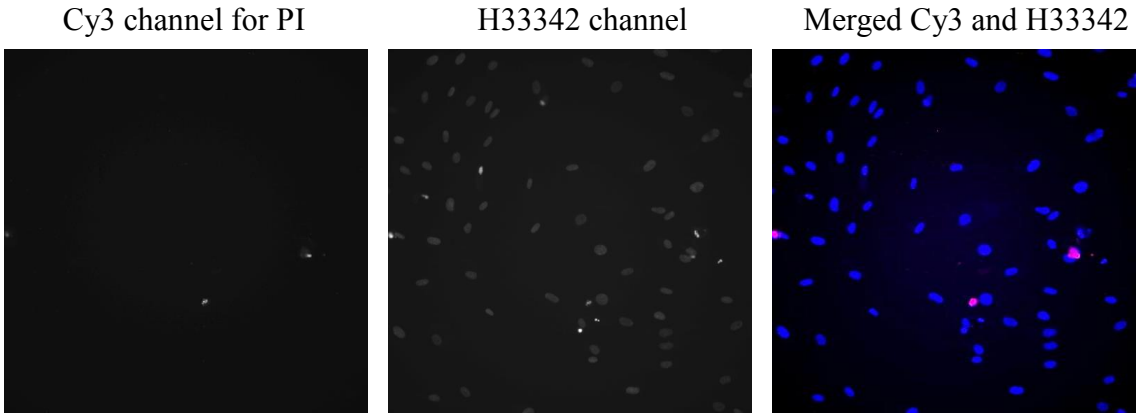

Fig. 4.6 Images recorded with the inCell analyser. From left to right: propidium iodide channel, Hoechst 33342 channel and merged.

It was previously mentioned that, together with the PI assay, adenosine triphosphate levels were also evaluated to provide additional information regarding cell metabolism and viability. This technique is described in the following section.

4.1.3.2 Adenosine triphosphate (ATP) assay

Adenosine triphosphate (ATP) is the energy currency of living organisms' cells [20, 21]. Its quantification is used as a technique to evaluate metabolic activity of cells and can be correlated to cytotoxicity [21-23].

In order to evaluate ATP variation, cells were seeded on 96 wells plates and incubated, at 37 ºC under 5% CO_2 atmosphere, together with increasing concentration of NGs and analysed at different time points (4 and 24 hours mainly) after being treated with **CellTiter-Glo®** luminescent kit. The assay consists in the lysis of cells and the measurement of fluorescence intensity resulting from the binding between ATP molecules and luciferase [23]. As for PI assays, cells were cultured in Dulbecco's modified Eagle's medium (DMEM) supplemented with 10% (v/v) of fetal bovine serum and 1% (v/v) penicillin/streptomycin. PI and ATP assays involve different procedures and apparatuses. While in the case of PI the cell culture plate is directly analysed at the InCell analyser, ATP levels are measured via a fluorescence plate reader that analyses the fluorescence of the cell media, containing the cell lysate, transfered

on cell plates which are not transparent but completely white to ensure accurate fluorescence readout.

These measurements were recorded by using a microplate reader that determines the total fluorescence of each well of the culture plate.

After the overview on skin organisation and biological assays selected, the following section describes the cell lines employed in this work and the results obtained.

4.2 **Cell Studies**

Before starting to discuss the biological results, the nanogel formulations evaluated in this work are presented in the Table below (Table 4.1). This should provide the reader a faster correlation of the data presented in this chapter with the chemical composition of the nanoparticles.

NG	tBAEMA	EGMMA	MAA	MAF	MBA	C_M%	Solvent	Yield	Size N
209	55%	0%	20%	5%	20%	0.5%	W:Ac 1:1	69%	70 ±5nm
211	55%	20%	0%	5%	20%	0.5%	W:Ac 1:1	51%	70 ±5nm
213	60%	0%	20%	0%	20%	0.5%	W:Ac 1:1	91%	6 ±3nm
214	60%	20%	0%	0%	20%	0.5%	W:Ac 1:1	86%	9 ±3nm

Table 4.1 Summary of preparations selected for biological assays. Experimental codes (MRGC) are reported in the first column

4.2.1 Immortalised human keratinocytes (HaCaT)

HaCaT cells (Figure 4.7) are immortalised human keratinocytes. The first attempt to promote their spontaneous transformation from normal human skin keratinocytes was achieved by Azzarone et all. In 1976 and later improved by Baden et all. in 1987 and Boukamp et all. in 1988 [24]. The cells are extensively used to understand the epidermal

functioning, as model for skin treatment testing and to perform toxicological studies on particles [25-29]. Their wide use is due to their ease of propagation and almost normal phenotype [30]. On the contrary non-immortalised keratinocytes are more complex to maintain in culture and are not suitable for long term investigation as they rapidly die [30].

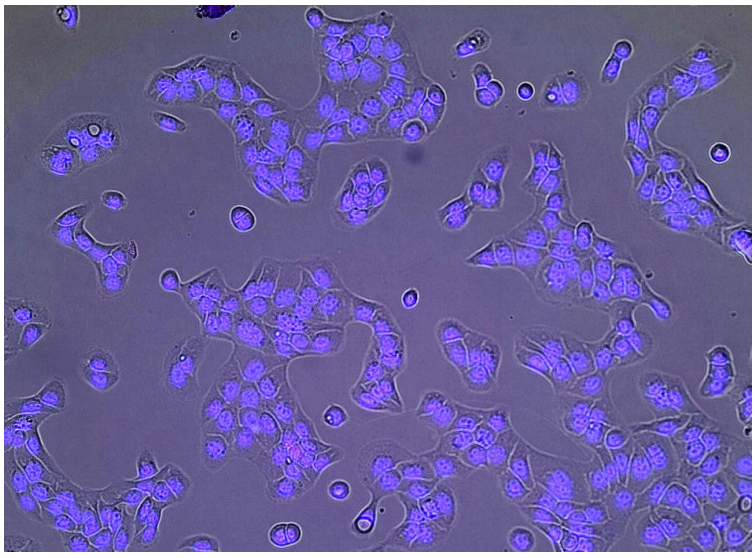

Fig. 4.7 HaCaT cell line culture where nuclei are stained with 4',6-diamidin-2-fenilindolo (HOECHST 3342). Image recorded by Ms. Josephine Blersch and obtained by using an InCell analyser.

Before describing the biological results obtained it is important to note that each individual data reported or shown in the pictures, in this chapter, were extrapolated by calculating the mean value of triplicates. Furthermore, the assays were repeated on different dates to minimise experimental error and in some cases performed by different users to increase randomisation and obtain more significant data.

As previously mentioned cytotoxicity of nanogel in this cell line was assessed using the propidium iodide assay. Upon exposure of HaCaT cell cultures to increasing concentrations of nanogels, ranging from 10 up to 400 µg/mL, no cytotoxicity was observed up to 24 hours incubation (Figures 4.8 and 4.9). Moreover, very low standard deviation (SD) < 1% was observed confirming consistency of results obtained. The concentration range was based on literature research [31-36] and suggestions provided by Dr. Ferreira's group, targeting higher concentrations of nanoparticles in order to induce a toxic effect. As observed in literature, the effect on cell viability of nanoparticles is often observed at concentration lower than 400 µg/mL. A further test on nanogel

cytotoxicity could have been an increase in nanogel concentration in order to identify the toxicity starting point. However, particles concentration higher than 400 µg/mL would never be used *in vivo*. Therefore, these experiments were not performed as they were considered not relevant for the intended application.

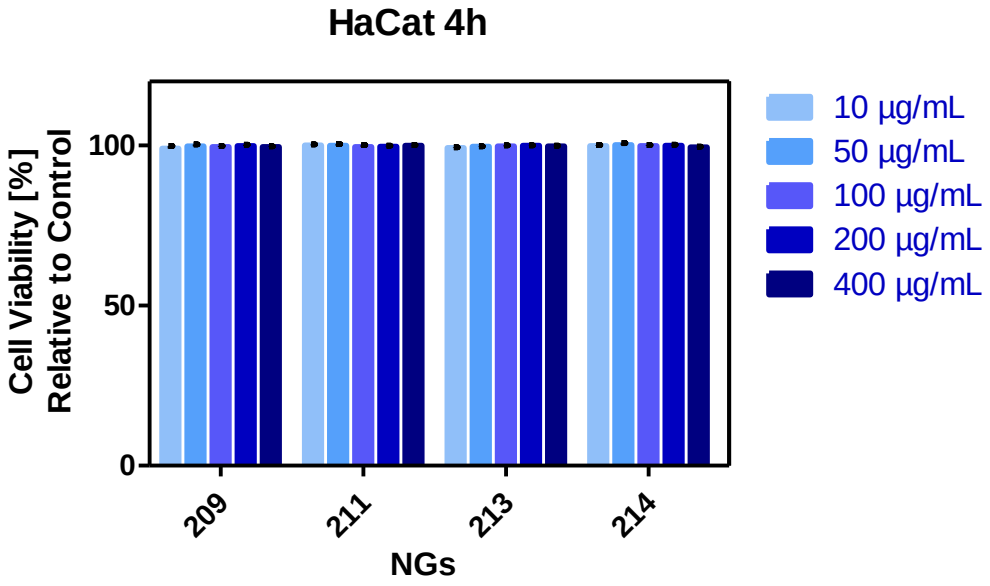

Fig. 4.8 Cytotoxicity of nanogels in HaCaT cells after 4 hours incubation reported as a mean value of triplicates plus the standard deviation (SD).

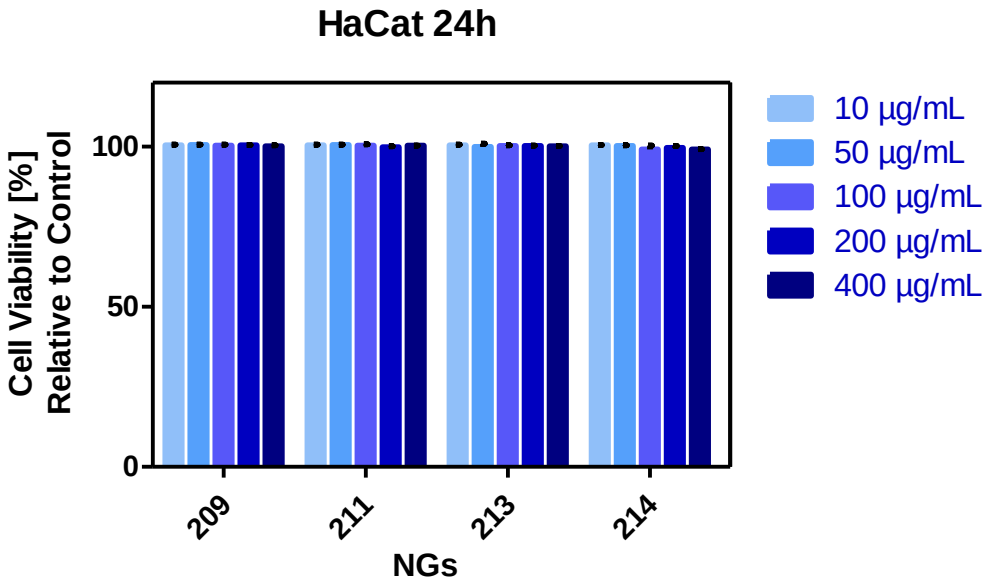

Fig. 4.9 Cytotoxicity of nanogels in HaCaT cells after 24 hours incubation reported as a mean value of triplicates plus the standard deviation (SD).

To assess nanoparticles cytotoxicity HaCaT cells were incubated in the presence of nanogels. After 4 and 24 hours incubation the cell media was removed and replaced with fresh medium containing Hoechst 33342 and PI and the entire plate was screened at the InCell analyser. Cell viability was then calculated using the Hoechst 33342 channel to create a mask layer (Figure 4.10) able to measure number of cell by counting cells' nuclei. This layer was then overlapped with the PI channel to determine the number of dead cells. Cells with 10% overlap of PI and H33342 stains were considered positive to cell toxicity (dead cells) and substracted to overall number of nuceli previously counted. The overlapping allowed avoidance of false positive resulting from binding between propidium iodide and free DNA or RNA in the medium. All results obtained for cells treated with nanogels were correlated with a control of untreated cells cultured in normal media and not exposed to nanogels.

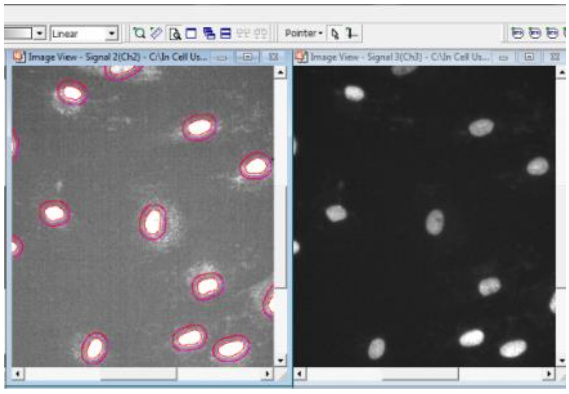

Fig. 4.10 Example of segmentation implemented on Hoechst 33342 channel.

To further confirm and expand viability data obtained with PI assay, visual analyses of cellular morphology modifications were carried out also to assess possible effects not immediately detectable with PI assay. Figure 4.11 and 4.12 below show the comparison between control cells and cell incubated for 24 hours with both MRGC 213 and 214, at the maximum concentration (400 µg/mL). The images show no morphological differences between cells incubated with or without NGs. Furthermore, no variation of cell growth was observed (cell density). This result provides an additional evidence the NGs were nontoxic, in HaCaT cells, under the condition tested.

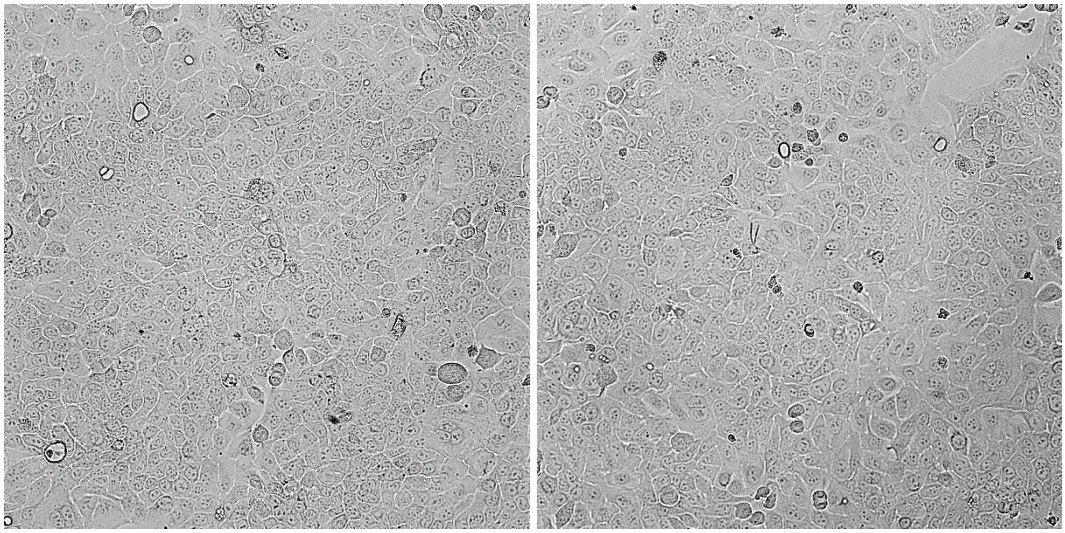

Fig. 4.11 Control cells (untreated) on the left and cells incubated with MRGC 213 at 400 µg/mL on the right, after 24 hours

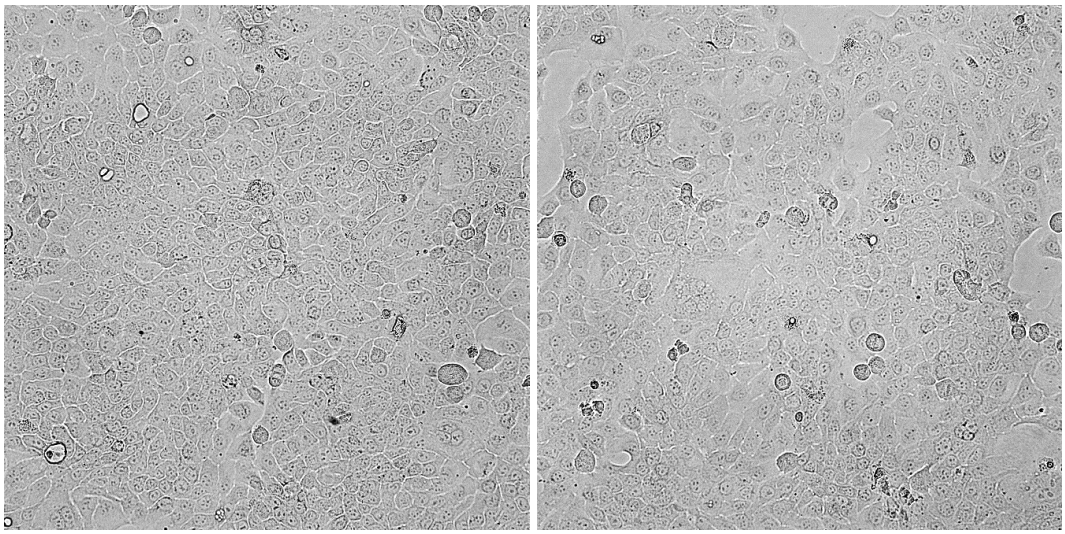

Fig. 4.12 Control cells on the left and cells incubated with MRGC 214 400 at µg/mL on the right after 24 hours

ATP levels assays were then performed in order to understand the metabolic behaviour of cells in the presence of NGs and to further confirm biocompatibility of NPs (Figures 4.13 and 4.14).

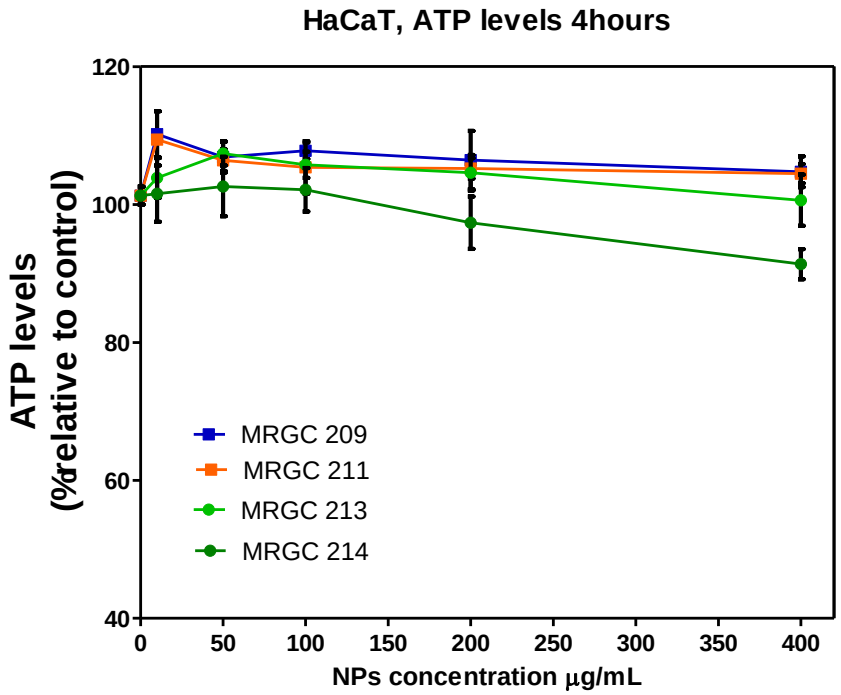

Fig. 4.13 ATP levels relative to control in HaCaT cells incubated for 4 hours with various concentration of NGs reported as a mean value of triplicates plus the standard deviation (SD).

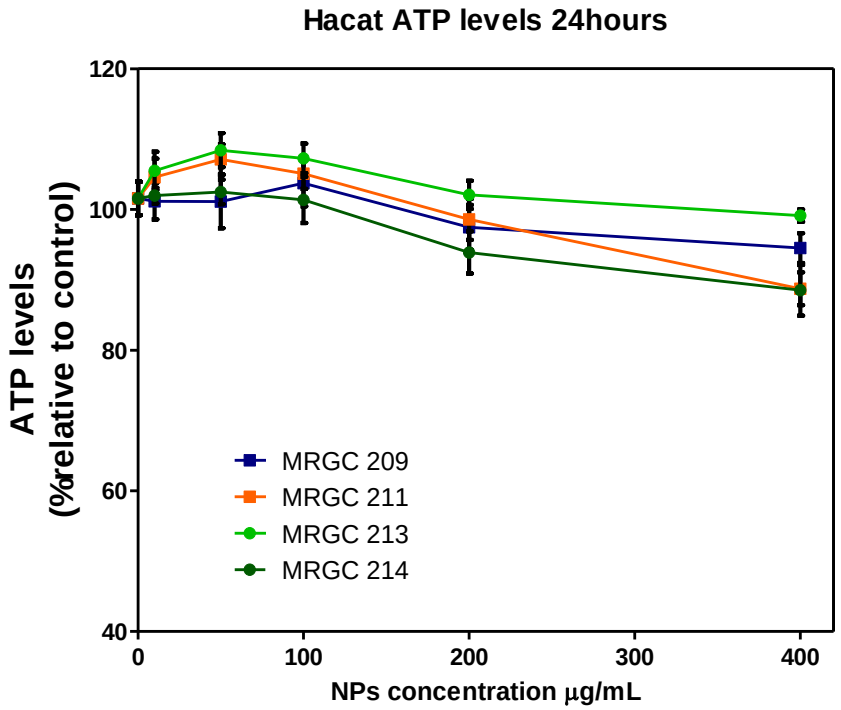

Fig. 4.14 ATP levels relative to control in HaCaT cells incubated for 24 hours with various concentration of NGs reported as a mean value of triplicates plus the standard deviation (SD).

After the incubation of cells, in 96 well plates for 4 and 24 hours, half of the cell medium was removed and replaced with **CellTiter-Glo®** kit which induce complete lysis of cells with consequent release of ATP able to bind with luciferase and therefore emit yellow fluorescence. The yellow fluorescent medium was then transfered in a new opaque white 96 well plate and screened using a microplate reader equipped with a fluorimeter. Intensity readings were normalised to the control (untreated cells) and baselined using cell media plus **CellTiter-Glo®** kit as value 0.

While figures 4.13 and 4.14 display ATP levels data in a condensed way, Figure 4.15 below show in a more clear manner the ATP level variation for each individual nanogel.

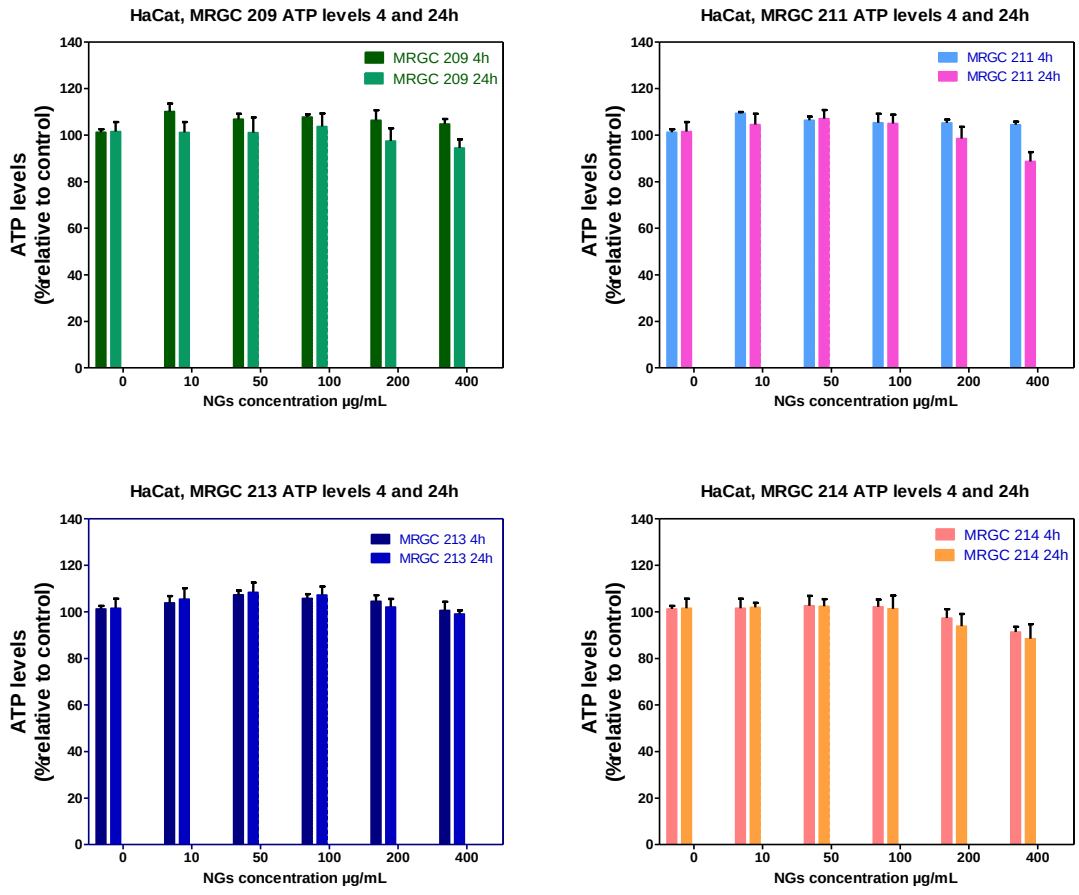

Fig. 4.15 ATP levels relative to control in HaCaT cells incubated for 4 and 24 hours with various concentration of NGs reported as mean value of triplicates plus the standard deviation (SD).

Slightly higher (in the range of 2-8%) ATP levels in cells treated for instance with MRGC 213 may indicate interactions between nanogels and cell components that may trigger ATP synthesis. However, with the experiments performed it was not possible to identify the real cause of this positive variation which is anyway of a very small extent.

Results obtained demonstrated no significant and within experimental error variations in ATP concentrations (in the range of ± 5% relative to control cells) in cells treated with NGs up to 24 hours supporting previous findings. Standard deviation of each nanogel concentration was also found low (≤ 3%) further confiming data consistency. It is important to note that generally higher values of SD are observed in ATP assays compared to PI assays due to the higher complexicty of the first which involve the extra step of medium transfer leading to higher variability.

It should also be considered that HaCaT cells are generally quite resistant to stress and exogenous compounds. As an example of this resistance, A. Schmidtt et al. were able to develop an HaCat cell line resistant to the extremely toxic sulphur mustard. [37] Therefore, in order to confirm nanogel biocompatibility and to obtain results with higher consistency it was decided to extend and repeat the same analyses on a more sensitive cell line, fibroblast.

4.2.2 Normal dermal human fibroblast (NDHF)

Fibroblast (Figure 4.16) are long, flat, and star-shaped cells extensively distributed in the connective tissue and are responsible for the secretion of fibres in the extracellular matrix (ECM) [38-40]. They are involved in wound healing, the regulation of epithelial differentiation and inflammation [40].

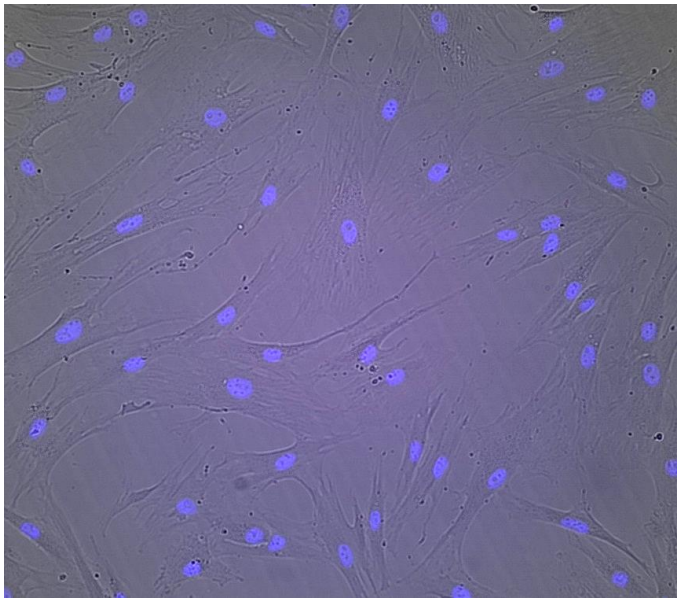

Fig. 4.16 Fibroblast cell line culture where nuclei are stained with 4',6-diamidin-2-fenilindolo (HOECHST 3342). Image recorded by Miss Josephine Blersch and obtained by using an InCell analyser.

Incubation of fibroblast with MRGC 209, 211 and 213, for 24 hours, at concentration up to 400 µg/mL did not indicate any reduction of cell viability however incubation with MRGC 214 showed small signs of cellular death for concentration equal and higher than 200 µg/mL (Figures 4.17 and 4.18). Also in this case a low SD < 1% was observed demonstrating high data consistency.

As for HaCaT cell line, PI assay was performed for the assessment of cytotoxicity in fibrobalst following the same protocol as for HaCaT cells with the only difference of seeding concentration. NDHF were in fact seeded at a density of 5×10^3 cells (due to their larger size) while immortalised keratinocytes at 2×10^4 cells.

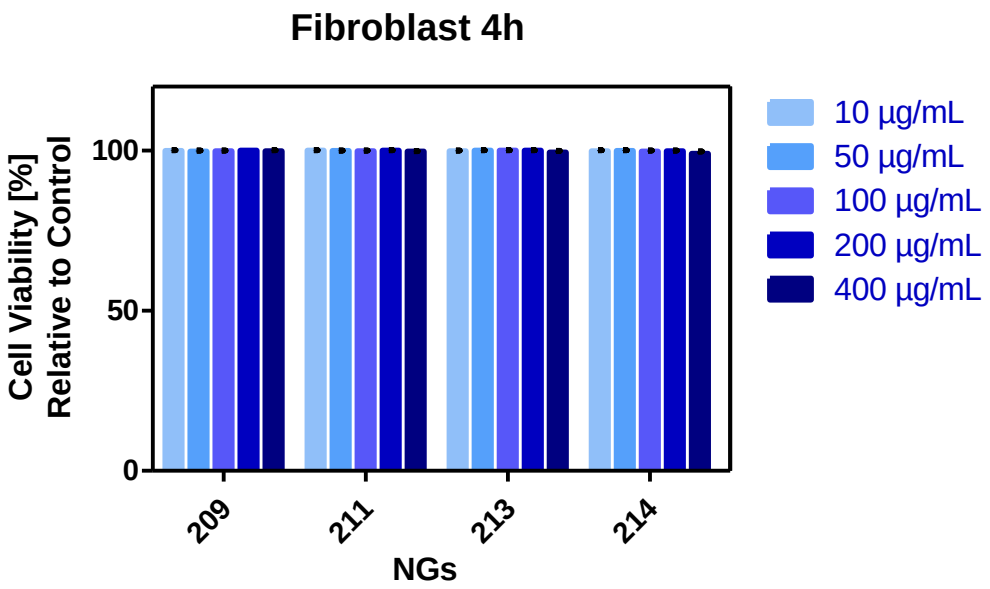

Fig. 4.17 Cytotoxicity of NGs in Fibroblast after 4 hours incubation reported as a mean value of triplicates plus the standard deviation (SD).

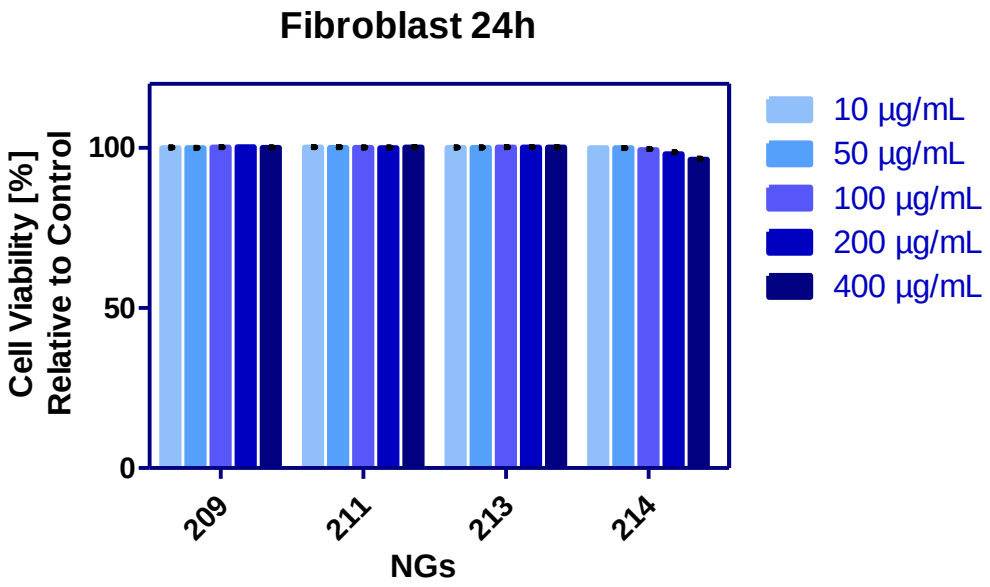

Fig. 4.18 Cytotoxicity of NGs in Fibroblast after 24 hours incubation reported as a mean value of triplicates plus the standard deviation (SD).

In the previous paragraph the strength and chemical resistance of HaCaT was mentioned, which make them not the most reliable cell line in the estimation of cytotoxicity. On the contrary fibroblasts can provide a more accurate view on viability

due to their higher sensitivity. Moreover, NDHF are expressed in almost all the tissues of human body making them an excellent model for a general toxicological study.

In addition, fibroblasts are more suitable for shape and growth variation analysis than HaCaT cells, as they are bigger in size, possess slower division rate and are generally more sensitive to external compounds. Therefore, as for HaCaT cells, a visual investigation on NDHF was performed to individuate a correlation between PI assay data and the eventual morphological and growth rate changes (Figures 4.19-4.21)

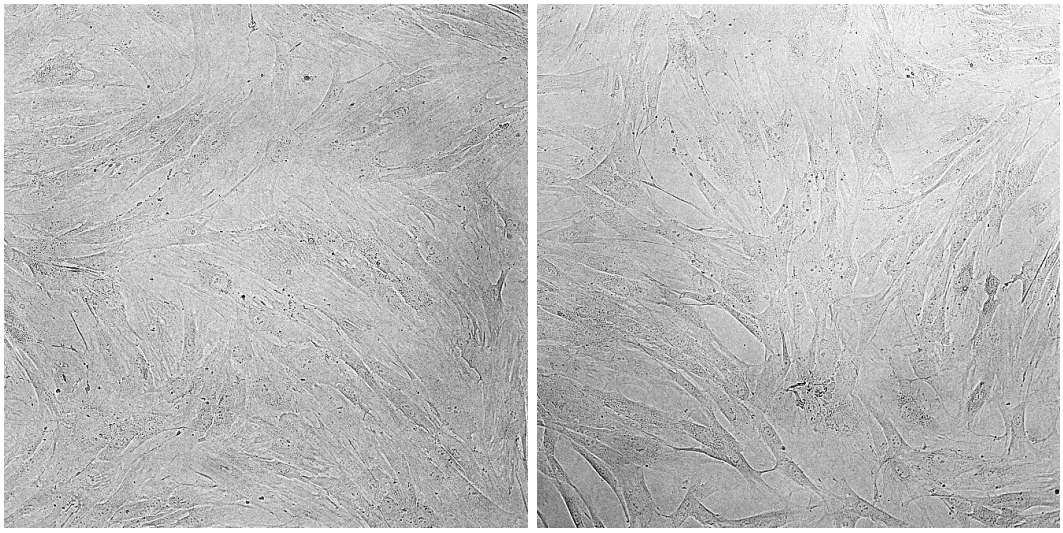

Fig. 4.19 Control cells on the left and cells incubated with MRGC 213 at 400 µg/mL on the right, after 24 hours

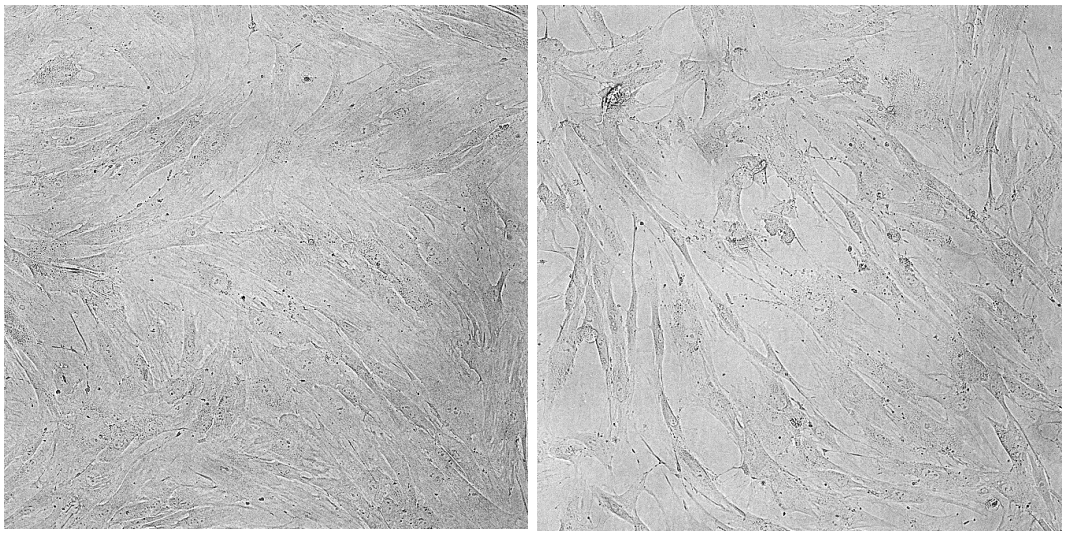

Fig. 4.20 Control cells on the left and cells incubated with MRGC 214 at 200 µg/mL on the right, after 24 hours

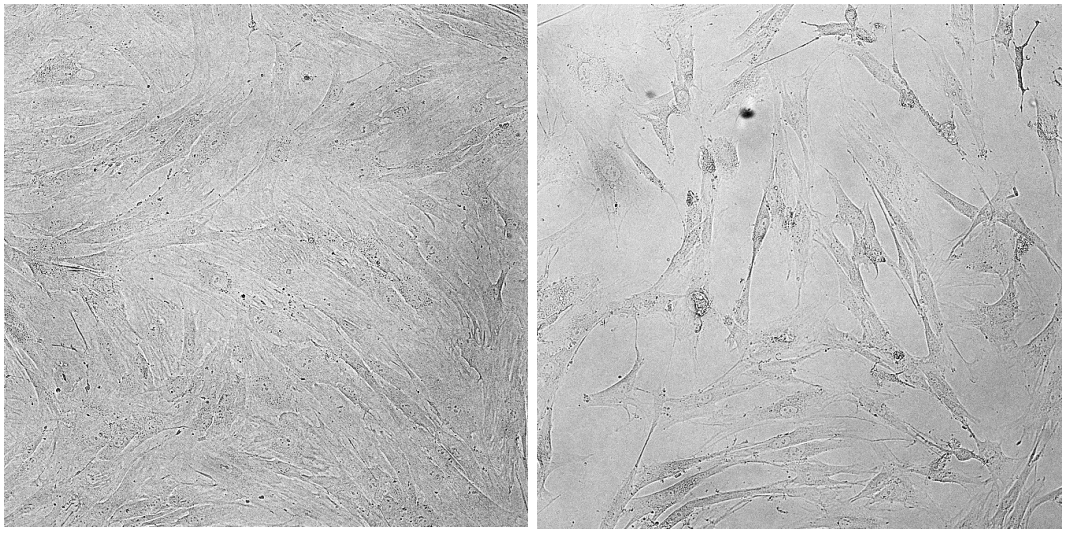

Fig. 4.21 Control cells on the left and cells incubated with MRGC 214 at 400 µg/mL on the right, after 24 hours

Figure 4.19-4.21 confirmed results obtained with PI assays. While there was no effect on morphology and cell viability for MRGC 213, in the case of MRGC 214 it is clear that organisational changes and reduction in cell growth were occurring starting from a concentration of 200 µg/mL and to a greater extent at 400µg/mL. However, these were considered high concentrations and realistically cells would never be exposed to this amount of NGs in vivo.

ATP levels were then evaluated by employing the same protocol used for immortalised keratinocytes and with seeding density at 5×10^3 cells as for PI assay.

Adenosine trisphosphate assay confirmed results achieved with cytotoxicity and morphological analyses (Figures 4.22 and 4.23). MRGC 214 at 400µg/mL in particular produced a significant decrease in ATP levels, suggesting irreversible effects on cellular homeostasis. As the cells dies their energy production decreases giustifying the lower levels of ATP observed.

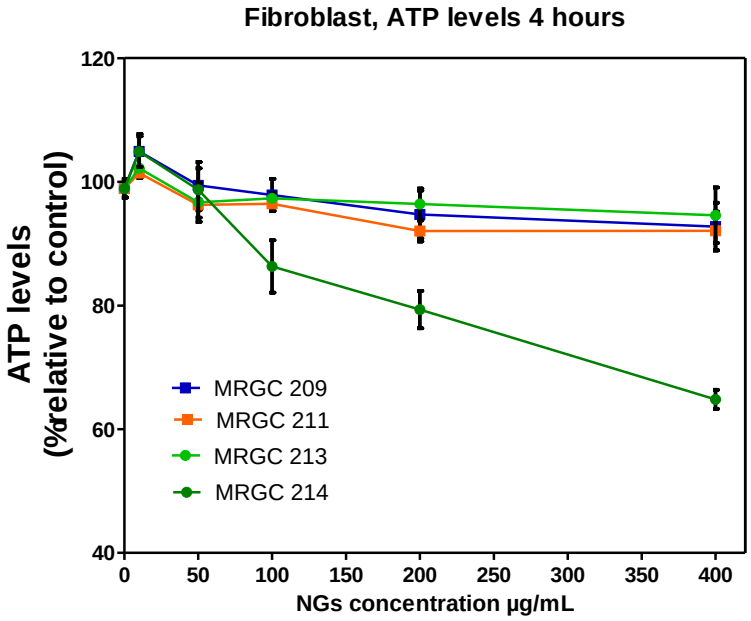

Fig. 4.22 ATP levels relative to control in NDHF incubated for 4 hours with various concentration of NGs reported as mean value of triplicates plus the standard deviation (SD).

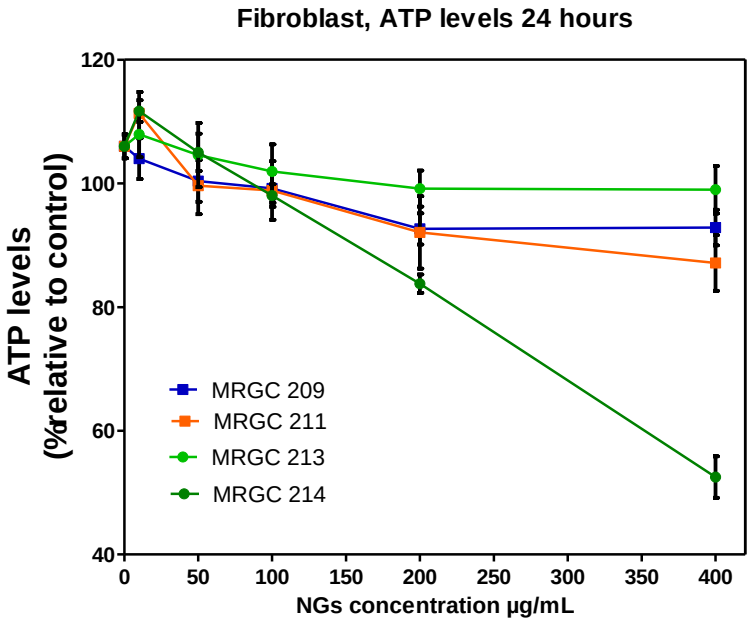

Fig. 4.23 ATP levels relative to control in NDHF incubated for 24 hours with various concentration of NGs reported as mean value of triplicates plus the standard deviation (SD).

As for HaCaT cells, Figures 4.22 and 4.23 are condensed ATP levels graphs of data while Figure 4.24 below show in a more clear manner the ATP level variation for each individual nanogel.

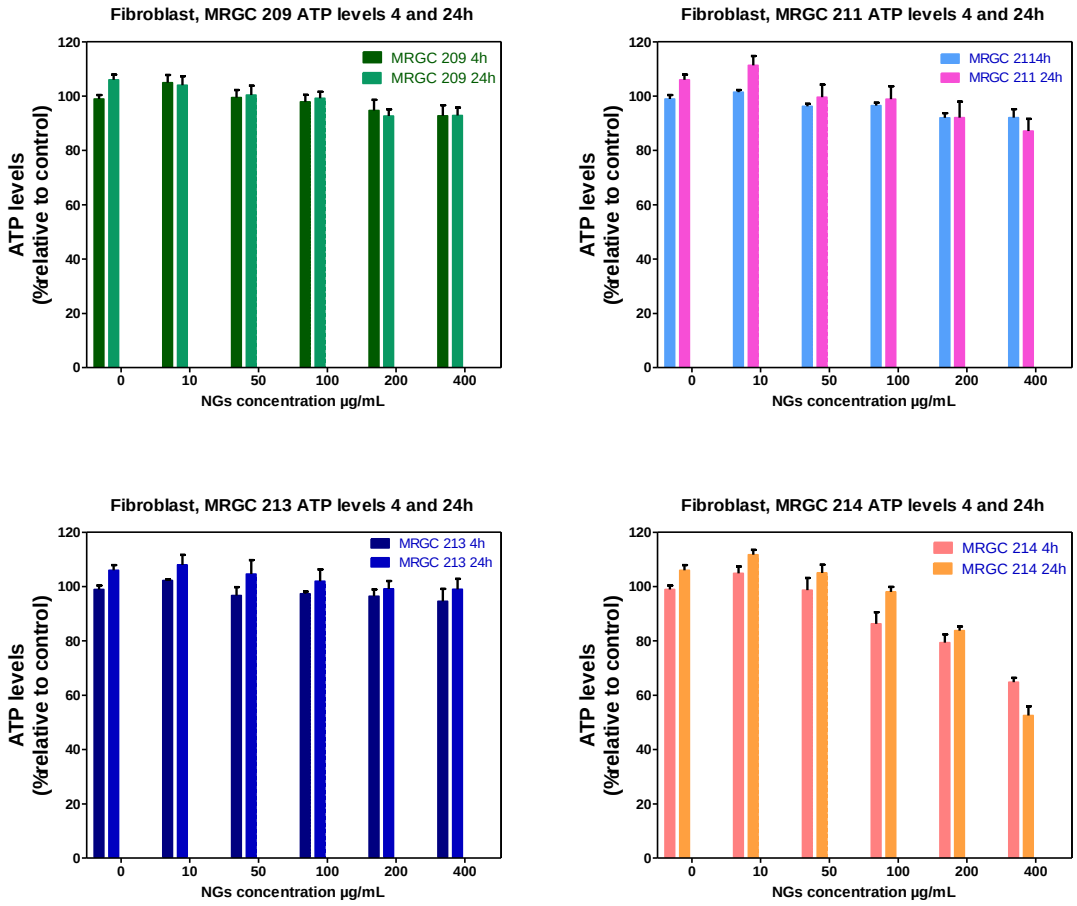

Fig. 4.24 ATP levels relative to control in NDHF incubated for 4 and 24 hours with various concentration of NGs reported as mean value of triplicates plus the standard deviation (SD).

These novel methacrylate based nanogels proved not to affect cell viability, after 24 hours incubation, up to a concentration 100 µg/mL both on NDHF and HaCaT cell lines herein tested and up to 400 µg/mL in HaCaT. Furthermore, no morphological or metabolic variation were observed after cell exposure to nanoparticle, for 24 hours, up to 100 µg/mL in fibroblast and up to 400 µg/ml in immortalised keratinocytes, in agreement with cytotoxicity results. Replicates, randomisation together with the fact that all the three analyses were confirming the same results, were promising findings that laid solid foundations for the further development of this novel drug delivery system, which then involved the testing of pharmaceutically active molecules loading and releasing capabilities of nanogels, described in chapter four.

Having demonstrated the nanoparticles suitability for transdermal delivery applications, the focus was then directed toward the assessment of cellular internalisation of nanogels and their drug delivery capabilities, in particular understanding the possibility to use the nanoparticles as a vehicle for gene therapy. Therefore, a third cell line was included in this work to test siRNA release ability of nanoparticles and at the same time confirm their uptake by cells.

The cell line selected was a genetically modified HeLa, expressing green fluorescent protein (GFP), able to switch the fluorescence off upon treatment with short interfering RNA (siRNA) specific for GFP's gene. Because an additional cell line was used cytotoxicity studies were performed also on HeLa cells and are presented in the next paragraph. The internalisation and siRNA release studies are instead described in depth in chapter four in order to maintain more defined structure and content of each chapter.

4.2.3 HeLa cells

HeLa are an established cell line originating from cervical carcinoma of a patient named Henrietta Lacks (Figure 4.25) [41]. They are among the most widely used cell lines for biological studies [42-45]. Furthermore their use have lead to the discovery of a vaccine for polio and the award of various Nobel prises [42].

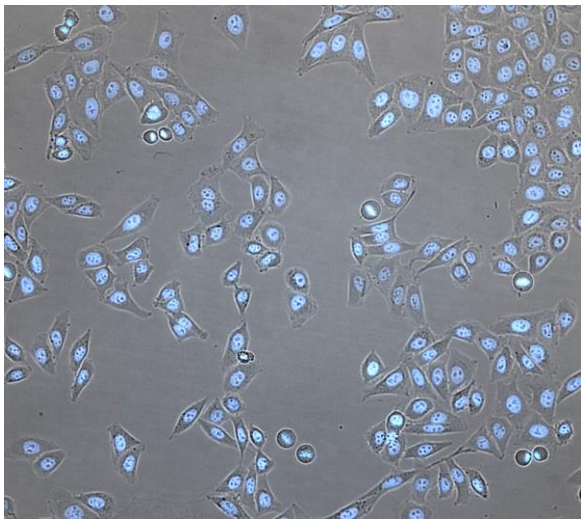

Fig. 4.25 HeLa cell line culture where nuclei are stained with Hoechst 3342. Image recorded by Miss Josephine Blersch and obtained by using an InCell analyser.

Propidium iodide assay was carried out in order to test cell viability on HeLa cell cultures seeded at a cellular density of 5×10^4. As for immortalised keratinocytes, nanogels did not show significant cytotoxicity after 24 hours incubation, with the exception of MRGC 214 at a concentration of 400 µg/mL which showed slight decrement of viability (Figure 4.26). Also in for this assay SD was found to be very low (< 1%)

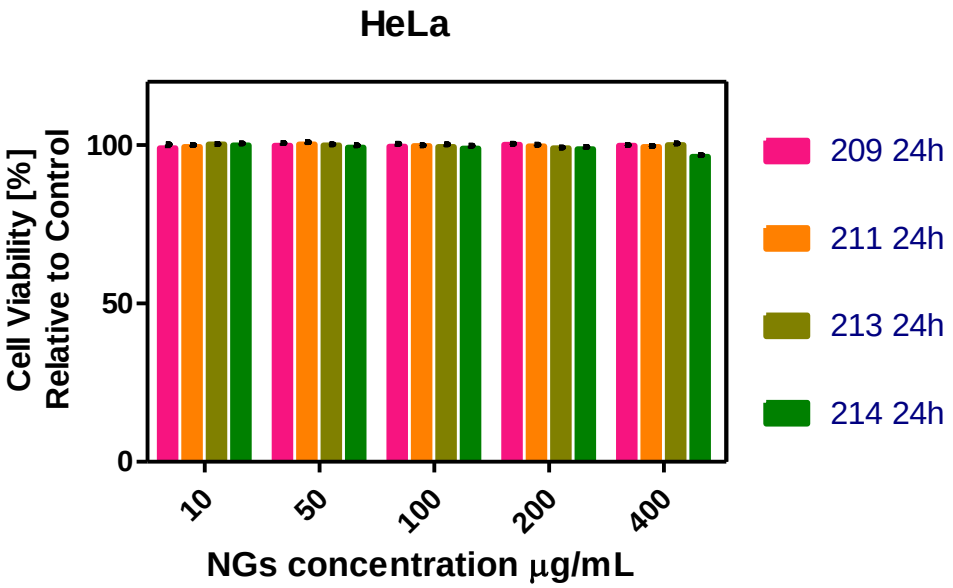

Fig. 4.26 Cytotoxicity of NGs in HeLa cells after 24 hours incubation reported as mean value of triplicates plus the standard deviation (SD).

In this case toxicological assessment was not performed on cells incubated for 4 hours due to time and resources constrains. Although the minor decrease of viability observed for MRGC 214, visual comparison between control cells and HeLa incubated in the presence of nanogel did not show any morphological or cellular density differences (Figure 4.27 and 4.28)

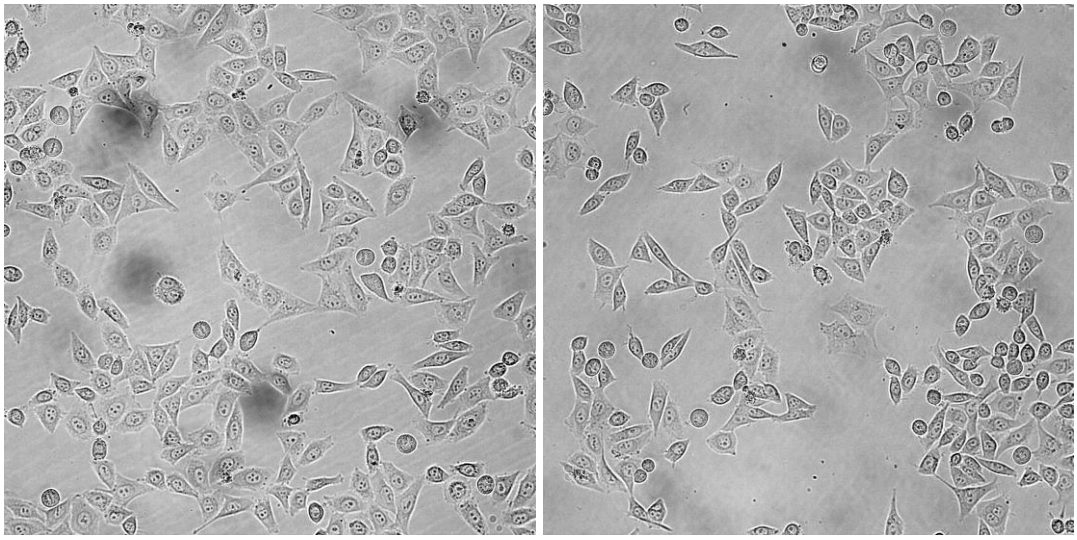

Fig. 4.27 Control cells on the left and cells incubated with MRGC 213 at 400 µg/mL on the right, after 24 hours

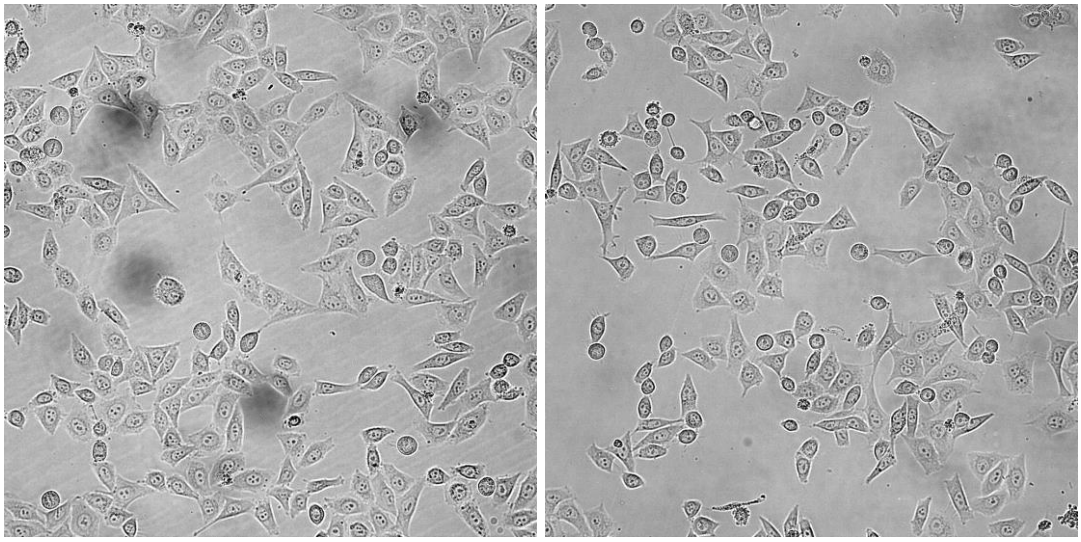

Fig. 4.28 Control cells on the left and cells incubated with MRGC 214 at 400 µg/mL on the right, after 24 hours

In depth cell viability studies were carried out in NDHF and HaCaT cells, therefore ATP levels assay was not performed on HeLa cells as beyond the scope of this study.

4.3 Conclusions

In conclusion nanogels proved to be non-toxic, after 24 hours incubation, up to a concentration of 100 µg/mL in all the cell lines herein tested and up to 400 µg/mL both in HaCaT and HeLa cell lines. The results were confirmed by morphological studies, cell viability and ATP levels assays and further strengthened by data consistency achieved (low SD) These promising results were considered essential for the further development of this novel methacrylate based nanogel for drug delivery applications.

Therefore, after assessing the biocompatibility on different dermal and not dermal cell lines, the next step was to assess the capability of nanogels to upload and realease both small conventional drugs and macromolecule of biological significance like RNA in order to verify their functional capability to be employed in drug delivery. These characteristics are analysed in the following chapter.

Image reference

a) M. Pasparakis, I. Haase; F. O. Nestle. Mechanisms Regulating Skin Immunity and inflammation. *Nat Rev. Immunol.*, **2014**, 14, 289-301. **License Number:** 3962990247987.
b) M. A. Farage, K. W. Miller, P. Elsner; H. I. Maibach. Structural Characteristics of the Aging Skin: A Review. *Cutan. Ocul. Toxicol.*,**2007**, 26, 343-357. Permission granted free of charge from Taylor & Francis for thesis use.
c) J. J. Escobar-Chávez, I. M. Rodríguez-Cruz, C. L. Domínguez-Delgado, R. Díaz- Torres, A. Luisa Revilla-Vázquez; N. C. Aléncaster. Nanocarrier Systems for Transdermal Drug Delivery, Recent Advances in Novel Drug Carrier Systems, PhD. *Ali Demir Sezer (Ed.), InTech*, **2012** DOI: 10.5772/50314. (OPEN ACCESS) Available from: http://www.intechopen.com/books/recent-advances-in-novel-drug-carrier-systems/nanocarrier-systems-for-transdermal-drug-delivery.

References

1. M. R. Prausnitz; R. Langer. Transdermal drug delivery**.** *Nat Biotechnol.,* **2008**, 26 (11) 1261–1268.
2. E. Proksch, J. M. Brandner; J.-M. Jensen. The skin: an indispensable barrier. *Exp. Dermatol.,* **2008**, 17, 1063–1072.
3. C. Pegoraro, S. MacNeil; G. Battaglia. Transdermal drug delivery: from micro to nano. *Nanoscale*, **2012**, 4, 1881–1894.
4. Devraj, D.C. Bhatt; M. Aqil. A Review: Different Generation Approaches of Transdermal drug delivery System. *J. Chem. Pharm. Res.,* **2010**, 2(4), 184-193.
5. B. Baroli. Penetration of Nanoparticles and Nanomaterial in the skin: Fiction or Reality? *J. Pharm. Sci*., **2010,** 99, 21-50.
6. A. Vogt, B. Combadiere, S. Hadam, K. M. Stieler, J. Lademann, H. Schaefer, B. Autran, W. Sterry; U. Blume-Peytavi. 40 nm, but not 750 or 1,500 nm, Nanoparticles Enter Epidermal CD1aþ Cells after Transcutaneous Application on Human Skin. *J. Invest. Dermatol.,* **2006**, 126, 1316-1322.
7. G. Sonavane, K. Tomoda, A. Sanoa, H. Ohshima, H. Terada; K. Makino. In vitro permeation of gold nanoparticles through rat skin and rat intestine: Effect of particle size. *Colloid Surface B*, **2008**, 65 1–10.
8. M. M. Suter, F. M. Crameri, T. Olivry, E. Mueller, C. Von Tscharner; P. J. Jensen. Keratinocyte biology and pathology**.** *Vet. Dermatol.,* **1997**, 8, 67-100.
9. J. A. McGrath, R. A. J. Eady; F. M. Pope. Anatomy and Organization of Human Skin, in Rook's Textbook of Dermatology, Seventh Edition (eds T. Burns, S. Breathnach, N. Cox and C. Griffiths), Blackwell Publishing, Inc., Malden, Massachusetts, USA. doi: 10.1002/9780470750520.ch3 **2004**.
10. B. Ekwall, V. Silano, A. Paganuzzi-Stammati; F. Zucco. Chapter 7: Toxicity Tests with Mammalian Cell Cultures. *Short-term Toxicity Tests for Non-genotoxic Effects,* **1990,** SCOPE. Published by John Wiley & Sons Ltd.
11. J. Lackie. A Dictionary of Biomedicine. *Oxford University* Press, **2015**, eISBN 9780191727948.
12. I. Vermes, C. Haaanen, H. Steffens-Nakken; C. Reutelingsperger. A novel assay for apoptosis Flow cytometric detection of phosphatidylserine expression on early apoptotic cells using fluorescein labelled Annexin V. *J. Immunol. Methods*, **1995**, 184(1), 39-51.
13. M. K. Gould, X. L. Vu, T. Seebeck; H. P. de Koning. Propidium iodide-based methods for monitoring drug action in the kinetoplastidae: Comparison with the Alamar Blue assay. *Anal. Biochem.,* **2008**, 382, 87-93.
14. A. M. Rieger, B.E. Hall, L. Thuong Luong, L. M. Schang; D. R. Barreda. Conventional apoptosis assays using propidium iodide generate a significant number of false positives that prevent accurate assessment of cell death. *J. Immunol. Methods*, **2010**, 358, 81-92.

15. H. Zhao, J. Oczos, P. Janowski, D. Trembecka, J. Dobrucki, Z. Darzynkiewicz; D. Wlodkowic. Rationale for the Real-Time and Dynamic Cell Death Assays Using Propidium Iodide. *Cytom. Part A*, **2010**, 77, 399-405.
16. R. C. Wilkins, B.C. Kutzner, M. Truong, J. Sanchez-Dardon; J. R. N. McLean. Analysis of Radiation-Induced Apoptosis in Human Lymphocytes: Flow Cytometry Using Annexin V and Propidium Iodide Versus the Neutral Comet Assay. *Cytometry*, **2002**, 48, 14-19.
17. High Content-Analysis. From: GE Healthcare Life Sciences website. http://www.gelifesciences.com/webapp/wcs/stores/servlet/catalog/en/GELifeSciences-uk/applications/high-content-analysis
18. S. A. Latt, G. Stetten, L. A. Juergens, H. F. Willard; C. D. Scher. Recent developments in the detection of deoxyribonucleic acid synthesis by 33258 hoechst fluorescence. *J. Histochem. Cytochem.,* **1975**, 23, 493-505.
19. D. J. Brayden, S.-A. Cryan, K. A. Dawson, P. J. O'Brien; J. C. Simpson. High-content analysis for drug delivery and nanoparticle applications. *Drug Discov. Today,* **2015,** 8, 942-957.
20. R. Rennie. A Dictionary of Chemistry 7th edition. *Oxford University* Press, **2016**, eISBN 9780191789540.
21. J. Wang, Y. Jiang, C. Zhou; X. Fang. Aptamer-Based ATP Assay Using a Luminescent Light Switching Complex**.** *Anal. Chem.,* **2005,** 77, 3542-3546.
22. H. S. Garewal, F. R. Ahmann, R. B. Schifman; Abbie Celniker. ATP Assay: Ability To Distinguish Cytostatic From Cytocidal Anticancer Drug Effects. *J. Natl. Cancer I.,* **1986**, 77(5), 1039-1044
23. CellTiter-Glo® Luminescent Cell Viability Assay **(**Instructions for Use of Products **G7570, G7571, G7572 and G7573).** Technical bulletin, Promega Corporation, **2015**.
24. P. Boukamp, R. T. Petrussevska, D. Breitkreutz, J. Hornung, A. Markham; N. E. Fusenig. Normal Keratinization in a Spontaneously Immortalized Aneuploid Human Keratinocyte Cell Line. *J. Cell Biol.,* **1988**, 106, 761-771.
25. J.-J. Yin, J. Liu, M. Ehrenshaft, J. E. Roberts, P. P. Fu, R. P. Mason, B. Zhao**.** Phototoxicity of nano titanium dioxides in HaCaT keratinocytes-Generation of reactive oxygen species and cell damage. *Toxicol. Appl. Pharm.,* **2012**, 263, 81-88.
26. M. Schoop, N. Mirancea; N. E. Fusenig. Epidermal Organization and Differentiation of HaCaT Keratinocytes in Organotypic Coculture with Human Dermal Fibroblasts. *J. Invest. Dermatol.,* **1999**, 112, 343–353.
27. A. D. McNeilly, J. A. Woods, S. H. Ibbotson, C. R. Wolf; G. Smith. Characterization of a Human Keratinocyte HaCaT Cell Line Model to Study the Regulation of CYP2S1. *Drug. Metab. Dispos.,* **2012**, 40, 283-289.
28. H. Lianga, C. Jin, Y. Tang, F. Wang, C. Ma; Y. Yang. Cytotoxicity of silica nanoparticles on HaCaT cells. *J. Appl. Toxicol.,* **2014**, 34, 367-372.
29. Y. Zhao, J. Sun, W. Dou; J.-H. Hu. Curcumin inhibits proliferation of interleukin-22-treated HaCaT cells. *Int. J. Clin. Exp. Med.,* **2015**, 8(6), 9580-9584.

30. A. F. Deyrieux; V. G. Wilson. In vitro culture conditions to study keratinocyte differentiation using the HaCaT cell line. *Cytotechnology*, **2007**, 54, 77-83.
31. C.-H. Pan, W.-T. Liu, M.-Y. Bien, I-C. Lin, T.-C. Hsiao, C.-M. Ma, C.-H. Lai, M.-C. Chen, K.-J. Chuang; H.-C. Chuang. Effects of size and surface of zinc oxide and aluminum-doped zinc oxide nanoparticles on cell viability inferred by proteomic analyses. *Int. J. Nanomed.,* **2014**, 9, 3631-3643.
32. C. Hoskins, L. Wang, W. P. Cheng; A. Cuschieri. Dilemmas in the reliable estimation of the in-vitro cell viability in magnetic nanoparticle engineering: which tests and what protocols? *Nanoscale Res. Lett.,* **2012**, 7:77.
33. S. Vijayakumar; S. Ganesan. In Vitro Cytotoxicity Assay on Gold Nanoparticles with Different Stabilizing Agents. *J. Nanomater.,* **2012**, (Special issue on Biocompatibility and Toxicity of Nanobiomaterials, Article N. 14).
34. Cha, K. Eun; H. Myung. Cytotoxic Effects of Nanoparticles Assessed In Vitro and In Vivo. *J. Microbiol. Biotechnol.,* **2007**, 17(9), 1573-1578.
35. Synthesis and characterization of pH-sensitive poly(N-2-hydroxyethyl acrylamide)–acrylic acid (poly(HEAA/AA)) nanogels with antifouling protection for controlled release. *Soft Matter,* **2012**, 8, 7848-7857.
36. R. Salehi, S. Rasouli; H. Hamishehkar. Smart thermo/pH responsive magnetic nanogels for the simultaneous delivery of doxorubicin and methotrexate. *Int. J. Pharm.,* **2015**, 487, 274-284.
37. A. Schmidt, D. Steinritz; H. Thiermann. Development of the sulfur mustard resistant keratinocyte cell line HaCaT/SM. *Toxicol. Lett.,* **2016**, 244, 44-48.
38. E. Martin. Concise medical dictionary 9th edition. *Oxford University* Press, **2015**, eISBN 9780191767302.
39. R. Hein; E. Martin. A Dictionary of Biology 7th edition. *Oxford University* Press, **2015**, eISBN 9780191059445.
40. R. Kalluri; M. Zeisberg. Fibroblasts in cancer. *Nat. Rev. Cancer,* **2006**, 6, 392-401.
41. R. C. King, P. K. Mulligan; W. D. Stansfield. A Dictionary of Genetics 8th edition. *Oxford University* Press, **2014**, eISBN 9780199376865.
42. J. J. M. Landry, P. T. Pyl, T. Rausch, T. Zichner, M. M. Tekkedil, A. M. Stütz, A. Jauch, R. S. Aiyar, G. Pau, N. Delhomme, J. Gagneur, J. O. Korbel, W. Huber; L. M. Steinmetz. The Genomic and Transcriptomic Landscape of a HeLa Cell Line. *G3: Genes, Genome, Genetics,* **2013**, 3, 1213-1224.
43. A. Topete, D. Melgar, M. Alatorre-Meda, P. Iglesias, B. Argibay, S. Vidawati, S. Barbosa, J. A. Costoya, P. Taboada; V. Mosquera. NIR-light active hybrid nanoparticles for combined imaging and bimodal therapy of cancerous cells. *J. Mater. Chem. B,* **2014**, 2, 6967–6977
44. R. Y. Gaji, M.-H. Huynh; V. B. Carruthers. A Novel High Throughput Invasion Screen Identifies Host Actin Regulators Required for Efficient Cell Entry by Toxoplasma gondii. *PLoS One,* **2013**, 8(5), e64693.
45. O. Donzé; D. Picard. RNA interference in mammalian cells using siRNA synthesized with T7 RNA polymerase. *Nucleic Acid Res.,* **2012**, 30, 10, e46.

Chapter V: Drug uploading and release

5.1 Introduction

Chapter 3 illustrated the promising biological properties of the methacrylate based nanogels (NGs) that have been obtained. In particular, nanogels transfected into cells at concentrations up 100 µg/mL did not induce any cytotoxicity in fibroblasts, HaCat and Hela cells. Furthermore, the nanoparticles in the concentrations ranging from 10 to 100 µg/mL did not show any evidence of inducing cellular morphology or growth variations and did not lead to disruption of normal cell metabolism, measured via quantification of adenosine triphosphate (ATP) levels. Following the cell studies the next step focused on the evaluation of the properties of the nanogels in terms of drug uploading and release.

Table 5.1, shown below, summarises the chemical composition of the NGs used for these studies in order to facilitate correlation between chemical structure and data herein reported.

NG	tBAEMA	EGMMA	MAA	MBA	C_M%	Solvent	Yield	Size
213	60%	0%	20%	20%	0.5%	W:Ac 5:5	91%	6 ±3nm
214	60%	20%	0%	20%	0.5%	W:Ac 5:5	86%	9 ±3nm

Table 5.1 Experimental details of the polymer preparations that were used for this part of the work, together with data regarding chemical yield of the polymerisation and particle size (by number) determined by DLS with 1mg/mL polymer solution in water. Chemical composition of the polymerisation mixtures is given as molar percentage. tBAEMA is tert-butyl amino ethyl methacrylate, EGMMA is ethylene glycol methyl methacrylate, MAA is methacrylic acid and MBA is methylene bis-acrylamide

In order to expand the range of applicability of the methacrylate based nanogels, it was decided to test the ability of nanoparticles to encapsulate large macromolecules as well as small drug molecules. In particular as a result of collaborations of the Resmini's group with other research teams, siRNA was identified as a suitable macromolecule candidate, while the anti-inflammatory fenoprofen was chosen as small compound. While the latter provides an indication of the nanogel suitability for the delivery of

conventional therapeutics, siRNA incorporation may extend the nanoparticles' pharmaceutical employment in the promising field of gene therapy.

This chapter is therefore divided into two main parts: the first one describes siRNA incorporation and release studies while the second one focuses on the encapsulation efficiency of the naogels in the uploading of the small molecule fenoprofen.

5.2 Large biologically active molecules, siRNA delivery

The biological experiments described in this section are the result of a 2 months secondment that was undertaken by the candidate presenting this thesis at the Biocant Technological Park of Cantanhede in Portugal, under the co-supervision of Dr. L. Ferreira and with the collaboration of his research team, in particular Ms. J. Blersch and Ms. M. Comune. The candidate himself obtained all the data presented in this section.

Short interfering RNA (siRNA), also known as small interfering RNA or silencing RNA is a 20-25 nucleic acids chain, arranged to form a double stranded RNA, that reduces gene transcription by either directly suppressing transcription (transcriptional gene silencing [TGS]) or by promoting sequence-specific messenger RNA (mRNA) degradation process (posttranscriptional gene silencing [PTGS]) [1] (Figure 5.1).

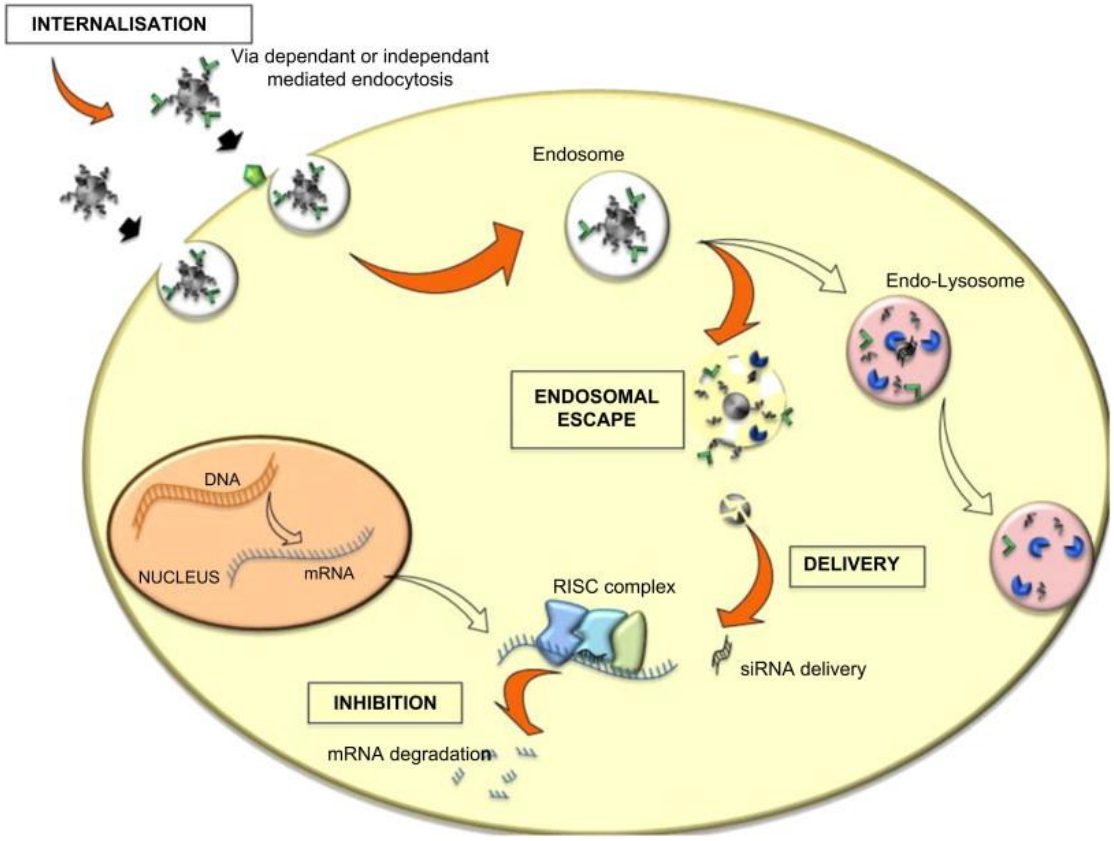

Fig. 5.1 Scheme of siRNA carrier mediated internalisation and gene silencing. From: P. Resnier et al. *Biomaterials*, **2013**, 34, 6429-6443. **License Number:** 3970170454005. [a]

Since its discovery in the late 1990s an increasing number of RNA-based therapies have been developed and are currently undergoing clinical trials, significantly expanding the pharmacological spectrum of conventional drugs, as in principle all the genes can be silenced [2]. Short interfering RNA is in fact being tested for the treatment of cancer, HIV, cardiovascular diseases, ocular treatment, hypercholesterolaemia etc. [3-7]

Although siRNA has great therapeutic potential, its usability is limited by several factors: the low stability in vivo caused by the presence of ribonucleases (enzymes that degrades RNA) both in the serum and in cells; the inability to cross cellular membranes due to siRNA's negative charge; the triggering of an immune response and the high glomerular permeability of siRNA which leads to fast kidneys' excretion rate. [3, 8, 9]

RNA chemical modification was the initial strategy employed, in the first years following the siRNA discovery, in order to avoid ribonucleases degradation and elimination by the immune system [10, 11]. However, this approach was not sufficient to achieve targeted delivery and overcome most of the biological barriers [3]. Today there

are two main approaches used for nucleic acid delivery: viral and non-viral methods. Viral vectors are genetic material extracted from viruses where a therapeutic gene is inserted, replacing those coding for pathogenic viral proteins, while the genetic sequences responsible for viral replication are kept [12]. A vast library of viral vectors, including gammaretrovirus, lentivirus and adenovirus to name few, is currently under investigation with the most successful ones already undergoing clinical trials. [12-13] Despite the high efficiency of viral vectors, this approach has its own limitations. Viral vectors are expensive and difficult to produce. Furthermore, concerns have been raised regarding their oncogenic, immunogenic and inflammatory potential effects [10, 13-15].

Non-viral methods include both the use of nanoparticles as vectors for genetic material and physical methods such as ultrasound or electroporation gene administration [13]. Although the efficiency of non-viral approaches is still not as high as for viral vectors, their wide range of characteristics and tuneable properties together with lower cost, absence or reduced immunogenic and carcinogenic power, makes them a promising alternative for gene delivery [8, 13-14].

In recent years a large number of non-viral carriers for siRNA delivery have been reported. Some examples are gold or lipid nanoparticles, polymers synthesised via reversible addition-fragmentation chain transfer (RAFT) polymerisation and nanogels [16-21]. Advantages of using nanogels for drug delivery were discussed in chapter 1 and 2 together with the potential and limitations of transdermal delivery described in chapter 3. It must be however mentioned that topical skin administration of siRNA offers potential applications in the modulation of genes responsible for various cutaneous or subcutaneous disorders such as psoriasis, pachyonychia congenital, rheumatoid arthritis etc. [22]

When considering a suitable carrier for siRNA delivery, the negative charge and chemical composition of the RNA interference strand have to be taken into account (Figure 5.2). Positive charged particles are in fact employed for successful RNA complexation [23-25].

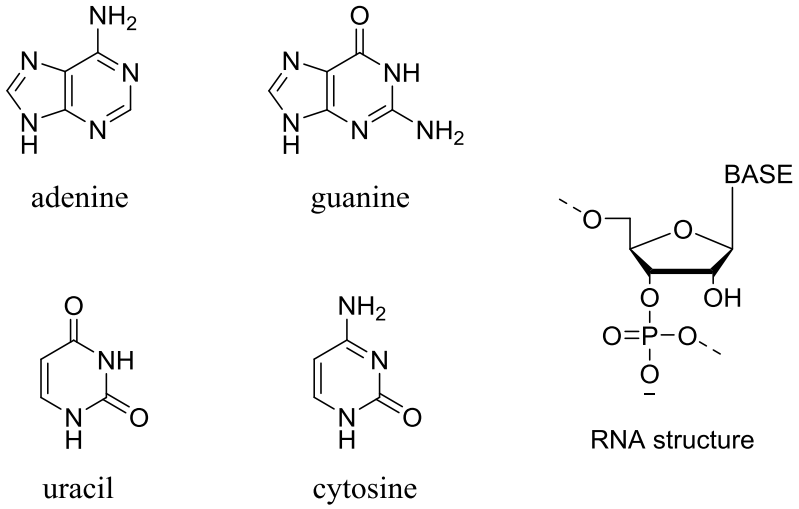

Fig. 5.2 Chemical structure of nucleic bases and basic unit of RNA.

The chemical structures of the methacrylate based nanogel's functional groups (Figure 5.3), the nucleic acid bases and the RNA strand (Figure 5.2) allow several ionic and electrostatic interactions between the two entities.

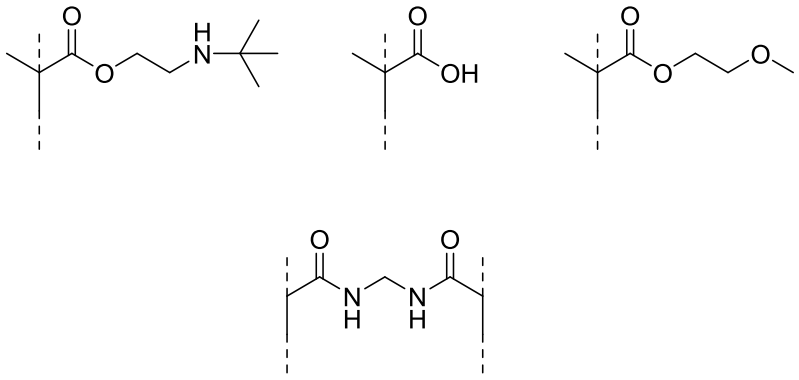

Fig. 5.3 Chemical structures of NGs' functional groups. Clockwise: tert-butyl amino ethyl methacrylate (tBAEMA), methacrylic acid (MAA), ethylene glycol methyl methacrylate (EGMMA) and methylene bis-acrylamide (MBA)

A few examples of these interactions are shown in Figure 5.4 shown below.

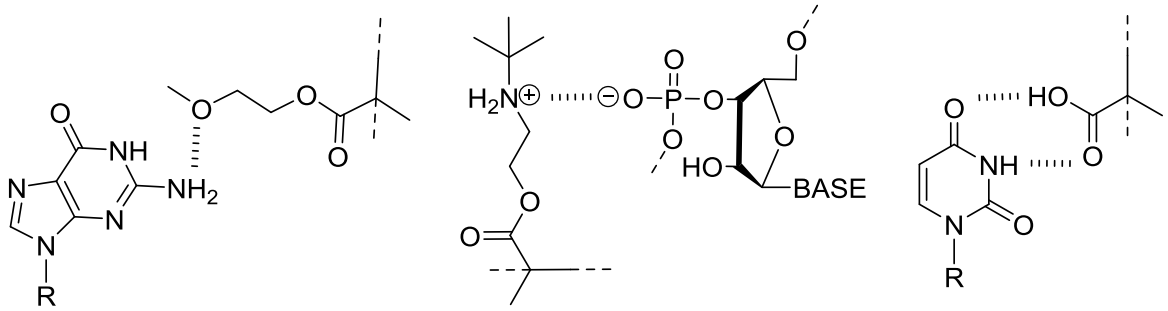

Fig. 5.4 Examples of electrostatic interactions between functional groups and nucleic acid bases together with ionic interactions between NGs and RNA strand. R is the rest of the RNA filament.

The great potential of siRNA for transdermal delivery and the affinity between silencing RNA and nanogels' chemical structures were the premises for testing siRNA encapsulation and release capability of the nanogels.

In order to confirm the ability of the nanopartocles to successfully bind and deliver siRNA inside the cells, therefore avoiding the premature degradation of the RNA, it was decided to employ a model constituted by genetically modified HeLa cell expressing green fluorescent protein (GFP) in combination with a siRNA specific for the knock down of GFP (GFP Duplex I). HeLa GFP is a well-established biological cell model for the evaluation of gene expression and for visualisation purposes [26-28]. The details of the HeLa GFP assay are reported later in this chapter.

The first step in the evaluation of siRNA incorporation and release was the complexation of GFP Duplex I with the nanogels.

5.2.1 siRNA (GFP Duplex I) complexation

To promote electrostatic interactions between nanoparticles (NPs) and siRNA, MRGC 213 and MRGC 214 were suspended in sterile molecular grade, nuclease free, water together with GFP Duplex I and GFP Duplex I fluorescently labelled with cyanine 5 (CY5) (Figure 5.5) at a mass ratio NG : siRNA of 25:1.

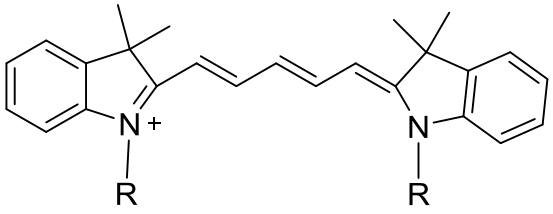

Fig. 5.5 Chemical structure of basic cyanine 5.

The labelling of GFP Duplex I with CY5 served as a way to visually localise the siRNA during cellular imaging and to evaluate the degree of complexation of siRNA with the nanogels.

The complexation efficiency was determined indirectly by measuring the CY5 residual fluorescence in the supernatant of the centrifuged solution of NG : siRNA complexes. The protocol was based on the assumption that unbounded siRNA would have remained in solution while heavier complexes would have precipitated. The values obtained were subtracted from fluorescence intensity of standard solutions of CY5 tagged siRNA previously measured. Furthermore, the fluorescence intensity of a solution of NGs in water non-complexed with RNA interference was used as baseline for the analysis of GFP Duplex I-CY5 complexed nanogels.

MRGC 213 and MRGC 214 were both shown to possess high loading efficiency, 99.4%±0.2. These data were calculated as mean values of triplicates. Although the results may seem high, several other studies, reported in literature, show the achievement of similar siRNA uploading efficiency in nanogels as well as for other nanoparticles such as liposomes. [23, 29-30] Furthermore the almost identical complexation efficiency achieved by the two different nanogel formulations seemed to suggest that the ionic interaction between the positive charges of tBAEMA with the negatively charged RNA strand plays the key role in the complexation. After this study the next step focused on cell transfection.

5.2.2 Cell transfection

HeLa cells were transfected with increasing concentration of nanogels ranging from 20 to 100 μg/mL. The three concentrations used (20, 50 and 100) were selected taking into account results obtained while testing cytotoxicity and cell metabolism as described in chapter 4, which showed no sign of toxicity, cell morphology changes and adenosine triphosphate fluctuations.

In order to prepare the cells for transfection with the nanogels : siRNA complexes, HeLa GFP cells were seeded 24 hours prior to transfection and cultured in full medium consisting of DMEM (without phenol red) containing 5% fetal bovine serum (FBS), penicillin-streptomycin (PenStrep) and Blasticidin. Phenol red confers a red color to the medium. This visually facilitates pipetting into the well plates. However, this color could also interfere with the red fluorescence of CY5. For this reason, it was decided to employ phenol red free medium. After the pre-transfection, the medium was replaced with fresh one containing nanogel-siRNA complexes or Lipofectamine RNAiMAX (a transfection vector) for the control cells, in order to compare cells exposed to similar conditions. The transfection was performed in starvation medium consisting of DMEM only, for 4 hours. The starvation medium was characterized by the absence of the essential proteins contained in FBS. This particular medium was used to mimic stress condition of cells (the target of nanoparticles employed for drug delivery) and to further promote the internalization of the nanogels.

After 4 hours of transfection, additional medium was added to the cells to give a final FBS concentration of 2.5%, reduced from the standard 5%, to decelerate cellular proliferation and avoid 100% cell confluency. These conditions were maintained for 48 hours. When 100% cell confluency is reached there is no more growing space for cells. Therefore, new cells, resulting from cellular division, replace old cells leading to their detachment from the wells' walls. When the cells detach from the walls of the well they undergo cellular death. In these conditions it becomes difficult to evaluate cell toxicity by comparing control cells with nanogel transfected ones, as it would be impossible to discriminate between the cell deaths associated with 100% confluency and the eventual cytotoxicity caused by the nanoparticles.

5.2.3 HeLa GFP knock down

Following 48 hours incubation with nanogels, HeLa GFP cells were stained with propidium iodide (PI) and Hoechst H33342 (nuclei staining) to assess cell viability, as reported in chapter 4. Dead cells, with compromised cell membrane, were stained by both Hoechst H33342 and PI, while live cells were stained only by Hoechst H33342.

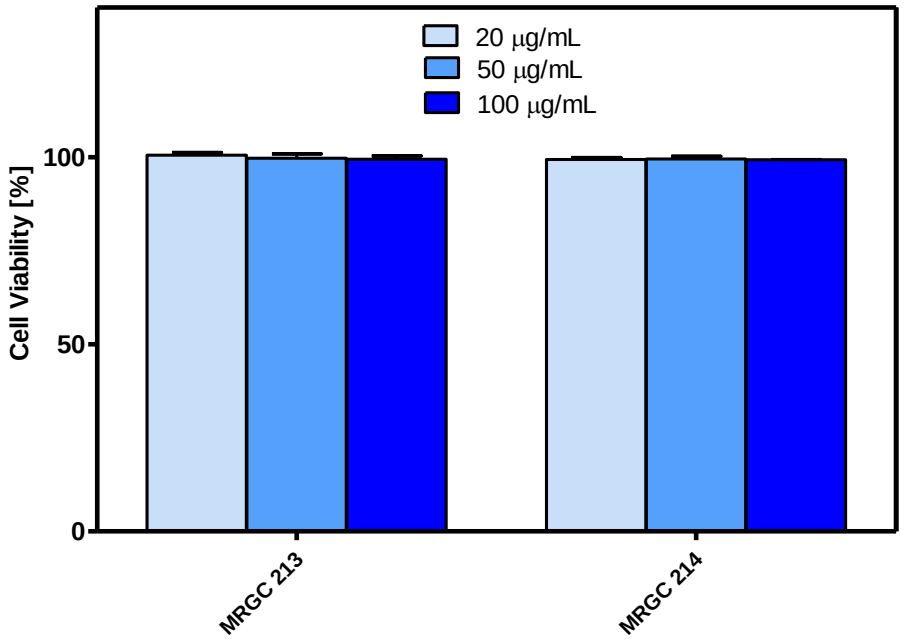

Fig. 5.6 Cytotoxicity of NGs in HeLa GFP cells after 48 hours transfection. Reported as a mean value of triplicate plus the standard deviation (SD). All values are relative to control cells not treated with nanogels.

Data (shown in Figure 5.6) demonstrated no signs of cytotoxicity for HeLa GFP at concentrations ranging from 20 to 100 μg/mL, after 48 hours transfection with nanogels.

Together with cell viability, assessment of the fluorescence intensity of the channel for CY5 was measured, using high content imaging paired with the automated fluorescence microscope, to evaluate siRNA internalisation into cells. As seen in Figure 5.7 intensity grows proportionally to nanogel concentration fed to cells.

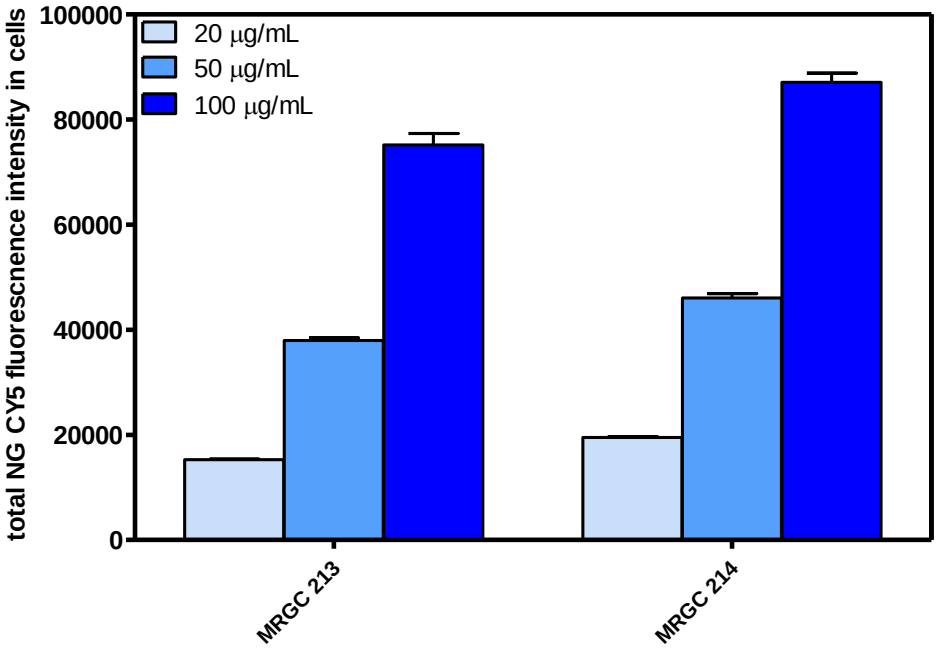

Fig. 5.7 CY5 channel fluorescence intensity in cells. Reported as a mean value of triplicate plus the standard deviation

The results provided further evidence that the different chemical composition of nanogels did not affect significantly the percentage of siRNA complexation and confirmed that interaction between tBAEMA with siRNA strand provided the highest contribution for the complexation.

However, these data of CY5 fluorescence intensity alone were not enough to confirm nanogel internalisation and siRNA release, as fluorescence intensity increase could have been due, exclusively, to the presence of loaded NGs in the medium, not necessarily internalised inside cells. However, this first result was taken as further confirmation that the nanogels were complexed with siRNA.

Microscope imaging provided additional indications of nanogel internalisation as an intense red fluorescence, produced by CY5 (attached to siRNA), was observed in the immediate proximity of the nuclei and inside the cells' cytoplasm (Figure 5.8).

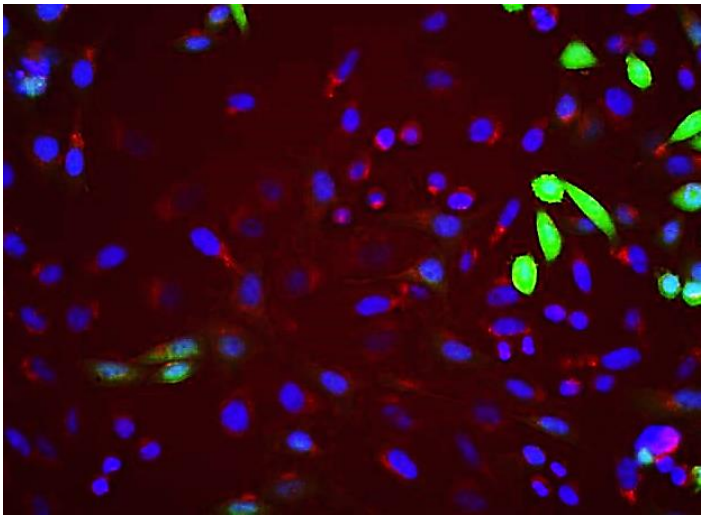

Fig. 5.8 HeLa GFP 48 hours after transfection with MRGC 213 – GFP Duplex I/CY5 100 μg/mL. Cell nuclei stained with Hoechst H33342. Image recorded by Ms. Josephine Blersch and obtained by using an InCell analyser.

Furthermore, the final evidence of successful nanoparticles' internalization and siRNA release was provided by the analysis of green fluorescence reduction, as a result of GFP knock down operated by GFP Duplex I (Figure 5.9). The inability of "naked" silencing RNA to enter the cells and withstand ribonucleases biodegradation was already mentioned in this chapter (section 5.1). As a result, the gene silencing effect can only be explained by the ability of the novel methacrylate based nanogels to act as carriers for the siRNA intracellular delivery.

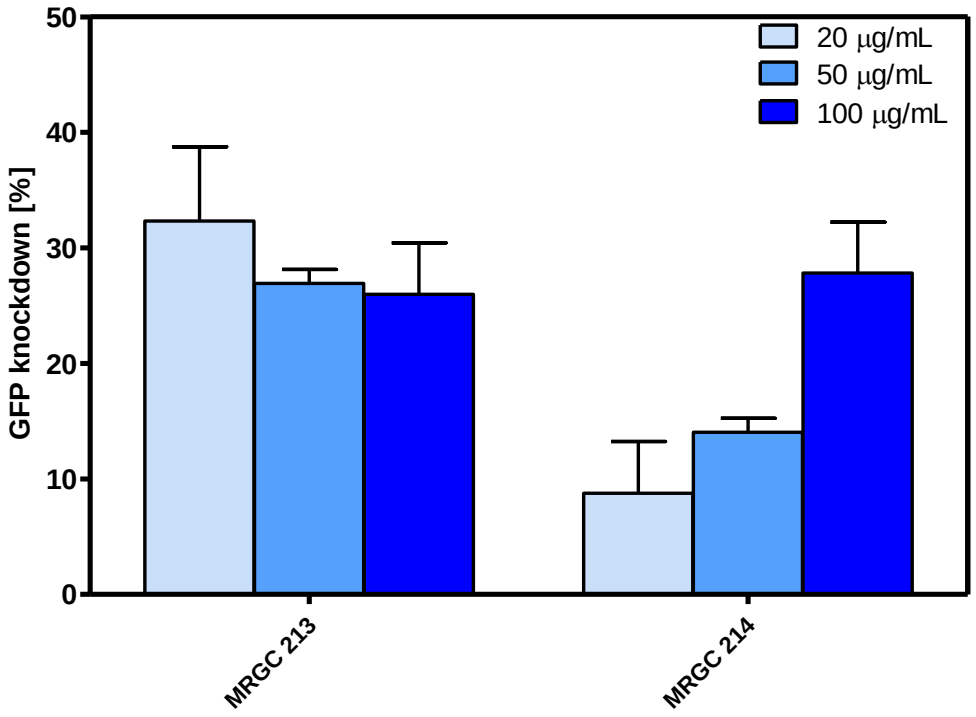

Fig. 5.9 Percentage of GFP knock down, relative to control cells, induced by MRGC 213 and 214 complexed with GFP Duplex I-CY5. Reported as a mean value of triplicates plus the standard deviation

GFP knock down was evaluated by comparing overall well fluorescence of the control HeLa GFP cells with nanogel transfected cells. All data were reported as mean values of triplicates however due to time constrains this experiment was performed only once. Preliminary results seemed to indicate that MRGC 213 induced a green fluorescent protein knock down of 32% ±4 which was independent from nanogel-GFP Duplex I/CY5 complex concentrations, ranging from 20 to 100 μg/mL; on the other hand MRGC 214 produced a GFP silencing effect going from 8 ±3 to 28% ±3 and proportional to the concentration of nanogel-siRNA complexes used to transfect HeLa GFP cells (Figure 5.9). It was hypothesised that the different chemical composition between MRGC 213 and 214 may have played a role in the endocytic pathway and siRNA release profile of the nanogels.

Endocytosis is an energy dependent process used by cells to internalise biomolecules, ions, signalling molecules and it is also the major route of nanoparticles' cellular access [31, 32]. The purposes of the process are the acquisition of nutrients, the defence against pathogens and communication with other cells. [31, 33] Although there are several

endocytic mechanisms, such as phagocytosis, macropinocytois clathrin-dependent and independent etc. (Figure 5.10), they all involve the invaginations of the cellular membrane resulting in the formation of vesicles called endosomes [34, 35].

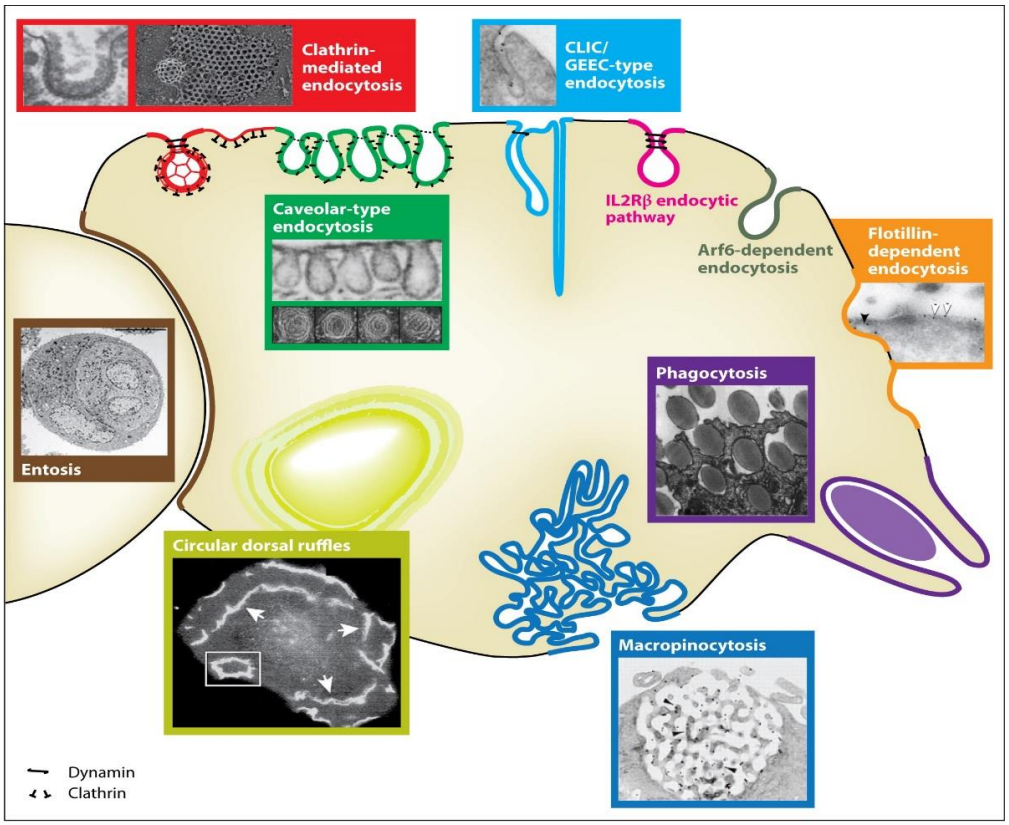

Fig. 5.10 Representation of endocytosis pathways. From G. J. Doherty et al. *Annu. Rev. Biochem.*, **2009**, 78, 857-902. (OPEN PERMISSION for thesis/dissertation)[b]

Endosomes undergo a maturation process that can be divided in 4 key stages (Figure 5.11): 1) early endosomes (EE) are the cell compartments immediately after they receive the cargo from the extracellular environment; 2) late endosome (LE) are more mature vesicles, where the pH ranges from 6 to 4.9 and that progress toward spherical shape; 3) LE then grows in size by fusing with other endosome and 4) endosomes fuse with lysosome forming endolysosome which are vesicles where their content gets degraded by enzymes.

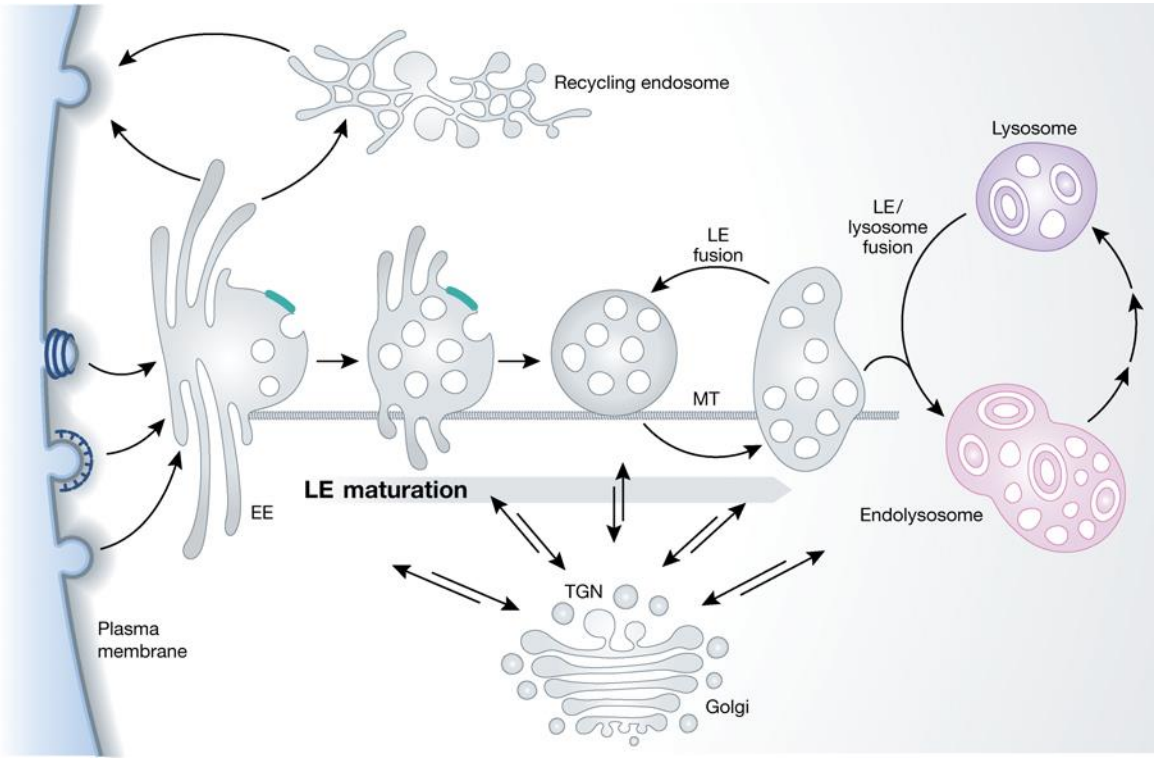

Fig. 5.11 Schematic for endosome/lysosome system (MT= microtubules, TGN= trans-Golgi network). From J. Huotari et al. *EMBO J.*, **2011**, 30, 3481-3500. (**License Number:** 3926480288417). [c]

In order to exert its biological activity, siRNA needs to be released in the cytosplasm [36]. To achieve cytosol release, the nanoparticles need to be able to escape endosome pathway as it would eventually lead to their digestion inside the endolysosome (Figure 5.12). There are several mechanisms of endosomal escape [36, 37]. However, in the case of particles rich in proton acceptor groups (such as the amino group of tert-butylamino ethyl methacrylate) the so called proton sponge effect is the main mechanism of endosomal escape. Essentially the protonation of nanoparticles leads to a flow of H^+, Cl^- and water inside the endosomes, resulting in osmotic swelling and endosome burst. [37]

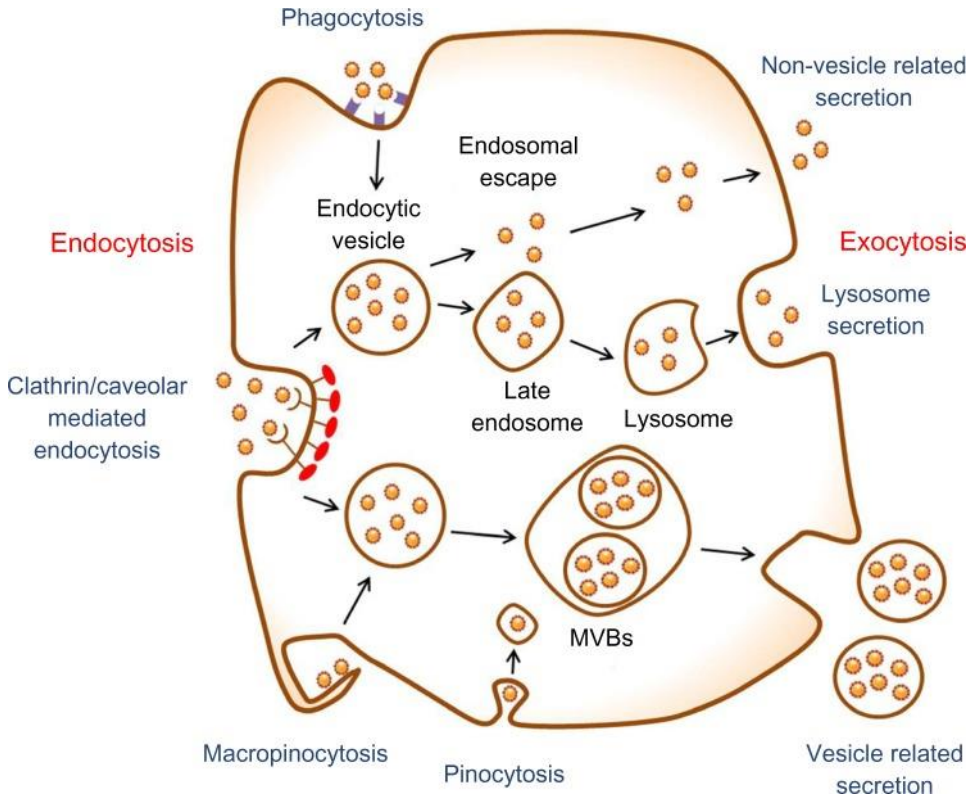

Fig 5.12 Schematic of nanoparticles' endocytosis and exocytosis pathways (MVB**s**, multivesicular bodies). From N. Oh et al.. *Int. J. Nanomedicine,* **2014**, 9 (1), 51-63. (**Order License Id:** 3926421408563). [d]

In view of these facts, it was hypothesised that MRGC 213, due to the presence of additional proton acceptor groups (methacrylic acid moieties), could have escaped endosome at an earlier stage than MRGC 214. Therefore, even the lowest MRGC 213 –siRNA complex concentration of 20 µg/mL was sufficient to obtain the maximum GFP knockdown value of around 30 %, probably the highest gene silencing achievable with the siRNA employed. However as previously mentioned this experiment was performed only once thus this hypothesis will require further experiments in order to be confirmed, but due to time constrains additional analyses could not be performed.

Visual evidences of green fluorescent protein knock down were also shown by fluorescent microscopy imaging (Figures 5.13-5.18). Figure 5.13 and 5.14, below, are images from the control cells, characterised by intense green fluorescence (Figure 5.13) and absence of red CY5 signal (Figure 5.14).

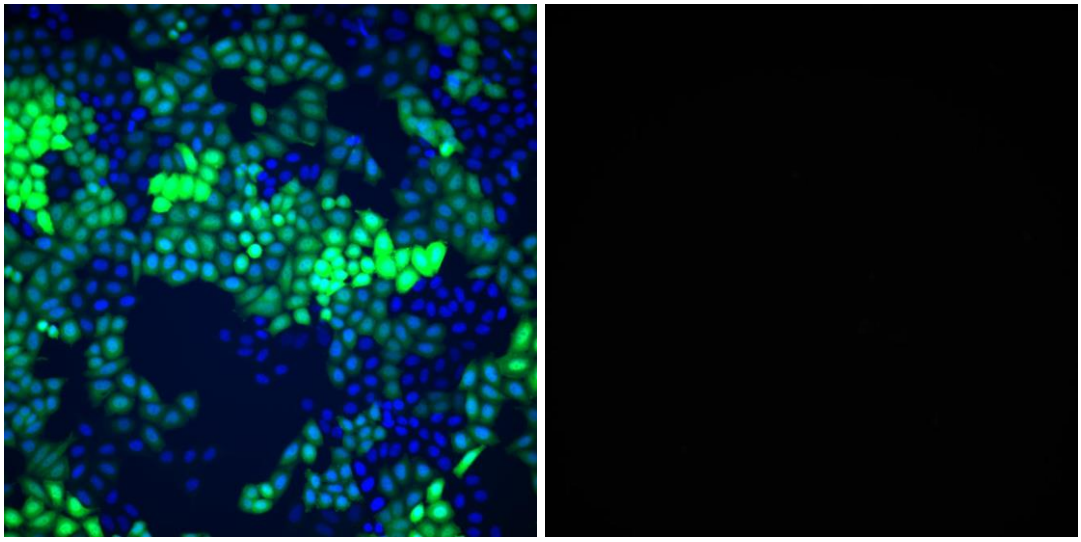

Fig. 5.13-5.14 Left: HeLa GFP 48 hours after incubation with Lipofectamine RNAiMAX. Cell nuclei stained with Hoechst H33342. Merged of CY5, Hoechst H33342 and green channels. Right: CY5 channel. Image recorded by Ms. Josephine Blersch and obtained by using an InCell analyser.

Images of HeLa GFP transfected with NGs-GFP Duplex I/CY5 (Figures 5.15-5.18) showed instead decrease of green fluorescence and intense red signal visible both in the merged channels images (Figure 5.15 and 5.17) and in the CY5 channel (Figures 5.16 and 5.18).

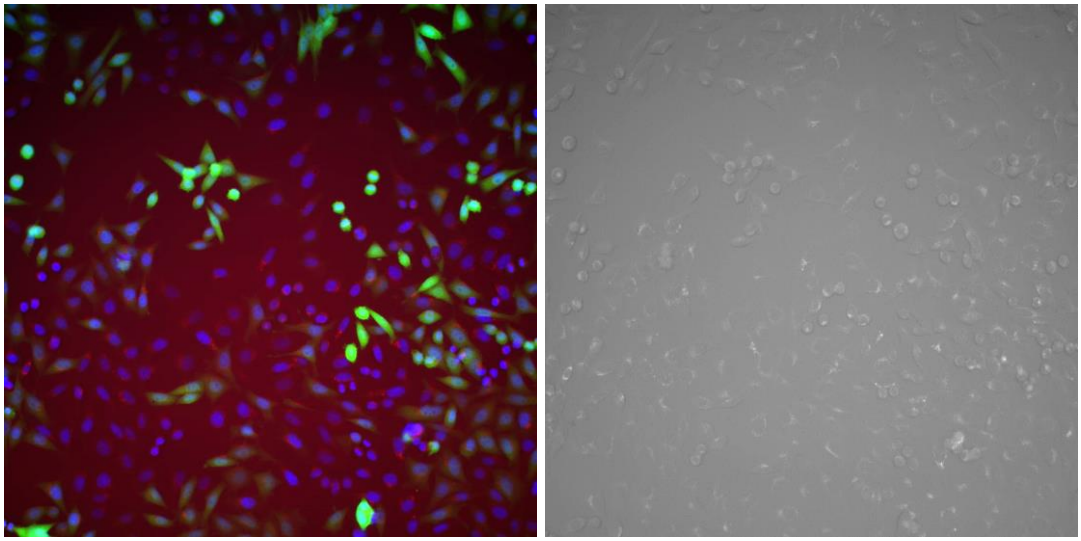

Fig. 5.15-5.16 Left: HeLa GFP 48 hours after transfection with MRGC 213 – GFP Duplex I/CY5 100 μg/mL. Cell nuclei stained with Hoechst H33342. Merged of CY5, Hoechst H33342 and green channels. Right: CY5 channel. Image recorded by Ms. Josephine Blersch and obtained by using an InCell analyser.

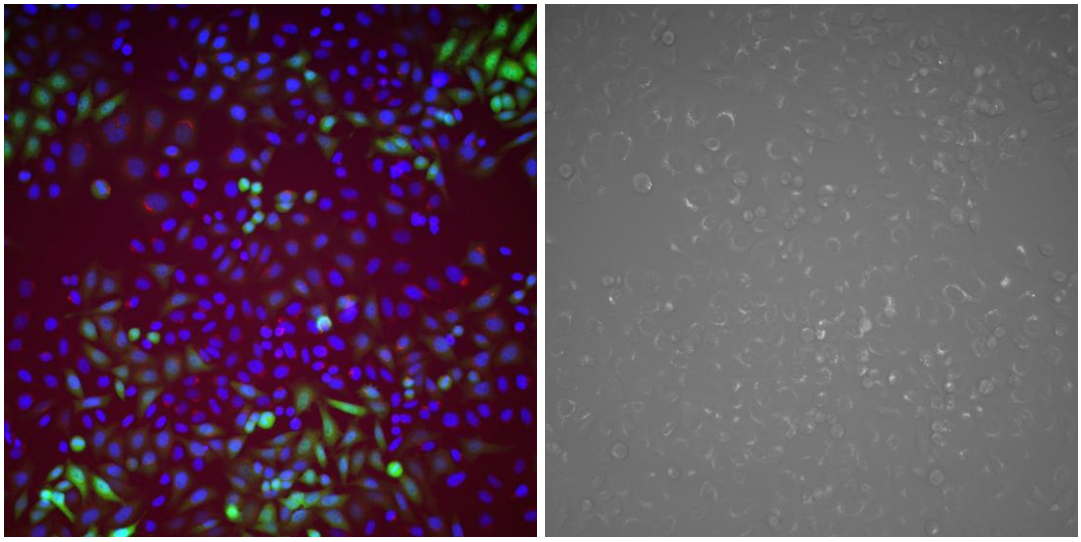

Fig. 5.17-5.18 Left: HeLa GFP 48 hours after transfection with MRGC 214 – GFP Duplex I/CY5 100 µg/mL. Cell nuclei stained with Hoechst H33342. Merged of CY5, Hoechst H33342 and green channels. Right: CY5 channel. Image recorded by Ms. Josephine Blersch and obtained by using an InCell analyser.

Although higher GFP knock down has been elsewhere achieved [38], also thank to formulation improvements [39] or with the use of high efficiency viral vector [40], the results herein presented are comparable, in terms of GFP knock down percentage, to previously reported works. [39, 41]

HeLa GFP cannot be considered a disease model, therefore additional studies will be required for the implementation of these nanoparticles for drug delivery purposes. Nevertheless, the proven ability of nanogels to enter the cells and release their payload provided good basis for the further development of the system.

In the next section the ability of methacrylate based nanogels to incorporate and release conventional small drugs is presented.

5.3 Drug uploading of small molecule

Following the promising results of cytotoxicity, cell metabolism, nanogels cellular internalisation and siRNA release (chapter 3 and 4), it was decided to test encapsulation

and release capability of nanogels for small molecules to assess their usability for more conventional pharmaceutical applications.

When evaluating possible drug candidates to be tested for incorporation, the focus was directed towards anti-inflammatory drugs that could be used also for the treatment of skin disease. In the past years, flufenamic acid was frequently used as model drug within the Resmini's group, therefore it was initially considered [42]. However due to the availability of a chondrocytes model for rheumatoid arthritis via a recent collaboration with Prof M. Perretti and its research team from Queen Mary University of London, fenoprofen was selected as a more suitable molecule as it was already employed in the treatment of rheumatoid arthritis.

Before presenting the results regarding the loading and release of fenoprofen a brief introduction on the drug and rheumatoid arthritis is given in the following section.

5.3.1 Rheumatoid arthritis and fenoprofen

Rheumatoid arthritis (RA) is a chronic inflammatory disease which affects cartilages and bones of the joints. [43] It is a common condition that affects around 1% of the adult population in the developed world, with higher incidence in woman [44-45]. RA is triggered by both genetic (predominantly) and environmental risk factors such as smoking, the diet, socioeconomic status etc. [43-44]. Several are the treatments employed today. They can be divided in: 1) non pharmaceutical involving surgery; 2) pharmaceutical including non-steroidal anti-inflammatory drugs (NSAIDs) like fenoprofen, analgesics and corticosteroids paired with chemical disease-modifying anti-rheumatic drugs (DMARDs) such as methotrexate and 3) biological consisting of tumor necrosis factor (TNF) and interleukin (IL) antagonists, B and T cells blocker, stem cells and gene therapy. [43-44]

Despite the large number of therapeutic approaches that are investigated, an ideal therapy has yet to be identified, as all the previously mentioned strategies are either under development or associated with moderate to high toxic effects [43-44].The use of NSAIDs remains the main treatment of choice for RA, with careful consideration of the side effects.

Fenoprofen (Figure 5.19) is a non-steroidal anti-inflammatory drug (NSAID), also analgesic, which is used to treat arthritic conditions and pain [46-47].

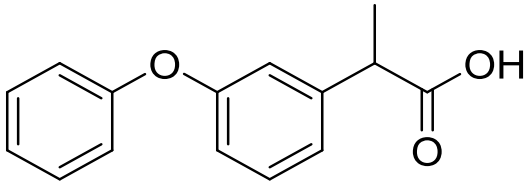

Fig. 5.19 Chemical structure of fenoprofen

It is administered orally and it's commonly associated with headache, drowsiness, dizziness, heartburn, constipation, dyspepsia, myalgia, nausea, vomiting etc. [46-47] Furthermore, long-term NSAIDs therapies are well known to induce severe gastrointestinal, renal, and cardiovascular toxicity when administered for the treatment of chronic diseases. [48] This is due to their poor water solubility resulting in reduced bioavailability, thus requiring high doses which then cause the side effects [49]. In the view of this, the topical and local therapeutic effect achieved via transdermal delivery could potentially avoid the side effect associated with NSAIDs.

It was therefore proposed to employ methacrylate based nanogels as potential carrier for fenoprofen with the final purpose of improving the therapeutic profile of the drug.

The drug incorporation protocol, the evaluation of encapsulation efficiency and loading capacity are reported in the following section.

5.3.2 Drug uploading, encapsulation efficiency and drug release

Particles which are not formed via self-assembly are generally uploaded with drugs, after their synthesis has been completed. Post polymerisation drug encapsulation can be achieved in different ways such as:

- simple drug impregnation by dissolution of both drug and nanoparticles into the same solvent followed by sonication or stirring in order to accelerate and force interactions

- emulsion solvent evaporation method, where an hydrophobic drug is dissolved together with the nanoparticles in a volatile non-miscible organic solvent then dispersed into water containing surfactants and homogenised via sonication or fast agitation letting the organic solvent evaporate
- the thin layer evaporation method, the technique selected in this work which is described later in this paragraph
- spray drying of either one solutions containing both nanoparticles and drug or two separate solutions mixed together, to name few. [50-52]

This latter technique consists in the fast drying of solution droplets extruded at high speed into a cyclone chamber were dry air is circulating through [50]. While spray drying offers the advantage of scalability it is also associated with high cost. [50]

Emulsion evaporation incorporation techniques are widely employed however their use is limited to hydrophobic drugs and to drugs and particles which are soluble in the same organic solvent. Moreover, the use of surfactants requires further purification processes and increase complexity and cost of the system [50]. Simple drug impregnation instead is limited by the use of a solvent able to dissolve both drug and NPs at the same time and able to allow interaction between the two.

In order to overcome all the limitations previously discussed, it was decided to use a combination between the simple drug impregnation and the emulsion solvent evaporation methods. This technique was called thin layer evaporation method. Essentially nanogel (MRGC 213) and the drug were added to a volatile organic solvent (acetone) in which the drug was soluble but not the nanogel. Then the mixture was sonicated for a few minutes and left under stirring in order to let nanoparticles and drug interact. The solvent was then removed by rotary evaporation to produce a thin layer of particles and drugs on the wall of the flask containing the mixture. Finally, the film was re-suspended in high pressure liquid chromatography (HPLC) grade water where the nanoparticles were soluble while the drug was only partially soluble. HPLC grade water was used since drug encapsulation efficiency was evaluated by employing high pressure liquid chromatography coupled with UV detection, using modifications of HPLC analytical methods reported in literature [53-54]. The water mixture was left under stirring for a few minutes in order to fully dissolve the remaining film and to homogenise the system. After the stirring, the mixture was left resting for few minutes in order to allow

insoluble fenoprofen to deposit at the bottom of the vessel. The top portion of the mixture was filtered through 0.45µm syringe filters an injected at the HPLC. Another portion was instead transferred in a centrifuge Eppendorf equipped with a polyethersulfone (PES) membrane placed in the middle of the tube and centrifuged (Figure 5.20).

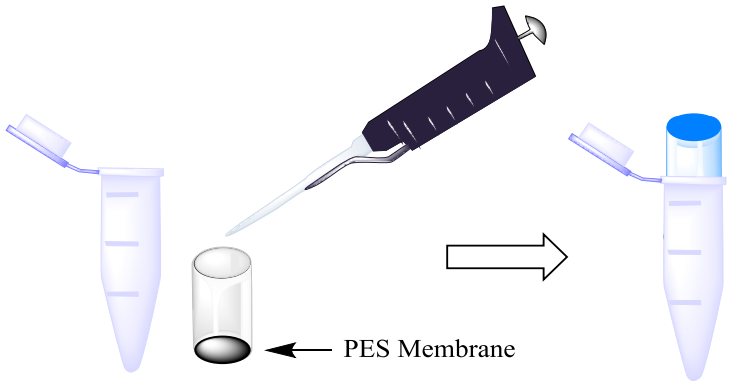

Fig. 5.20 Representation of centrifugal filter equipped with PES membrane

These two procedures were used to compare two different purification techniques. They were in facts used to remove any insoluble fenoprofen and disaggregate any possible dispersed nanogels' clusters not visible to the naked eye. During centrifugation the nanogel-drug suspension was forced through the membrane. Insoluble drug (larger than membrane's molecular cut-off) remained trapped on to the cellulose membrane while soluble and adsorbed drug were passing in the acceptor compartment of the Eppendorf. The content of the acceptor compartment was then injected showing comparable results to injection of filtrate. HPLC grade water was also added into the donor compartment in order to re-dissolve the fenoprofen left and then filtered through 0.45µm syringe filters prior HPLC injection. Although MRGC 213 nanogel was used, the experiment was named MRGC 219 in order to avoid confusion.

Previously the partial water solubility of fenoprofen was mentioned, therefore the drug alone, without the presence of nanonogels, was treated by using the same procedure carried out for MRGC 219 in order to discriminate the amount of fenoprofen dissolved in water from the one uploaded into nanogels.

Fenoprofen elution time, between 12.5 and 13 minutes (Figure 5.21), was achieved by using a mobile phase constituted by acetonitrile : water containing 0.5% acetic acid in a volume ratio of 1:1.

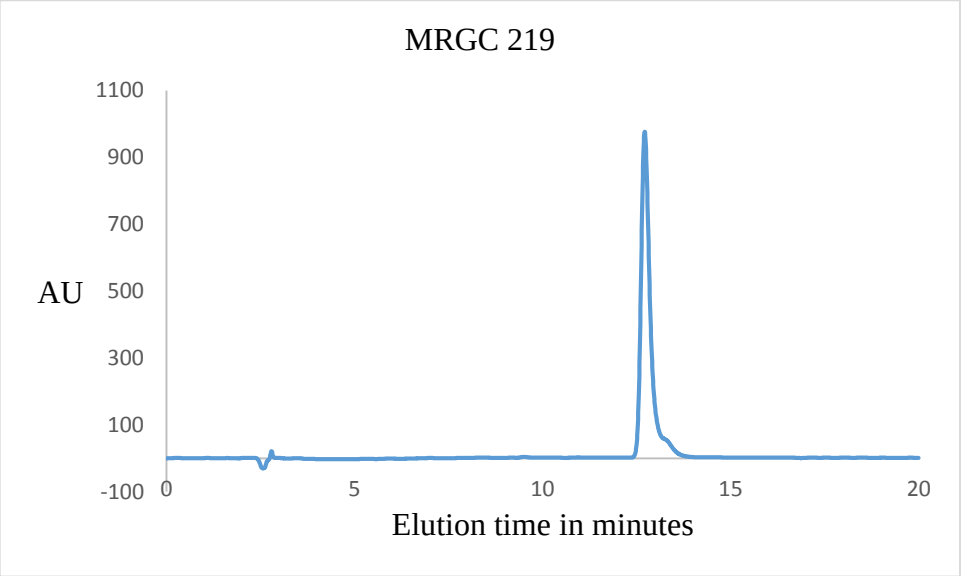

Fig. 5.21 Chromatographic signal of co-dispersed nanogels and fenoprofen filtrate.

Two parameters regarding quantification of drug uploading into the nanogels were evaluated: 1) the encapsulation efficiency which is the percentage of drug uploaded onto the nanoparticles in respect to the total amount of drug used in the experiment, this provides indications on how efficient are the conditions used for drug incorporation and the amount of drug loss 2) the loading capacity which is a percentage that express the maximum amount of drug that a given mass of nanoparticle is able to carry.

Knowing the fenoprofen amount fed into the mixture, the encapsulation efficiency was then assessed by fitting the data of HPLC injections into the equation of a calibration curve previously obtained and adjusting these values by subtracting the amount of drug dissolved in water. Via calculations (Equations 5.1 and 5.2), encapsulation efficiency was found to be 56% ±1 and loading capacity, 84% ±7, was achieved. [55] This latter value was found to be comparable with nanogel uploading capacity attained via similar uploading techniques. [52, 56-57] The values were calculatated from two set of experiment repeated twice.

$$Encapsulation\ efficiency\ (\%) = \frac{\text{weight of drug into nanogels}}{\text{weight of drug fed initially}} x100$$

$$Loading\ capacity\ (\%) = \frac{\text{weight of drug into nanogels}}{\text{weight of nanogels fed initially}} x100$$

Equation 5.1 and 5.2

The release profile of the fenoprofen-loaded nanogels was obtained by dissolving the loaded nanoparticles in phosphate buffer (PBS pH 7.4), transferring the solution in dialysis cassette (M.W. cut off 5 KDa) and dyalising it against PBS (pH 7.4) at 37º C to mimic body temperature (Figure 5.22).

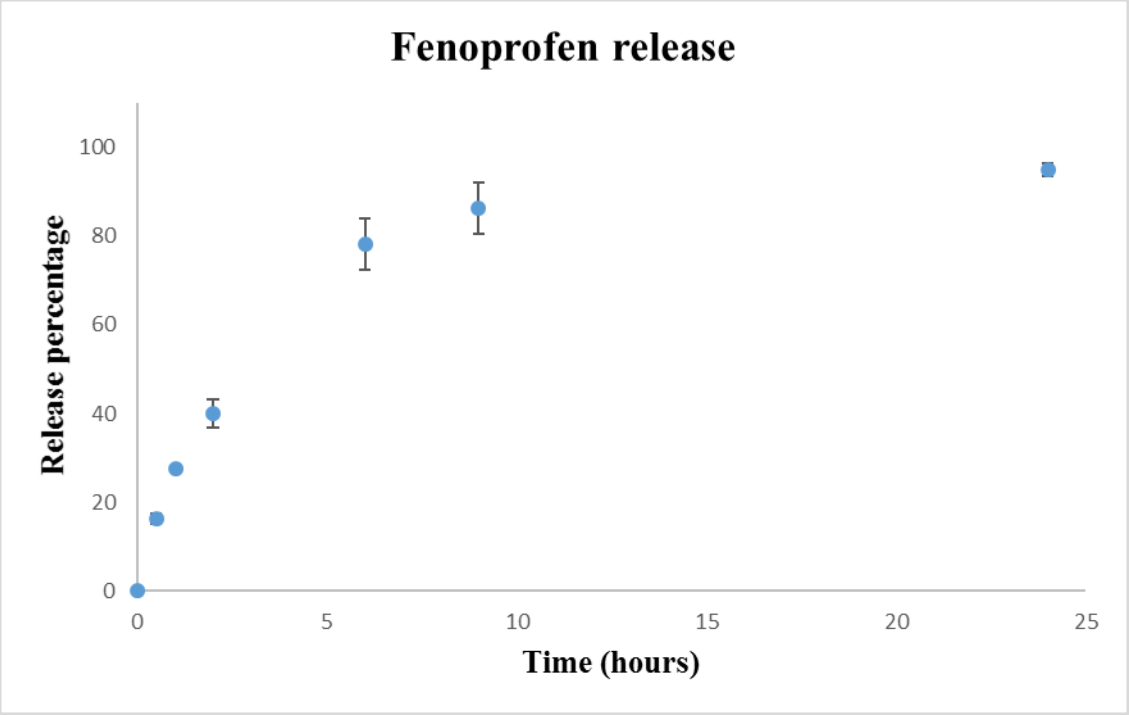

Fig. 5.22 Release profile of fenoprofen from nanogel MRGC 213 at 37º C in PBS (pH 7.4).

Release of fenoprofen was monitored over 24 hours by collecting fenoprofen-loaded nanogel solution aliquots at differen time points. Results obtained showed almost full drug release (86 % ± 3 %) within 10 hours.

Dialysis was selected as release evaluation technique due to its well established and diffuse use. [58-60] At present only few studies on fenoprofen release from drug delivery systems were identified in literature. Available literature evaluates the drug release kinetics of fenoprofen from drug delivery systems, which share few similarities with nanogels object of this study, such as modified chitosan polymers, chewing gum tablets and prodrugs. [61-63] For this reason, an exact and direct comparison may not be possible. Moreover, it is important to note that fenoprofen release profile varies depending not only on polymers or particles chemical composition but also on the environment conditions, such as temperature or buffer solutions, used to carry out the release evaluation. [61-63] However, combining fenoprofen release studies available [61-63] with drug release profiles achieved with nanogels, [64, 65] it was possible to make a comparison with the results herein obtained. In particular doxorubicin release studies from pullulan based and polymethacrylic acid based nanogels, performed by K. Na et al. and Y.-J. Pan et al. respectively, [64, 65] showed that in certain conditions release profiles were comparable to the one shown in Figure 5.23 in terms of time frame and drug release percentage.

5.4 **Conclusions**

In conclusion, preliminary data suggest that methacrylates based nanogels were suitable for incorporation and release of both small conventional pharmaceutical compounds and large bio-macromolecules. Although more analysis will need to be performed before the safe employment of these nanogels in drug delivery, these promising findings provided an excellent platform for the further development of these nanoparticles.

Before providing conclusions and discuss possible future developments of this nanogel system, experimental details are reported in the following chapter.

Images references

a) P. Resnier, T. Montier, V. Mathieu, J.-P. Benoit; C. Passirani. A review of the current status of siRNA nanomedicines in the treatment of cancer. *Biomaterials,* **2013**, 34, 6429-6443. **License Number:** 3970170454005
b) G. J. Doherty; H. T. McMahon. Mechanisms of Endocytosis. *Annu. Rev. Biochem*., **2009**, 78, 857-902. (OPEN PERMISSION)
c) J. Huotari; A. Helenius. Endosome maturation. *EMBO J.*, **2011**, 30, 3481-3500.
d) N. Oh; J-H. Park. Endocytosis and exocytosis of nanoparticles in mammalian cells. *Int. J. Nanomedicine,* **2014**, 9 (1), 51-63. **Order License Id:** 3926421408563.

References

1. N. Agrawal, P. V. N. Dasaradhi, A. Mohmmed, P. Malhotra, R. K. Bhatnagar; S. K. Mukherjee. RNA Interference: Biology, Mechanism, and Applications. *Microbiol. Mol. Biol. R.,* **2013**, 67, 657-685.
2. J. C. Burnett; J. J. Rossi. RNA-Based Therapeutics: Current Progress and Future Prospects. *Chem. Biol.,* **2012**, 19, 60-71.
3. R. Kanasty, J. Robert Dorkin, A. Vegas; D. Anderson. Delivery materials for siRNA therapeutics. Nat. Mater., **2013**, 12, 967-977.
4. Y. Tang, Y.-z. GE; J. Q Yin. Exploring in vitro roles of siRNA in cardiovascular disease. *Acta Pharmacol. Sin.,* **2007**, 28, 1-9.
5. A. Thakur, S. Fitzpatrick, A. Zaman, K. Kugathasan, B. Muirhead, G. Hortelano; H. Sheardown. Strategies for ocular siRNA delivery: Potential and limitations of non-viral nanocarriers. *J. Biol. Eng.,* **2012**, 6, 1-16.
6. P. Resnier, T. Montier, V. Mathieu, J.-P. Benoit; C. Passirani. A review of the current status of siRNA nanomedicines in the treatment of cancer. *Biomaterials,* **2013**, 34, 6429-6443.
7. J. Zhou; J. J. Rossi. Therapeutic Potential of Aptamer-siRNA Conjugates for Treatment of HIV-1. *BioDrugs*, **2012**, 26, 393-400.
8. J. Wang, Z. Lu, M. G. Wientjes; J. L.-S. Au. Delivery of siRNA Therapeutics: Barriers and Carriers. *AAPS J.,* **2010**, 12, 492-503.
9. A. Wittrup, J. Lieberman. Knocking down disease: a progress report on siRNA therapeutics. *Nat. Rev. Genet.,* **2015**, 16, 543-552.
10. A. Ardana, A. K. Whittaker, N. A. J. McMillanb; K. J. Thurecht. Polymeric siRNA delivery vectors: knocking down cancers with polymeric-based gene delivery systems. *Chem Technol Biotechnol*, **2015**, 90, 1196-1208.
11. S. A. Dar, A. Thakur, A. Qureshi; M. Kumar. siRNAmod: A database of experimentally validatedchemically modified siRNAs. *Sci. Rep.,* **2016**, 6, Article number: 20031, 1-8.
12. M. Giacca; S. Zacchigna. Virus-mediated gene delivery for human gene therapy. *J. Control. Release,* **2012**, 161, 377-388.
13. N. Nayerossadat, T. Maedeh; P. A. Ali. Viral and nonviral delivery systems for gene delivery. *Adv. Biomed. Res.,* **2012**, 1:27.
14. K. Gao; L. Huang. Nonviral Methods for siRNA Delivery. *Mol. Pharm.,* **2008**, 6(3), 651-658.
15. D. Castanotto; J. J. Rossi. The promises and pitfalls of RNAinterference-based therapeutics. *Nature*, **2009**, 457, 426-433.
16. M. Uz, S. K. Mallapragada; S. A. Altinkaya. Responsive pentablock copolymers for siRNA delivery. *RSC Adv.*, **2015**, 5, 43515-43527.
17. Y. Yang, J. Li, F. Liu; L. Huang. Systemic Delivery of siRNA *via* LCP Nanoparticle Efficiently Inhibits Lung Metastasis. Mol. Ther., **2012**, 20, 3, 609-615.

18. D. S. W. Benoit, S. Srinivasan, A. D. Shubin; P. S. Stayton. Synthesis of Folate-Functionalized RAFT Polymers for Targeted siRNA Delivery. *Biomacromolecules*, **2011**, 12, 2708-2714.
19. L. De Backer, K. Braeckmans, M. C. A. Stuart, J. Demeester, S. C. De Smedt; K. Raemdonck. Bio-inspired pulmonary surfactant-modified nanogels: A promising siRNA delivery system. *J. Control. Release,* **2015**, 206, 177-186.
20. M. H. Smith; L. A. Lyon. Multifunctional Nanogels for siRNA Delivery. *Acc. Chem. Res.*, **2012**, *45*(7), 985-993
21. G. Aguirre, J. Ramos; J. Forcada. Advanced Design of T and pH Dual-Responsive PDEAEMA–PVCL Core–Shell Nanogels for siRNA Delivery. **J. Polym. Sci. A Polym. Chem., 2016,** DOI: 10.1002/pola.28207 (Online Version of Record published before inclusion in an issue).
22. F. Testa Moura de Carvalho Vicentini, L. Neves Borgheti-Cardoso, L. Vieira Depieri, D. de Macedo Mano, T. Fedatto Abelha, R. Petrilli; M. V. Lopes Badra Bentley. Delivery Systems and Local Administration Routes for Therapeutic siRNA. Pharm. Res., **2013**, 30, 915-931.
23. G. Soni; K. S. Yadav. Nanogels as potential nanomedicine carrier for treatment of cancer: A mini review of the state of the art. *Saudi Pharm. J.,* **2016**, 24, 133-139.
24. K. Raemdonck, B. Naeye, K. Buyens, R. E. Vandenbroucke, A. Høgset, J. Demeester; S. C. De Smedt. Biodegradable Dextran Nanogels for RNA Interference: Focusing on Endosomal Escape and Intracellular siRNA Delivery. *Adv. Funct. Mater.,* **2009**, 19, 1406-1415.
25. H. Mimi, K. M. Ho, Y. S. Siu, A. Wu; P. Li. Polyethyleneimine-Based Core-Shell Nanogels: A Promising siRNA Carrier for Argininosuccinate Synthetase mRNA Knockdown in HeLaCells. *J. Control. Rel.*, **2012**, 158, 123-130.
26. K. E. Shopsowitz, C. Wu, G. Liu, E. C. Dreaden; P. T. Hammond. Periodic-shRNA molecules are capable of gene silencing, cytotoxicity and innate immune activation in cancer cells. *Nucleic Acids Res.*, **2016**, 44, 2, 545-557.
27. R. Rizzuto, M. Brini, P. Pizzo, M. Murgia; T. Pozzan. Chimeric green fluorescent protein as a tool for visualizing subcellular organelles in living cells. *Curr. Biol.,* **1995**, 5, 635-642.
28. C. Tschuch, A. Schulz, A. Pscherer, W. Werft, A. Benner, A. Hotz-Wagenblatt, L. Serra Barrionuevo, P. Lichter; D. Mertens. Off-target effects of siRNA specific for GFP. *BMC Mol. Biol.*, **2008**, 9:60.
29. K. Buyens, B. Lucas, K. Raemdonck, K. Braeckmans, J Vercammen, J. Hendrix, Y. Engelborghs, S. C. De Smedt; N. N. Sanders. A fast and sensitive method for measuring the integrity of siRNA carrier complexes in full human serum. *J. Control. Rel.,* **2008**, 126, 67-76.
30. T. Furst, V. Bettonville, E. Farcas, A. Frere, A. Lechanteur, B. Evrard, M. Fillet, G. Piel, A.-C. Servais. Capillary electrophoresis method to determine siRNA complexation with cationic liposomes. *Electrophoresis*, **2016**, *00*, 1-7.
31. N. Oh; J-H. Park. Endocytosis and exocytosis of nanoparticles in mammalian cells. *Int. J. Nanomedicine,* **2014**, 9 (1), 51-63.

32. L. Kou, J. Sun, Y. Zhai; Z. He. The endocytosis and intracellular fate of nanomedicines. *Asian J. Pharm. Sci.,* **2013**, 8 1-10.
33. M. Miaczynska; H. Stenmark. Mechanisms and functions of endocytosis. *J. Cell Biol.,* **2008**, 180, 7-11.
34. G. J. Doherty; H. T. McMahon. Mechanisms of Endocytosis. *Annu. Rev. Biochem.,* **2009**, 78, 857-902.
35. J. Huotari; A. Helenius. Endosome maturation. *EMBO J.,* **2011**, 30, 3481-3500.
36. M. Dominska; D. M. Dykxhoorn. Breaking down the barriers: siRNA delivery and endosome escape. *J. Cell Sci.,* **2010**, 123, 1183-1189.
37. A. K. Varkouhi, M. Scholte, G. Storm, H. J. Haisma. Endosomal escape pathways for delivery of biologicals. J. Control. Release, **2011**, 151, 220-228.
38. A. R. Shrivats, Y. Mishina, S. Averick, K. Matyjaszewski; J. O. Hollinger. In Vivo GFP Knockdown by Cationic Nanogel-siRNA Polyplexes. *Bioengineering,* **2015**, 2, 160-175.
39. M. Benfer; T. Kissel. Cellular uptake mechanism and knockdown activity of siRNA-loaded biodegradable DEAPA-PVA-g-PLGA nanoparticles. *Eur. J. Pharm. Biopharm.,* **2012**, 80, 247-256.
40. G. Tiscornia, O. Singer, M. Ikawa; I. M. Verma. A general method for gene knockdown in mice by using lentiviral vectors expressing small interfering RNA. *Proc. Natl. Acad. Sci. USA,* **2003**, 100(4), 1844-1848.
41. D. T. Auguste, K. Furman, A. Wong, J. Fuller, S. P. Armes, T. J. Deming, R. Langer. Triggered release of siRNA from poly(ethylene glycol)-protected, pH-dependent liposomes. *J. Control. Rel.,* **2008**, 130, 266–274.
42. G. Saito. Novel cholesterol and glycerol based nanoparticles for dermal drug delivery. PhD thesis, **2016**.
43. J. S. Smolen, D. Aletaha; I. B. McInnes. Rheumatoid arthritis. *The Lancet,* **2016**, doi:10.1016/S0140-6736(16)30173-8 (Online Version of Record published before inclusion in an issue).
44. J. D. Isaacs; L. W. Moreland. Fast Facts: Rheumatoid Arthritis (2nd edition). *Health Press,* **2011**, ISBN: 9781905832910, 1905832915.
45. L. Carmona, M. Cross, B. Williams, M. Lassere; L. March. Rheumatoid arthritis. *Best Pract. Res. Cl. Rh.,* **2010**, 24, 733-745.
46. E. Martin. Concise medical dictionary 9th edition. *Oxford University* Press, **2015**, eISBN 9780191767302.
47. Fenoprofen from Drug.com https://www.drugs.com/cdi/fenoprofen.html
48. M. Agotegaray, F. Gumilar, M. Boeris, R. Toso; A. Minetti. Enhanced Analgesic Properties and Reduced Ulcerogenic Effect of a Mononuclear Copper(II) Complex with Fenoprofen in Comparison to the Parent Drug: Promising Insights in the Treatment of Chronic Inflammatory Diseases. *BioMed Research International,* **2014**, Article ID 505987, 1-9.
49. J. Majumder, P. Yedoti; P. Dastidar. A supramolecular topical gel derived from a nonsteroidal anti-inflammatory drug, fenoprofen, is capable of treating skin inflammation in mice. *Org. Biomol. Chem.,* **2015**, 13, 2300-2309.
50. K. Miladia, S. Sfar, H. Fessi; A. Elaissari. Drug carriers in osteoporosis: Preparation, drug encapsulation and applications. *Int. J. Pharm.,* **2013**, 445, 181-195.

51. D. Cunha, M. B. Yahia, S. Hall, S. R. Miller, H. Chevreau, E. Elkaïm, G. Maurin, P. Horcajada; C. Serre. Rationale of Drug Encapsulation and Release from Biocompatible Porous Metal-Organic Frameworks. *Chem. Mater.,* **2013**, 25, 2767-2776.
52. F. O. M. S. Abreua, E. F. Oliveiraa, H. C. B. Paulaa; R. C. M. de Paula. Chitosan/cashew gum nanogels for essential oil encapsulation. *Carbohyd. Polym.*, **2012**, 89, 1277-1282.
53. R. Mehvar; F. Jamali. Stereospecific high-performance liquid chromatographic (HPLC) assay of fenoprofen enantiomers in plasma and urine. *Pharm. Res*., **1988**, 5(1), 53-6.
54. D. Purnachand, A. Veerareddy, B. Ramadevi; B. Madhusudhanreddy. Development and Validation of Stability Indicating RP-HPLC Method for Determination of Related Substances in Fenoprofen Calcium. *J. Chem. Pharm. Res*.**, 2016**, 8(5), 251-259.
55. S. Papadimitriou; D. Bikiaris. Novel self-assembled core–shell nanoparticles based on crystalline amorphous moieties of aliphatic copolyesters for efficient controlled drug release. *J. Control. Release,* **2009**, 138, 177-184.
56. J. K. Oh, D. J. Siegwart; K. Matyjaszewski. Synthesis and Biodegradation of Nanogels as Delivery Carriers for Carbohydrate Drugs. *Biomacromolecules,* **2007,** 8, 3326-3331.
57. S. Zhaveh, A. Mohsenifar, M. Beiki, S. T. Khalili, A. Abdollahi, T. Rahmani-Cherati, M. Tabatabaei. Encapsulation of Cuminum cyminum essential oils in chitosan-caffeic acid nanogel with enhanced antimicrobial activity against *Aspergillus flavos. Ind. Crop. Prod.,* **2015**, 69, 251-256.
58. S. S. D'Souza; P. P. DeLuca. Methods to Assess in Vitro Drug Release from Injectable Polymeric Particulate Systems. *Pharmaceut. Res.,* **2006**, 23, 3, 460-474.
59. S. Modi; B. D. Anderson. Determination of Drug Release Kinetics from Nanoparticles: Overcoming Pitfalls of the Dynamic Dialysis Method. *Mol. Pharmaceutics,* **2013**, 10, 3076-3089.
60. E. Leo, R. Cameroni; F. Forni. Dynamic dialysis for the drug release evaluation from doxorubicin-gelatin nanoparticle conjugates. *Int. J. Pharm.,* **1999**, 180, 23-30.
61. W. Duan, C. Shen, H. Fang, G. H. Li. Synthesis of dehydroabietic acid-modified chitosan and its drug release behaviour. *Carbohyd. Res.,* **2009**, 344, 9-13.
62. A. E. El Assassy, M. M. Amin; A. A. Abdelbary. Immediate release three-layered chewing gum tablets of fenoprofen calcium: preparation, optimization and bioavailability studies in healthy human volunteers. *Drug Dev. Ind. Pharm.*, **2012**; 38, 5, 603-615.
63. T. van der Merwe, B. Boneschans, B. Zorc, J. Breytenbach; M. Zovko. Macromolecular prodrugs X. Kinetics of fenoprofen release from PHEA-fenoprofen conjugate. *Int. J. Pharm.,* **2002**, 241, 223-230.
64. K. Na, E. S. Lee; Y. H. Bae. Self-Organized Nanogels Responding to Tumor Extracellular pH: pH-Dependent Drug Release and *in Vitro* Cytotoxicity against MCF-7 Cells. *Bioconjugate Chem.,* **2007,** 18, 1568-1574.
65. Y.-J. Pan, Y.-Y. Chen, D.-R. Wang, C. Wei, J. Guo, D.-R. Lu, C.-C. Chu; C.-C. Wang. Redox/pH dual stimuli-responsive biodegradable nanohydrogels with varying responses to dithiothreitol and glutathione for controlled drug release. *Biomaterials*, **2012**, 33, 6570-6579.

Chapter VI: Materials and methods

6.1 Materials

6.1.1 Chemicals reagents

Ammonium persulfate, tert-buthylamminoethyl methacrylate (tBAEMA), N,N'-methylenebis(acrylamide) (MBA), ethylene glycol methyl ether methacrylate (EGMMA), diethylamminoethyl methacrylate (DEAEMA), methacrylic acid (MAA), bromoacetyl chloride, 2-hydroxyethyl methacrylate, 2,3-dibromomaleimide, tetrabutylammonium iodide, 1-butanethiol, oleic acid, methyl myristate, esterase from porcine liver and fenoprofen calcium salt hydrate were purchased from Sigma Aldrich.

High pressure liquid chromatography (HPLC) grade water, HPLC grade acetone, HPLC grade acetonitrile, HPLC grade methanol, anhydrous dimethyl sulfoxide (DMSO), ethyl acetate, petroleum ether, acetic acid, 1-octanol, paraffin oil, hydrochloric acid 35%, potassium chloride, citric acid monohydrate, citrate dehydrate, sodium hydrogen phosphate, potassium dihydrogen phosphate, sodium bicarbonate and sodium carbonate were obtained from VWR.

Sodium hydroxide and sodium chloride were acquired from Fisher scientific.

Nitrogen (oxygen free) gas was purchased from BOC gases.

Deuterium oxide (D_2O), deuterated chloroform ($CDCl_3$), deuterated DMSO ($(CD_3)_2SO$) from Goss Scientific.

6.1.2 Biological reagents

Normal dermal human fibroblasts (NDHF) and penicillin/streptomycin were obtained from Lonza; HaCaT keratinocyte cell line from CLS service; Dulbecco's modified Eagle's medium (DMEM), Hoechst H33342, HeLa (non GFP) and propidium iodide from Sigma Aldrich; sterile molecular grade, nuclease free water from 5prime; fetal bovine serum and DMEM (without Phenol Red) from Gibco; GFP Duplex I and CY5 tagged GFP Duplex I from GE Dharmacon; HeLaGFP cells from CellBiolabs Inc.;

Lipofectamine RNAiMAX from Thermo Fisher Scientific and CellTiter-Glo® Luminescent Cell Viability Assay from Promega.

6.1.3 Additional consumables

Graphene oxide support film on Lacey carbon on 400 mesh Cu TEM grids were acquired from Agar scientific; UV cuvettes high precision quartz suprasil 10 mm from Hellma; DLS disposable cuvettes DTS0012 and zeta potential disposable cuvettes DTS1060 from Malvern; PTFE-faced rubber septa and wheaton transparent glass bottles (various volumes) from Sigma Aldrich; acrodisc 13mm syringe filter with 0.45µm GHP membrane, thin layer chromatography (TLC) plates TLC Silica gel 60G F254 20x20 cm and 500 µL centrifugal filters modified polyethersulfone (PES) membrane from VWR; 96 well plates from Costar; microliter syringes (various volumes) from Hamilton; Research plus pipettes from Eppendorf (various volumes); crossover forceps watchmaker 5X steel from Scientific Laboratory Supplies Limited; M2 minishaker vortex from IKA and dialysis tubing 3500 Da molecular weight cut-off (MWCO) from Medicell,

6.2 Instruments

Dynamic light scattering (DLS) measurements and ζ-potential measurements were performed using a Zetasizer NaNO ZS from Malvern equipped with a 4 mV He-Ne laser operating at $\lambda = 633$ nm with a detector placed at 173º angle.

Imaging were recorded using a transmission electron microscope (TEM) Jeol JEM 1230 operating at 80 kV equipped with camera from Morada (instrument operated by Dr. G. Mastroianni); Leica DMRA2 light microscope equipped with QICLICK CCD camera from QImaging for emulsion imaging; high content imaging for the assessment of cell toxicity and nanogels' internalization was performed using the automated fluorescence microscope In Cell 2200 from GE Healthcare equipped with a 20x

objective and data analyses were then performed on the In Cell Developer software from GE Healthcare.

Samples and chemicals weight was determined using a Radwag AS 60/220 R2. pH measurements were carried out using a MP 220 pH meter (Mettler Toledo) equipped with inlab micro probe (Mettler Toledo).

Deionised water was obtained from water purifier Purelab Option (ELGA); evaporation processes were performed using a Buchi Rotavapor R-200 and Heidolph G1 and sample freeze drying was performed on a Labconco 7752060

High performance liquid chromatography (HPLC) experiments were performed on Infinity series 1200 equipped with UV detector and carbon 18 HPLC column H1-5C18-250A from Hichrom; Cary Eclipse fluorescence spectrophotometer and Cary 100 UV-VIS spectrophotometer from Agilent Technologies, both equipped with a thermostat, were used for fluorescence and UV analyses respectively.

FT-IR analyses were performed using a Perkin Elmer Spectrum 100.

^{1}H-NMR (400 MHz) spectra were recorded using a Bruker 400 MHz instrument and analysed using MestReNova software.

^{1}H-NMR peak multiplicity was reported as seen on NMR spectra and as follow: s (singlet), br (broad), d (doublet), t (triplet), q (quartet), quin (quintet), sex (sextet), m (multiplet), NMR chemical shift (δ) was reported in part per million (ppm) and J coupling constant was reported in Hz.

6.3 Methods

6.3.1 Synthesis of nanogels in dymethylsulfoxide, water and mixtures of solvents.

A classic NGs synthesis was performed as follow: monomers, cross-linker, initiator and fluorophore (in some cases) were all placed into a wheaton bottle. The solvent was

poured into the flask which was then sealed with PTFE-faced rubber septa. Through the use of a vacuum/nitrogen line, 3 cycles of vacuum, each one followed by a nitrogen (oxygen free) cycle, were applied to the polymerisation mixture until no gas bubbling was observed. The process served to remove all traces of oxygen which act as radical scavenger. After the vacuum/nitrogen cycle the whaeton bottle was placed in a sonicating bath for 30 second and then in a oven with the temperature set at 70 ºC for a time ranging from 6 to 48 hours.

The volume required for the nanogel polymerisation together with the moles of initiator employed, given a certain mass concentration (C_M) and initiator percentage, were calculated using the following equations:

$$\boldsymbol{Solvent\ volume\ required}\ (\boldsymbol{L}) = \frac{\frac{[(\mathrm{MSmons} + \mathrm{MScl})\ \mathrm{x}\ (100 - \mathrm{CM\%})]}{\mathrm{CM\%}}}{\text{density of solvent}}$$

Equation 6.1 MSmons is the mass of monomers and **MScl** is the mass of crosslinker.

$$\boldsymbol{Moles\ initiator\ required} = \frac{(\mathrm{Nmons} + 2x\mathrm{Ncl})\ x\ \%initiator}{100}$$

Equation 6.2 Nmons are the number of moles of monomers and **Ncl** are the number of moles of crosslinker.

When solvent mixtures were employed the density value used were calculated according to the contribution of each solvent by using the following equation.

$$Solv.mix\ density = (\%\ Solv.A\ x\ den.Solv.A) + (\%\ Solv.B\ x\ dens.Solv.B) + \cdots$$

Equation6.3 Solv. is solvent and dens. is density.

Nanogels MRGC 213 and MRGC 214 were found to be the most promising preparations. For this reason, their synthesis is described in dedicated sections reported below.

6.3.2 Synthesis of MRGC 213

Commercially available tert-buthylamminoethyl methacrylate (91.4 mg, 0.49 mmol), N,N'-methylenebis(acrylamide) (24.7 mg, 0.16 mmol), methacrylic acid (13.8 mg, 0.16 mmol) and ammonium persulfate (11.0 mg, 0.05 mmol) were placed into a wheaton bottle and dissolved in 28.9 mL of a mixture water : acetone in a ratio 1:1 (v/v) to obtain a final C_M of 0.5%. The bottle was then sealed with a PTFE-faced rubber septa. To avoid evaporation of acetone, due to its low boiling point, the bottle was placed into ice, let cool down for 2 minutes and vacuum was applied for only 5 seconds. With the bottle kept in to the ice bath, nitrogen (oxygen free) was bubbled through the solution for 10 minutes by using a long syringe needle (going through the rubber septa) reaching the bottom of the bottle and a short syringe needle to allow oxygen exhaustion. After nitrogen saturation, the solution was placed in an oil bath set at 40 ºC and left reacting for 72 hours. After this time the polymerisation mixture was let cool down at room temperature and then dialysed against deionised water to get rid of unreacted materials and acetone. The dialysed mixture was then freeze dried to yield 118.9 mg of a white soft powder (yield 91.3%).

Synthesis of fluorescently tagged nanogels was performed following the same procedure herein reported, reducing the number of moles of tBAEMA by the number of fluorofore's moles used.

6.3.3 Synthesis of MRGC 214

Commercially available tert-buthylamminoethyl methacrylate (91.4 mg, 0.49 mmol), N,N'-methylenebis(acrylamide) (24.7 mg, 0.16 mmol), ethylene glycol methyl ether methacrylate (23.5 mg, 0.16 mmol) and (11.0 mg, 0.05 mmol) were placed into a wheaton bottle and dissolved in 31 mL of a mixture water : acetone in a ratio v/v 1:1 to obtain a final C_M of 0.5%. Bottle was then sealed with a PTFE-faced rubber septa. To avoid evaporation of acetone, due to its low boiling point, the bottle was placed into ice, let cool down for 2 minutes and vacuum was applied for only 5 seconds. With the

bottle kept in to the ice bath, nitrogen (oxygen free) was bubbled through the solution for 10 minutes by using a long syringe needle (going through the rubber septa) reaching the bottom of the bottle and a short syringe needle to allow oxygen exhaustion. After nitrogen saturation, the solution was placed in an oil bath set at 40 ºC and left reacting for 72 hours. After this time the polymerisation mixture was let cool down at room temperature and then dialysed against deionised water to get rid of unreacted materials and acetone. The dialysed mixture was then freeze dried to yield 120.1 mg of a white soft powder (yield 86.0%).

Synthesis of fluorescently tagged nanogels was performed following the same procedure herein reported, reducing the number of moles of tBAEMA by the number of fluorofore's moles used.

6.3.4 Fluorescent tag synthesis

As the synthesis of the fluorescent tag was already reported, each intermediate compound was only characterised by ^{1}H-NMR. [1-3]

Synthesis of 3,4-bis(butylsulfanyl)-2,5-dihydro-1H-pyrrole-2,5-dione (1)

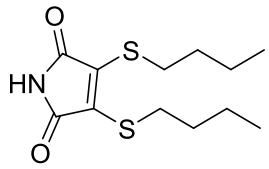

2,3-Dibromomaleimide (2.32 g, 9.10 mmol) was dissolved in diethyl ether (70 mL) and cooled to 0 °C in an ice bath. Butanethiol (1.68 g, 18.66 mmol) was added and stirred for 5 minutes. Triethylamine (1.844 g, 18.66.33 mmol) was added dropwise to the cooled solution. An immediate yellow colour was observed and a white precipitate. After the addition of trimethylamine was completed, the solution was allowed to warm to room temperature and left to stir for 16 hours. The reaction was monitored by thin

layer chromatography (TLC) R_f = 0.31 (ethyl acetate : petroleum ether, 1:9). Diethyl ether (70 mL) was added, and the organic solution washed with water (150 mL) and then brine (150 mL). The organic layer was dried over anhydrous $MgSO_4$. The solution was then filtered and concentrated under vacuum to obtain a crude as an orange oil. The crude was purified by flash chromatography on silica gel (ethylacetate : petroleum ether, 1:9) to yield the product as an orange oil (0.91 g, 37 %). **^{1}H-NMR** (400 MHz, $CDCl_3$) δ 7.45-7.30 (N-H, br, 1H), 3.29 (-CH_2-, t, 4H, J = 7.5 Hz), 1.64 (-CH_2-, quin, 4H, J = 7.5 Hz), 1.45 (-CH_2-, sex, 4H, J = 7.5 Hz), 0.93 (-CH_3, t, 3H, J = 7.5 Hz).

Synthesis of 2-(2-bromoacetoxyl) ethyl methacrylate. (2)

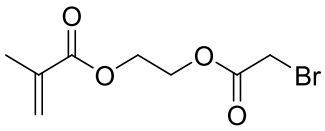

2-Hydroxyethyl methacrylate (HEMA) (13.0 g, 0.1 mol) and triethyl amine (TEA) (10.9 g, 0.107 mol) were dissolved in Chloroform (300 mL) and placed in an ice bath. Bromoacetyl chloride (15.7 g, 0.1 mol) was then added dropwise. The mixture was let reach room temperature and was left stirring for 48 hours. The reaction was monitored by TLC R_f = 0.45 (ethyl acetate : hexane, 2:8). The unreacted bromoacetyl chloride was quenched via the addition of methanol (5 mL). The solution was then stirred for additional 30 min. The reaction mixture was washed saturated aqueous $NaHCO_3$ (100 mL) and with water twice (2 × 100 mL). The organic layer was dried over anhydrous $MgSO_4$, filtered and concentrated under vacuum to give a brown oil. The crude was further purified by flash chromatography on silica gel (ethylacetate : hexane, 2:8) to give a colourless oil,(10.8 g, 37%). **^{1}H-NMR** (400 MHz, $CDCl_3$) δ 6.13 (CH_{trans}=C(CH3)-COO, pseudo d, 1H,), 5.61 (CH_{cis}=C(CH3)-COO, pseudo t, 1H), 4.45 (-CH_2-CH_2-COO-CH_2-Br, pseudo quin, 2H), 4.39 (-CH_2-CH_2-COO-CH_2-Br, pseudo quin, 2H), 4.09 (-CH_2-Br, s, 2H), 1.95 (OOC-C(CH_3)=CH_2, pseudo t, 3H).

Synthesis of 2-(2-(3,4-bis(butylthio)-2,5-dioxo-2,5-dihydro-1H-pyrrol-1-yl)acetoxy)ethyl methacrylate {methacrylate fluorophore} (MAF)

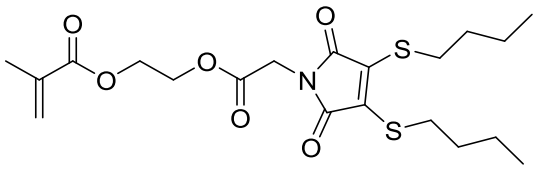

K_2CO_3 (228.0 mg, 1.65 mmol) and tetrabutylammonium iodide (40.6 mg, 0.11 mmol) were suspended in acetone (30 mL). Acetone solutions of **1** (300.0 mg, 1.10 mmol) (10mL) and bromoacetyl methacrylate (**2**) (274.3 mg, 1.10 mmol) (10 mL) were added to the suspension. The mixture was then stirred at room temperature for 50 h and monitored by TLC R_f = 0.35 (dichloromethane : petroleum ether, 3:7). After completion the reaction solution was filtered and the solvent removed under vacuum. The crude product was purified by flash chromatography on silica gel (dichloromethane : petroleum ether, 3:7) to yield the product as a yellow oil (280 mg, 57.4%). **^{1}H-NMR** (400 MHz, $CDCl_3$) δ 6.11 ($C\underline{H}_{trans}$=C(CH3)-COO, br, 1H), 5.59 ($C\underline{H}_{cis}$=C(CH3)-COO, t, 1H, J = 1.5 Hz), 4.41 (-CH_2-$C\underline{H}_2$-COO-CH_2-NR_2, m, 2H) 4.35 (-$C\underline{H}_2$-CH_2-COO-CH_2- NR_2, m, 2H), 4.27 (-$C\underline{H}_2$- NR_2, s, 2H), 3.30 (-$C\underline{H}_2$-, t, 4H, J = 7.5 Hz), 1.95 (OOC-C($C\underline{H}_3$)=CH_2, t, 3H, J = 1.5 Hz), 1.64 (-$C\underline{H}_2$-, quin, 4H, J = 7.5 Hz), 1.44 (-$C\underline{H}_2$-, sex, 4H, J = 7.5 Hz), 0.93 (-$C\underline{H}_3$, t, 3H, J = 7.5 Hz).

6.3.5 General procedure for nanogel purification

After polymerisation was completed, the mixture was was allowed to cool down at room temperature. At the same time dialysis tubing (molecular weight cut-off 3500 Da) were submerged into warm water and kept hydrating for around 30 minutes. The mixture was poured into the dyalisis bag using a glass funnel equipped with filter paper. The bag was then immersed in a conical flask containing deionised water and equipped with a magnetic flea. The water was replaced up to 6 times at increasing time intervals in order to allow equilibration between mixture inside the bag and water solution

outside it. This procedure allowed the removal of any unreacted materials, short polymer chains, traces of initiator and unbounded drugs from the polymerisation mixture prior to the isolation of nanogels by freeze drying.

6.3.6 Freeze dry

The content of the dialysis bag was transferred into a round bottom flask (RBF) of at least 3 times the volume contained in the dialysis bag using a funnel equipped with filter paper. The solution was then rapidly frozen by immerging the flask into liquid nitrogen. By holding the RBF from the neck, tilting it 45º degrees and gently turning it, the solution was let freezing on the wall of the RBF. This way the ice surface was increased leading to a faster and more even ice sublimation. After freezing, the RBF was connected to the freeze dryer and let dry for 12-24 hours. The nanogel powder obtained appeared as a fluffy white powder for non-fluorescent nanogels and yellow for fluorescently labelled nanoparticles. The powder was then collected and transferred into glass vial for storage. The vials were sealed and kept at room temperature.

6.3.7 UV thermal analyses

Thermo-responsive behaviour of nanogels was assessed by monitoring UV transmittance percentage variations upon thermal treatment of aqueous solutions of NGs in the temperature range between 20 to 60 ºC. Nanogel powders (obtained after freeze drying) were dissolved in deionised water at a concentration of 1 mg/mL, sonicated for 1 minute and then transferred into 1 cm UV quartz cuvettes. The cuvettes were placed in a thermostat and exposed to increasing temperature, ramping up at 1 ºC per minutes, in the range between 20 to 60 ºC. UV readings (500 nm) were recorded every minute for each temperature point.

6.3.8 Fluorophore incorporation assessment

MRGC 209 and 211 were dissolved in a mixture water : acetone 3:7 (v/v) at a concentration of 0.5 mg/mL. The solutions were transferred into 1 cm quarts UV cuvettes, equilibrated at 25 ºC and their absorbance, in the wavelength range between 200 and 800 nm (1nm resolution), was recorded. The maximum absorbance values, achieved at 411 nm, were then fitted into a calibration curve previously obtained and the incorporation efficiency was measured following the equations reported below.

$$\boldsymbol{MAF\ incorporation\ percentage} = \frac{\mu M\ of\ MAF\ obtained\ from\ calibration}{theoretical\ MAF\ \mu M\ in\ 0.5\ mg\ of\ NGs}$$

Equation 6.4 used for the determination of MAF incorporation into NGs.

Theoretical MAF concentration was previously calculated by using equations shown as follow (equation 6.5 and 6.6).

$$\boldsymbol{theo.MAF\ \mu M\ in\ 0.5\ mg\ of\ NGs} = \frac{theo.MAF\ mg\ in\ 0.5\ mg\ of\ NGs\ x\ 1000}{\text{M. W. of MAF}}$$

$$\boldsymbol{theo.MAF\ mg\ in\ 0.5\ mg\ of\ NGs} = \frac{\text{mg of MAF fed } x \text{ fraction yield}}{\text{total mg of NGs obtained } x\ 2}$$

Equations 6.5 and 6.6 used to determine theoretical MAF concentration. M.W is the molecular weight.

Calculation were based on the assumption that all nanogel's components contributed to the final yield proportionally to their molar percentages initially fed into the polymerisation mixture.

6.3.9 DLS sample preparation

Nanogel powder (obtained after freeze drying) was dissolved in deionised water (or DMSO) at a concentration of 0.1 to 1 mg/mL. The mixture was then sonicated for 1 minute at room temperature. With the use of a graduated 1 or 2 mL syringe, 1mL of the

solution was transferred on a disposable plastic cuvette after being passed through a 0.45µm filter (in order to remove eventual dust particle or fibres). The cuvette was then capped and the sample size was analysed. Particle size was analysed 3 times to prevent analytical errors. Material method was set to polymer latex, temperature at 25 ºC and data were obtained by cumulated analyses of the correlation function using Stokes-Einstein equation.

ζ-potential samples were prepared following the same procedure but using a ζ-potential cuvette and without the involvement of a filtration step.

6.3.10 TEM sample preparation

Nanogel powder (obtained after freeze drying) was dissolved in deionised water at a concentration of 1 mg/mL (0.25 mg/mL for MRGC 214 second attempt). The solution was then sonicated for 2 minutes at room temperature (10 minutes for MRGC 214 second attempt). Using a graduated pipette, 15µl of the solution obtained were deposited on to a carbon oxide coated TEM grid (held by the corner using a crossover forcep), forming a drop on top of the grid. After 2 minutes of interaction (in order to let some particle deposit onto the grid) the excess of water was removed using paper triangles cut out from filter paper. The triangles were placed perpendicularly to the grid in order to remove the water by capillarity and avoid any contaminations that could have resulted from the paper entering in direct contact with the surface of the grid. The grid was then let dry completely for 1 or 2 minutes and then stored in the grid holder provided by the manufacturer until it was analysed.

The same process was employed for MRGC 214 nanogels complexed with bovine serum albumin (BSA) with the only exception that after sonication 0.5 mL of MRGC 214 (1 mg/mL) were mixed with 0.5 mL of a deionised water solution of BSA (0.5 mg/mL).

6.3.11 Emulsion oil phase and w/o ratio selection

Nanogel powder was dissolved in deionised water at a concentration of 1 mg/mL and then sonicated for 1 minute at room temperature. 1mL of this solution was placed in a 4 mL tall and narrow glass vial and a mark was drawn with a marker pen to indicate the phase separation level. Then increasing amount of oil phase were poured into the vial starting from 0.1 mL going up to 2 mL. For each volume added the mixture was stirred on a vortex at 2500 rpm for 1 minute. Then the mixture was observed for sign of emulsion formation. If emulsion was not formed that mixture was discarded, otherwise observations were recoded (either reported in a laboratory book or by taking pictures) over time until the emulsion was dissolved. If emulsion appeared to be stable, the sample was kept for further analysis under the optical microscope.

6.3.12 Emulsion pH test

Five aqueous solutions with various pH were prepared: 1) 0.01M hydrochloric acid (HCl) in water; 2) 0.01M NaOH in water; 3) 0.1M citrate buffer solution (pH 4) prepared by mixing 0.1M aqueous solution of citric acid monohydrate (59 mL) with 0.1M aqueous solution of trisodium citrate dehydrate (41 mL); 4) phosphate buffer saline (PBS) solution (pH 7.4) prepared by dissolving NaCl (0.8 g), KCl (0.2 g), Na_2HPO_4 (1.44g) and KH_2PO_4 (0.24g) in deionised water (800 mL), pH was then adjusted with HCl and deionised water was added up to a final volume of 1 litre; 5) 0.1M carbonate buffer (pH 9.2) prepared by mixing 0.1M aqueous solution of sodium bicarbonate (84 mL) with 0.1M aqueous solution of sodium carbonate (16 mL).

Nanogel powders were dissolved in one of the five solutions previously mentioned, at a concentration of 1 mg/mL and then sonicated for 1 minute at room temperature. 1 mL of this solution was placed in a 4 mL tall and narrow glass vial and a mark was drawn with a marker pen to indicate the level of phase separation. Oleic acid (1 mL) was added and the two phases were homogenised by stirring on a vortex at 2500 rpm for 1 minute. Emulsion formed were monitored over time by taking picture and recording observations in laboratory book.

6.3.13 Optical microscopy protocol

One drop of emulsion was casted and spread onto a microscope glass by using a glass pipette. Pictures were then quickly recorded due to the emulsion breakage caused by the spreading onto the glass.

6.3.14 Nanogels for cell cultures

Nanogels were dissolved, at a concentration of 2 mg/mL, in cell medium constituted by Dulbecco's modified Eagle's medium (DMEM) supplemented with 10% (v/v) of fetal bovine serum and 1% (v/v) penicillin/streptomycin (PenStrep). The solutions were sonicated for 1 minute and then diluted in cell medium to obtain the 5 concentration used for cell transfection (10, 50, 100, 200 and 400 μg/mL).

6.3.15 HaCat/nanogels incubation

Immortalised human keratinocytes (HaCaT) were seeded at a density of 2×10^4 cells per well respectively and cultured in a 96-well plate for 24 hours (37 ºC, 5% CO_2) prior to nanogel transfection. After 24 hours the medium was removed and the cell were incubated with MRGC 209, 211, 213 and 214, dissolved in culture medium at different concentrations (10, 50, 100, 200 and 400 μg/mL). All transfections were performed with three technical replicates. Cell medium was constituted by Dulbecco's modified Eagle's medium (DMEM) supplemented with 10% (v/v) of fetal bovine serum and 1% (v/v) penicillin/streptomycin (PenStrep), as recommended by cells' providing company. After 4 and 24 hours (two different 96-well plates), CellTiter-Glo® luminescent cell viability assay was used to evaluate the adenosine triphosphate (ATP) production of the cells following the supplier's instructions. ATP level values were calculated as the mean value of triplicates normalised for the control cells and baselined with the auto-fluorescence of cell medium treated with CellTiter-Glo®. For propidium

iodide (PI) cytotoxicity assay, HaCaT cells were seeded at a density of 2×10^4 cells per well in 96-well plates and cultured for 24 hours before incubation with nanogels. NPs suspended in culture medium at different concentrations (see above) were then added to cells. After 4 and 24 hours (two different 96-well plates), PI and Hoechst H33342 both at a concentration of 1 μg/mL were added to cells and incubated for 15 min at room temperature (RT) prior to the acquisition of images on In Cell Microscope 2200 equipped with a 20x objective. Automated image analyses were performed on the In Cell Developer software provided with the instrument. Dead cells, with compromised cell membrane, are stained for both Hoechst H33342 and PI, while live cells stained only for Hoechst H33342. Cell nuclei stained with Hoechst H33342 were segmented and counted via software. Cell viability was calculated as the % of dead nuclei from the total count of nuclei normalised for the control (untreated cells).

6.3.16 Fibroblast/nanogel incubation

Normal dermal human fibroblasts (NDHF) were seeded at a density of 5×10^3 cells per well respectively and cultured in a 96-well plate for 24 hours (37 ºC, 5% CO_2) prior to nanogel transfection. After 24 hours the medium was removed and the cell were incubated with MRGC 209, 211, 213 and 214, dissolved in culture medium at different concentrations (10, 50, 100, 200 and 400 μg/mL). All transfections were performed with three technical replicates. Cell medium was constituted by Dulbecco's modified Eagle's medium (DMEM) supplemented with 10% (v/v) of fetal bovine serum and 1% (v/v) penicillin/streptomycin (PenStrep), as recommended by cells' providing company. After 4 and 24 hours (two different 96-well plates), CellTiter-Glo® luminescent cell viability assay was used to evaluate the ATP production of the cells following the supplier's instructions. ATP level values were calculated as the mean value of triplicates normalised for the control cells and baselined with the auto-fluorescence of cell medium treated with CellTiter-Glo®. For Propidium Iodide (PI) cytotoxicity assay, NDHF cells were seeded at a density of 5×10^3 cells per well in 96-well plates and cultured for 24 hours before incubation with nanogels. NPs suspended in culture medium at different concentrations (see above) were then added to cells. After 4 and 24 hours (two different 96-well plates), PI and Hoechst H33342 both at a

concentration of 1 μg/mL were added to cells and incubated for 15 min at room temperature (RT) prior to the acquisition of images on In Cell Microscope 2200 equipped with a 20x objective. Automated image analyses were performed on the In Cell Developer software provided with the instrument. Dead cells, with compromised cell membrane, are stained for both Hoechst H33342 and PI, while live cells stained only for Hoechst H33342. Cell viability was calculated as the % of dead nuclei from the total count of nuclei normalised for the control (untreated cells).

6.3.17 HeLa/nanogel incubation

HeLa cells were seeded at a density of 4×10^3 cells per well respectively and cultured in a 96-well plate for 24 hours (37 ºC, 5% CO_2) prior nanogel transfection. After 24 hours the medium was removed and the cell were incubated with MRGC 209, 211, 213 and 214, dissolved in culture medium at different concentrations (10, 50, 100, 200 and 400 μg/mL). All transfections were performed with three technical replicates. Cell medium was constituted by Dulbecco's modified Eagle's medium (DMEM) supplemented with 10% (v/v) of fetal bovine serum and 1% (v/v) penicillin/streptomycin (PenStrep), as recommended by cells' providing company. After 24 hours, propidium iodide (PI) cytotoxicity assay was performed. PI and Hoechst H33342 both at a concentration of 1 μg/mL were added to cells and incubated for 15 min at room temperature (RT) prior to the acquisition of images on In Cell Microscope 2200 equipped with a 20x objective. Automated image analyses were performed on the In Cell Developer software provided with the instrument. Dead cells, with compromised cell membrane, are stained for both Hoechst H33342 and PI, while live cells stained only for Hoechst H33342. Cell viability was calculated as the % of dead nuclei from the total count of nuclei normalised for the control (untreated cells).

6.3.18 siRNA complexation

To evaluate Nanogels capability to electrostatically bind siRNA, nanogels (NGs) MRGC 213 and MRGC 214 were complexed with siRNA against eGFP (GFP Duplex

I and CY5 tagged GFP Duplex I) in a mass ratio of NG:siRNA of 25:1. Therefore, NGs were dissolved in sterile molecular grade, nuclease free water to a concentration of 2 mg/mL. A solution containing 40 μg/mL siRNA and 40 μg/mL CY5 tagged siRNA was prepared in sterile molecular grade, nuclease free water. For complexation, equal volumes of NGs and siRNA were added to a 1.5 mL Eppendorf tube and incubated at room temperature while shaking, at 250 rpm, for two hours on an orbital shaker. The 2 mg/mL stock solution was then diluted in DMEM (without phenol red) to sample concentrations of 20, 50 and 100 μg/mL and directly used for cell transfection and determination of complexation efficiency. Complexation efficacy was determined indirectly from CY5 tagged siRNA after separating NPs and non-complexed siRNA by centrifugation (4ºC, 14000 *g*; 15 minutes), quantifying CY5 fluorescence in three replicates in the supernatant. Concentration was determined relative to a standard curve.

6.3.19 HeLa GFP nanogel transfection and GFP knockdown

HeLaGFP cells, cultured in full medium constituted by DMEM (without phenol red) containing FBS (10%, v/v), PenStrep (0.5%, v/v, 50 μg/mL,) and Blasticidin (10 μg/mL), were seeded 24 hours (37 ºC, 5% CO_2) prior to experiment in 96 well plates at a density of 4×10^3 cells per well. HeLaGFP cells were then transfected with MRGC 213 and 214 GFP Duplex I/CY5 complexes (20, 50, 100 μg/mL) and with Lipofectamine RNAiMAX (1.5 μL/mL) for the control cells in starvation medium constituted by DMEM (without phenol red) only. After 4 h of transfection, medium was added with final concentration of 2.5% FBS v/v (to decelerate growth in order for the cells not to overpass 100% confluency while the assay time) 0.25 % PenStrep (0.5%, v/v, 50 μg/mL) and Blasticidin (5 μg/mL). At 48 hours post transfection, cells were stained and placed in an automated incubator for further incubation and analysis by High Content Imaging with the automated fluorescence microscope In Cell 2200. Cell nuclei were stained at 48 h with Hoechst H33342 and propidium iodide (PI). Dead cells, with compromised cell membrane, are stained for both Hoechst H33342 and PI, while live cells stained only for Hoechst H33342. At 48 h four random fields per well were imaged on an In Cell 2200 with a 20x objective. Automated image analyses were

performed on the In Cell Developer software. GFP knockdown was accessed from mean GFP fluorescence intensity in the cytoplasm of live cells. GFP knockdown was expressed in percent with reference to 100% fluorescence in control conditions (untreated HelaGFP cells) after subtracting fluorescence background of Hela cells. Cell viability was calculated as the % of dead nuclei from the total count of nuclei.

6.3.20 Post polymerisation drug uploading protocol

MRGC 213 (10.40 mg) and fenoprofen (10.90 mg) were placed in a round bottom flask (RBF) equipped with a magnetic flea and 15 mL acetone were added. The dispersion was sonicated for 10 minutes and then left under stirring (400 rpm) for 6 hours. The acetone was evaporated under reduced pressure using a rotavapor until formation of white film around the wall of the RBF. The film was suspended in 10 mL of water and left stirring (360 rpm) for 2 minutes to homogenise the suspension and then let settle for 5 minutes in order to allow precipitation of eventual unsoluble fenoprofen. 1 mL from the top of the dispersion was filtered through 0.45 µm syringe and analysed with high pressure liquid chromatography coupled with UV detection instrument. 0.5 mL of the same dispersion were placed inside a 500 µL centrifugal filters equipped with a polyethersulfone (PES) membrane and centrifuged (13200 rpm for 15 minutes).

The procedure described was employed for the comparison between the two purification techniques. However, for the evaluation of encapsulation efficiency and loading capacity of nanogels the conditions used were different, as it was necessary to work at a fenoprofen concentration over the water saturation point of the drug.

Therefore, MRGC 213 (4.04 mg) and fenoprofen (10.05 mg) were placed in a round bottom flask equipped with a magnetic flea and 10 mL acetone were added. The dispersion was sonicated for 10 minutes and then left under stirring (400 rpm) for 6 hours. The acetone was evaporated under reduced pressure using a rotavapor until formation of white film around the wall of the RBF. The film was then suspended in 4 mL of water and left stirring (360 rpm) for 2 minutes to homogenise the suspension and then let settle for 5 minutes in order to allow precipitation of eventual unsoluble

fenoprofen. 1 mL from the top of the dispersion was filtered through 0.45 µm syringe, diluted by a factor of 2 and analysed at the HPLC.

At the same time fenoprofen (9.75 mg) was placed in a round bottom flask equipped with a magnetic flea and 10 mL acetone were added. The solution was sonicated for 10 minutes, then the acetone was evaporated under reduced pressure using a rotavapor until formation of white film around the wall of the RBF. The film was then suspended in 4 mL of water and left stirring (360 rpm) for 2 minutes to homogenise the suspension and then let settle for 5 minutes in order to allow precipitation of unsoluble fenoprofen. 1 mL from the top of the dispersion was filtered through 0.45 µm syringe, diluted by a factor of 2 and analysed at the HPLC. This sample was prepared to determine amount of fenoprofen dissolved in water.

6.3.21 Fenoprofen uploading quantification

High pressure liquid chromatography coupled with UV detection was used for the evaluation of fenoprofen upload. The mobile phase used was constituted by acetonitrile/water containing 0.5% acetic acid in a volume ratio of 50:50. Flow was set at 1 mL/min and UV spectra were recorded at 230 nm wavelength. Column C18 used was kept at 25 ºC by the use of a thermostat. In these conditions the trace of fenoprofen had a retention time of 12.5-13 minutes.

In order to evaluate the percentage of drug incorporated into the nanoparticles a calibration curve for fenoprofen was produced by using 5 different concentration points of fenoprofen solutions in acetone (Figure 6.1).

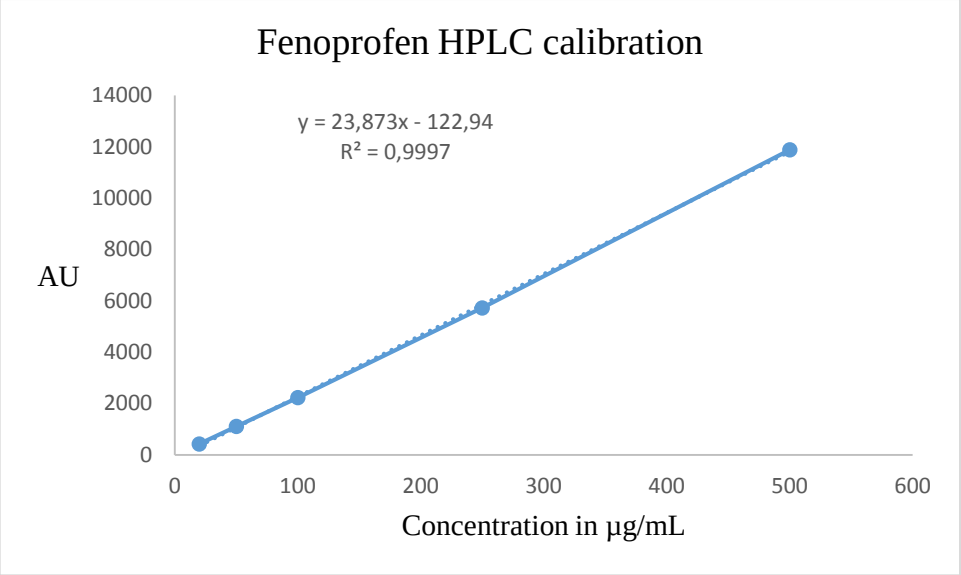

Fig. 6.1 Calibration curve of fenoprofen in acetone. AU = arbitrary units.

Knowing the fenoprofen amount fed into the mixtures and fitting the results, obtained after HPLC injections, into the equation of the calibration curve, the encapsulation efficiency and loading capacity of nanogels were determined using equations 5.7, 5.8 and 5.9.

$$\boldsymbol{encapsulation\ efficiency}\ (\boldsymbol{EE})\% = \frac{fen.conc.\ into\ nanogels}{fen.conc.fed - fen.conc.in\ solution} x100$$

$$\mathbf{fen.conc.\ into\ nanogels} = solution\ nanogels\ plus\ fen. - fen.in\ water$$

Equation 6.7 and 6.8 where fen. is fenoprofen

$$\boldsymbol{Loading\ capacity}\ \% = \frac{\text{mass of fen. incorporated}}{\text{mass of nanogel}} x100$$

Equation 6.9

6.3.22 Fenoprofen release

MRGC 213 and fenoprofen (mass ratio 1:2.5) were placed in a round bottom flask (RBF) equipped with a magnetic flea and 10 mL acetone were added. The dispersion was sonicated for 10 minutes and then left under stirring (400 rpm) for 6 hours. The acetone was evaporated under reduced pressure using a rotavapor until formation of white film around the wall of the RBF. The film was suspended in an amount of phosphate buffer (pH 7.4) necessary to achieve a nanogel concentration of 1 mg/mL and left stirring (360 rpm) for 2 minutes to homogenise the suspension and then let settle for 5 minutes in order to allow precipitation of eventual unsoluble fenoprofen. The superatant was then filtered through 0.45 µm syringe in order to remove precipitate still dispersed in the supernatant. 5 mL of the filtrate were placed in a 5.5 mL dyalisis cassette (3500-4000 M.W. cutoff). The cassette was then immersed in 50 mL of PBS. Fenoprofen release profile was evaluated by collecting aliquotes of either the solution inside and outside the cassette at different time points from 0 to 24 hours. The aliquots were then injected in to an HPLC equipped with UV detector using the same method descibed in section 6.3.20.

References

1. Y. Kang, A. Lu, A. Ellington, M. C. Jewett; R. K. O'Reilly. Effect of Complementary Nucleobase Interactions on the Copolymer Composition of RAFT Copolymerizations. *ACS Macro Lett.* **2013**, 2, 581−586.
2. M. P. Robin, P. Wilson, A. B. Mabire, J. K. Kiviaho, J. E. Raymond, D. M. Haddleton; R. K. O'Reilly. Conjugation-Induced Fluorescent Labeling of Proteins and Polymers Using Dithiomaleimides. *J. Am. Chem. Soc.*, **2013**, 135, 2875−2878.
3. M. P. Robin; Rachel K. O'Reilly. Fluorescent and chemico-fluorescent responsive polymers from dithiomaleimide and dibromomaleimide functional monomers. *Chem. Sci.*, **2014**, 5, 2717-2723.
4. Y. Kang, A. Lu, A. Ellington, M. C. Jewett; R. K. O'Reilly. Effect of Complementary Nucleobase Interactions on the Copolymer Composition of RAFT Copolymerizations. *ACS Macro Lett.* **2013**, 2, 581−586.
5. M. P. Robin, P. Wilson, A. B. Mabire, J. K. Kiviaho, J. E. Raymond, D. M. Haddleton; R. K. O'Reilly. Conjugation-Induced Fluorescent Labeling of Proteins and Polymers Using Dithiomaleimides. *J. Am. Chem. Soc.*, **2013**, 135, 2875−2878.
6. M. P. Robin; Rachel K. O'Reilly. Fluorescent and chemico-fluorescent responsive polymers from dithiomaleimide and dibromomaleimide functional monomers. *Chem. Sci.*, **2014**, 5, 2717-2723.

Chapter VII: Conclusion and future works

7.1 Conclusions

The work described in this thesis focused on the development of a novel methacrylate based nanogel for drug delivery application. The study was divided in three main objectives: 1) synthesis and characterisation of the nanogels; 2) *in vitro* toxicity and cell metabolism studies and 3) preliminary evaluation of drug upload and release.

The synthesis of nanogels was achieved via high dilution radical polymerisation using N,N′-methylenebis(acrylamide) (MBA) as cross-linker, azobisisobutyronitrile and ammonium persulfate as initiators, a selection of monomer concentration (C_M) and diverse methacrylates molecules, at various concentration, including: lauryl methacrylate (LMA), ethylene glycol methyl methacrylate (EGMMA), 2-(diethylamino)ethyl methacrylate (DEAEMA), 2-(tert-butylamino)ethyl methacrylate (tBAEMA) and methacrylic acid (MAA), all used with a variety of solvent systems, depending on the combinations. This polymerisation technique was shown to give significant advantages in terms of good reproducibility, low costs and easy removal of unreacted materials.

As a result of the initial studies, aiming to achieve optimal chemical composition of polymerisation mixtures and synthetic conditions, two preparations (MRGC 213 and MRGC 214) were identified as the most promising nanogels for dermal drug delivery applications due to their reduced particle size (ranging between 5 and 20 nm) confirmed both by dynamic light scattering and transmission electron microscopy; good water solubility ($\geq$ 3 mg/mL) and emulsion formation capabilities.

MRGC 213 and 214 were synthesised in a mixture of water : acetone 1:1 using ammonium persulfate as initiator and with a C_M of 0.5%. Their chemical composition was tBAEMA : MAA : MBA and tBAEMA : EGMMA : MBA respectively, in a molar ratio of 60:20:20. In order to visually evaluate the fate of nanogels crossing the skin or internalising inside cells, nanoparticles covalently labelled with a fluorescent tag (MRGC 209 and 211) were prepared. The fluorescent nanoparticles were prepared using the same protocol and with similar composition as for MRGC 213 and 214, with the only difference being a moles reduction of 5% of tBAEMA in favour of 5% moles of 2-(2-(3,4-bis(butylthio)-2,5-dioxo-2,5-dihydro-1H-pyrrol-1-yl)acetoxy)ethyl

methacrylate {methacrylate fluorophore} (MAF), for a final chemical composition of tBAEMA : MAA : MBA : MAF and tBAEMA : EGMMA : MBA : MAF 55:20:20:5.

Excellent results were also obtained, in terms of nanogels' biocompatibility, by testing cell cytotoxicity, cellular morphology modifications and adenosine triphosphate levels inside cells incubated with various concentrations of fluorescent and non-fluorescent nanogels (10, 20, 50, 100, 200 and 400 µg/mL).Viability and cellular morphology modification studies were performed on immortalised human keratinocytes (HaCaT), normal dermal human fibroblast (NDHF) and HeLa cells while adenosine triphosphate levels were carried out only on NDHF and HaCaT cells. No evidence of cell toxicity was observed after 24 hours incubation, up to a nanogel's concentration of 100 µg/mL on NDHF and up to 400 µg/mL in HaCaT and HeLa cell lines. Furthermore, no morphological or metabolic (ATP levels) variations were observed after cell exposure to nanoparticle, for 24 hours, up to 100 µg/mL in fibroblast and up to 400 µg/mL in immortalised keratinocytes and HeLa cells, in agreement with cytotoxicity results.

An important aspect, in the development of these novel nanogels for drug delivery, was the evaluation of the nanoparticles ability to incorporate and then release pharmaceutically active molecules. Two different therapeutic profiles were considered. The first envisaging the use of siRNA as large biomolecule to assess the nanogels' suitability to be used as a vector for gene delivery and the second regarding the employment of fenoprofen, a non-steroidal anti-inflammatory drug (NSAID), as a more conventional small pharmaceutic. Silencing RNA encapsulation and release were evaluated by transfecting genetically modified HeLa cells, expressing green fluorescent protein (GFP), with nanogels complexed with a fluorescently labelled siRNA (mass ratio 25:1) specific for the knock down of GFP gene (siRNA Duplex I/CY5), at various concentration ranging from 20 to 100 µg/mL. A siRNA's complexation efficiency of 99% was achieved and GFP knockdown up to 30% was observed, confirming capability of nanoparticles to act as vector for silencing RNA release. Preliminary studies on fenoprofen incorporation were also performed showing an encapsulation efficiency over 55% and high loading capacity over 70%. These results proved the potential of nanogels to function as cargo for the drug.

The time available for this project did not allow to achieve all the desired objectives, in particular regarding further characterisations in terms of pharmacology. In view of the

promising physico-chemical and biological features of these methacrylate based nanogels, demonstrated in this work so far, further studies are proposed for future development and are briefly described in the following section.

7.2 Future works and perspectives

7.2.1 Materials studies

More extensive polymerisation studies could be performed in order to create an exhaustive library of methacrylate based nanogels. Additionally, important information could be obtained by an in-depth polymerisation kinetic studies which could lead to further optimisation of nanogel synthesis. Lastly tests on physicochemical properties of nanogel (rheology, thermal properties, resistance to compression and traction etc.) could provide additional information on material characteristics and physical behaviour.

7.2.2 Emulsion studies

In order to identify a suitable formulation composition and to fully understand the action of nanogels at the interface, more tests need to be carried out. In regards to formulation composition it is essential to determine the best combination of water/oil phases and the optimal nanogels concentration. At the same time, it would be ideal to gain information on emulsion performance in function of physical-chemical changes such as temperature, ionic strength, presence of impurities etc.

7.2.3 Small drug incorporation and release studies

Following the promising results of fenoprofen incorporation it was considered to assess nanogels' encapsulation efficiency using a molecularly imprinting approach of drug

uploading profiting from the expertise of the Resmini's research group in the field. Although these experiments were planned they could not be completed due to time constrains. Moreover, further analyses will be performed in order to further evaluate the release profile of the nanogels herein presented.

7.2.4 Biological studies

Additional siRNA complexation and release studies will need to be carried out in order to gain an exhaustive understanding of potential gene therapy applications, nanogels cell internalisation and content release mechanisms. Furthermore, as a results of a collaboration with Prof. M. Perretti and his research team, at Queen Mary university of London, a chondrocyte model for rheumatoid arthritis will be available to evaluate the ability of the nanogels to target this disease. This experiment has already received funding and will be performed by the candidate presenting this thesis. After chondrocytes analyses and implementation of siRNA delivery, the system will require *ex vivo* and *in vivo* testing to bring the nanogels one step closer to the development of a final pharmaceutical formulation. *Ex vivo* models comprise Franz cells equipped with membranes or pig skin and penetration studies on human skin obtained from surgery procedures, available via a partner research group led by Prof. D. Kelsell from the medical school of Queen Mary University of London. Possible animal models include zebrafish and mice, accessible via present and past collaborations with research groups led by Dr. C. Brennan from the school of biological and chemical of Queen Mary University of London (zebrafish) and Prof. V. Preat from the Univerité Cahtolique de Louvain, Belgium (mice).

7.2.5 Further development

Although an extensive amount of work still needs to be carried out before the pharmaceutical employment of these nanogels, the study highlighted the potential to use 2-(*tert*-butylamino)ethyl methacrylate (tBAEMA) based crosslinked nanoparticles as a drug delivery carrier for transdermal application. However, many more

applications can be taken into account not only in terms of different route of drug administration but also in the development of nano-emulsion synthetic environment or as coating agent for organic and inorganic nanoparticles.